

Substituted Fischer carbene complexes of molybdenum(0)

By

Tamzyn Joyce Levell

Submitted in partial fulfilment of the requirements for the degree

Magister Scientiae

In the Faculty of Natural & Agricultural Sciences

University of Pretoria

Pretoria

June 2014

Supervisor: Dr M. Landman

Declaration

I, Tamzyn Joyce Levell declare that the dissertation, which I hereby submit for the degree Magister Scientiae at the University of Pretoria, is my own work and has not previously been submitted by me for a degree at this or any other tertiary institution.

June 2014

Abstract

Substituted Fischer carbene complexes of molybdenum(0)

By Tamzyn Joyce Levell

Supervisor: Dr. M. Landman

Department of Chemistry

University of Pretoria

MSc Dissertation

The synthesis and structure elucidation of fourteen novel Fischer ethoxy- and amino carbene complexes of molybdenum and chromium metals of the type $[(CO)_3L_2M=C(X)R]$ were performed. Substitution of the parent pentacarbonyl complex $[(CO)_5M-C(OEt)(R)]$; $M = Mo, Cr$; $R = 2$ -thienyl, 2-furyl; with mono- and bidentate phosphine ligands yielded the corresponding tetracarbonyl complexes $[(CO)_4(PR'_3)M-C(OEt)R]$ with $M = Mo, Cr$, $R = 2$ -thienyl, 2-furyl and $R' = Ph, Cy$ or tricarbonyl complexes $[(CO)_3(DPPE)Mo-C(OEt)(2-furyl)]$, respectively. Aminolysis of these novel complexes resulted in substitution of the ethoxy substituent with an amino group. Full characterisation of these novel complexes included infrared spectroscopy, NMR (1H , ^{13}C , ^{31}P) spectroscopy, x-ray crystallography and mass spectral analyses. From the characterisation data, it was found that the *cis* isomer was dominant for the tetracarbonyl carbene complexes whereas the *mer* isomer was favoured in most cases for the tricarbonyl carbene complexes.

Structural elucidation of nine of the novel complexes was confirmed with x-ray crystallography. The amino carbene complexes showed preference for a *syn* conformation of the oxygen atom of the furyl moiety and the nitrogen atom of the amino moiety in the crystal form. The ethoxy carbene complexes showed a preference for the *anti* conformation in the crystal form. The NMR analysis showed that resonance between the metal-carbene carbon-heteroatom stabilisation is more prevalent in the case of the amino carbene complexes.

DFT calculations were performed for eleven of these complexes and their isomers. The infrared stretching modes were calculated and compared to experimental data. The HOMO and LUMO position and energy gaps were calculated. It was observed that the HOMO in all calculated complexes lay on the metal centre, while the LUMO was centred on the carbene carbon. It was found that the HOMO-LUMO gap was larger for the amino Fischer carbene complexes than for the ethoxy Fischer carbene complexes. From frontier orbital considerations, it is concluded that ligand substitution of carbonyls by phosphines as well as carbene substituent alterations does not seem to improve the reactivity of the novel complexes of this study particularly for the potential application as metathesis catalysts. The performed DFT calculations, in the future, can help determine which type of catalytic reactions these fourteen complexes would be most effective for.

Acknowledgements

Dr Landman – Ma, for steering me in the right direction throughout this project and for the countless hours we spent editing my very many drafts

Prof. van Rooyen – Pa, for solving my crystal structures and for helping me make sense of them and for “adding value” to me, my crystals and my thesis

Prof. Vlegaar – Who will always be remembered for his jokes and for lending a hand and advice even when he did not quite know what I was talking about

Eric Palmer – For obtaining clear NMR spectra and for helping me when I could not get the same quality spectra when doing it myself

Roan, Wynand, Lauren and Dom – The team + honorary member, for teaching me so many things, for the camaraderie, for the French and the fun, you guys are the best

Grant – My lief, for all his computer related ingenuity, for putting up with all my tears and for being my sounding board even when my sentences made no sense

Dwayne Koot and Elise Smit – For all your work and assistance in interpreting my MS data

Thank you to Jeanette Conradie, Marrigje Conradie and Blenerhassit Buitendach from UFS for working with us on the two articles which resulted from this work. (DOI: 10.1016/j.molstrc.2014.02.014; submitted to Organometallics)

The financial assistance of the University of Pretoria and the National Research Foundation (NRF) towards this research is hereby acknowledged. Opinions expressed and conclusions arrived at, are those of the author and are not necessarily to be attributed to the NRF.

Table of Contents

Abstract.....	iii
List of complexes.....	ix
List of abbreviations.....	xii
Chapter 1: Introduction	1
1.1 History	2
1.2 Structure, reactivity and catalysis of carbenes.....	3
1.3 Application.....	12
1.4 This study.....	13
1.5 Aims of this study	14
Chapter 2: Ethoxy Carbene Complexes.....	15
2.1 Introduction.....	16
2.2 Molybdenum pentacarbonyl ethoxy carbene complexes.....	21
2.2.1 Infrared spectroscopy	23
2.2.2 ¹ H NMR spectroscopy.....	27
2.2.3 ¹³ C NMR spectroscopy	30
2.2.4 X-Ray crystallography	33
2.3 Chromium and molybdenum tetracarbonyl phosphine-substituted ethoxy carbene complexes	36
2.3.1 Infrared spectroscopy	38
2.3.2 ¹ H NMR spectroscopy.....	40
2.3.3 ¹³ C NMR spectroscopy.....	42
2.3.4 ³¹ P NMR spectroscopy.....	44
2.3.5 X-Ray crystallography	45
2.4 Molybdenum tricarbonyl diphosphine-substituted ethoxy carbene complexes	48
2.4.1 Infrared spectroscopy	49
2.4.2 ¹ H NMR spectroscopy.....	52

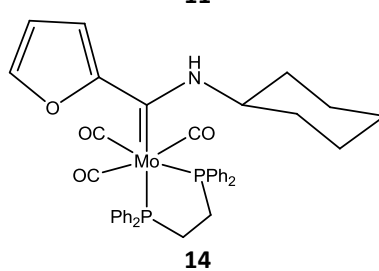
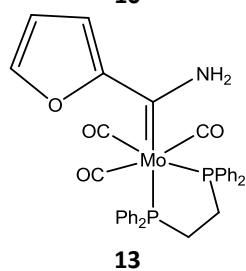
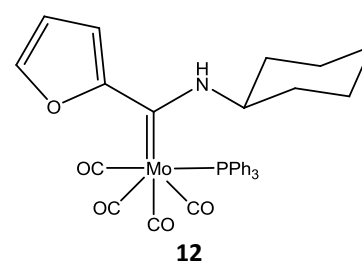
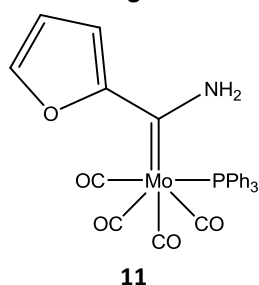
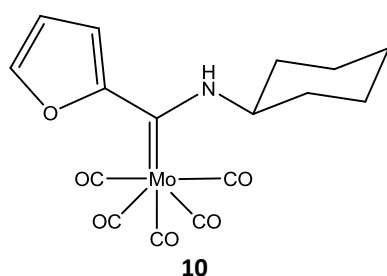
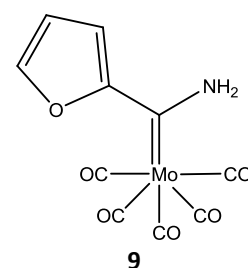
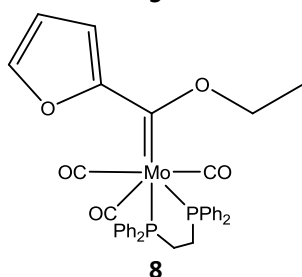
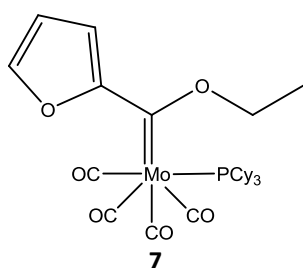
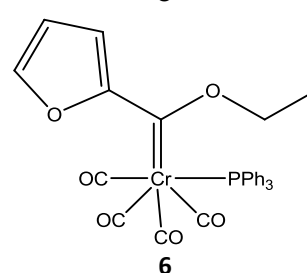
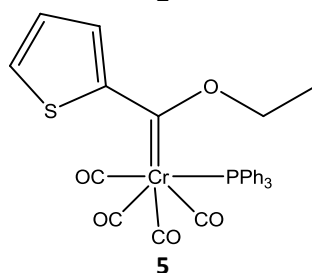
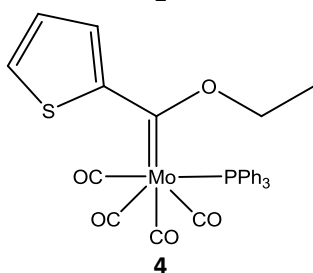
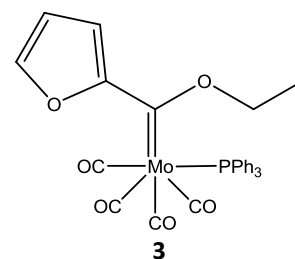
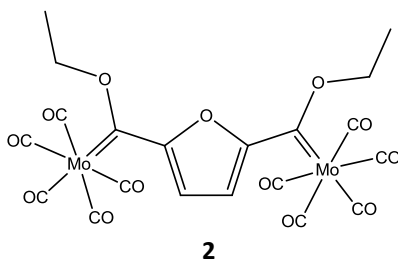
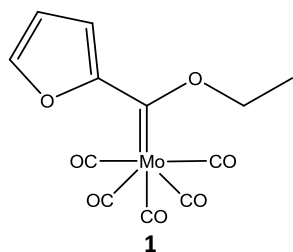
2.4.3 ^{13}C NMR spectroscopy.....	54
2.4.4 ^{31}P NMR spectroscopy.....	55
2.4.5 X-Ray crystallography.....	57
2.5 Computational analysis	61
Chapter 3: Amino Carbene Complexes	70
3.1 Introduction.....	71
3.2 Molybdenum pentacarbonyl amino carbene complexes.....	75
3.2.1 Infrared spectroscopy	78
3.2.2 ^1H NMR spectroscopy.....	79
3.2.3 ^{13}C NMR spectroscopy.....	82
3.2.4 X-Ray crystallography.....	83
3.3 Molybdenum tetracarbonyl phosphine-substituted carbene complexes.....	86
3.3.1 Infrared spectroscopy	87
3.3.2 ^1H NMR spectroscopy.....	88
3.3.3 ^{13}C NMR spectroscopy.....	90
3.3.4 ^{31}P NMR spectroscopy.....	91
3.3.5 X-Ray crystallography.....	92
3.4 Molybdenum tricarbonyl diphosphine-substituted amino carbene complexes.....	94
3.4.1 Infrared spectroscopy	96
3.4.2 ^1H NMR spectroscopy.....	97
3.4.3 ^{13}C NMR spectroscopy.....	99
3.4.4 ^{31}P NMR spectroscopy.....	101
3.4.5 X-Ray crystallography.....	102
3.5 Computational analysis	104
Chapter 4: Comparisons and Conclusions	111
4.1 Introduction.....	112
4.2 Comparisons.....	112

4.2.1 Infrared spectroscopy	112
4.2.2 NMR spectroscopy	113
4.2.3 X-Ray crystallography	115
4.2.4 Computational analysis	118
4.3 Conclusions	120
Chapter 5: Experimental	122
5.1 General comments	124
5.2 Synthesis of $[\text{Mo}(\text{CO})_5[\text{C}(\text{OEt})(\text{C}_4\text{H}_3\text{O})]]$ (1) and $[\text{Mo}(\text{CO})_5\text{C}\{(\text{OEt})\}_2(\text{C}_4\text{H}_3\text{O})]$ (2)	125
5.3 Synthesis of $[\text{Mo}(\text{CO})_4(\text{PPh}_3)[\text{C}(\text{OEt})(\text{C}_4\text{H}_3\text{O})]]$ (3)	126
5.4 Synthesis of $[\text{Mo}(\text{CO})_4(\text{PPh}_3)[\text{C}(\text{OEt})(\text{C}_4\text{H}_3\text{S})]]$ (4)	127
5.5 Synthesis of $[\text{Cr}(\text{CO})_4(\text{PPh}_3)[\text{C}(\text{OEt})(\text{C}_4\text{H}_3\text{S})]]$ (5)	128
5.6 Synthesis of $[\text{Cr}(\text{CO})_4(\text{PPh}_3)[\text{C}(\text{OEt})(\text{C}_4\text{H}_3\text{O})]]$ (6)	128
5.7 Synthesis of $[\text{Mo}(\text{CO})_4(\text{P}(\text{C}_6\text{H}_{11})_3)[\text{C}(\text{OEt})(\text{C}_4\text{H}_3\text{O})]]$ (7)	129
5.8 Synthesis of $[\text{Mo}(\text{CO})_3(\text{DPPE})[\text{C}(\text{OEt})(\text{C}_4\text{H}_3\text{O})]]$ (8)	129
5.9 Synthesis of $[\text{Mo}(\text{CO})_5[\text{C}(\text{NH}_2)(\text{C}_4\text{H}_3\text{O})]]$ (9)	130
5.10 Synthesis of $[\text{Mo}(\text{CO})_5[\text{C}(\text{NC}_6\text{H}_{12})(\text{C}_4\text{H}_3\text{O})]]$ (10)	130
5.11 Synthesis of $[\text{Mo}(\text{CO})_4(\text{PPh}_3)[\text{C}(\text{NH}_2)(\text{C}_4\text{H}_3\text{O})]]$ (11)	131
5.12 Synthesis of $[\text{Mo}(\text{CO})_4(\text{PPh}_3)[\text{C}(\text{NC}_6\text{H}_{12})(\text{C}_4\text{H}_3\text{O})]]$ (12)	131
5.13 Synthesis of $[\text{Mo}(\text{CO})_3(\text{DPPE})[\text{C}(\text{NH}_2)(\text{C}_4\text{H}_3\text{O})]]$ (13)	132
5.14 Synthesis of $[\text{Mo}(\text{CO})_3(\text{DPPE})[\text{C}(\text{NC}_6\text{H}_{12})(\text{C}_4\text{H}_3\text{O})]]$ (14)	133
5.15 Synthesis of $[\text{Mo}(\text{CO})_5[\text{C}(\text{OEt})(\text{C}_4\text{H}_3\text{S})]]$ (C)	133
5.16 Synthesis of $[\text{Cr}(\text{CO})_5[\text{C}(\text{OEt})(\text{C}_4\text{H}_3\text{S})]]$ (L)	134
6. Appendices	135
6.1 Appendix A: Crystal data and structure refinement for 1	135
6.2 Appendix B: Crystal data and structure refinement for 3	136
6.3 Appendix C: Crystal data and structure refinement for 5	137
6.4 Appendix D: Crystal data and structure refinement for 8	138

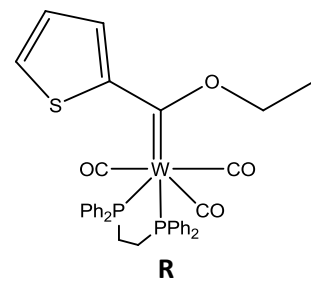
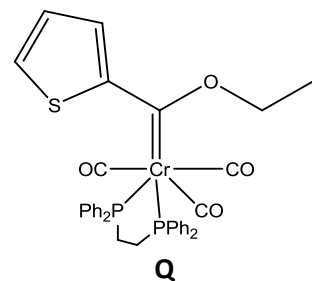
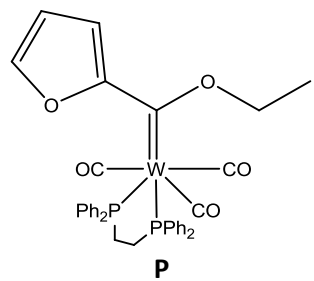
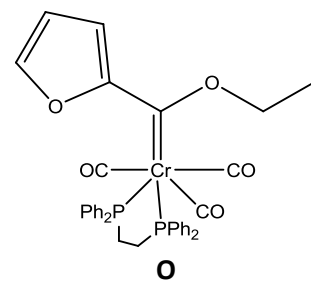
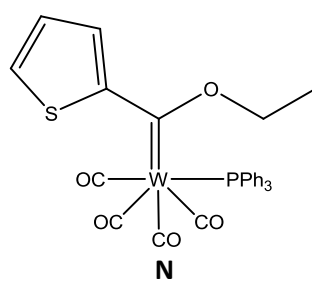
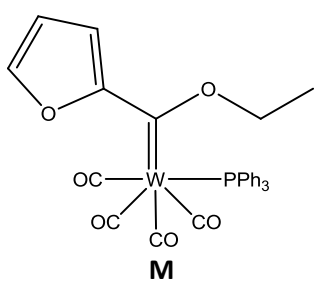
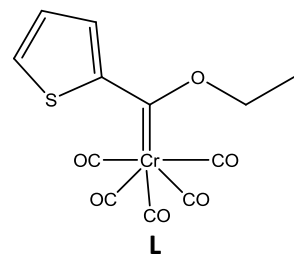
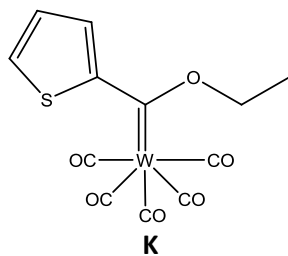
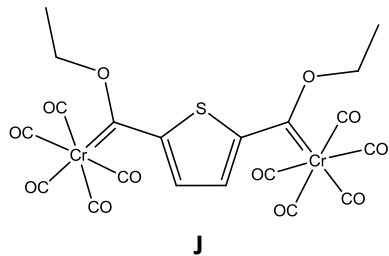
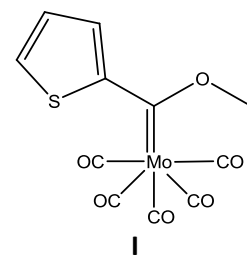
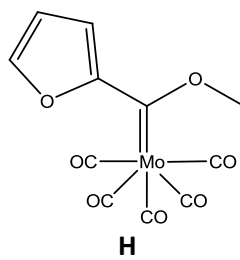
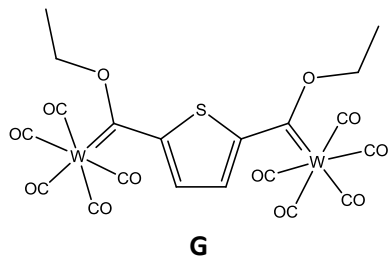
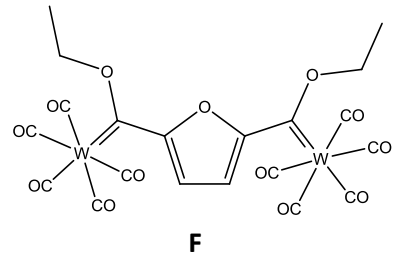
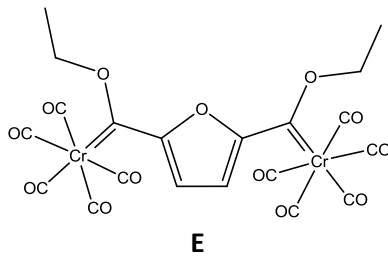
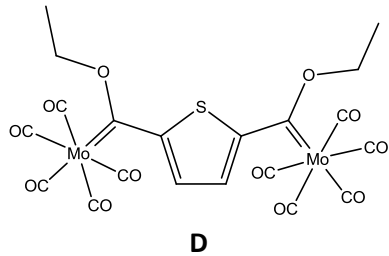
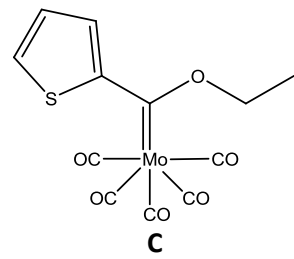
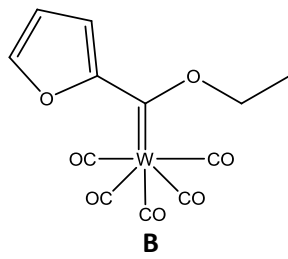
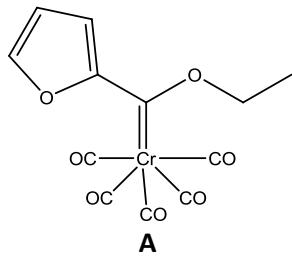
6.5 Appendix E: Crystal data and structure refinement for 9	139
6.6 Appendix F: Crystal data and structure refinement for 10	140
6.7 Appendix G: Crystal data and structure refinement for 11	141
6.8 Appendix H: Crystal data and structure refinement for 12	142
6.9 Appendix I: Crystal data and structure refinement for 13	143

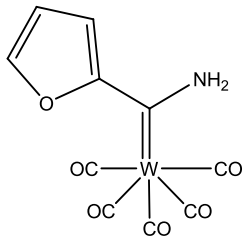
List of complexes

Novel Complexes

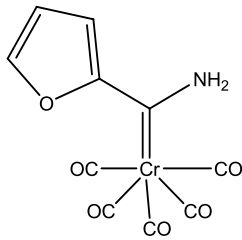


Known Complexes

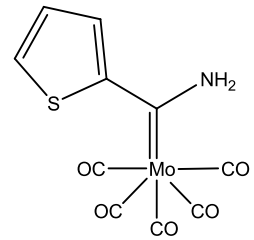




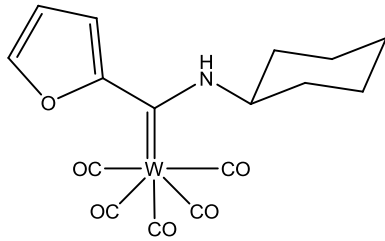
S



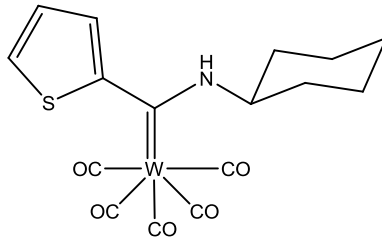
T



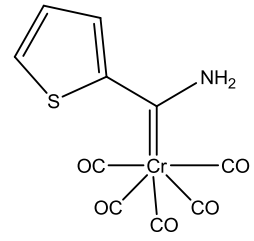
U



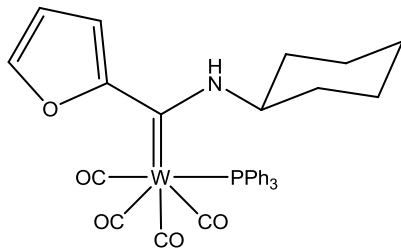
V



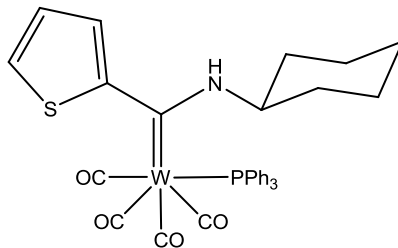
W



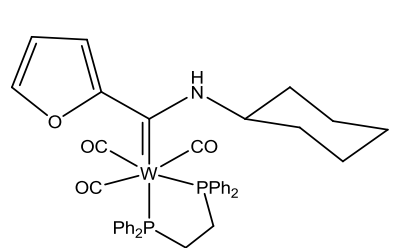
X



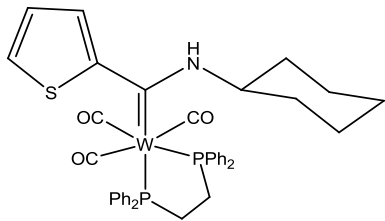
Y



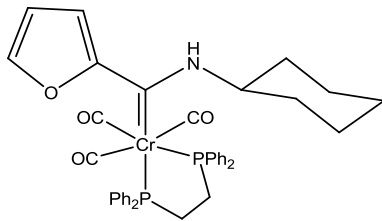
Z



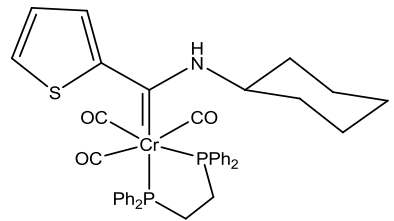
AA



AB



AC



AD

List of abbreviations

Ad	Adamantyl
APCI	Atmospheric pressure chemical ionisation
b	Broad peak (NMR spectroscopy)
CAAC	Cyclic alkyl amino carbene
CO	Carbonyl
COSY	Correlation spectroscopy
Cy	Cyclohexyl
d	Doublet
DCM	Dichloromethane
dd	Double doublet
DFT	Density functional theory
DPPE	1,2-Bis(diphenylphosphino)ethane
ESI	Electrospray ionisation
ESP	Electrostatic potential
Et	Ethyl
<i>fac</i>	Facial isomer
HOMO	Highest occupied molecular orbital
HSQC	Heteronuclear single quantum coherence
IR	Infrared
LUMO	Lowest unoccupied molecular orbital
m	Multiplet (NMR spectroscopy)
m	Medium intensity (IR spectroscopy)
Me	Methyl
<i>mer</i>	Meridional isomer

mes	Mesityl
mmol	Millimole
MS	Mass spectrometry
ⁿ BuLi	n-Butyl lithium
NHC	N-heterocyclic carbene
NHP	N-heterocyclic phosphonium
NMR	Nuclear magnetic resonance spectroscopy
Ph	Phenyl
q	Quartet
R	Alkyl group
RT	Room temperature
s	Strong intensity (IR spectroscopy)
t	Triplet
THF	Tetrahydrofuran
TLC	Thin layer chromatography
vs	Very strong intensity (IR spectroscopy)
w	Weak intensity (IR spectroscopy)

Chapter 1:

Introduction

Wherever we look, the work of the chemist has raised the
level of our civilisation and has increased the
productive capacity of our nation.”

– Calvin Coolidge

1.1 History

The first notion toward the existence of a carbenic species was detailed by Geuther and Hermann¹ in 1855. They suggested a divalent carbon intermediate for the alkaline hydrolysis reaction of chloroform. The same intermediate was suggested for the Reimer-Tiemann reaction performed in chloroform by Nef² 40 years later. These suggestions were quite bold, since the first free radical was only synthesised and characterised in 1900 by Gomberg.³ Throughout the 1920's and 30's, carbenes were considered to be diradicals.⁴ In 1951, quantum mechanics was used to determine the geometry around the methylene carbene.⁵ It could not, however, be discerned whether the triangular geometry (singlet state) or the linear geometry (triplet state) had the lowest energy.⁵ Shortly after, it was proven that the triangular geometry, singlet state, had the lowest energy.⁶

The first fully characterised, stable metal carbene complex was published in 1964 by Fischer and Maasböl⁷ (Figure 1.1). This was the advent of this field of organometallic chemistry which has since developed at an immense rate over the last 50 years. Today three main classes of carbene complexes are recognized namely Schrock-, Fischer- and N-heterocyclic carbenes (NHCs). Each of the three carbene types have their own unique characteristics and reactivity patterns which will be discussed later in this chapter. The impetus for research in this area was the catalytic properties of these species and their effectiveness at catalysing industrial processes such as olefin metathesis.

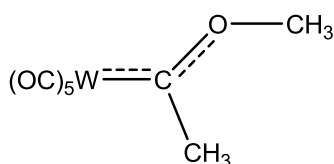


Figure 1.1: First stable metal carbene complex published by Fischer and Maasböl⁷

Shortly after the first Fischer carbene complex was synthesised and characterised, Öfele⁸ and Wanzlick *et al.*⁹ described complexes with one or two N-heterocyclic carbene moieties, respectively. Öfele continued to work on these types of complexes and elucidated some basic features. In 1991, Arduengo¹⁰ synthesised and characterised the first free N-heterocyclic carbene (Figure 1.2).

¹ Geuther, A., Hermann, M., *Liebigs Ann. Chem.*, 95, **1855**, 211

² Nef, J.U., *Justus Liebigs Ann. Chem.*, 298, **1897**, 202

³ Gomberg, M., *J. Am. Chem. Soc.*, 22, **1900**, 757

⁴ de Frémont, P., Marion, N., Nolan, S.P., *Coord. Chem. Rev.*, 253, **2009**, 862

⁵ Lennard-Jones, J., Pople, J. A., *Discuss. Faraday. Soc.*, 10, **1951**, 9

⁶ Duchesne, J., Burnelle, L., *J. Chem. Phys.* 21, **1953**, 2005

⁷ Fischer, E.O., Maasböl, A., *Angew. Chem. Int. Ed. Engl.* 3, **1964**, 645

⁸ Öfele, K., *J. Organomet. Chem.*, 12, **1968**, 42

⁹ Wanzlick, H.W., Schönherr, H.J., *Angw. Chem. Int. Ed. Engl.*, 7, **1968**, 141

¹⁰ Arduengo III, A.J., Harlow, R.L., Kline, M., *J. Am. Chem. Soc.*, 113, **1991**, 361

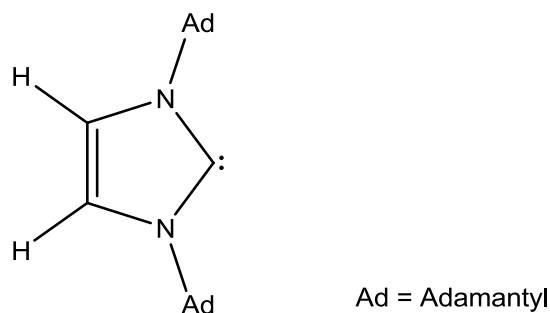


Figure 1.2: First free N-heterocyclic carbene synthesised by Arduengo¹⁰

In 1974, the first synthesis and elucidation of a high oxidation state metal-alkylidene complex was reported by Schrock.¹¹ Grubbs¹² subsequently synthesised a ruthenium-containing Schrock carbene complex (Grubbs I) that was catalytically active for the metathesis reaction. A few short years later, he synthesised another catalyst - this time an NHC carbene complex: Grubbs II.¹³ This work resulted in Grubbs, together with two other scientists, being awarded a Nobel prize in 2005.¹⁴

In 2002, Bertolini *et al.*¹⁵ detailed the use of molybdenum Fischer carbene complexes to successfully convert a dienyne to 4,3,1-propellane. Barluenga *et al.*¹⁶ soon after published a paper which detailed a method to interchange diphosphinated molybdenum Fischer carbene complexes from *fac* isomers to *mer* isomers and *vice versa*. This was done for the purpose of producing enantiomerically pure reagents.

1.2 Structure, reactivity and catalysis of carbenes

As outlined in Fischer's Nobel prize lecture,¹⁷ carbenes are very reactive derivatives of divalent carbon. These compounds are stabilised upon coordination with metals which results in two distinct types of carbene complexes - Fischer-type carbene complexes and Schrock-type carbene complexes. More recently, an additional and controversial third type of carbene has been added - N-heterocyclic carbenes (Figure 1.2).¹⁸ These are controversial because some consider them to be a subsection of Fischer carbenes.¹⁸ Each of the three types of carbene has their own reactivities and characteristics.

The crux of the carbene classification matter is the metal-carbene bond. There are two different types of metal-carbene bonds - one characterised by spin triplet fragments and one characterised by

¹¹ Schrock, R.R., *J. Am. Chem. Soc.*, 96, **1974**, 6796

¹² Nguyen, S.T., Johnson, L.K., Grubbs, R.H., Ziller, J.W., *J. Am. Chem. Soc.*, 114, **1992**, 3974

¹³ Schwab, P., France, M.B., Ziller, J.W., Grubbs, R.H., *Angew. Chem. Int. Ed. Engl.*, 18, **1995**, 2039

¹⁴ Grubbs, R.H., *Adv. Synth. Catal.*, 349, **2007**, 34

¹⁵ Bertollini, T.M., Nguyen, Q.H., Harvey, D.F., *J. Org. Chem.*, 67, **2002**, 8675

¹⁶ Barluenga, J., Muniz, K., Tomas, M., Ballesteros, A., Garcia-Granda, S., *Organometallics*, 22, **2003**, 1756

¹⁷ Fischer, E.O., *Angew. Chem.* 86, **1974**, 651

¹⁸ Salzer, A., Elschenbroich, C.H., *Organometallics: A Concise Introduction*, Second Ed., **1992**, VCH Verlag, Weinheim, 210-241

spin singlet fragments.¹⁹ Triplet fragments are associated with Schrock carbenes, and the singlet fragments are associated with both Fischer and NHC complexes. The efficiency of the metal carbon σ -bonding and the efficiency of the π -back bonding is integral to the complex's reactivity.¹⁹

The multiplicity of the carbene is, to a large extent, determined by the electronegativity of the substituents on the carbene carbon. Electron-withdrawing groups favour the singlet state because they stabilise the non-bonding orbital.⁴

Vyboishchikov and Frenking²⁰ use the following definitions to classify compounds as Fischer carbenes or Schrock carbenes:

Fischer carbenes: "Compounds that have a heteroatom linked to the carbenoid carbon; they usually have a metal in a low oxidation state, π -acceptor ligands, and electrophilic character at the carbene carbon atom."

Schrock carbenes: "[Compounds] with alkyl groups or hydrogen atoms at the carbene centre; these usually present higher oxidation states of the metal atom, a variety of ligands, which are usually not closed shell species as free molecules, and they have nucleophilic character at the carbene carbon atom."

With this in mind, the characteristics of the three classes of carbene complexes can now be discussed.

Schrock-type carbene complexes typically occur for metals which are in a higher oxidation state (non-zero oxidation state). These types of carbene complexes typically have less than 18 electrons,¹⁹ have nucleophilic carbene carbons,²¹ are triplet carbene complexes,¹⁹ and are stabilised only by alkyl or hydride substituents.¹⁸ The carbene ligand has σ -donor, π -donor characteristics.¹⁸ A lone electron in a sp^2 hybrid orbital of the carbene carbon atom is shared in a σ -fashion with the single electron in the metal's dz^2 orbital. This is a formal covalent bond. Additionally, a single electron in an unhybridised p-orbital on the carbene carbon is shared, in a π -fashion, with a single electron in the metal's valence shell. This results in the carbene-metal bond being a formal covalent double bond (Figure 1.3).

¹⁹ Du Toit, J.I., van Sittert, C.G.C.E., Vosloo, H.C.M, *J. Organomet. Chem.*, 738, **2013**, 76

²⁰ Vyboishchikov, S.F., Frenking, G., *Chem. Eur. J.*, 4, **1998**, 1428

²¹ Schrock, R.R., *Acc. Chem. Res.*, 12, **1979**, 98



Figure 1.3: Metal–ligand bonding in a Schrock-type carbene¹⁸

Good ligands for Schrock carbene complexes are non- π -acceptors, and good R-groups to have on the carbene are non- π -donors (π -donors will destabilise the metal-carbene bond).¹⁹

Some typical reactions which Schrock carbenes undergo include¹⁹ Wittig-type reactions, electrophilic attack of the nucleophilic carbene carbon and reactions with methylene transfer agents.^{18,21}

NHC complexes can stabilise high or low oxidation state transition metals. This carbene is a singlet carbene, and as a ligand, it is a σ -donor ligand,¹⁸ and thus only forms a single bond with the metal. The σ -bond formation is due to an electron lone pair donation from a hybrid orbital of the carbene carbon atom that is donated to an unoccupied orbital of the metal (Figure 1.4). This is known in conventional chemistry as a dative covalent type bond.

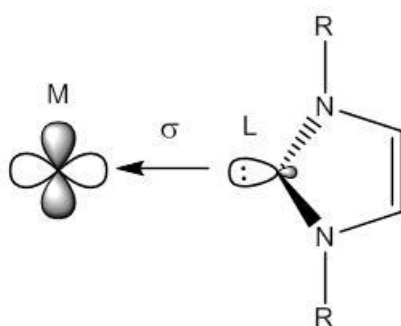


Figure 1.4: Metal-ligand bond formation in NHC carbene complexes¹⁸

Back-bonding from the metal does not occur because of the presence of the two nitrogen heteroatoms adjacent to the carbene carbon.¹⁸ These heteroatoms donate an electron pair in a π -fashion to the un-hybridised p-orbital on the carbene carbon. Thus no extra electron density is required from the metal, implying that the carbene can stabilise itself (Figure 1.5).

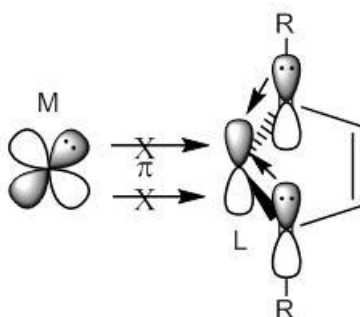


Figure 1.5: Nitrogen-carbene carbon bonding¹⁸

NHCs as ligands are found to be strong σ -donors, but weak π -acceptors; as a result, they tend to labilise other ligands around a metal while they themselves are tightly bound to the metal. The heteroatom substituents on the carbene carbon result in the orbitals on the carbon, which were originally degenerate, to be unequal in energy. This makes the carbene more nucleophilic and more thermodynamically stable.²²

Finally, in Fischer-type carbene complexes the transition metals involved are generally strong π -donors,¹⁹ are in low oxidation states¹⁸ and the complexes which are formed have 18 electrons.¹⁹ This carbene as a ligand is a σ -donor, π -acceptor ligand.¹⁸ Fischer-type carbene complexes are electrophilic at the carbene carbon.⁷ These carbene complexes are singlet carbenes, which have at least one heteroatom bonded directly to the carbene carbon atom.^{4,18,23,24} In these complexes, good ligands are π -acceptor ligands, and good carbene R-groups are π -donors.¹⁹ A lone pair in a hybrid orbital on the carbene carbon is donated to the metal d_{z^2} orbital in a dative covalent sigma bond fashion, while a lone pair in the metal valence shell is back donated into an un-hybridised p-orbital on the carbene carbon (also dative covalently), as shown in Figure 1.6.

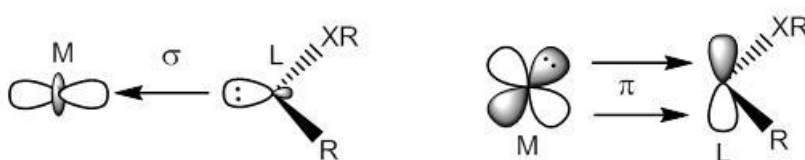


Figure 1.6: Metal-ligand bonding in a Fischer-type carbene complex¹⁸

It should be stated that the stronger the back-bonding is between the metal and the carbene moiety, the weaker the back bonding is to the carbonyl carbon *trans* to the carbene carbon, such as in the case of a pentacarbonyl carbene complex. The electrophilic character of the carbene carbon is stabilised by the back-bonding¹⁸ (Figure 1.6) as well as resonance effects¹⁸ from contributions from the heteroatom. The resonance structures are shown in Figure 1.7. As the carbene attains more stabilisation from the heteroatom, the double bond character of the metal-carbene bond diminishes.⁴

²² Herrmann, W.A., Köcher, C., *Angew. Chem. Int. Ed. Engl.*, 36, **1997**, 2162

²³ Sierra, M.A., *Chem. Rev.*, 100, **2000**, 3591

²⁴ Fey, N., Haddow, M.F., Harvey, J.N., McMullin, C.L., Orpen, A.G., *Dalton Trans.*, **2009**, 8183

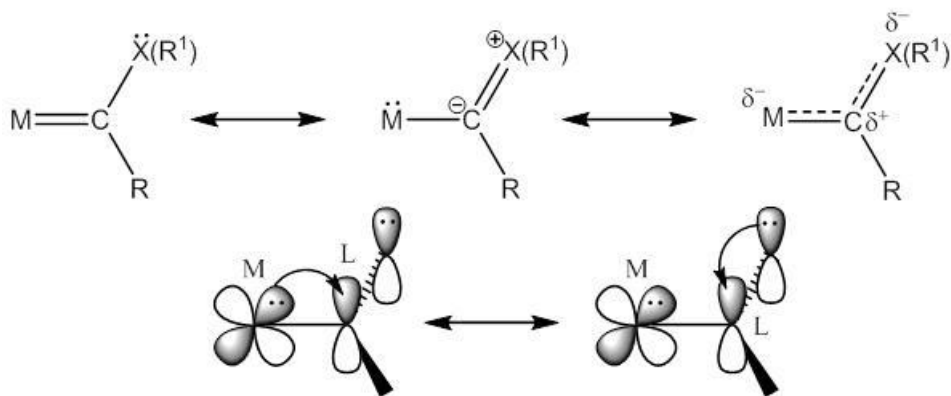


Figure 1.7: Resonance observed in Fischer-type carbenes¹⁸

Fischer carbene complexes undergo a number of different reactions, including reactions with nucleophiles, reactions with carbene transfer agents and reactions with alkynes^{18,25} (Figure 1.8).

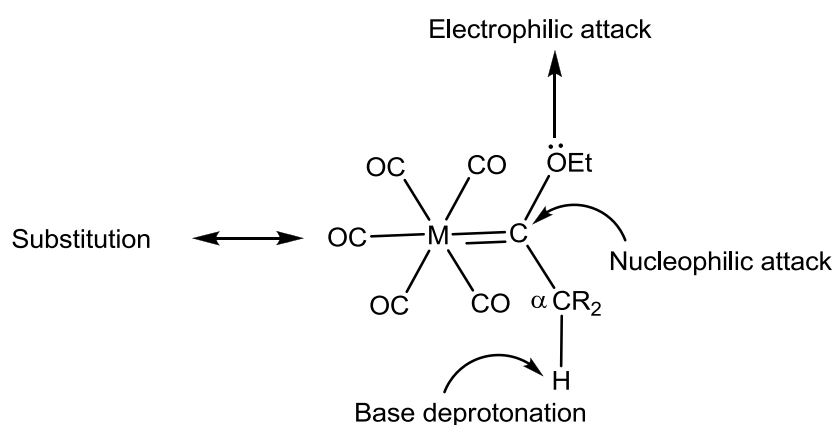


Figure 1.8: Reactivity of Fischer carbenes²⁶

Dötz²⁶ reported many reactions that Fischer carbene complexes can undergo. These include functionalization of the carbene ligand, carbene transfer reactions, carbonyl-carbene transfer reactions, synthesis of natural products and catalytic reactions. Functionalization of the carbene ligand occurs by α -H deprotonation resulting in a carbene complex anion and substitution of the carbene ligand. Carbene-transfer reactions take various forms, namely cleavage of the metal-carbene bond, alkenylation reactions, cycloaddition reactions and insertion reactions. The substitution reactions that the carbonyls of the carbene can undergo should only be considered with neutral ligands.^{26,27} This is to ensure that the oxidation state of the metal remains low in order to comply with the Fischer carbene characteristic.

²⁵ Collman, J.P., Hegedus, L.S., Norton, J.R., Finke, R.G., Principles and Application of Organotransition Metal Chemistry, **1987**, University Science Books, Mill Valley, CA, US.

²⁶ Dötz, K.H., *Angew. Chem. Int. Ed. Engl.*, **23**, **1984**, 587

²⁷ Landman, M., Pretorius, R., Buitendach, B.E., van Rooyen, P.H., Conradie, J., *Organometallics*, **32**, **2013**, 5491

It has been found that the most promising Schrock type carbene complex, for catalytic activity, is a molybdenum complex. A molybdenum catalyst is more reactive in the olefin metathesis catalytic cycle than the traditionally used ruthenium catalyst,²⁸ as it allows for tri- and tetra-substituted olefins to be made.²⁸

Fischer carbenes are the least exploited for their catalytic activity. These carbenes on group VI metals have been used as catalysts in the Fischer-Tropsch process, and have been very successful in this reaction.²⁹ However, Fischer carbene complexes are renowned to be poor metathesis catalysts compared to Schrock carbene complexes.¹⁹ This activity is mainly ascribed to frontier orbital considerations. For Schrock carbene complexes, the HOMO is positioned on the carbene carbon, and the LUMO is found on the metal atom while for Fischer carbene complexes, the opposite is observed - the LUMO is located the carbene carbon and the HOMO is centred on the metal. There are many examples of group VI metals being used in industrially important organic synthesis reactions,²⁹ thus this is a very valuable avenue of research.

Carbene complexes have very diverse chemistry associated with them, from catalysts³⁰ to electrochemical probes³¹ to self assemblies and signalling molecules³² to organic synthetic reactions.³³ Oh *et al.*³⁴ synthesised a manganese complex and showed that it has the ability to self assemble (Figure 1.9). The position of the oxygen atoms on the benzene ring was the factor that determined the method of self assembly.^{30,35} Aoki *et al.*³⁶ reports a method to temporarily protect the carbene against nucleophilic attack by forming an anion adjacent to the carbene. The anion can be a carbanion which affords significant stereoselectivity or a hetero-anion. The anion mitigates the electrophilicity of the carbene complex.

²⁸ Clayden, J., Greeves, N., Warren, S., Wothers, P., *Organic Chemistry*, **2009**, Oxford University Press, Oxford.

²⁹ Dötz, K.A., Fischer, H., Hofmann, P., Kreissl, F.R., Schubert, U., Weiss, K. *Transition Metal Carbene Complexes*, **1983**, Verlag Chemie, Weinheim.

³⁰ Dialer, H., Polborn, K., Beck, W., *J. Organomet. Chem.*, **589**, **1999**, 21

³¹ (a) Baldoli, C., Cerea, P., Falcicola, L., Giannini, C., Licandro, F., Maiorana, S., Mussini, P., Perdiccia, D.J., *J. Organomet. Chem.*, **690**, **2005**, 5777. (b) Hoskovcova, I., Rohacova, J., Meca, L., Tobrman, T., Dvorak, D., Ludvik, J., *Electrochim. Acta*, **50**, **2005**, 4911. (c) Hoskovcova, I., Rohacova, J., Dvorak, D., Tobrman, T., Zalis, S., Zverinova, R., Ludvik, J., *Electrochim. Acta*, **55**, **2010**, 8341. (d) Raubenheimer, H. G., du Toit, A., du Toit, M., An, J., van Niekerk, L., Cronje, S., Esterhuysen, C., Crouch, A. M., *Dalton Trans.*, **2004**, 1173. (e) Hoskovcova, I., Zverinova, R., Rohacova, J., Dvorak, D., Tobrman, T., Zalis, S., Ludvik, J., *Electrochim. Acta*, **56**, **2011**, 6853. (f) Pombeiro, A.J.L, *J. Organomet. Chem.*, **690**, **2005**, 6021.

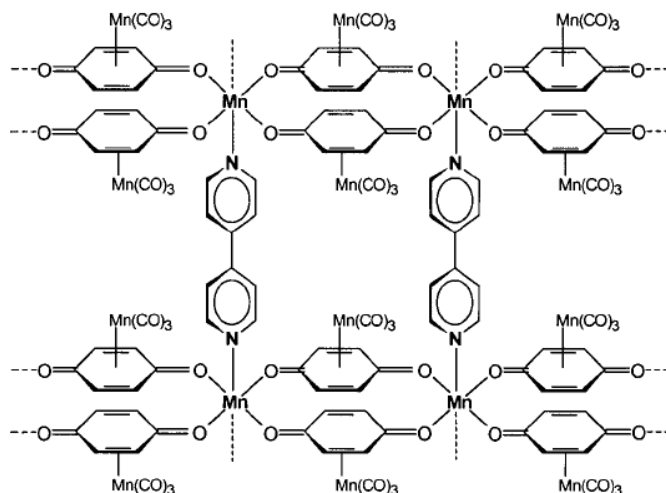
³² Merlic, C.A., You, Y., McInnes, D.M., Zechman, A.L., Miller, M.M., Deng, Q., *Tetrahedron*, **57**, **2001**, 5199

³³ Herndon, J.W., *Coord. Chem. Rev.*, **206**, **2000**, 237

³⁴ Oh, M., Carpenter, G.B., Sweigert, D.A., *Angew. Chem. Int. Ed.*, **41**, (19), **2002**, 3650

³⁵ Bezuidenhout, D.I., van der Westhuizen, B., van Jaarsveld, N.A., Lotz, S., *J. Inorg. Organomet. Polym.*, **24**, **2014**, 39

³⁶ Aoki, S., Fujimura, T., Nakamura, E., *J. Am. Chem. Soc.*, **114**, (8), **1992**, 2985



*This figure has been reproduced from the article itself³⁴
Figure 1.9: Self-assembling manganese complex³⁴

In 1988, Hegedus and D'Andrea³⁷ first posited the notion that group VI metal carbene complexes could undergo photochemistry and generate ketene-like intermediates, reversibly. Hegedus³⁸ (Figure 1.10), Arrieta³⁹ and the Fernandez group⁴⁰ found that molybdenum and chromium Fischer-type carbene complexes are able to form electron-rich, metal-containing ketenes upon visible light irradiation. Upon addition of nucleophiles, these complexes are able to produce numerous products without dimerising the ketenes. Rivero *et al.*⁴¹ discovered that these electron-rich metalloketene type molecules serve as a source of C₂ units for [5+2] and [6+2] cycloaddition reactions.

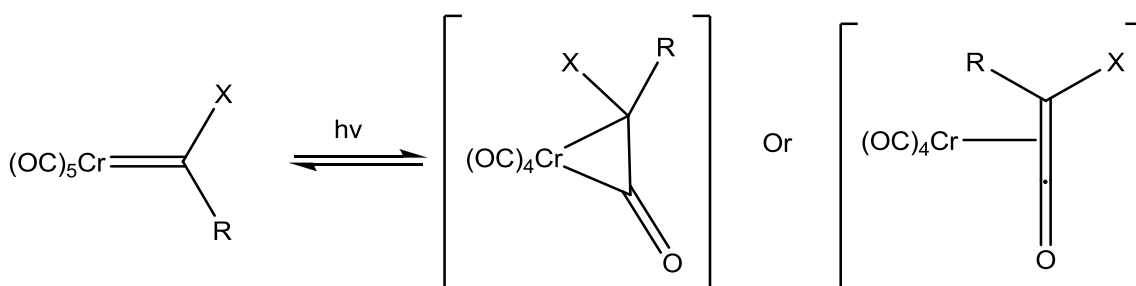


Figure 1.10: Synthesis of electron rich, metal-containing ketenes of chromium³⁸

³⁷ Hegedus, L.S., de Weck, G., D'Andrea, S., *J. Am. Chem. Soc.*, 110, **1988**, 2122

³⁸ Hegedus, L.S., *Tetrahedron*, 53, **1997**, 4105

³⁹ Arrieta, A., Cossío, F.P., Fernández, I., Gómez-Gallego, M., Lecea, B., Mancheño, M.J., Sierra, M.A., *J. Am. Chem. Soc.*, 122, **2000**, 11509

⁴⁰ a) Fernández, I., Sierra, M.A., Gómez-Gallego, M., Mancheño, M.J., Cossío, F.P., *Chem. Eur. J.*, 11, **2005**, 5988.

b) Fernández, I., Sierra, M.A., Mancheño, M.J., Gómez-Gallego, M., Cossío, F.P., *J. Am. Chem. Soc.*, 130, **2008**, 13892. c) Fernández, I., Cossío, F.P., Sierra, M.A., *Acc. Chem. Res.*, 44, **2011**, 479. d) Fernández, I., Sierra, M.A., *Top. Heterocycl. Chem.*, 30, **2012**, 65.

⁴¹ Rivero, A.R., Fernández, I., Sierra, M.A., *Chem. Eur. J.*, 20, **2014**, 1359

Before 2005, the use of group VI metals as catalysts have been neglected.⁴² Gómez-Gallego *et al.*⁴² undertook to rectify this. The possibility of performing transmetallation reactions with complexes of group VI metals were investigated. Fischer *et al.*⁴³ produced an iron carbene complex using a molybdenum carbene complex and pentacarbonyl iron. A transmetallation reaction occurring between chromium alkoxy carbene and tungsten hexacarbonyl has also been reported.⁴⁴ Additionally gold carbene complexes have been produced from tungsten carbene complexes.⁴⁵ There have been reports of trinuclear nickel carbene complexes by Fischer⁴³ and trinuclear platinate complexes by Ashworth⁴⁶ obtained from mononuclear carbene complexes.

Instead of transmetallation, a carbene has been made where one of the substituents on the carbene carbon is an ethoxy group, and the other is ferrocene.⁴⁷

In a review by Wulff *et al.*,⁴⁸ it was stated that there are more than twenty different types of products which can be obtained using phenyl- and alkyl-substituted complexes of chromium, tungsten and molybdenum. N-heterocyclic carbenes have been successfully used as catalysts,⁴⁹ but the method of synthesis of these carbenes is problematic since they are not well understood. These problems are accentuated by the fact that there are limited examples of these carbene complexes in literature, and indeed limited examples of molybdenum carbene complexes in general.

It has been found that cyclohexylamino carbene complexes are easier to oxidise or reduce than their ethoxy analogues. Similarly, DPPE-containing complexes are easier to reduce or oxidise than non-phosphine containing complexes.⁵⁰ Van der Westhuizen *et al.*⁵¹ found that the Cr(0) → Cr(I) electron transfer step is irreversible whereas the Cr(I) → Cr(II) electron transfer step is reversible. It was also found that the Cr(II) species was stabilised by true CH-Cr agostic interactions. This study also revealed that the reduction and oxidation processes occurred at lower potentials for furan complexes than for thiophene complexes.⁵¹

⁴² Gómez-Gallego, Mancheño, M.J., Sierra, M.A., *Acc. Chem. Res.*, 36, **2005**, 44

⁴³ (a) Fischer, E.O., Beck, H.J., *Angew. Chem., Int. Ed.*, 9, **1970**, 72. (b) Fischer, E. O., Beck, H. J., Kreiter, C. G., Lynch, J., Mueller, J., Winkler, E., *Chem. Ber.*, 105, **1972**, 162

⁴⁴ Casey, C.P., Anderson, R.L., *J. Chem. Soc., Chem. Commun.*, **1975**, 895

⁴⁵ Aumann, R., Fischer, E.O., *Chem. Ber.*, 114, **1981**, 1853

⁴⁶ Ashworth, T.W., Berry, M., Howard, J.A.K., Laguna, M., Gordon, F., Stone, A., *J. Chem. Soc., Dalton Trans.*, **1980**, 1615

⁴⁷ López-Cortés, J.G., de la Cruz, L.F.C., Ortega-Alfaro, M.C., Toscano, R.A., Alvarez-Toledano, C., Rudler, H., *J. Organomet. Chem.*, 690, **2005**, 2229

⁴⁸ Wulff, W.D., Tax, B.M., Brandvold, T.A., Chan, K.S., Gilbert, A.M., Hsung, R.P., Mitchell, J., Clardy, J., *Organometallics*, 13, **1994**, 102

⁴⁹ Nolan, S.P., *Heterocyclic carbenes in synthesis*, **2006**. Wiley VCH Verlag Weinheim.

⁵⁰ Landman, M., Liu, R., Fraser, R., van Rooyen, P.H., Conradie, J., *J. Organomet. Chem.*, 752, **2014**, 171

⁵¹ Van der Westhuizen, B., Swarts, P.J., van Jaarsveld, L.M., Liles, D.C., Siegert, U., Swarts, J.C., Fernández, I., Bezuidenhout, D.I., *Inorg. Chem.*, 52, **2013**, 6674

The first stable chiral complexes of molybdenum were synthesised by Barluenga⁵² in 2002 (Figure 1.11). These complexes contained a chiral biphosphite ligand and it was shown that the *fac* isomer can interchange to the *mer* isomer with the application of heat.⁵² Ning *et al.*⁵³ found that by using group VI metals, specifically chromium and molybdenum, with dinitrogen and phosphine ligands, the synthesis of a vinylcarbyne hydride complex whose intermediate is a vinylcarbene could be achieved. Up until 2012, there were two types of catalysts that played a large role in the metathesis catalyst market. The first is the Grubbs catalyst, a ruthenium catalyst that was developed by Grubbs *et al.*⁵⁴ in 1995. The second is a molybdenum catalyst which was developed by Schrock.⁵⁵ Schrock's molybdenum catalyst exhibits exceptional reactivity toward a variety of substrates. The possibility of variations in electronic and steric properties, indicate the versatility and pliability of this molecule to make it 'fit for purpose'. The only disadvantage to molybdenum-containing catalysts is their sensitivity toward oxygen, water and solvent impurities.⁵⁶

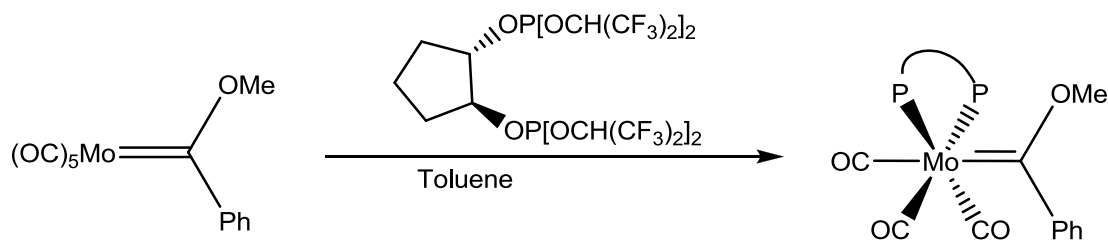


Figure 1.11: Synthesis of the chiral molybdenum complex⁵²

Using bimetallic complexes of molybdenum with multiple thiophene rings as bridging units has been investigated by Landman *et al.*⁵⁷ These have potential uses in polymer science⁵⁸ and for conduction⁵⁹ and superconduction⁶⁰ purposes.

⁵² Barluenga, J., Muniz, K., Tomás, M., Ballesteros, A., Garcia-Granda, S., *Organometallics*, 22, **2003**, 1756

⁵³ Ning, Y., Froese, R.D.J., Margl, P., Lee, E.L., Nguyen, S.T., Peterson, T.H., Wagner, N., Stern, C.L., Sarjeant, A.A., *Organometallics*, 33, **2014**, 1120

⁵⁴ Schwab, P., France, M.B., Ziller, J.W., Grubbs, R.H., *Angew. Chem. Int. Ed. Engl.*, 34, **1995**, 2039

⁵⁵ Schrock, R.R., *Chem. Commun.*, **2005**, 2773

⁵⁶ Kotha, S., Dipak, M.K., *Tetrahedron*, 68, **2012**, 397

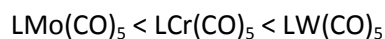
⁵⁷ a) Lotz, S., Crause, C., Olivier, A.J., Liles, D., Görls, H., Landman, M., Bezuidenhout, D.I., *Dalton Trans.*, **2009**, 697; b) Landman, M., Görls, H., Lotz, S., *Z. Anorg. Allg. Chem.*, 628, **2002**, 2037; c) Lotz, S., Landman, M., Görls, H., Crause, C., Nienaber, H., Olivier, A., *Z. Naturforsch., B: Chem. Sci.*, **2007**, 419.

⁵⁸ Musmann, S., Ferraris, J.P., *J. Chem. Soc., Chem. Commun.*, **1993**, 172

⁵⁹ Yui, K., Ishida, H., Aso, Y., Otsubo, T., Ogura, F., Kawamoto, A., Tanaka, J., *Bull. Chem. Soc. Jpn.*, 62, **1989**, 1547

⁶⁰ Kobayashi, O., *Phosphorus, Sulphur Silicon Relat. Elem.*, 43, **1989**, 187

Molybdenum is renowned for having more labile carbonyls than either chromium or tungsten.¹⁸ Fischer⁶¹ posited that, in increasing order, the stability of the group VI pentacarbonyl carbene complexes is the following:



Although this makes it somewhat more difficult to work with in terms of stability and isolating the desired synthetic product for analysis, it also opens many opportunities for ligand substitution.

1.3 Application

There are many applications of carbene complexes, which range from organic synthesis to catalysis and industrial waste management. Schrock, Fischer and N-heterocyclic carbene complexes are typically used for catalytic processes. Catalysts are essential to modern industry and modern life, for several reasons. Almost 90% of goods in industrialised countries are manufactured using catalysts at some point during the manufacturing process. It will be plain why catalysts are so important if one should consider one of the largest role players in the South African economy - SASOL. SASOL's main production output uses catalysts for their Fischer-Tropsch process which elongates carbon chains. Catalysts are so important to them that they are in the process of building a R1bn catalyst manufacturing plant, after which they will be spending R40bn on local projects.⁶² Additionally it is essential to consider that the Fischer-Tropsch method utilises a slurry of reagents in water. The water that is used is taken from the Vaal river and has to be recovered to either use again in the plant or be returned to the river. SASOL uses tonnes of water annually⁶³ and if a catalyst could be embedded in the filters they use as a primary treatment method, secondary treatment may become cheaper. Thus it becomes apparent why these compounds should be studied with a view to benefit industry and the environment.

Carbenes are also used extensively in organic syntheses. The original catalysts used for synthesis were unstable and thus their use was limited.²⁸ Metal carbene complexes are stabilised transition metal complexes which are fit for the purpose of catalysis. Metal carbene complexes are used as catalysts for many reactions including olefin metathesis reactions, carbonyl alkylation, cyclopropanation reactions, C-H insertions and ylide forming reactions,¹⁹ to name a few.

⁶¹ Dötz, K.H., Fischer, H., Hoffmann, P., Kreissl, F.R., Schubert, U., Weiss, K., Transition metal complexes, VCH Verlag Chemie, Weinheim. **1983**.

⁶² Lazenby, H. SASOL unveils new cobalt catalyst plant. Engineering news online, 25 November 2011. [Accessed 13/08/2012] <http://www.engineeringnews.co.za/article/sasol-unveils-new-cobalt-catalyst-plant-2011-11-25>

⁶³ Sasolburg SH&E brief, September 2006. [Accessed 13/08/2012] http://www.sasol.com/sasol_internet/downloads/SH_E_2006_1165306867013.pdf

Using the area of olefin metathesis as an illustrative topic to explain the applications available in so little as one area of industry; the olefin metathesis reaction was discovered 40 years ago at the Philips Petroleum Co.⁶⁴ In their triolefin process, a molybdenum catalyst supported by aluminium was used. This process produced propene from ethene and butene. Propene is used to make polypropylene, acrylonitrile, oxo alcohol and acrylic acid, among others.⁶⁴ In 2004, there was more demand for propene than there was supply of it.⁶⁴ Olefin metathesis has many possibilities in petrochemicals, pharmaceuticals, agrochemicals, fragrance industries and polymer industries.⁶⁴ Metathesis provides a cheaper and easier alternative to obtain a double bond in a complex synthetic structure - as would be found in trying to synthesise natural products.

1.4 This study

There are numerous reasons to study carbene complexes, such as the importance of carbenes to catalysis and the importance of catalysts to the world's economy. In this project Fischer carbene complexes of molybdenum metal were synthesised. Additionally it is important to study these complexes since there is a significant gap in the knowledge surrounding molybdenum carbene complexes, whereas there is a lot of data available for chromium- and tungsten carbene complexes.⁶⁵ This project will serve to bridge the knowledge gap in group VI complexes and provide some comparable complexes and data on molybdenum. In future, periodic trends can be studied using this research.

The investigation of the substitution of carbonyl ligands on molybdenum metal with the view of potential applications in catalysis may be invaluable to the knowledge of the reactivity of the group VI metals, and indeed the catalyst chemistry and data of this group. To conclude, this project has the potential to increase the availability and variety of catalysts available to industry by the potential discovery of an applicable catalyst, thus benefiting industry and the environment (in waste management) and thus the economy of the country as a whole.

⁶⁴ Mol, J.C., *J. Mol. Catal. A: Chem.*, 213, **2004**, 39

⁶⁵ a) Landman, M., Pretorius, R., Buitendach, B.E., van Rooyen, P.H., Conradie, J., *Organometallics*, 32, **2013**, 5491; b) Landman, M., Fraser, R., Pretorius, R., Prinsloo, R., Liles, D.D., van Rooyen, P.H., *Acta Crystallogr. Sect. E: Struct. Rep. Online*, E68, **2012**, m930; Landman, M., Liu, R., Fraser, R., van Rooyen, P.H., Conradie, J., *J. Organomet. Chem.*, 752, **2014**, 171; Landman, M., Pretorius, R., Fraser, R., Buitendach, B.E., Conradie, M.M., van Rooyen, P.H., Conradie, J., *Electrochim. Acta*, 130, **2014**, 104 and references therein.

1.5 Aims of this study

The primary aims of this study are

1. To synthesise and fully characterise the following novel molybdenum carbene complexes
 - Mo Fischer pentacarbonyl carbene complexes with ethoxy and furyl substituents
 - Mo Fischer tetracarbonyl monophosphine carbene complexes with ethoxy and furyl substituents
 - Mo Fischer tricarbonyl diphosphine carbene complexes with ethoxy and furyl substituents
 - Amino and cyclohexylamine analogues of the abovementioned Fischer carbene complexes
 - Cr and W analogues which had been neglected by our labs to date, were synthesised for comparison and to complete the series

The secondary aims are:

1. To study the substitution of the carbonyl ligands around a molybdenum metal atom and how this affects the complexes' reactivity.
2. To model theoretically the physical data and behaviour of the synthesised complexes to provide comparison mutually as well as with analogous group VI complexes; to evaluate the effect, if any, that ligand substitution and carbene substituent exchange of Fischer carbene complexes of molybdenum may have on the frontier orbital distribution of these complexes to enhance reactivity in the metathesis reaction.

Future prospects:

1. Use the theoretical studies to assist in predicting catalytic activity of the group VI compounds.
2. To study the electrochemical behaviour of the synthesised complexes to provide information regarding how electrons move within the molecule; how reduction and oxidation affect the molecular orbitals of the complex; and lastly whether these changes are reversible or not.

Chapter 2:

Ethoxy Carbene Complexes

[Science is] an imaginative adventure of the mind seeking truth in a world of mystery.

– Sir Cyril Herman Hinshelwood (1897-1967)

Nobel Prize 1956

2.1 Introduction

Phosphine as a ligand

The synthesis and purification of monophosphinated Fischer carbene complexes with various ligands and metals have been described in literature.¹ Between 1966 and 1969, modification of the ligand sphere of a carbonyl carbene complex using a phosphine moiety was first studied and reported.^{1a,2,3} These new complexes were more stable in air than the carbonyl carbene complexes.^{1a} There are two mechanisms that are generally followed by phosphines in order to substitute a carbonyl. The first mechanism is a dissociative process, Figure 2.1a,⁴ where the carbonyl first dissociates and then the phosphine coordinates; this mechanism is followed by phosphines such as triphenylphosphine which is minimally nucleophilic.⁴ The second mechanism is an associative process, Figure 2.1b,⁴ and substitutes the carbene itself through an ylide intermediate.⁴ The properties of phosphines can be vastly different depending on their substituents. This can lead to differences in electronic⁵ as well as steric⁶ properties.

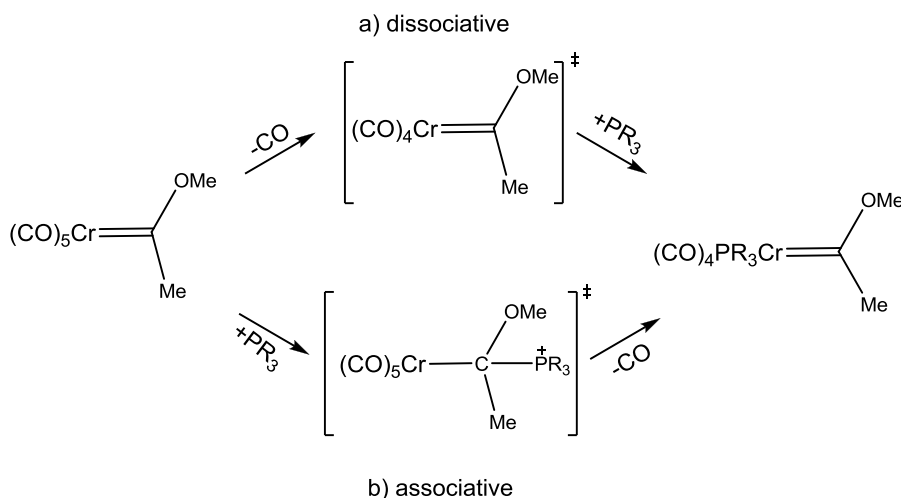


Figure 2.1: Mechanisms whereby phosphines can substitute carbonyls a) dissociative, b) associative⁴

Most of the monophosphinated Fischer carbene complexes that can be found in literature are *cis* structures, with the *trans* isomer being simply too unstable to isolate, characterize and/or crystallize.

¹ a) Fischer, E. O.; Aumann, R. *Chem. Ber.*, **102**, **1969**, 1495, b) Elowe, P.R.; West, N. M.; Labinger, J. A.; Bercaw, J. E. *Organometallics*, **28**, **2009**, 6218, c) Stumpf, R.; Jaeger, M.; Fischer, H. *Organometallics*, **20**, **2001**, 4040, d) Dötz, K. H.; Larbig, H.; Harms, K. *Chem. Ber.* **125**, **1992**, 2143, e) Caputo, C.A.; Jennings, M.C.; Tuononen, H. M.; Jones, N. D. *Organometallics*, **28**, **2009**, 990, f) Weberndörfer, B.; Werner, H. *J. Chem. Soc., Dalton Trans.*, **2002**, 1479, g) Jahr, H. C.; Nieger, M.; Dötz, K. H. *Chem. Eur. J.* **11**, **2005**, 5333

² Mills, O.S.; Redhouse, A.D., *Chem. Commun.*, **22**, **1966**, 814

³ Werner, H.; Rascher, H., *Inorg. Chim. Acta*, **2**, **1968**, 181

⁴ Arndtsen, B.A.; Schoch, T.K.; McElwee-White, L., *J. Am. Chem. Soc.*, **114**, **1992**, 7041

⁵ Crotti, C.; Farnetti, E.; Celestino, T.; Stener, M.; Fontana, S., *Organometallics*, **23**, **2004**, 5219

⁶ Brown, T.L.; Lee, K.J., *Coord. Chem. Rev.*, **128**, **1993**, 89

In 1968 Fischer and Aumann synthesised monophosphinated carbene complexes of molybdenum, chromium and tungsten although no crystal structures were obtained.^{1a} Similar complexes to these, with different carbene moieties, were made by Stumpf *et al.*^{1c} on tungsten (Figure 2.2). The molybdenum analogues were made by Dötz *et al.*^{1d} Elowe, West, Labinger and Bercaw^{1b} synthesised diphosphinated complexes of rhenium and manganese. Although the phosphines are *trans* to each other in these complexes, they are all *cis* to the carbene. These complexes however, are not M(0) complexes.

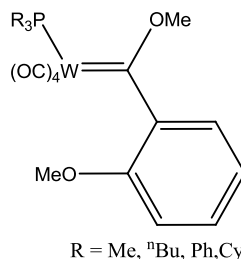


Figure 2.2: Complexes made by Stumpf *et al.*^{1c}

In general, phosphine complexes which have been synthesised are abundant and as diverse as they are interesting. Mills and Redhouse² were the first to characterise *cis*-methylmethoxycarbene-triphenylphosphinetetracarbonylchromium. Fernández *et al.*⁷ synthesised phosphine complexes where the phosphine moiety was a substituent of the carbene carbon. Phosphine-containing alkoxy and amino carbene complexes that were imbedded in a polymer by the phosphine ligand, were investigated by Maiorana *et al.*⁸ Klapdohr⁹ synthesised amino carbene complexes rooted in a silica matrix by their phosphine ligands. By using chiral phosphines the stereoselectivity of a complex can be altered, which means isomerically different organic molecules can be produced by simply altering the phosphine moiety.¹⁰ Phosphite ligands have been used to introduce chirality into a complex.¹¹ Arrieta *et al.*¹² has used chiral phosphine complexes to study photocarbonylation reactions. Alteration of the carbene complexes ligand sphere using phosphine, and indeed diphosphine

⁷ Fernández, I., Sierra, M.A., Gómez-Gallego, M., Mancheño, M.J., *Angew.Chem.*, 118, **2005**, 131

⁸ Maiorana, S., Seneci, P., Rossi, T., Baldoli, C., Ciraco, M., de Magistris, E., Licandro, E., Papagni, A., Provera, S., *Tetrahedron Lett.*, 40, **1999**, 3635

⁹ Klapdohr, S., Dötz, K.H., Assenmacher, W., Hoffbauer, W., Hüsing, N., Nieger, M., Pfeiffer, J., Popall, M., Schubert, U., Trimmel, G., *Chem. Eur. J.*, 6, **2000**, 3006

¹⁰ Cooke, M.D., Fischer, E.O., *J. Organomet. Chem.*, 56, **1973**, 279

¹¹ Barluenga, J., Muniz, K., Tomas, M., Ballesteros, A., Garcia-Granda, S., *Organometallics*, 22, **2003**, 1756

¹² Arrieta, A., Cossío, F.P., Fernández, I., Gómez-Gallego, M., Lecea, B., Mancheño, M.J., Sierra, M.A., *J. Am. Chem. Soc.*, 122, **2000**, 11509

ligands,¹³ has been a minimally explored area of research. Heteroaryl phosphine carbene complexes have been explored in our labs¹⁴ and the study of them, here, is an extension of that work.

It has been said that the properties of the singlet carbenes can be likened to phosphorous(III) complexes in terms of their reactivity and stability.¹⁵ Although their binding differs, they are similar in their innocence during reactions.¹⁵ For example the reactivity of the Grubbs catalyst was greatly enhanced by the substitution of a phosphine ligand for an NHC ligand. As a result of this, the popularity of research into NHCs increased, but phosphine research has not been abandoned as of yet.¹⁵ Phosphorous-containing ligands are widely available. There is a great amount of diversity among them and they are extensively described in literature.¹⁵ Compared to this, less is known about NHCs and hence the phosphorous-containing ligands continue to be used for ligand design and synthesis.¹⁵

There has been a resurgence of interest in the production of oil from synthesis gas (syngas) and from coal.¹⁶ In general, this is achieved using the Fischer-Tropsch process where the production of methane is undesirable.¹⁶ Elowe *et al.*^{1b} proposed a manganese triphenylphosphine complex to act as an intermediate catalyst; They showed that their catalyst, when stabilised by electron-deficient boranes, is effective in producing methyl acetate - a C₂ compound - which can be used as one of the feedstocks of the Fischer-Tropsch process.^{1b}

Phosphine chemistry even extends to the area of N-heterocyclic phosphonium (NHP) complexes. Caputo *et al.*^{1e} studied the differences between NHP complexes and NHC complexes (Figure 2.3). It was found that the bonding characteristic between the metal and the phosphorous was dominated by the π -contribution from the metal into the phosphorous d-orbitals. On the other hand, the bonding characteristic between the metal and the carbon (in the NHC) was found to be dominated by the σ -contribution. Both can be saturated or unsaturated. NHPs are weak σ -donors and strong π -acceptors, and NHCs are the opposite on both counts.¹⁷ The first NHP was studied by Parry¹⁸ in 1978, and it has sparked a bit of interest. Nakazawa studied NHPs of chromium and tungsten,^{19,20}

¹³ Reinheimer, E.W., Kantardjieff, K.A., Herron, S.R., Tisserat, C.G., Casalnuovo, J.A., *J. Chem. Crystallogr.*, **33**, **2003**, 503

¹⁴ Landman, M., Pretorius, R., Fraser, R., Buitendach, B.E., Conradie, M.M., van Rooyen, P.H., Conradie, J., *Electrochim. Acta*, **130**, **2014**, 104

¹⁵ Fey, N., Haddow, M.F., Harvey, J.N., McMullin, C.L., Orpen, A.G., *Dalton Trans.*, **2009**, 8183

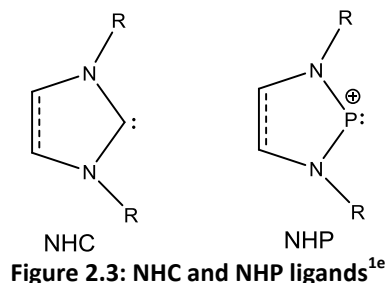
¹⁶ Henrici-Olivé, G., Olivé, S., *The Chemistry of the Catalyzed Hydrogenation of Carbon Monoxide*; Springer-Verlag: New York, **1984**.

¹⁷ Tuononen, H. M., Roesler, R., Dutton, J. L., Ragona, P. J., *Inorg. Chem.*, **46**, **2007**, 10693

¹⁸ Montemayor, R. G., Sauer, D. T., Fleming, S., Bennett, D. W., Thomas, M. G., Parry, R. W., *J. Am. Chem. Soc.*, **100**, **1978**, 2231

¹⁹ Nakazawa, H., Yamaguchi, Y., Miyoshi, K., *J. Organomet. Chem.*, **465**, **1994**, 193

molybdenum,^{21,22} iron²³ and ruthenium.²⁴ An NHP version of the Wilkinson catalyst was made by Richeson and co-workers²⁵ and Baker and co-workers.²⁶



The carbonyl ligands and the trans effect

The triphenylphosphine- and the 1,2-bis(diphenylphosphino)ethane (DPPE) ligands both have σ -donor, π -acceptor character weaker than that of a carbonyl ligand. A prediction can thus be made that the carbonyl *trans* to one of these groups will have a lower frequency in the IR spectrum²⁸ as a result of the increase in the M-CO bond order and a decrease in the C=O bond order.^{28,27} The π -acceptor character results from back-bonding into the d-orbitals of the phosphorus.²⁸ Modification of the carbene complex can be achieved without changing the untargeted groups significantly. Phosphine-substituted carbene complexes will thus still allow for the classical Fischer ligand sphere.

If one were to look at the carbonyl region of the IR spectra, many deductions can be made regarding the structure of the complex. The carbonyl ligand is characteristic to a Fischer carbene complex. It is a good σ -donor, π -acceptor ligand and coordinates to the metal centre by donating an electron pair in a σ -fashion to the metal. Extra electron density is back-donated into the empty anti-bonding orbitals of the carbonyl ligand.²⁸ The highest occupied molecular orbital (HOMO) in this ligand is carbon-centred, designated the $3\sigma^*$ orbital, while the lowest unoccupied molecular orbital (LUMO), designated $2\pi^*$, is degenerate with ideal symmetry for acceptance of electron density from the metal.²⁸

²⁰ Yamaguchi, Y., Nakazawa, H., Itoh, T., Miyoshi, K., *Bull. Chem. Soc. Jpn.*, **69**, **1996**, 983

²¹ Gudat, D., Haghverdi, A., Nieger, M., *J. Organomet. Chem.*, **383**, **2001**, 617

²² Nakazawa, H., Miyoshi, Y., Katayama, T., Mizuta, T., Miyoshi, K., Tsuchida, N., Ono, A., Takano, K., *Organometallics*, **25**, **2006**, 5913

²³ Nakazawa, H., Kishishita, M., Nakamoto, T., Nakamura, N., Ishiyama, T., Miyoshi, K., *Chem. Lett.*, **2000**, 230

²⁴ Kawamura, K., Nakazawa, H., Miyoshi, K., *Organometallics*, **18**, **1999**, 4785

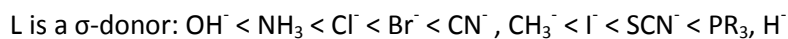
²⁵ Spinney, H. A., Yap, G. P. A., Korobkov, I., DiLabio, G., Richeson, D. S., *Organometallics*, **25**, **2006**, 3541

²⁶ Abrams, M. B., Scott, B. L., Baker, R. T., *Organometallics*, **19**, **2000**, 4944

²⁷ Cotton, F.A., *Inorg. Chem.*, **3**, (5), **1964**, 703

²⁸ Salzer, A., Elschenbroich, C. H., *Organometallics: A Concise Intro.*, Second Ed., **1992**, 210

The *trans* effect states that “a strong σ -donor ligand or π -acceptor ligand greatly accelerates substitution of a ligand that lies in the *trans* position”.²⁹ This means that the ligand *trans* to the stronger σ -donor, π -acceptor ligand will be preferentially substituted. The *trans* effect follows the order:²⁹



In a Fischer carbene complex, substitution *trans* to a carbonyl ligand is therefore predicted instead of *trans* to the carbene ligand. The *trans* effect arises as a result of two other factors - the *trans* influence and the transition state effect.

The *trans* influence is the extent to which the π -acceptor *trans* to the carbonyl ligand influences the back-bonding to the carbonyl group in the ground state.²⁹ The *trans* influence is experienced by the carbonyl ligand whereas in the systems under study a ligand such as a phosphine ligand will exhibit a *trans* influence.²⁹ The net result is a stronger M-C bond and a weaker C \equiv O interaction which will affect the stretching frequencies observed in the infrared spectra of the complexes under study here. The stretching frequencies will decrease in frequency as the M-C bond increases in strength.²⁸

The transition state effect is considered to be the result of the increased electron density on the metal as a result of an incoming ligand.²⁹ Any other ligand on the metal which can accept this increased electron density will stabilise the transition state of the complex.²⁹

Focus of this study

Molybdenum is a group VI transition metal and is the central metal in the series (Cr, Mo, W). In this study hexacarbonyl molybdenum is reacted with monolithiated furan to form an alkoxy pentacarbonyl Fischer carbene complex, after alkylation. The pentacarbonyl carbene complex will then be substituted by triphenylphosphine (PPh₃) to form the corresponding tetracarbonyl carbene complexes. Reaction of the ethoxy pentacarbonyl Fischer carbene complex with DPPE will yield the corresponding tricarbonyl carbene complex. The metal will remain in the zero oxidation state throughout.

There has been extensive work done on tungsten and chromium carbene complexes, in terms of properties and effects of changing the ligand sphere on the pentacarbonyl coordination compounds

²⁹ Atkins, P., Overton, T., Rourke, J., Weller, M., Armstrong F., Shriver and Atkins Inorganic Chemistry, Fourth Edition, Oxford University Press, **2006**

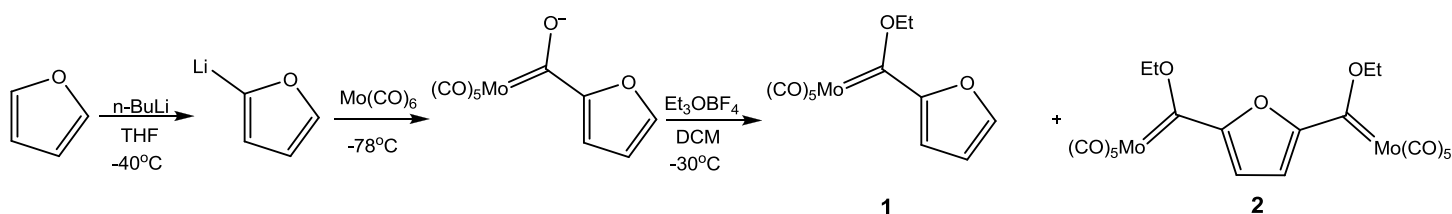
as well as in Schrock, NHC and phosphorus compounds.³⁰ Very little literature exists for molybdenum complexes and this study aims to address some of these limitations. The synthesis, characterisation data and theoretical properties of eight novel complexes (**1-8**) will be presented in this chapter. Crystal structures of five of these complexes (**1-3**, **5** and **8**) will be discussed.

Known complexes (**A-R**) obtained from literature will be utilised for comparison with the novel complexes. The references for these literature complexes can be found where the data is first presented for that particular complex.

2.2 Molybdenum pentacarbonyl ethoxy carbene complexes

The complexes that will be discussed here are the $[\text{Mo}(\text{CO})_5\text{C}\{(\text{OEt})(\text{C}_4\text{H}_3\text{O})\}]$ (**1**) as well as the $1,3\text{-}[\text{Mo}(\text{CO})_5\text{C}\{(\text{OEt})\}]_2\text{C}_4\text{H}_3\text{O}$ (**2**).

For the synthesis of **1**, the following reaction scheme was followed:



Scheme 2.1: The synthetic route to obtain **1** and **2**

Complex **1** is synthesised using classic Fischer methodology.³¹ Furan is monolithiated in THF, which results in a solution that is pale yellow in colour. Metallation using hexacarbonyl molybdenum followed, which yields a red solution. This red solution is alkylated in dichloromethane using triethyloxonium tetrafluoroborate to yield **1** with 40 % yield. The lithiation step can result in a dilithiated furan which results in the formation of the by-product, **2**. Complex **2** is synthesised with 0.6 % yield.

Conformations which are conceivably possible for **1** in the solid state are shown in Figure 2.4 below.

³⁰ a) Ardon, M., Hogarth, G., Oscroft, D.T.W., *J. Organomet. Chem.*, 689, **2004**, 2429; b) Gómez-Gallego, M., Mancheño, M.J., Sierra, M.A., *Acc. Chem. Res.*, 38, **2005**, 44; c) Connor, J.A., Jones, E.M., Randall, E.W., *J.C.S. Dalton*, **1972**, 2419; d) Pariya, C., Theopold, K.H., *Curr. Sci.*, 78, (11), **2000**, 1345 and references therein

³¹ Fischer, E.O., Maasböl, A., *Angew. Chem. Int. Ed. Engl.* 3, **1964**, 645

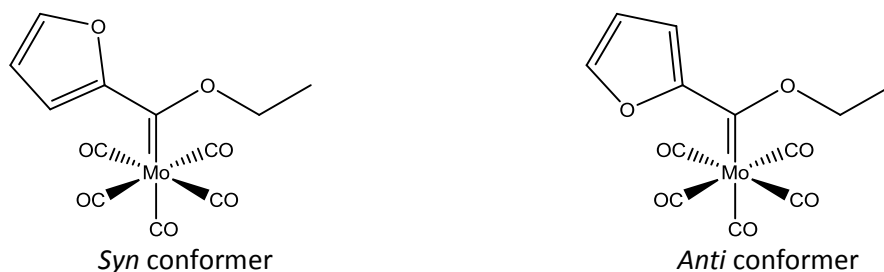


Figure 2.4: The possible conformations of **1** in the solid state

It was found that only one conformer was isolated in the solid state, namely the *anti*-conformer (Figure 2.13). Literature shows that most frequently the *anti*-conformer is the conformer that is characterised.^{32,33,34}

The biscarbene complex is formed as a side-product of the reaction used to synthesise **1**. Different conformations are possible in the case of **2**, depending on the rotation around the carbene-furyl bonds. The conformers which could possibly be formed in this reaction are shown in Figure 2.5 below. The most predominant conformer found in solid state in literature is the *syn, syn* conformer.^{35,36}

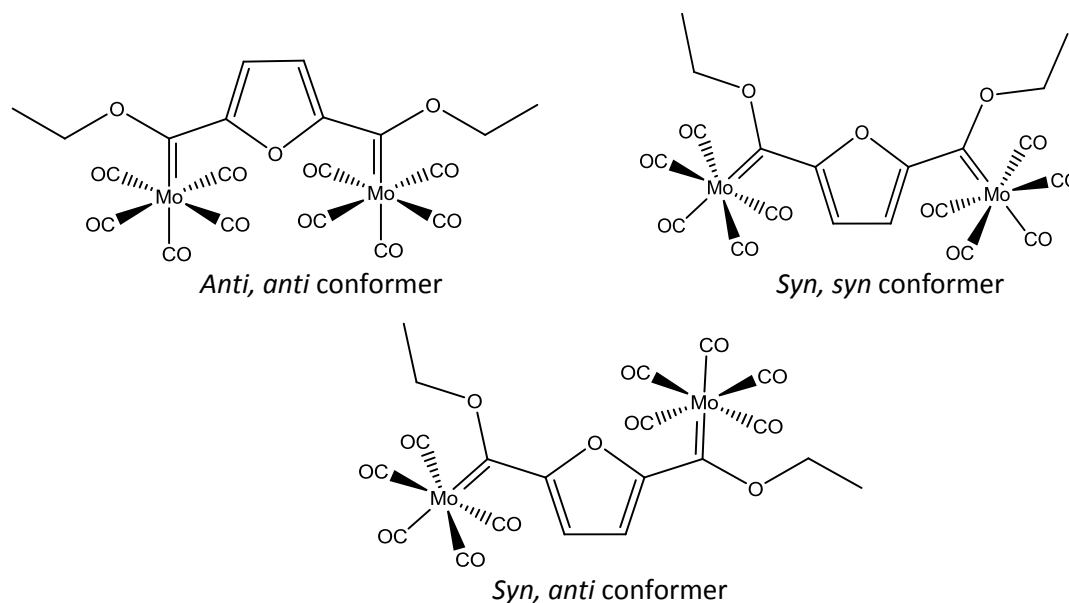


Figure 2.5: The conceivable conformations of **2**

³² Thompson, S., Wessels, H.R., Fraser, R., van Rooyen, P.H., Liles, D.C., Landman, M., *J. Mol. Struct.*, 1060, **2014**, 111

³³ Landman, M., Lui, R., van Rooyen, P.H., Conradie, J., *Electrochim. Acta*, 114, **2013**, 205

³⁴ Connor, J.A., Jones, E.M. *J. Am. Chem. Soc.(A)*, **1971**, 1974

³⁵ Terblans, Y.M., Roos, H.M., Lotz, S., *J. Organomet. Chem.*, 566, **1998**, 133

³⁶ Lotz, S., van Jaarsveld, N.A., Liles, D.C., Crause, C., Görls, H., Terblans, Y.M., *Organometallics*, 31, **2012**, 5371

2.2.1 Infrared spectroscopy

The carbonyl region ($1500\text{--}2200\text{ cm}^{-1}$) of the IR spectrum is characteristic and relatively easy to analyse. The characteristic peaks that are observed have their basis in the symmetry of the molecule being observed.³⁷ This implies that they allude to the bonding of the molecule, as well as the symmetry and geometry of the molecule. The peaks are sharp, well defined and sensitive to the environment in which they are found.³⁷ The carbonyls themselves interact strongly with one another, adding to the resolution of the carbonyl region of the spectrum.³⁷

A great deal of mathematics governs the prediction of the patterns that arise in the carbonyl region of IR spectra. A summary of the conclusions of this mathematics will be given here.

Each of the metals in **1** and **2** are of the type $M(\text{CO})_5\text{L}$ - the carbene moiety is treated as one generic ligand. Although the type of substituents on the carbene ligand can change, this does not change the symmetry around the metal; the nature of the substituent does, however, influence the carbonyl frequencies. The symmetry associated with an octahedral molecule of type $M(\text{CO})_5\text{L}$ is C_{4v} . Since the ligand takes up one position of the octahedron, the remaining carbonyls are in a square pyramidal geometry. This geometry gives rise to the four IR active bands resulting from the stretches shown in Figure 2.6:³⁷

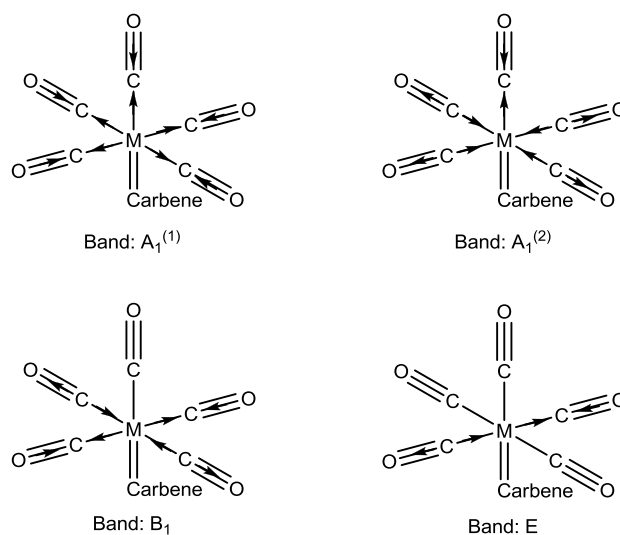


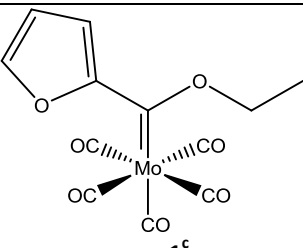
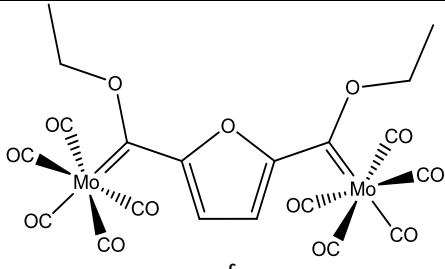
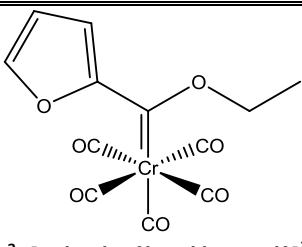
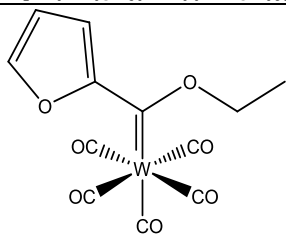
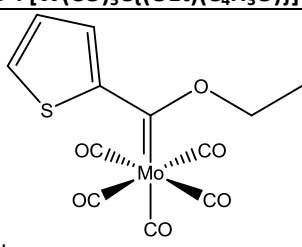
Figure 2.6: Illustration of the origin of the IR stretching frequencies observed for C_{4v} symmetry

The band found at the highest frequency should be the $A_1^{(1)}$, this should also be the weakest band - in some cases too weak to be observed.³⁷ It is characterised by a symmetric compression of all of the carbonyls (i.e. from the point of origin toward the metal centre). The frequency order of the $A_1^{(2)}$ and the E bands depends on the identity of the complexes involved.³⁷ The E band will have the strongest

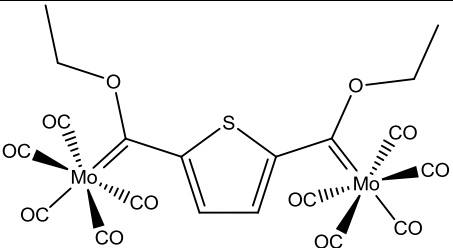
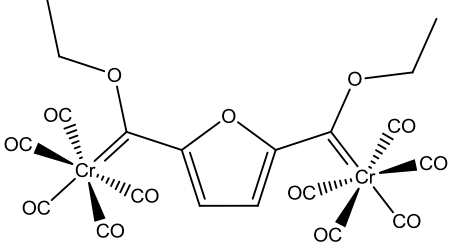
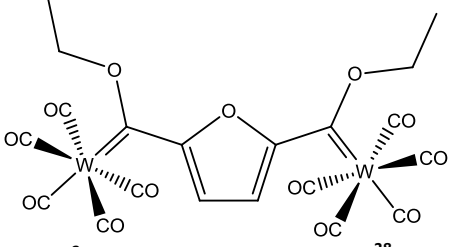
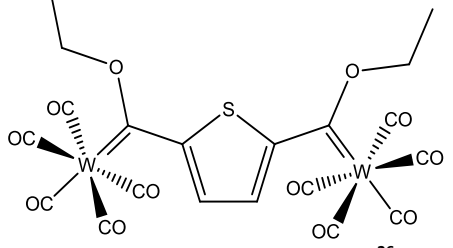
³⁷ Braterman, P.S., *Metal Carbonyl Spectra*, Academic Press, 1975

intensity in the carbonyl region.³⁷ The $A_1^{(2)}$ band is characterised by symmetric stretching (i.e. from the point of origin away from the metal centre), while the E band is characterised by the stretching of one carbonyl and compression of another. Lastly, the B_1 band is characterised by stretching of two carbonyls and compression of another two.

Table 2.1: IR Frequency assignments for 1 and 2, including literature values

Complexes	Carbonyl Stretching frequency (cm^{-1})			
	$A_1^{(1)}$	B_1	E	$A_1^{(2)}$
 1^c	2068 (m)	1988 (m)	1923 (vs)	1942 (s)
 2^c	2062 (m)	1999 (w)	1919 (vs)	1947(s)
 $A^a: [\text{Cr}(\text{CO})_5\text{C}\{(\text{OEt})(\text{C}_4\text{H}_3\text{O})\}]^{38}$	2061 (s)	1990 (w)	1946 (s)	1960(vs)
 $B^a: [\text{W}(\text{CO})_5\text{C}\{(\text{OEt})(\text{C}_4\text{H}_3\text{O})\}]^{38}$	2069 (s)	1986 (w)	1943 (s)	1956 (vs)
 $C^b: [\text{Mo}(\text{CO})_5\text{C}\{(\text{OEt})(\text{C}_4\text{H}_3\text{S})\}]^{39}$	2066 (m)	1983 (vw)	1942 (vs)	1942 (vs)

³⁸ Crause, C., Görls, H., Lotz, S., *Dalton Trans.*, **2005**, 1649

Complexes	Carbonyl Stretching frequency (cm ⁻¹)			
	A ₁ ⁽¹⁾	B ₁	E	A ₁ ⁽²⁾
 D^b: [Mo(CO)₅C{(OEt)}]₂(C₄H₃S)³⁹	2064 (m)	1985 (vw)	1943 (vs)	1943 (vs)
 E^a: [Cr(CO)₅C{(OEt)}]₂(C₄H₃O)³⁸	2054 (s)	1995 (w)	1955 (s)	1962 (vs)
 F^a: [W(CO)₅C{(OEt)}]₂(C₄H₃O)³⁸	2062 (s)	1990 (w)	1950 (s)	1957 (vs)
 G^a: [W(CO)₅C{(OEt)}]₂(C₄H₃S)³⁶	2062 (m)	1986 (w)	1960 (s)	1951 (vs)

Media: ^aHexane, ^bDCM, ^cKBr Pellet

Dötz found that the IR data for **H**: [Mo(CO)₅C{(OMe)(C₄H₃O)}]⁴⁰ was 2070 cm⁻¹, 1951 cm⁻¹ and 1966 cm⁻¹ when measured in a hexane solution. He also found the data for **I**: [Mo(CO)₅C{(OMe)(C₄H₃S)}]⁴⁰ was 2069 cm⁻¹, 1952 cm⁻¹ and 1961 cm⁻¹ when measured in a hexane solution.

The local symmetry of **1** is C_{4v}²⁸ and the four expected active IR-bands were observed. It can be seen from the data presented in Table 2.1 that the E vibration (which corresponds to an asymmetric stretch in the plane of four of the carbonyls²⁸) is the strongest band and the possibility arises for the E and A₁⁽²⁾ band to overlap.³⁸ The A band may also appear as a shoulder on the more intense E band, as seen in Figure 2.7a. The carbene ligand is a good π-acceptor ligand,³¹ which means that the A₁⁽²⁾

³⁹ Landman, M., Görls, H., Lotz, S., *Z. Inorg. Allg. Chem.*, 628, **2002**, 2037

⁴⁰ Dötz, K.H.; Larbig, H., *J. Organomet. Chem.*, 433, **1992**, 115

band may be found at higher wave numbers than the E band.³⁸ This was witnessed in this study, as shown by the data in Table 2.1. It can also be seen from the data in Table 2.1 that there is good correlation with literature^{38,39,40} values upon comparison of the $A_1^{(1)}$ and B_1 bands. The literature values found for similar molybdenum carbene complexes are comparable.³⁹ The data in Table 2.1 shows that neither a change in the metal nor a change in the carbene substituent affects the trend observed in the data.

Complex **2** has the same symmetry around each metal as **1**. This symmetry is C_{4v} and therefore the same number of stretching bands as well as the types of active modes will be expected (Figure 2.6).

Upon comparison of the IR stretching frequencies obtained for **1** and **2**, it can be seen that both of the A_1 bands lie at similar frequencies but the E and B_1 bands differ slightly. The intensity of the bands is similar as well. As shown in the data in Table 2.1, literature^{35,36,38,40} correlates well with observed trends. Literature values for similar biscarbene complexes, **G**³⁶ and **J**: $[Cr(CO)_5C\{(OEt)\}]_2(C_4H_3S)$ (2054 cm^{-1} , 1987 cm^{-1} , 1953 cm^{-1} , 1964 cm^{-1})³⁵ compare well.

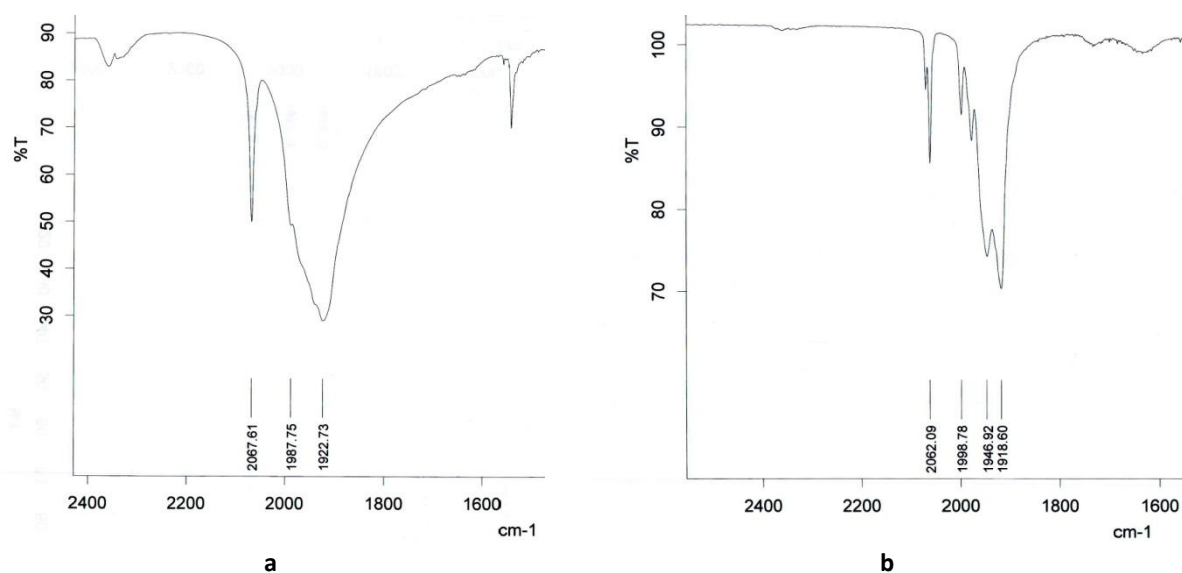


Figure 2.7: Carbonyl Region of the Experimental IR Spectra of a) **1** (KBr) and b) **2** (KBr)

Figure 2.7 shows the carbonyl regions of **1** and **2**. These show excellent correlation with theoretical expectations as laid out by Braterman³⁷ and discussed above. It will be seen in section 2.3.2 that two conformers can be seen in the 1H NMR spectrum of **2**. This indicates that the IR spectrum was recorded on a mixture of conformers which can explain the additional peaks observed in the IR spectrum of **2**.

2.2.2 ¹H NMR spectroscopy

The ¹H NMR data of **1** and **2** are summarised in Table 2.2, below. The following numbering system is imposed upon all complexes, both novel and known, presented in the table.

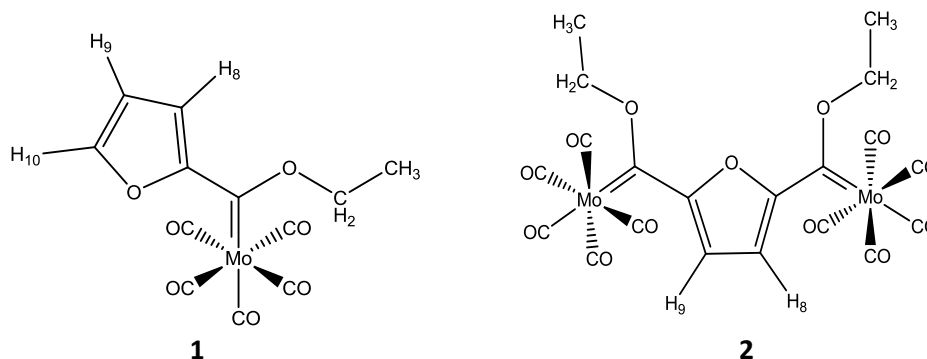


Table 2.2: ¹H NMR assignments for **1** and **2**, including literature values

Complexes	Chemical Shift (δ , ppm), Multiplicity and coupling Constants (J, Hz)				
	H ₁₀	H ₉	H ₈	CH ₂	CH ₃
1 ^a	7.83 dd J = 0.8, 1.7	6.58 dd J = 1.7, 3.7	7.09 dd J = 0.8, 3.6	5.03 q J = 7.1	1.62 t J = 7.2
2a ^a		6.91 s	6.91 s	4.13 q J = 6.9	1.45 t J = 7.1
2b ^a		7.06 d J = 3.9	7.00 d J = 3.9	4.13 q J = 6.9	1.45 t J = 7.1
H ^a : [Mo(CO) ₅ C{(OMe)(C ₄ H ₃ O)}] ⁴⁰	7.86 dd J = 0.6, 1.8	6.61 dd J = 1.8, 3.7	7.11 dd J = 0.6, 3.7		4.72 s
A ^a : [Cr(CO) ₅ C{(OEt)(C ₄ H ₃ O)}] ³⁸	7.82 dd J = 0.8, 1.6	6.56 dd J = 1.6, 3.6	6.96 dd J = 0.8, 3.6	5.13 q J = 7.0	1.63 t J = 7.0
B ^a : [W(CO) ₅ C{(OEt)(C ₄ H ₃ O)}] ³⁸	7.86 dd J = 0.8, 1.6	6.60 dd J = 1.6, 3.6	7.13 dd J = 0.8, 3.6	4.94 q J = 7.0	1.61 t J = 7.0
K ^a : [W(CO) ₅ C{(OEt)(C ₄ H ₃ S)}] ³⁶	8.14 d J = 4.2	7.20 d J = 4.1	7.80 d J = 4.1	4.99 q J = 7.0	1.66 t J = 7.05
L ^b : [Cr(CO) ₅ C{(OEt)(C ₄ H ₃ S)}] ³²	8.24 d J = 4.2	7.20 dd J = 4.2	7.67 d J = 4.6	5.16 q J = 7.0	1.65 t J = 7.0
E ^a : [Cr(CO) ₅ C{(OEt)} ₂ (C ₄ H ₃ O)] ³⁸		7.22 s	7.22 s	5.22 q J = 7.0	1.72 t J = 7.0
F ^a : [W(CO) ₅ C{(OEt)} ₂ (C ₄ H ₃ O)] ³⁸		7.29 s	7.29 s	4.97 q J = 7.0	1.70 t J = 7.0
G ^a : [W(CO) ₅ C{(OEt)} ₂ (C ₄ H ₃ S)] ³⁶		7.97 s	7.97 s	5.00 q J = 7.0	1.70 t J = 7.1

^aSolvent: CDCl₃ (7.24 ppm)

^bSolvent: (CD₃)₂CO (2.09 ppm)

The conformational forms of **2** as referred to above, are shown in Figure 2.8.

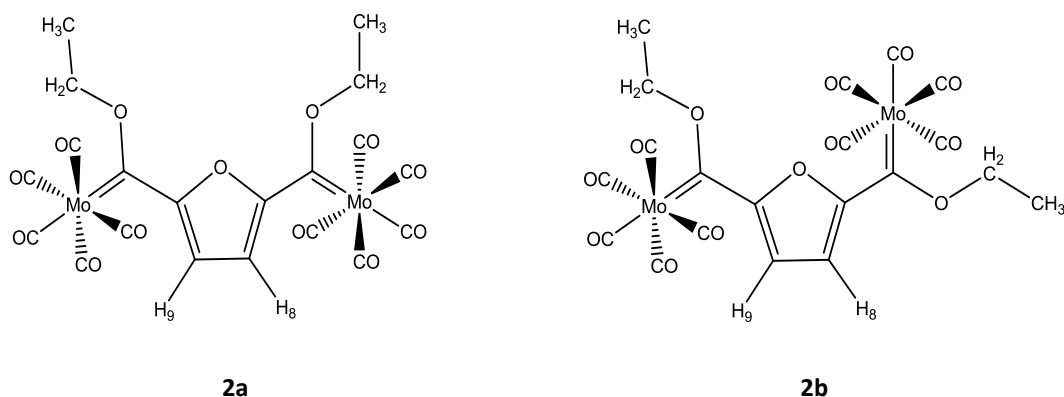


Figure 2.8: The conformational forms of **2**

The data in Table 2.2 shows that the resonance peaks of the CH₃ group on the ethoxy of **1** was shifted the furthest upfield and it was found to be a triplet, indicating that it has two equivalent neighbouring protons. Go through and rewrite all the NMRs to make sure you have the same format as the above sentence. To confirm this, it was found that it shared a coupling constant of 7.2 Hz with the adjacent CH₂ group (which showed a quartet of peaks, indicating three equivalent neighbouring protons). No further coupling was observed.

The protons on the furyl ring all showed double doublet peak patterns. This was expected for H₉, since H₉ has two non-equivalent neighbouring hydrogens; but not for H₈ and H₁₀, since they each only have one non-equivalent neighbouring proton. The appearance of double doublets for H₈ and H₁₀ can be explained by long range coupling through the π-system, and it can be seen that H₈ and H₁₀ are indeed coupled to one another with a characteristically small coupling constant of 0.8 Hz. H₉ is coupled to H₁₀ with a coupling constant of 1.7 Hz and to H₈ with a coupling constant of 3.6 Hz. The discrepancy between these two coupling constants is due to the presence of a heteroatom adjacent to H₁₀ but no heteroatom adjacent to H₈. The existence of the heteroatom, and its proximity decreases the coupling constant between H₉ and H₁₀.

The chemical shift of H₈ is affected by the proximity of the oxygen in the furyl group as well as the carbene moiety. Comparison with literature^{38,40} data in Table 2.2, excellent correlation is found with the values obtained.

Although the correlation is excellent, it is interesting to note that the ppm values of the chemical shifts between chromium, molybdenum and tungsten analogues for the heteroarene substituent increase in order of their positions in group VI; that is Cr < Mo < W. For the ethoxy moiety, this order is reversed: W < Mo < Cr.

The NMR analysis of **2** indicates that two different conformers were observed for this complex. In one conformer the metal moieties are orientated in the same direction on the furyl ring (**2a**) and an alternative 'conformer' is that they could be orientated in opposite directions (as depicted in Table 2.2 structure **2b**). This conformational shift will alter the symmetry of the molecule; as a result, the protons around each carbene will not be in the same environment and they will be distinguishable on a ^1H NMR spectrum.

The proximity of the metal moiety to H_8 or H_9 affects its chemical shift. If the metal is close to either of the above-mentioned protons (as in **2b** in Table 2.2), it results in the proton being more deshielded, causing a downfield chemical shift. This, indeed, was observed in the proton NMR spectrum.

Upon comparison to **1**, it can be seen that H_8 and H_9 are shifted slightly; in **2a**, H_8 and H_9 overlap because they are in identical chemical environments and the chemical shift is an intermediate value of the shifts for H_8 and H_9 that are found for **1**. Complex **2b** is the dominant conformer in the solid state; this was reiterated by the crystal structures on similar systems that were obtained by Crause.³⁸ In solution, however, the ratio of **2a:2b** is roughly equal. Comparison to literature³⁸ values (Table 2.2) shows that all the peaks that were obtained are shifted more upfield than the ethoxy furyl biscarbene complexes for chromium or tungsten metal complexes.³⁸

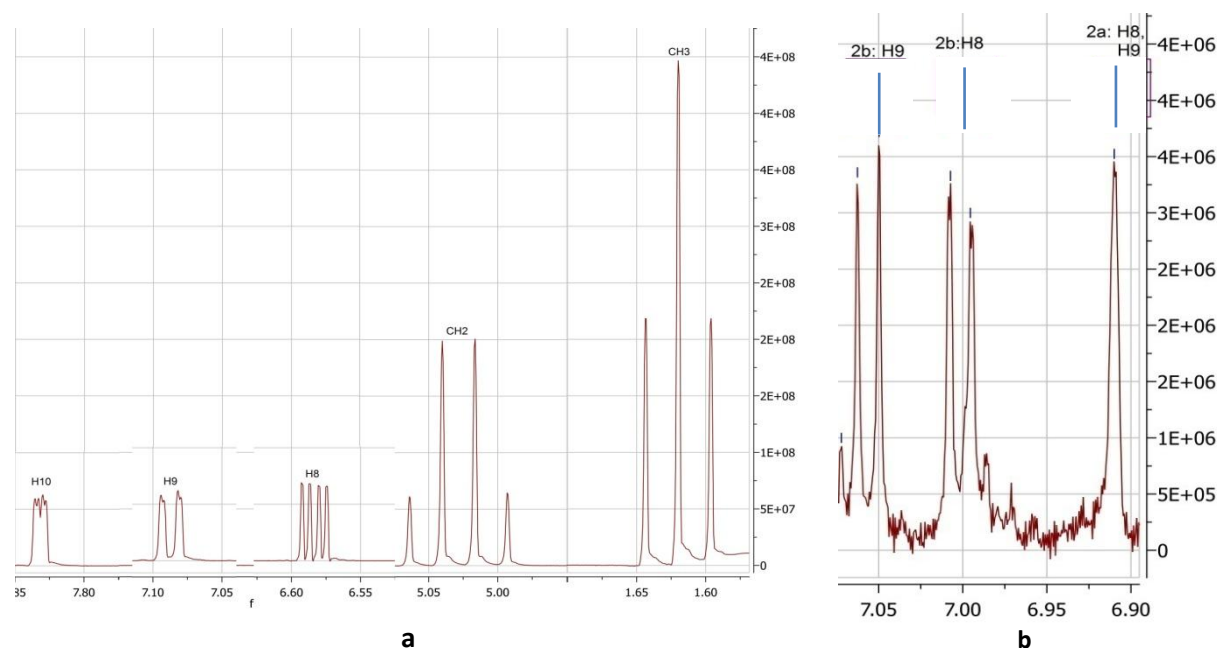


Figure 2.9: Experimental ^1H NMR spectrum of a) **1** (CDCl_3) and b) the H_8 and H_9 section of **2** (CDCl_3)

The experimental proton NMR spectra for **1** can be seen above; take note that the x-axis has been cut.

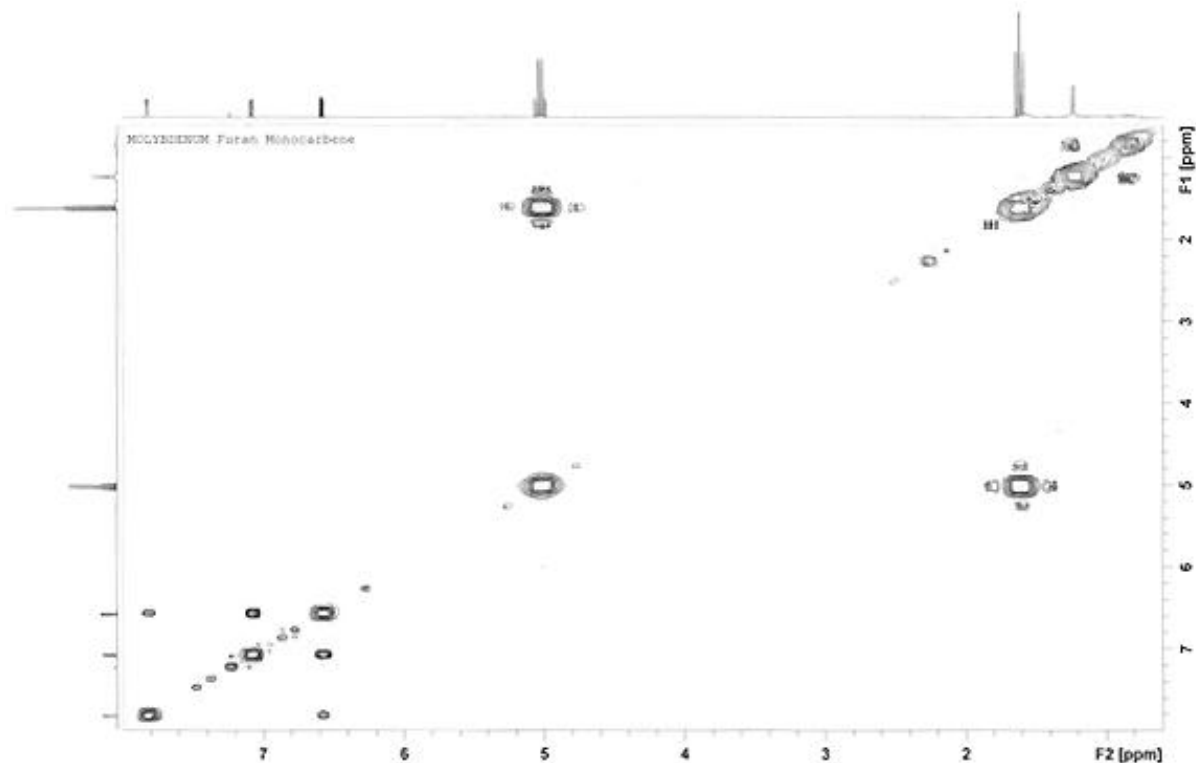


Figure 2.10: Two-Dimensional NMR spectroscopy - COSY spectrum of **1** (CDCl_3)

The COSY spectrum of **1** is shown above. This is a helpful technique, as it plots the proton NMR spectrum against itself. This allows for elucidation of which protons lie adjacent to each other in the molecule under study. The signals on the diagonal of Figure 2.10 show which proton signals on the x-axis correspond with the same proton signals on the y-axis. The remaining signals tell which proton signals are from protons on the adjacent carbon atom. For example, looking at the x-axis spectrum, the triplet CH_3 signal that is not on the diagonal is horizontally in line with the CH_2 (± 5 ppm) that occurs on the y-axis spectrum - indicating that the CH_2 and the CH_3 are adjacent.

2.2.3 ^{13}C NMR spectroscopy

Table 2.3 is compiled based on the following atom numbering system; this numbering system is also imposed on the literature values shown. Hydrogen atoms were omitted for clarity.

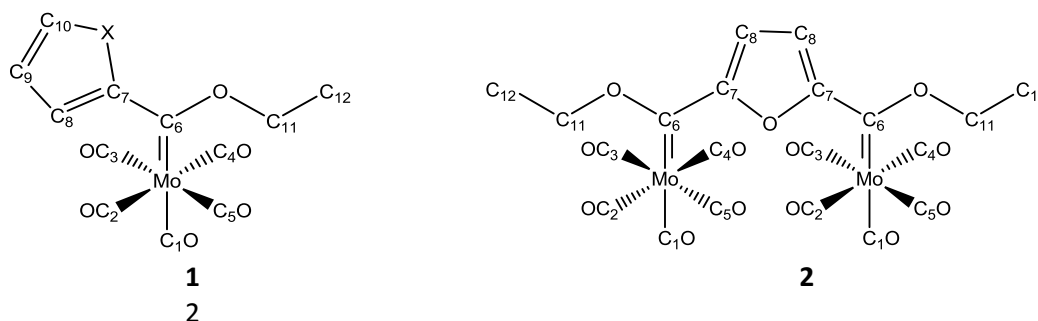


Table 2.3: ^{13}C NMR Assignments for **1** and **2**, including literature values

Complexes	Chemical Shift (δ , ppm)								
	C_1O (<i>trans</i>) [#]	$\text{C}_2\text{O}, \text{C}_3\text{O},$ $\text{C}_4\text{O}, \text{C}_5\text{O}$ (<i>cis</i>) [#]	C_6	C_7	C_8	C_9	C_{10}	C_{11}	C_{12}
1 ^a	213.5	206.0	301.1	164.4	114.6	113.2	150.0	76.6	15.2
2 ^a	211.5	206.2	302.8	164.8	112.7			77.4	14.1
A ^b : $[\text{Cr}(\text{CO})_5\text{C}\{\text{(OEt)}(\text{C}_4\text{H}_9\text{O})\}]^{41}$	225.5	218.4	313.6	165.6	113.5	113.0	150.7	76.7	15.3
L ^b : $[\text{Cr}(\text{CO})_5\text{C}\{\text{(OEt)}(\text{C}_4\text{H}_9\text{S})\}]^{41}$	224.9	218.7	319.8	157.5	135.8	129.8	141.5	77.2	15.5
B ^a : $[\text{W}(\text{CO})_5\text{C}\{\text{(OEt)}(\text{C}_4\text{H}_9\text{O})\}]^{38}$	203.4	197.3	284.8	166.1	114.8	113.4	150.0	78.3	15.0
K ^a : $[\text{W}(\text{CO})_5\text{C}\{\text{(OEt)}(\text{C}_4\text{H}_9\text{S})\}]^{36}$	205.0	197.6	312.5	162.0	135.9	128.9	141.4	79.0	14.9
C ^a : $[\text{Mo}(\text{CO})_5\text{C}\{\text{(OEt)}(\text{C}_4\text{H}_9\text{S})\}]^{39}$	212.8	206.1	307.2	150.1	136.2	128.9	141.4	77.8	15.1
D ^a : $[\text{Mo}(\text{CO})_5\text{C}\{\text{(OEt)}\}_2(\text{C}_4\text{H}_9\text{S})]^{39}$	212.9	205.6	312.4	154.5	136.9			78.3	15.0
E ^a : $[\text{Cr}(\text{CO})_5\text{C}\{\text{(OEt)}\}_2(\text{C}_4\text{H}_9\text{O})]^{38}$	224.0	216.4	312.9	161.9	118.6			76.6	15.3
F ^a : $[\text{W}(\text{CO})_5\text{C}\{\text{(OEt)}\}_2(\text{C}_4\text{H}_9\text{O})]^{38}$	203.2	196.9	286.1	165.6	120.7			79.1	15.0
G ^a : $[\text{W}(\text{CO})_5\text{C}\{\text{(OEt)}\}_2(\text{C}_4\text{H}_9\text{S})]^{36}$	202.7	197.0	294.6	162.5	137.3			79.1	14.9

^aSolvent: CDCl_3 (77.0 ppm)

^bSolvent: $\text{C}_3\text{D}_6\text{O}$ (29.8ppm)

[#]Position relative to carbene ligand

In the ^{13}C NMR spectrum of **1**, the carbene carbon (C_6) is very deshielded and is found to be the peak furthest downfield, as shown by the data in Table 2.3. These deshielding effects come from its proximity to the ethoxy moiety (which withdraws electron density), as well as the double bond environment to which the carbene carbon is attached. Interestingly the *trans* carbonyl carbon has the next highest shift on the spectra. This is because this group is directly across from the carbene carbon and thus it experiences the electron-withdrawing effects of the carbene carbon as well as the withdrawing effects of the metal. The carbonyl *trans* to the carbene is more deshielded than the carbonyls *cis* to the carbene because the carbene behaves as an electron “hole” which withdraws electron density from the metal, although the carbonyl ligand is a better π -acceptor than the carbene ligand. During the synthesis of **1**, the *trans* effect plays a role once the first carbonyl has dissociated - the other carbonyls will stabilise the transition state on the complex. It has been found that upon substituting a carbonyl, the chemical shift of the remaining carbonyls migrates more downfield in group VI metals.³⁷ Depending on the new ligand, the chemical shift value of the *trans* carbonyl increases across the following series:³⁷

Carbonyl < Phosphite < Phosphine, Arsine < Amine < Carbene

With regards to the carbons in the furyl backbone, the C_7 and C_{10} are the most deshielded - they are directly bonded to the oxygen atom; however it is found that C_7 is the most deshielded. This is because it experiences the withdrawing effects of the ethoxy and the carbene, as well as the oxygen adjacent to it, whereas C_{10} only feels the effects of the oxygen adjacent to it because it is furthest

⁴¹ Connor, J.A., Jones, E.M., Randall, E.W., Rosenburg, E., *J. Chem. Soc. A.*, **1972**, 2419

away from the point of attachment to the carbene carbon. C₈ and C₉ have similar shifts with C₈ being more downfield, this is as a result of it being adjacent to C₇ - the point of attachment to the carbene carbon.

Comparison to literature values³⁸ found in Table 2.3 shows excellent correlation, and an interesting trend - the molybdenum values always lie at an intermediate chemical shift compared to the same moieties on the spectra of the monocarbene complexes of chromium and tungsten; the trend in this case is increasing shift with decreasing mass: W < Mo < Cr. With this in mind, it can be said that the observed data correlates very well with the literature data.

The carbon spectrum of **2** shows no significant deviation from the carbene and carbonyl shifts on the carbon spectrum of **1** (data shown in Table 2.3). It also shows that the carbons on both carbenes are, for the most part, equivalent. It also shows that the carbons on the furyl ring are equivalent this indicates that rotation around the furyl-carbene bond does not influence the carbon's environment as it does the hydrogen environment. Upon comparison to literature³⁸ values shown in Table 2.3, it is found that the values obtained here are once again intermediate of those obtained for chromium and tungsten. There is a very good correlation between the data obtained for **1**; this was expected since **2** is a more symmetric version of **1**.

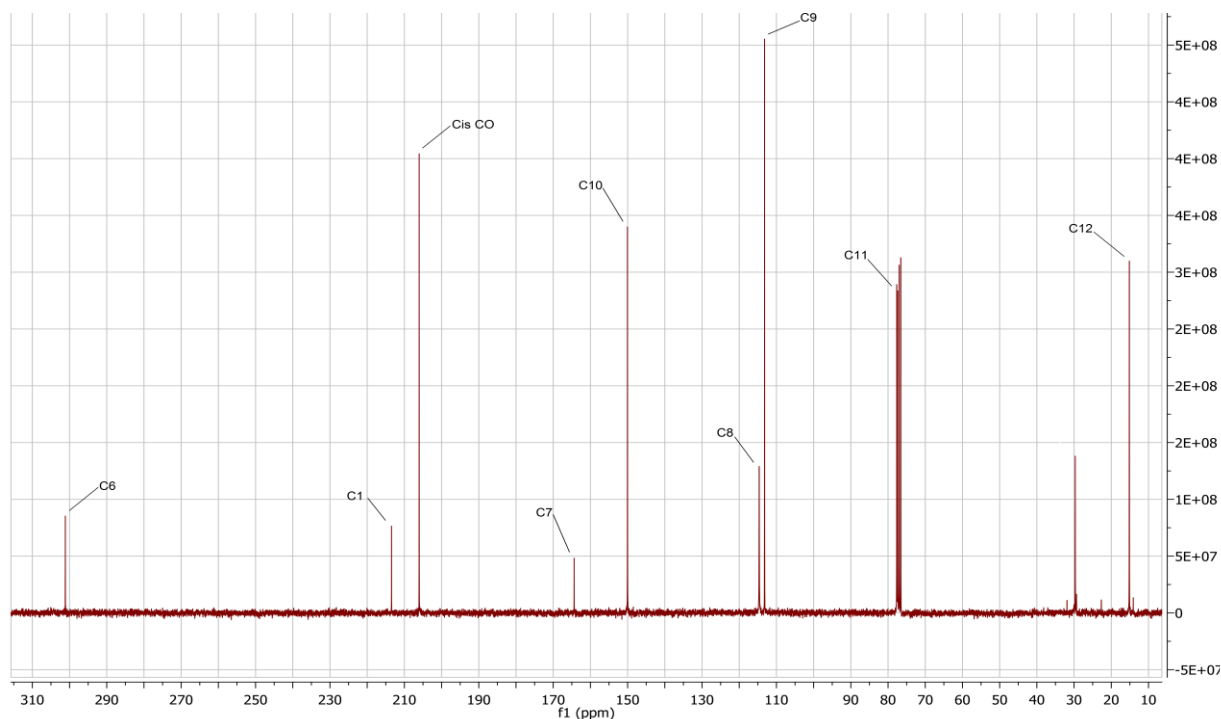


Figure 2.11: Experimental ¹³C NMR spectrum of **1** (CDCl₃)

The HSQC spectrum of **1** is shown below. This technique plots the proton NMR spectrum against the carbon-13 NMR spectrum. This has the direct implication of showing which proton signals are associated with which carbon signals. Using the triplet CH₃ signal on the x-axis spectrum as an example again, the signal vertically beneath it is horizontally in line with a signal on the ¹³C NMR (y-axis). This will be shown to be the CH₃ signal in section 2.3.3.

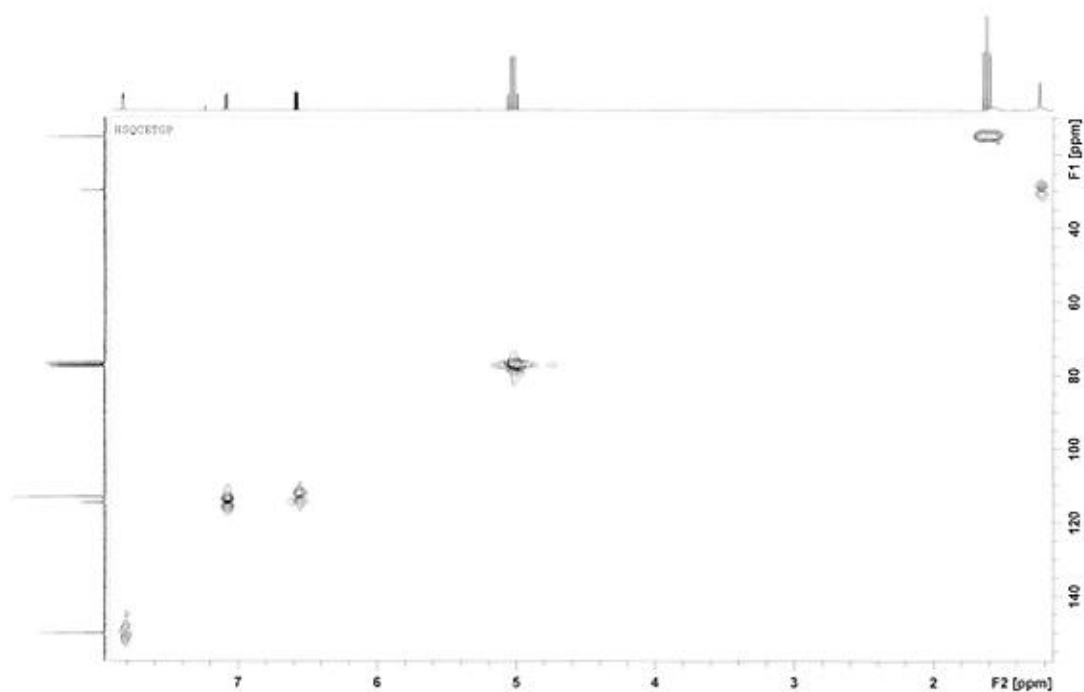


Figure 2.12: Two-Dimensional NMR Spectroscopy - HSQC spectrum of **1** (CDCl₃)

2.2.4 X-ray crystallography

Suitable crystals for x-ray ray diffraction were obtained for **1** from solvent diffusion of DCM and hexane. The crystals were red in colour. In all cases throughout the crystallography sections of this document, the atoms will be denoted with the following colours: red = oxygen, grey = carbon, white = hydrogen, yellow = sulfur, mustard = phosphorous, turquoise = molybdenum and blue =chromium.

The obtained crystal structure (Figure 2.13) shows that the ethoxy group is directly in the plane of the furyl ring and the carbene-metal bond, and that this plane is staggered with respect to the carbonyl groups. The oxygen atoms of the furyl group and the ethoxy group are orientated in an *anti*-conformation.

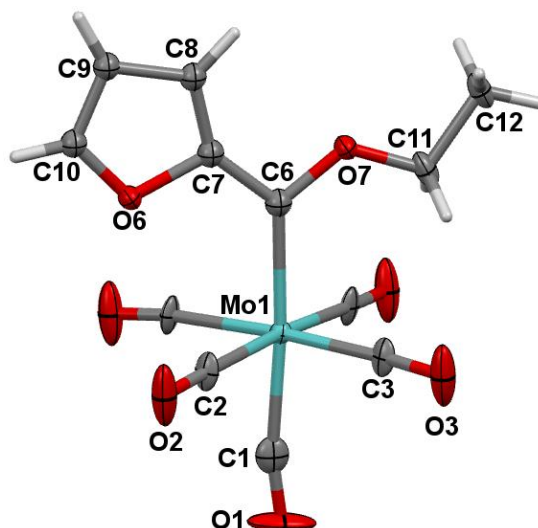


Figure 2.13: Crystal structure of 1 (ORTEP representation)

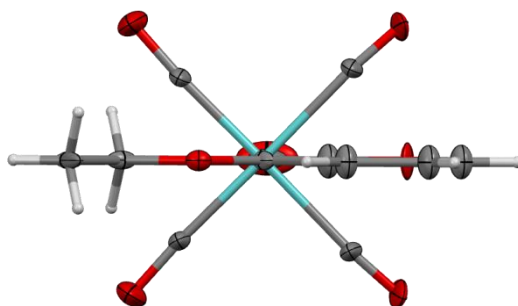


Figure 2.14: View down $C_6 \rightarrow Mo$ bond

As one views the molecule down the $C_6 \rightarrow Mo$ bond (Figure 2.14), it can be seen that the carbene substituents lie in a staggered position with respect to the equatorial carbonyls. Upon definition of a plane defined by $X-C_6-X-M$ where, in this case X refers to the oxygen atoms of the furan and the ethoxy moieties, the torsion angle is 0° . The orientation of the image in Figure 2.14 implies that three carbonyl peaks are expected to be seen on the carbon NMR spectrum (see section 3.3 for further explanation) but this is not the case. The orientation of the complex (Figure 2.14) results because the molecule was forced to adopt an orientation in the solid crystal state. The crystal structure has a crystallographic mirror plane through M , $C_6 \rightarrow C_{12}$, O_6 , O_7 . In solution, this mirror plane is not necessarily present. This results in the NMR signals of the carbon atoms of the carbonyl groups in the equatorial plane being degenerate rather than at separate chemical shifts.

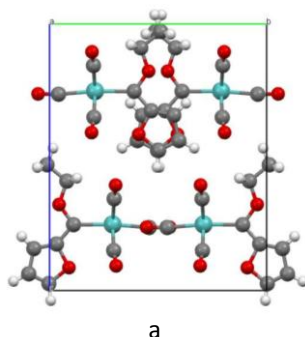


Figure 2.15: Crystal packing of **1** viewed down axis **a**

The crystal packing (Figure 2.15) indicates that there are four molecules in one unit cell. In Figure 2.15 it can be seen that at the top of the cell, the furfuryl rings are aligned over each other with an average π - π distance of 3.816 Å; in the bottom of the cell the *trans*-carbonyls are aligned over each other with a C-O distance of 3.797 Å.

Table 2.4: Bond lengths obtained from the crystal structure of **1**

Bond	Bond Length (Å)
O ₇ - C ₁₁	1.37(3)
O ₆ - C ₁₀	1.45(2)
O ₆ - C ₇	1.49(3)
C ₆ -C ₇	1.41(4)
O ₇ -C ₆	1.39(4)
C ₉ -C ₁₀	1.23(2)
C ₈ -C ₉	1.416(14)
C ₇ -C ₈	1.32(2)
Mo- C ₆	2.169(8)
Mo-CO _{cis} (ave)	2.045(13)
Mo-C ₁	2.037(11)

The average of the *cis* carbonyl bond lengths and the *trans* carbonyl bond length are very similar. The data of the furfuryl ring in Table 2.4 show that, since C₇-C₈, C₈-C₉ and C₉-C₁₀ are roughly 0.2 Å apart, resonance must play a sizeable role in the length of these bonds. C₇-C₈ and C₉-C₁₀ could be said to be a double bond in a nature. C₈-C₉ could be said to be a single bond in nature. In general, the bond length of a C-C single bond is 1.51(3)Å.⁴² All the C-C bond lengths in **1** are shorter than the general C-C single bond length. This indicates that resonance plays a significant role in this molecule. The

⁴² Cotton, F.A, Lukehart, C.M., *Prog. Inorg. Chem.*, 16, **1972**, 487

Mo-C₆ bond length (2.169(8)Å) is similar to that obtained by Erker *et al.* (2.195(6)Å).⁴³ This indicates that there is more double bond character in **1** compared to the complex analysed by Erker *et al.*

Table 2.5: Bond angles obtained from the crystal structure of Complex 1

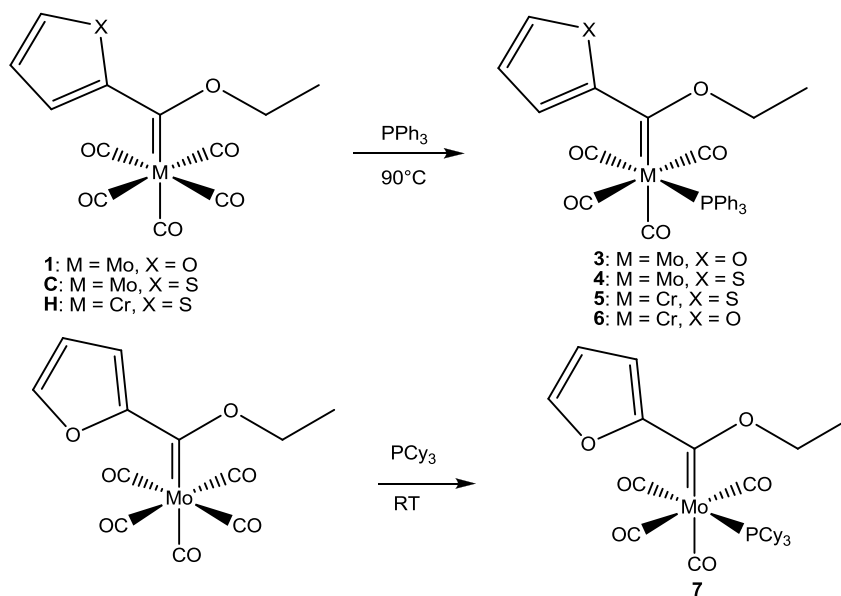
Angle	Angle size (°)
O ₇ -C ₆ -C ₇	102.7(7)
Mo-C ₆ -C ₇	130(2)
Mo-C ₆ -O ₇	127(2)
O ₇ -C ₁₁ -C ₁₂	110.1(18)
C ₂ -Mo-C ₃	89.61(19)
C ₂ -Mo-C ₆	91.6(7)
C ₃ -Mo-C ₆	92.6(7)
C ₁ -Mo-C ₆	176.7(16)

C₂ and C₅ are related by the symmetry element in the space group (mirror plane), and so are C₃ and C₄. This makes the observation that the angles between C₂-Mo-C₅ and C₃-Mo-C₄ are identical in size an expected one. The angles between C₂-Mo-C₃ and C₄-Mo-C₅ are different from those just mentioned, as well as different to each other. The angles around the molybdenum metal reported in Table 2.5, show that there is no significant deviation from the ideal octahedral bond angle of 90 °.

2.3 Chromium and molybdenum tetracarbonyl phosphine-substituted ethoxy carbene complexes

Substitution of the relevant pentacarbonyl ethoxy carbene complex (**1**, **C** or **H**) by triphenylphosphine or tricyclohexylphosphine resulted in the formation of tetracarbonyl ethoxy carbene complexes (**3-7**). The reaction schemes that were followed for the synthesis of **3** through **7** were as follows:

⁴³ Erker, G., Dorf, U., Kruger, C., Tsay, Y., *Organometallics*, 6, **1987**, 682



Scheme 2.2: Synthetic route followed to obtain **3** through **7**

In all of the complexes, more than one product was formed in the reaction; both a *cis* and a *trans* product. This was evident from TLC analysis. The complexes were purified using silica gel column chromatography. Although two products were visible on TLC, it was not possible to isolate both of these products for all of the complexes. On the other hand, for tungsten it is possible to isolate both products.⁴⁴

With regards to **3**, the first yellow-brown band which eluted from the silica gel column, was concluded to be the *trans* isomer based on polarity. It is less polar due to a more symmetrical structure compared to the *cis* complex. The *trans* isomer was markedly less stable than the *cis* complex, a red-brown complex eluting after the *trans* isomer. The *trans* complex transformed readily into the *cis* isomer. Elucidation of the *trans* isomer was especially difficult due to the conversion to the *cis* isomer being so rapid. According to the *trans* effect, the *cis* isomer should be favoured, as was the case here.

Complexes **4**, **5** and **7** were purified using silica gel column chromatography while **6** was purified using alox. The reaction to synthesise **4** was incomplete as the first band to elute was the starting material, **1**. The second band was the desired product which was a red-brown colour. In the column of **5**, **6** and **7**, two isomers were observable on the column. For all three complexes, the first product band to elute was the *trans* product which was yellow-brown in colour. It was not possible to characterise this product since it decomposed rapidly. The second product band to elute was pink/red-brown and was the *cis* isomer product.

⁴⁴ a) Landman, M., Levell, T., van Rooyen, P.H., Conradie, J., *J. Mol. Struct.*, 29, **2014**, 1065; b) Landman, M., Pretorius, R., Buitendach, B.E., van Rooyen, P.H., Conradie, J., *Organometallics*, 32, (19), **2013**, 5491

The possible isomers and conformers that can be products of this reaction can be found in Figure 2.16, below.

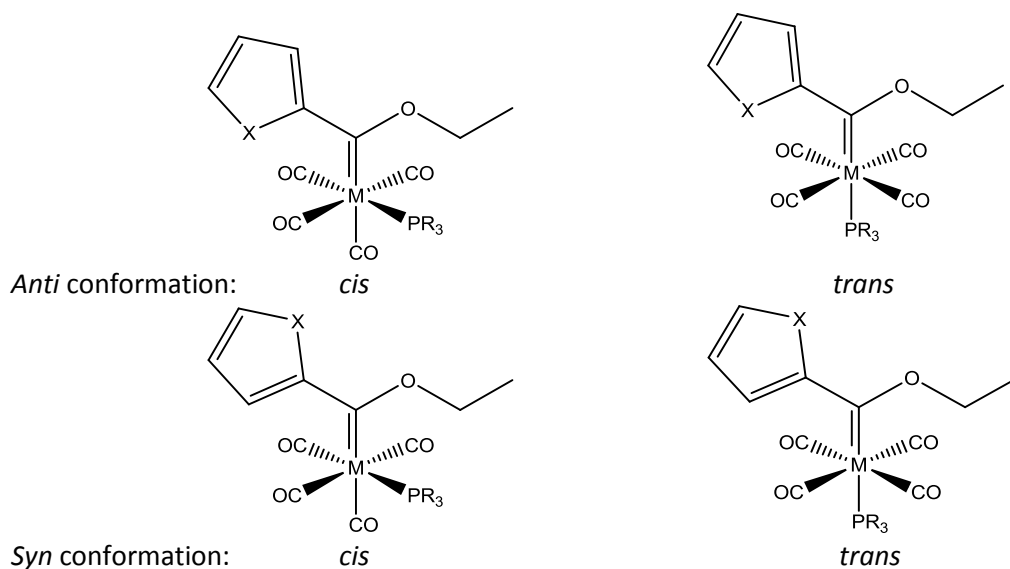


Figure 2.16: The possible conformations of a mono-phosphinated Fischer carbene complex

It is found from crystal structures that the *cis* isomer of **3** is in the *anti*-conformation (Figure 2.20), and the *cis* isomer of **5** is in the *syn*-conformation (Figure 2.20).

2.3.1 Infrared spectroscopy

The data of the *cis* complexes of **3-7** as well as the **3-trans** complex is reported in Table 2.6. Complexes **3** through **7** are of the molecular type *cis*-M(CO)₄LL'. This results in a symmetry of C_{2v}. In this case, the A₁⁽¹⁾ band has the highest frequency and the weakest intensity, and the B₁ has the lowest frequency and is of medium intensity³⁷. The order of A₁⁽²⁾ and B₂ is dependent on the compound; however A₁⁽²⁾ should be of medium intensity, and B₂ should exhibit the strongest intensity.³⁷

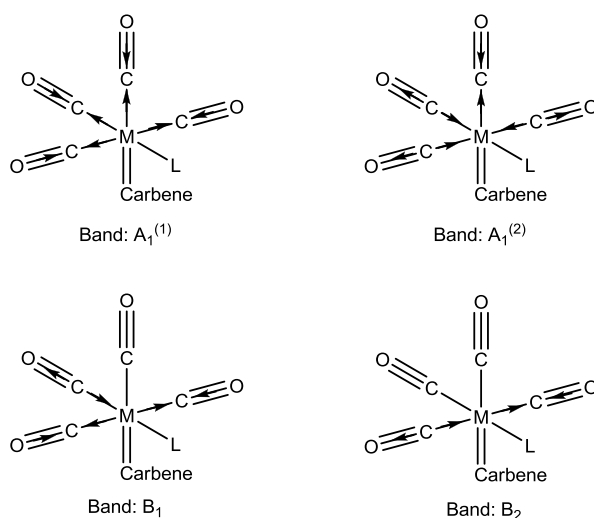
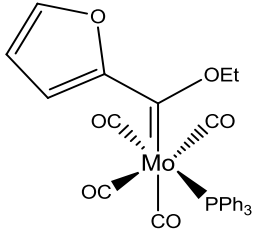
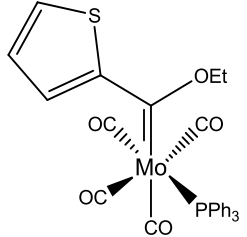
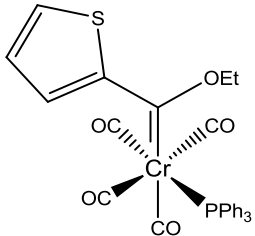
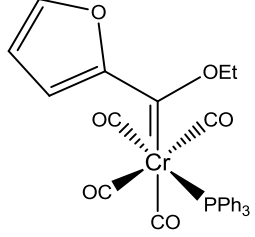
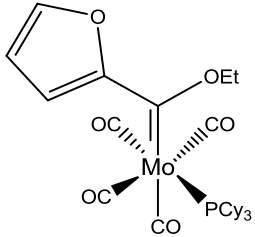


Figure 2.17: Illustration of the origin of the IR stretching frequencies observed for C_{2v} symmetry

The figure above shows the origin of the carbonyl stretching bands observed in octahedral complexes exhibiting C_{2v} symmetry.

Table 2.6: IR frequency assignments for 3 through 7

Complexes	Carbonyl Stretching Frequency (cm^{-1})			
	$A_1^{(1)}$	B_1	B_2	$A_1^{(2)}$
 <p>3 – Cis</p>	2013 (m)	1890 (vs)	1865 (s)	1924 (m)
 <p>4</p>	1994 (w)		1889 (vs)	1923 (m)
 <p>5</p>	2004 (vw)		1889 (m)	1940 (vs)
 <p>6</p>	2004 (w)	1921 (m)	1879 (vs)	1932 (m)
 <p>7</p>	2007 (w)		1880 (s)	1932 (m)
M: <i>cis</i> -[W(CO) ₄ (PPh ₃)C{(OEt)(C ₄ H ₃ O)}] ¹⁴	2009 (s)	1860 (s)	1888 (s)	1921 (s)
N: <i>cis</i> -[W(CO) ₄ (PPh ₃)C{(OEt)(C ₄ H ₃ S)}] ¹⁴	2009 (s)	1883 (s)	1894 (s)	1914 (s)

All IR measurements were made using KBr as the matrix.

The *trans* isomer of **3** that was isolated rapidly converted to the *cis* isomer in solution. This *trans* isomer showed peaks at 2018 cm⁻¹ (w), 1889 cm⁻¹ (vs) and 1944 cm⁻¹ (w). From section 2.3.1, the data obtained for **1** was A₁⁽¹⁾: 2068 cm⁻¹; B₁: 1989 cm⁻¹; E: 1923 cm⁻¹; A₁⁽²⁾: 1942 cm⁻¹. This data will be used for comparison in the text to follow.

The B₁ band of **3-cis**, **4**, **5**, **6** and **7** is expected to have the most intense peak; this is what is found for the *cis* isomer of **3** and **6**. The *trans* isomer of **3** is expected to have D_{4h} symmetry with one IR active stretching band⁴⁵ - one strong, broad peak is observed with three other noticeable, yet not always clearly discernible peaks. The presence of the bulky carbene ligand may account for this observation.¹⁴ Due to the differences in symmetry of the *trans* and the *cis* isomers which results in the different bands seen for the IR spectra of the two isomers of **3**, this complex illustrates Nakamoto's suggestion that the IR can be used to identify isomers.⁴⁵

In the case of **7**, the A₁⁽²⁾ and B₂ bands show good correlation to **3** and **5** (Table 2.6) even though there is a change in the phosphine groups' identity (triphenylphosphine in **3** and **5**, and tricyclohexylphosphine in **7**).

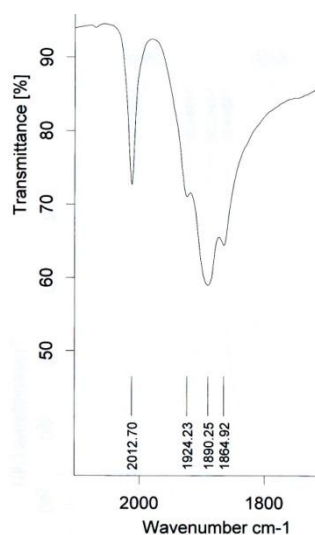


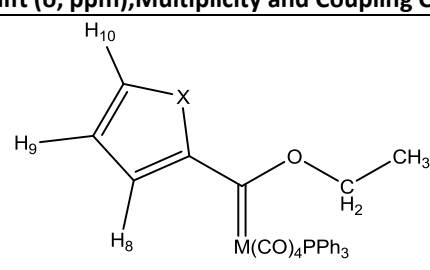
Figure 2.18: Carbonyl stretching region of experimental IR of **3-cis** (KBr)

[2.3.2 ¹H NMR spectroscopy](#)

The ¹H NMR data of **3** through **7** are summarised in Table 2.7, below.

⁴⁵ Nakamoto, K., *Infrared and Raman spectra of inorganic and coordination compounds*, 4th edition, John Wiley and Sons, 1986

Table 2.7: ^1H NMR Assignments for 3-7, including literature values

Complexes	Chemical Shift (δ , ppm), Multiplicity and Coupling Constants (J, Hz)						
							
	H ₁₀	H ₉	H ₈	CH ₂	CH ₃	PCylo	PPh ₃
3^c: M = Mo, X = O	7.54 s	6.37 dd J = 1.7, 3.6	6.76 dd J = 0.7, 3.6	4.79 q J = 7.1	1.36 t J = 7.1		7.21- 7.60 m
4^b: M = Mo, X = S	6.84 d J = 4.8	6.57 dd J = 3.9, 4.9	7.12 d J = 7.6	4.06 q J = 7.1	0.98 t J = 7.1		7.42- 7.72 m
5^b: M = Cr, X = S	6.79 s	4.70 s	7.45 s	4.03 q J = 7.3	0.94 t J = 7.1		6.92- 7.46 m
6^b: M = Cr, X = O	7.60 s	5.97 s	6.66 s	4.88 s	1.36 s		7.50- 7.87 m
7^b: M = Mo, X = O, P = PCy ₃	7.42 dd J = 1.2, 8.4	5.86 dd J = 1.7, 3.6	7.02 d J = 3.6	4.31 m	1.03 m	1.38, d, J = 14.4 1.55, d, J = 18.6 1.77, d, J = 11.5	
M^c: cis- [W(CO)₄PPh₃C((OEt)(C₄H₃O))] ¹⁴	7.30- 7.43 m	6.37 dd J = 1.7, 3.6	6.80 dd J = 0.8, 3.6	4.68 q J = 7.1	1.36 t J = 7.1		7.30- 7.43 m
N^c: cis- [W(CO)₄PPh₃C((OEt)(C₄H₃S))] ¹⁴	7.65 dd J = 1.1, 5.0	6.97 dd J = 4.0, 4.8	7.77 dd J = 1.1, 4.0	4.53 dq J = 7.0, 0.5	1.20 t J = 7.0		7.31- 7.46 m
1^a	7.83 dd J = 0.8, 1.7	6.58 dd J = 1.7, 3.7	7.09 dd J = 0.8, 3.6	5.03 q J = 7.1	1.62 t J = 7.0		

^aSolvent CDCl₃ (7.24 ppm)

^bSolvent: C₆D₆ (7.2 ppm)

^cSolvent: CD₂Cl₂ (5.32 ppm)

From Table 2.7, comparison to **1** shows that all of the protons attached to the carbene group are shifted upfield, indicating that they are now slightly more shielded. This is a result of the phosphine group not being as good a π -acceptor as the carbonyl, therefore there is more electron density available to be distributed to other atoms in the molecule. H₁₀ is found among the aromatic proton peaks from the triphenylphosphine. The protons on the phosphorous only provide a multiplet in the 7.21-7.60 ppm range of the spectrum. These protons also overlapped with the protons from the

furyl ring (namely H₈, H₉ and H₁₀) which is also aromatic. As a result, no specific assignments could be made to the phenyl protons. This data correlates very well with data available for the chromium and tungsten analogues.¹⁴ There is good correlation between the spectra of **M** and **3**. The data in Table 2.7 shows that with the change in the heteroatom on the carbene substituent, there is a large effect on the protons of the aromatic ring. All the protons are shifted upfield when the spectrum of **3** is compared to that of **N**, indicating experimentally that sulfur can accommodate more electron density than oxygen can - thus the furyl moiety is more shielded than the thienyl moiety.

Where the metal remains the same (compare the data of **3** with that of **4**, **5** with **6** and **M** with **N**) an inversion of assignments can be seen. In the furyl structures, the trend is H₁₀ > H₈ > H₉ but in the thienyl structures, the trend is H₈ > H₁₀ > H₉. This inversion of the trend is due to the electronegativities and withdrawing ability of the oxygen versus the sulfur. H₁₀ is closest to the sulfur atom in the thienyl and sulfur is less electronegative than oxygen, but still appreciably electronegative - the difference is that sulfur can accommodate the extra electron density because sulfur has access to d-orbitals whereas oxygen does not.

The same trend for the chemical shifts of furyl, regarding H₈, H₉ and H₁₀, is followed for **7**, although there is a wider spread for the data than seen in previous complexes. Three peaks are seen for all the cyclohexyl protons. This will be discussed in detail in chapter 3, section 3.3.2. The peaks represent the *ipso* proton, the axial protons and the equatorial protons.

Care should be exercised when drawing too many conclusions further than general trends from this data. This is due to the fact that the solvents used for the experiments were different. One solvent in particular was benzene which is known to cause isotropic effects in NMR experiments.

2.3.3 ¹³C NMR spectroscopy

Table 2.8 was compiled using the following numbering system; this numbering system is also imposed on the literature values shown. Hydrogen atoms have been omitted for clarity.

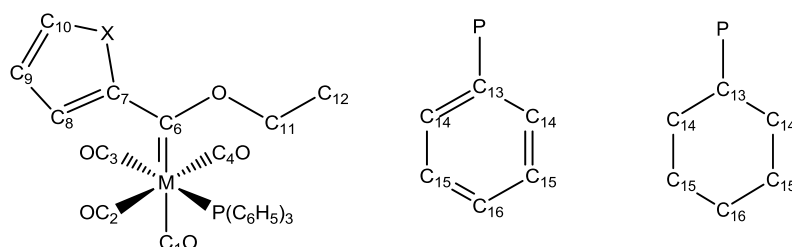


Table 2.8: ^{13}C NMR Assignments for **3** through **7**, including literature values

Complex	Chemical Shift (δ , ppm)													
	C_1O (<i>trans</i>) [#]	C_3O	$\text{C}_2\text{O},$ C_4O	C_{10}	C_9	C_8	C_7	C_6	C_{11}	C_{12}	C_{13}	C_{14}	C_{15}	C_{16}
3^c	220.2	216.8	211.9	148.7	112.1	112.9	164.8	304.8	76.9	15.2		129.5 - 130.1	128.6	128.5
4^b	212.6	210.7	206.7	136.5	136.0	135.2	162.3	n.o.	61.3	12.0		133.6	133.5	133.4
5^b	234.0	222.3	217.8	135.2	131.9	136.3	162.3	n.o.	61.3	14.6	134.7	132.4	130.7	129.1
6^b	228.0	222.6	217.8	130.7	110.2	112.6	164.9	315.2	75.1	14.7	134.6	132.8		129.2
7^b	227.3	223.7	214.9	145.8	132.1	138.9	155.5	319.3	70.1	26.3	70.0	113.2	104.8	108.1
M^c: cis- [W(CO)₄PPh₃ C(OEt) (C₄H₃O)]¹⁴	212.3	207.5	203.8	148.5	112.1	113.3	167.1	289.0	77.4	15.3	136.5	133.8	128.8	130.4
N^c: cis- [W(CO)₄PPh₃ C(OEt) (C₄H₃S)]¹⁴	211.4	207.3	203.8	133.1	128.7	140.2	159.9	294.5	77.8	14.8	135.9	133.7	129.0	130.4
1^a	213.5		206.0	150.0	113.2	114.6	164.4	301.1	76.6	15.2				

^aSolvent: CDCl_3 (77 ppm)

^bSolvent: C_6H_6 (128.0 ppm)

^cSolvent: CD_2Cl_2 (53.5 ppm)

[#]Position relative to carbene ligand

It can be seen from the data in Table 2.8 that there is no significant difference in the chemical shifts for the carbon NMR spectra shown, except for the shifts and/or number of peaks found for the carbonyls. This is because the carbonyls are in a significantly different environment when they are *trans* to a carbonyl (as in C_2O and C_4O), vs. *trans* to a phosphine ligand (C_3O), vs. *trans* to the carbene moiety (C_1O). Since the carbons in the carbene moiety are not notably shifted and a carbonyl peak is found for a carbonyl *trans* to a phosphine, this provides evidence that the phosphine group is not *trans* to the carbene (in other words, this is not the *trans* isomer). The carbonyl *trans* to a phosphine will be the most shielded because the carbonyl is a better π -acceptor than the phosphine ligand. The carbonyl *trans* to the carbene will be the most deshielded because the carbene ligand behaves as a void for electrons, strongly drawing electrons toward itself. Lastly the carbonyl *trans* to a carbonyl has an intermediary chemical shift. There is a good correlation of these values to available literature.¹⁴ The aromatic substituents on the carbene make no difference to the carbonyl shifts, but the thienyl is more deshielded and downfield when analysing the carbene shifts.

In the ^{13}C NMR spectrum, it is observed that the chromium complex (**5**) is consistently at higher carbonyl chemical shifts when compared to **3** or the tungsten analogue - reiterating the $\text{Cr} > \text{Mo} > \text{W}$ trend. There is a good correlation between the chemical shifts for **7** and **3**. The chemical shifts listed for C_{13-16} refer to the cyclohexyl ring, not the phenyl ring. Once again one cannot draw too many

direct conclusions due to the solvent effects between the benzene solvent and the furyl/thienyl rings as discussed previously.

2.3.4 ³¹P NMR spectroscopy

The data derived from the ³¹P spectra of **3** through **7** are summarised in Table 2.9, below.

Table 2.9: ³¹P NMR Assignments for **3** through **7**, including literature values

Complex	Chemical Shift (δ, ppm)	
	<i>Cis</i> [#]	<i>Trans</i> [#]
3^c-cis	40.00	
3^c-trans		37.67
4^b	37.83	
5^b	25.16	
6^b	25.09	
7^b	48.95	
M^c: cis-[W(CO)₄PPh₃C((OEt)(C₄H₃O))]¹⁴	25.25	
M^c-trans		23.00
N^c: cis-[W(CO)₄PPh₃C((OEt)(C₄H₃S))]¹⁴	25.00	
N^c-trans		22.78

^bSolvent: C₆D₆

^cSolvent: CD₂Cl₂

[#]Position relative to carbene ligand

The phosphorous-31 NMR chemical shift values for **3** (both *cis* and *trans*) are significantly different to the values obtained for the tungsten complexes, **M** and **N**, by Pretorius,¹⁴ as shown by the data in Table 2.9. The chromium analogue that also contains furyl, **6**, has a shift that is much lower than **3**. The same trend is observed for the thienyl set, **4** and **5**. The trend seen here is: Cr < W < Mo.

The phosphorous-31 chemical shift of the phosphorus atom in **7** is much further downfield than any of the triphenylphosphine complexes.

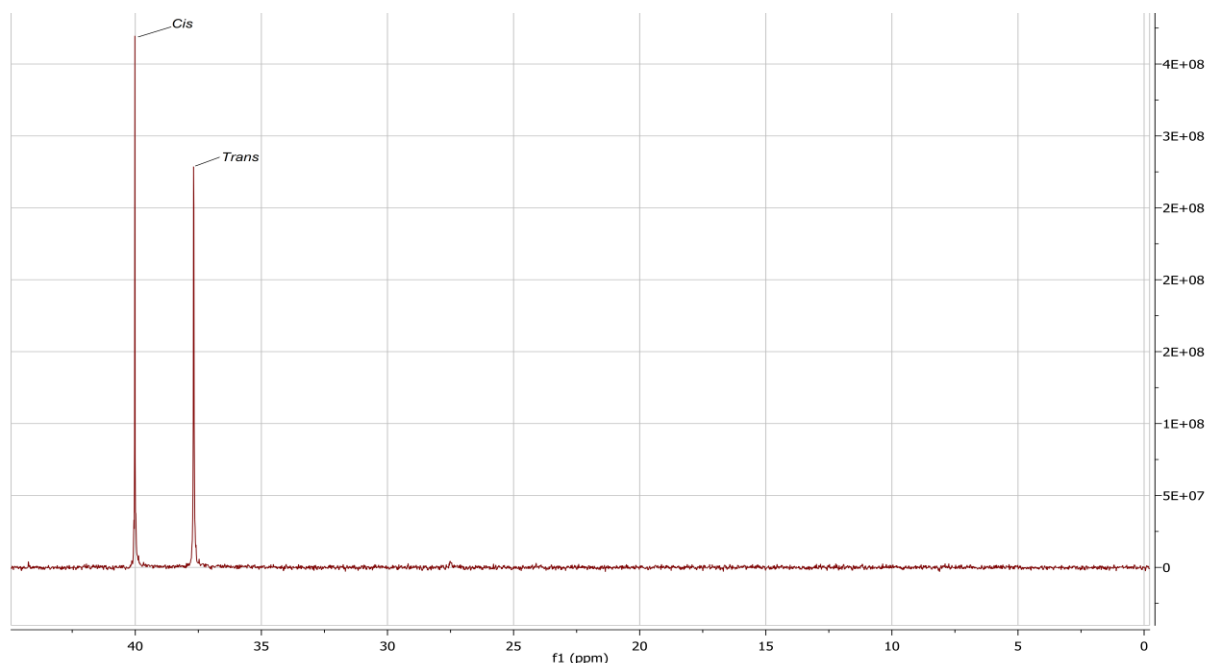


Figure 2.19: Experimental ^{31}P NMR of **3** (CD_2Cl_2)

The most abundant isomer in the NMR sample of **3** was the *cis* isomer (Figure 2.19). In general, the *cis* isomer peak is found more downfield than the *trans* isomer.

2.3.5 X-ray crystallography

The crystal structures obtained for **3-cis** and **5-cis** are shown in Figure 2.20.

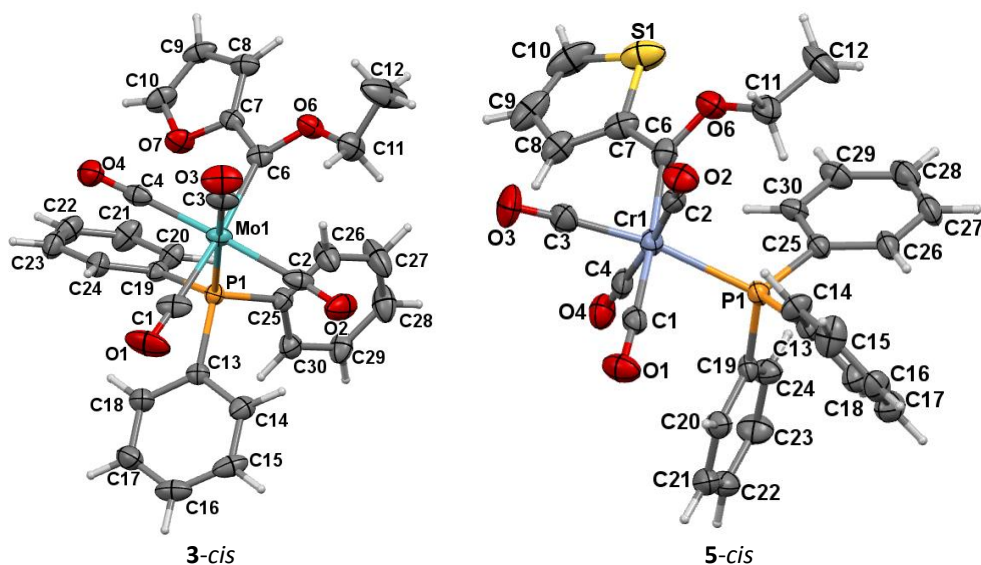


Figure 2.20: Crystal structure of **3-cis** (ORTEP Representation) and **5-cis** (ORTEP Representation)

Figure 2.20 shows that in **3-cis**, the oxygen atom of the furyl ring adopts an *anti*-conformation with respect to the oxygen atom of the ethoxy group. Conversely, in **5-cis** the sulfur atom of the thienyl moiety adopts a *syn* configuration with respect to the oxygen atom in the ethoxy group.³²

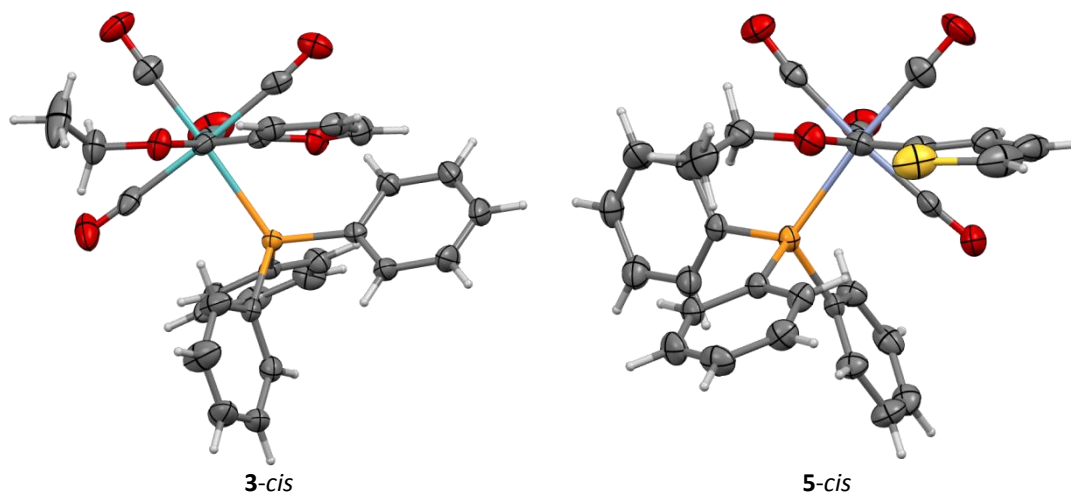


Figure 2.21: View down the $C_6 \rightarrow M$ bond for **3-cis** and **5-cis**

In Figure 2.21, it can be seen that both **3-cis** and **5-cis** adopt a staggered conformation in their crystal forms. The difference between the two is that the thienyl group is orientated away from the phosphine group in **5-cis**, and the furyl group towards the phosphine group in **3-cis**. The dihedral angle between the plane, $X-C_6-X-M$, and the furyl moiety is 7.56° out of this plane in **3-cis**, and the thienyl ring has a torsion angle of 14.81° out of this plane in **5-cis**. The furyl ring in **1** had a torsion angle of 0° out of this plane. This indicates that upon addition of the phosphine moiety, the carbene substituents are rotated to a staggered position, as a result of the steric bulk which is introduced by the phosphine moiety. The torsion angle between $P-M-C_6-C_7$ for **3-cis** is 60.91° , and for **5-cis** is 119.78° .

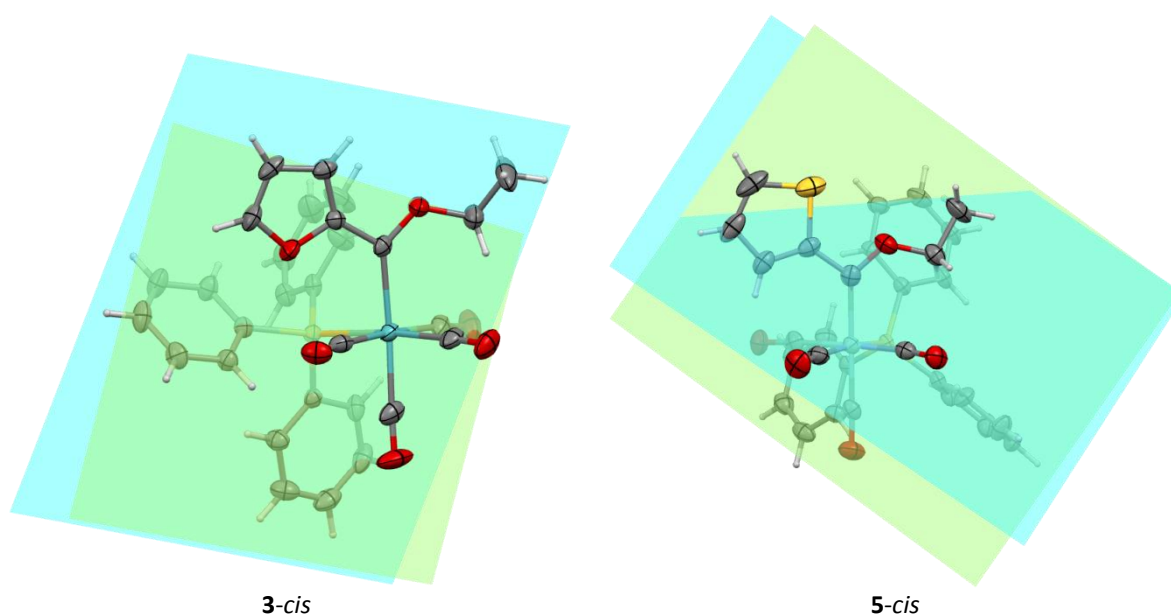
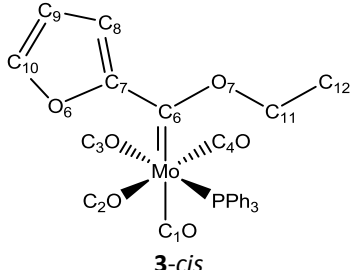
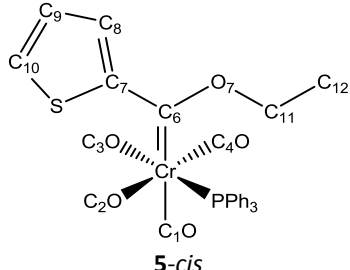
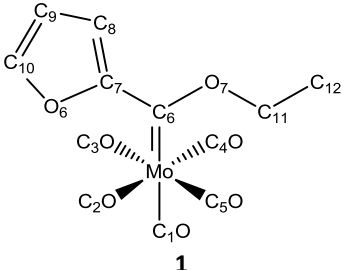


Figure 2.22: $C_7-C_8-C_9-C_{10}-O_6$ and $C_{12}-C_{11}-O_7$ planes in **3-cis** and **5-cis**

Figure 2.22 shows that the ethoxy group is rotated further out of the heteroaromatic ring plane in **3-cis** (19.70 °) than in **5-cis** (12.92 °). This could be a direct result of the phosphine ligand being closer to the furyl ring in **3-cis** and pushing the furyl ring away.

Table 2.10: Crystal structure bond lengths observed in **3-cis** and **5-cis** and compared with **1**

Bond	Bond Length (Å)		
	 3-cis	 5-cis	 1
M-P	2.562(8)	2.4287(16)	
M-C ₁	2.021(4)	1.876(6)	2.029(10)
M-C ₂	2.036(3)	1.888(6)	2.147(12)
M-C ₃	1.982(3)	1.867(6)	1.948(12)
M-C ₄	2.038(4)	1.892(6)	
M-C ₆	2.180(3)	2.038(6)	2.173(7)
O ₇ -C ₆	1.329(4)	1.365(7)	1.38(3)
O ₇ -C ₁₁	1.456(4)	1.451(10)	1.37(3)
O ₆ -C ₇	1.376(3)		1.49(3)
S-C ₇		1.721(8)	
C ₆ -C ₇	1.447(4)	1.457(9)	1.41(4)
C ₇ -C ₈	1.365(4)	1.411(12)	1.32(2)
C ₈ -C ₉	1.403(4)	1.357(12)	1.416(14)
C ₉ -C ₁₀	1.341(5)	1.373(16)	1.23(2)
C ₁₀ -O ₇	1.348(3)		1.45(2)
C ₁₀ -S		1.712(12)	

The data in Table 2.10 shows that the Mo-C₃ bond is slightly longer in **3-cis** (1.982(3) Å) when compared to **1** (1.948(12) Å). Since the PPh₃ is *trans* from this carbonyl, it would result in the back-bonding to the metal being increased since a carbonyl is a better π-acceptor than the PPh₃. With a PPh₃ *trans* to C₃, the double bond character of the carbonyl-metal bond is increased and it is expected that this carbonyl bond would be shorter in **3-cis** than in **1**, but this is not what is observed. All of the other carbonyl-metal bonds which are *cis* to the phosphine moiety are shorter in **3-cis** than in **1**; this could be due to the PPh₃, not because it is *trans* to these carbonyls, but simply because the metal has more electron density to distribute - thus making all the bonds to it shorter with more double bond character.

All of the bonds to the metal in **5-cis** are found (Table 2.10) to be shorter than in **3-cis**. This can be attributed to the change in the metal centre. Chromium is smaller than molybdenum by approximately 8 % and thus it cannot accommodate the extra electron density forced upon it by the phosphine moiety, so it distributes it - making shorter bonds and increasing double bond character

to ALL bonds that it is involved in. The M-P (2.4287(16) Å) bond is shorter in **5-cis** compared to **3-cis** (2.562(8) Å). The M-C₆ bond is shorter in **5-cis** (2.038(6) Å vs **3-cis'** 2.180(3) Å) indicating that there is more double bond character and more back bonding from the metal. It is expected then, that the O₇-C₆ bond should be longer in **5-cis** since the carbene has more stabilisation from the metal, so it does not need additional stabilisation from the ethoxy group. This is indeed the case - bond lengths of 1.365(7) Å and 1.329(4) Å in **5-cis** and **3-cis** respectively are observed. The same trend is observed in the chromium complexes synthesised by Meca *et al.*⁴⁶ and by Szesni *et al.*⁴⁷

The pentacarbonyl carbene analogue of **5-cis** shows a Cr-C₆ bond length of 2.054(5) Å.³² This bond has seen a slight change in character as a result of the addition of the phosphine moiety, and hence it is slightly shorter in **5-cis** (2.038(6) Å). The average Cr-carbonyl bond length is 1.897(10) Å³² in the pentacarbonyl monocarbene complex and 1.881(6) Å in **5-cis**, which is a small change in length. The carbonyl *trans* to the carbene, however, shortened from 1.891(6) Å³² in the pentacarbonyl monocarbene complex to 1.876(6) Å in **5-cis**.

Table 2.11: Crystal structure bond angles of **3-cis** and **5-cis**, as well as that of **1** for comparison

Angle	Angle size (°)		
	3-cis	5-cis	1
C ₁₂ -C ₁₁ -O ₇	106.5(3)	107.6(7)	110.1(18)
M-C ₆ -O ₇	131.5(2)	130.8(5)	127(2)
M-C ₆ -C ₇	124.8(2)	124.9(4)	130(2)
O ₇ -C ₆ -C ₇	103.6(2)	104.2(5)	102.6(7)
C ₆ -M-P	94.03(7)	98.54(16)	
C ₆ -M-C ₂	95.99(12)	88.8(3)	91.6(7)
C ₆ -M-C ₁	174.55(13)	175.3(2)	176.7(16)
C ₆ -M-C ₃	91.81(11)	89.4(3)	92.6(7)
C ₆ -M-C ₄	87.70(11)	92.2(3)	
P-M-C ₄	95.00(9)	83.9(2)	
P-M-C ₂	87.15(9)	100.2(2)	
C ₃ -M-C ₄	87.45(13)	89.9(3)	
C ₂ -M-C ₃	90.03(13)	85.7(3)	89.61(19)

Addition of the triphenylphosphine ligand does not affect the overall shape of the complex. There is no significant departure from the ideal octahedral bond angle of 90 ° (Table 2.11).

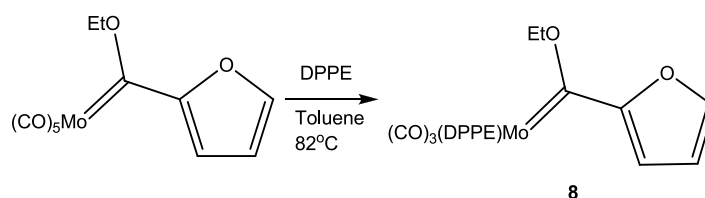
2.5 Molybdenum tricarbonyl diphosphine-substituted ethoxy carbene complexes

The complex that will be discussed is the [Mo(CO)₃(DPPE)C{(OEt)(C₄H₃O)}], **8**.

⁴⁶ Meca, L., Dvorak, D., Ludvik, J., Cisarova, I., Stepnicka, P., *Organometallics*, 23, **2004**, 2541

⁴⁷ Szesni, N., Hohberger, C., Mohamed, G.G., Burzlaff, N., Weibert, B., Fischer, H., *J. Organomet. Chem.*, 691, **2006**, 5753

For the synthesis of **8**, the following reaction scheme was followed:



Scheme 2.3: Synthetic route to obtain 8

Complex **8** was synthesised using the method outlined by Barluenga.¹¹ The starting materials, **1** and DPPE, were reacted under reflux in toluene. The solution turned from the red colour of **1** to the deep brown colour of **8**. The reaction was monitored by TLC analysis. Two product bands could be seen on the TLC plate. The product bands were *fac*- and *mer* isomers of **8**. The *fac* isomer was more polar and eluted last (in hexane); this isomer was pink-purple in colour. The *mer* isomer was brown-purple in colour and eluted before the *fac* isomer. Purification was achieved through recrystallisation with a yield of 65%.

Isomers and conformers which could be formed in this reaction are shown in Figure 2.23, below.

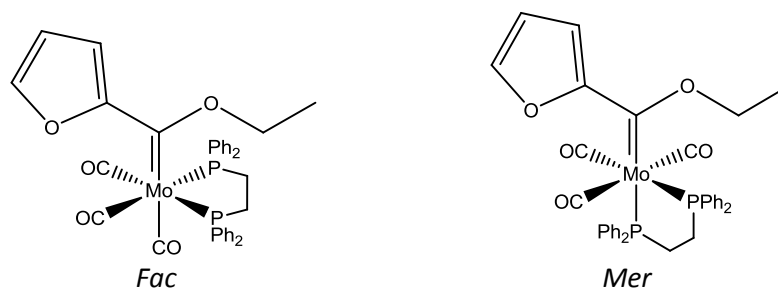


Figure 2.23: The isomers possible in a diphosphinated Fischer carbene complex, 8

There can be *syn* and *anti* conformers in addition to the isomers shown above in the solid state. This study showed that the *syn* set of conformers was isolated in the solid state (Figure 2.29).

2.4.1 Infrared spectroscopy

The *mer*-isomer of **8** is of the type $M(CO)_3L_2L'$ and has a symmetry of C_{2v} , with the carbonyls forming a T-structure geometry. The normal stretching modes of the carbonyls are shown below:³⁷

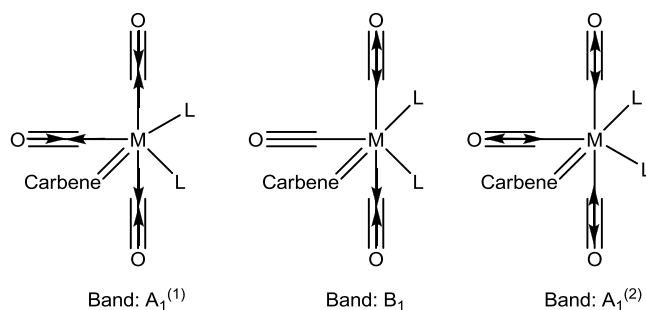


Figure 2.24: The stretching bands of a *mer* complex of the type $M(CO)_3L_2L'$

A *fac* complex of the type $M(CO)_3L_2L'$ is expected to have only two stretching bands characterised by the stretches in the following figure.

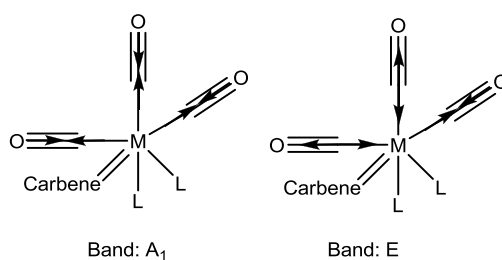


Figure 2.25: The stretching bands of a *fac* complex of the type $M(CO)_3L_2L'$

The band of highest frequency corresponds to $A_1^{(1)}$; it has a weak intensity which may result in it not being observed in the spectrum.³⁷ The frequency order of the $A_1^{(2)}$ band and the B_1 band depends on the nature of the complex under observation.³⁷ The B_1 band is expected to be intense.³⁷

The carbonyl stretching frequency observed in this complex is unlike any described before in this study, and indeed in literature for molybdenum complexes, and as a result no comparison can be drawn to previous complexes in this study. Comparisons will therefore necessarily come from chromium or tungsten analogues. This complex fits a three carbonyl IR pattern and the others in this study have fitted four- or five carbonyl IR patterns. This compound was purified using recrystallisation, and later column chromatography. However, before making the KBr pellets for the IR, the crystals were not manually separated. It can be said that the data in Table 2.12 is that of a mixture of isomers.

The molybdenum complex (**8**) in Table 2.12 shows very good correlation to the tungsten analogues (**P** and **R**). The same is true for the B_1 and $A_1^{(2)}$ bands for the chromium analogues (**Q** and **O**), but this observation does not hold for the $A_1^{(1)}$ band.

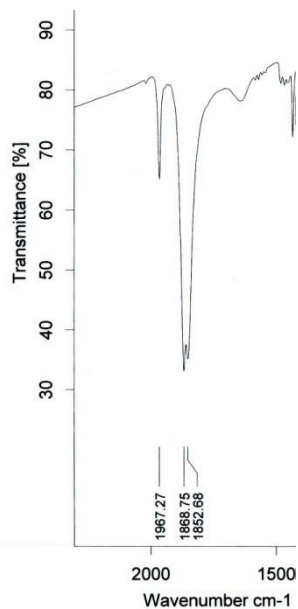
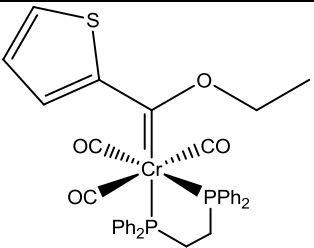
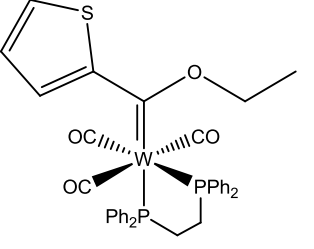


Figure 2.26: Carbonyl region of experimental IR spectrum of **8** (KBr)

Table 2.12: IR frequency assignments for **8**, including literature values

Complexes	Carbonyl Stretching frequency (cm ⁻¹)		
	A ₁ ⁽¹⁾	B ₁	A ₁ ⁽²⁾
<p>8</p>	1967 (m)	1869 (vs)	1853 (w)
<p>O: <i>Fac</i>-[Cr(CO)₃(DPPE)C{(OEt)(C₄H₃O)}]⁴⁸</p>	2007 (vw)	1863 (s)	1837 (s)
<p>P: <i>Mer</i>-[W(CO)₃(DPPE)C{(OEt)(C₄H₃O)}]¹⁴</p>	1962 (s)	1866 (s)	1841 (s)

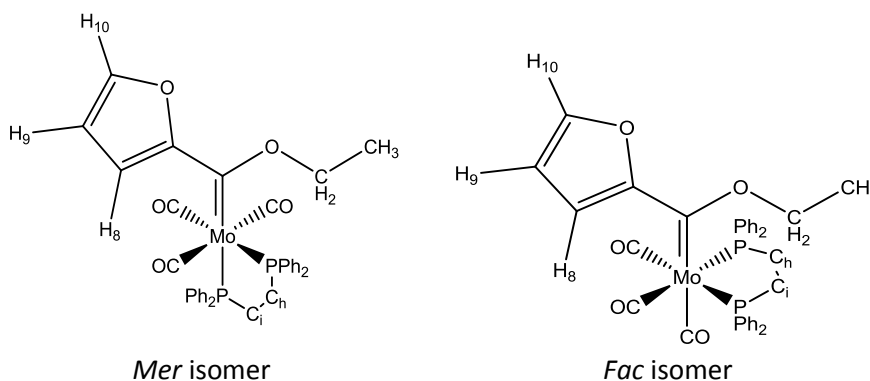
⁴⁸ Landman, M., Luj, R., Fraser, R., van Rooyen, P.H., Conradie, J., *J. Organomet. Chem.*, 752, **2014**, 171

Complexes	Carbonyl Stretching frequency (cm ⁻¹)		
	A ₁ ⁽¹⁾	B ₁	A ₁ ⁽²⁾
 Q: <i>Fac</i>-[Cr(CO)₃(DPPE)C{(OEt)(C₄H₃S)}]³²	2005 (vw)	1862 (s)	1840 (s)
 R: <i>Mer</i>-[W(CO)₃(DPPE)C{(OEt)(C₄H₃S)}]¹⁴	1966 (s)	1866 (s)	1846 (s)

All data was obtained using KBr pellets as the matrix.

2.4.2 ¹H NMR spectroscopy

The ¹H NMR spectral data for **8** is summarised in Table 2.13, below. The numbering system is illustrated below.



The two isomers were distinguishable on the one NMR spectrum (Figure 2.27) because the position of the second phosphine group influences the electron density in the whole molecule. When both phosphines are *cis* to the carbene (*fac* isomer) there is no *trans* influence between the carbene and a phosphine and therefore the carbene competes with a carbonyl for back bonding electrons and electron density. When one phosphine is *trans* to the carbene (*mer* isomer), the carbene will be competing against the weaker π-acceptor, the phosphine, for back-bonding electrons and electron density. This means that one would expect the carbene moiety's protons in the *mer* isomer to be more shielded and therefore more upfield than in the *fac* isomer. This is the general trend, as shown by the data in Table 2.13, and was not observed in this case. The dominant isomer was observed to be the *fac* isomer.

Upon comparison to **1**, it is found that the protons of both isomers are shifted upfield. This indicated that the DPPE ligand, regardless of which isomeric position it assumes, loses its electron density to the other ligands, resulting in their protons becoming more shielded. There is a very good correlation between observed peak shifts and literature peak shifts^{32,14} as shown by the data in Table 2.13.

Table 2.13: ¹H NMR assignments for **8**, including literature values

Complexes	Chemical Shift (δ , ppm), Multiplicity and coupling constants (J, Hz)							
	H ₁₀	H ₉	H ₈	CH ₂	CH ₃	PC _H H ₂	PC _I H ₂	P(Ph) ₂
8^c <i>Mer isomer*</i>	7.27 dd J = 1.6, 3.2	6.30 dd J = 1.7, 3.5	6.61 dd J = 0.7, 3.5	4.70 q J = 7.0	1.34 t J = 7.1	3.09- 2.86 m	2.61- 2.49 m	7.70-7.63 (m) 7.59-7.53 (m) 7.40-7.031 (m) 7.16-7.14 (m)
8^c <i>Fac Isomer</i>	7.60 dd J = 1.9, 2.3	6.00 dd J = 1.7, 3.6	6.70 dd J = 0.8, 3.5	4.84 q J = 7.1	1.21 t J = 7.1	2.82- 2.64 m	2.50- 2.36 m	7.70-7.63 (m) 7.59-7.53 (m) 7.40-7.31 (m) 7.16-7.14 (m)
1^a	7.83 dd J = 0.8, 1.7	6.58 dd J = 1.7, 3.7	7.09 dd J = 0.8, 3.6	5.03 q J = 7.1	1.62 t J = 7.2			
O^a: <i>Fac-</i> [Cr(CO)₃(DPPE)C{(OEt)(C₅H₃O)}] ⁴⁸	7.66 d J = 1.7	6.41 dd J = 1.7	6.54 d J = 3.4	4.60 q J = 7.0	1.28 t J = 7.0	2.79- 2.90 m	2.58- 2.74 m	7.30-7.46 (m) 7.67-7.78 (m)
P^c: <i>Mer-</i> [W(CO)₃(DPPE)C{(OEt)(C₅H₃O)}] ¹⁴	7.11 dd J = 0.8, 1.7	6.30 dd J = 1.7, 3.5	6.65 dd J = 0.8, 3.5	4.51 q J = 7.0	1.35 t J = 7.0	2.47- 2.80 m	2.47- 2.80 m	7.28-7.46 7.59-7.73 m
R^c: <i>Mer-</i> [W(CO)₃(DPPE)C{(OEt)(C₅H₃S)}] ¹⁴	7.36- 7.70 m	6.84 dd J = 3.9, 5.1	7.53 dd J = 1.1, 3.9	4.39 q J = 7.0	1.24 t J = 7.0	2.66- 2.82 m	2.53- 2.66 m	7.30-7.47 7.63-7.70 m

*It was ascertained that this is the *mer* isomer from comparison to the data obtained by Pretorius¹⁴

^aSolvent: CDCl₃ (7.24 ppm)

^cSolvent: CD₂Cl₂ (5.32 ppm)

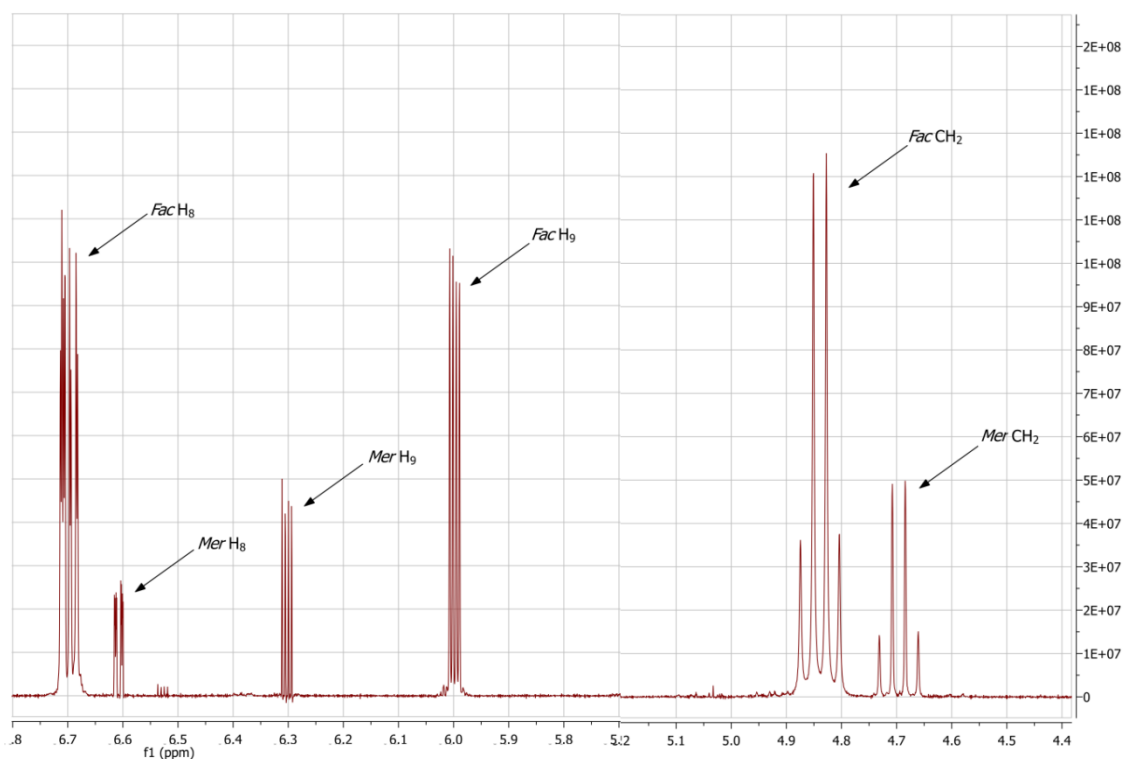


Figure 2.27: Experimental ^1H NMR of **8** (CD_2Cl_2)

2.4.3 ^{13}C NMR spectroscopy

The ^{13}C NMR data for **8** is summarised in Table 2.14, below. The data has been presented based on the following numbering system.

Since the concentration of the *mer* isomer was so low, no assignable peaks for this isomer was observed in the carbon spectrum. A carbonyl *trans* to a carbene is the most deshielded and is found the furthest downfield, while a carbonyl *trans* to a phosphine group is the most shielded and its peak appears the most upfield of the carbonyl peaks. Additionally it is interesting to note that the carbons in the $\text{Ph}_2\text{P}-\text{CH}_2-\text{CH}_2-\text{PPh}_2$ groups are discernible from each other even when both phosphine moieties are attached to the metal *cis* to the carbene.

In comparison to **1** and **3**, there is no significant shift in the position of the peaks observed (Table 2.14). These values correlate well with the available literature.^{32,14}

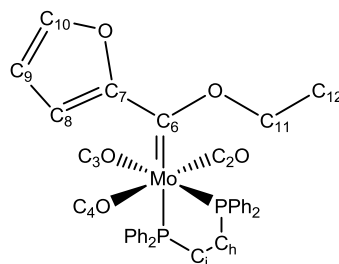


Table 2.14: ^{13}C NMR Assignments for **8**, including literature values

Complexes	Chemical shift (δ , ppm)												
	C ₁ O	C ₂ O, C ₄ O	C ₃ O	C ₁₀	C ₉	C ₈	C ₇	C ₆	C ₁₁	C ₁₂	PC _h	PC _i	Aromatic Protons
8^c <i>Fac</i> isomer	225.1 6	224. 6	214. 8	146. 0	112. 4	112. 7	163. 1	308. 1	75. 7	15. 3	27. 4	30. 6	131.7- 131.2 128.6- 128.5
3^c	220.2	211. 9	216. 8	148. 7	112. 1	112. 9	164. 8	304. 8	76. 9	15. 2			128.5- 130.1 128.6 128.5
1^a	213.5	206.0		150. 0	113. 2	114. 6	164. 4	301. 1	76. 6	15. 2			
O^a: <i>Fac</i>- [Cr(CO)₃(DPPE)C{(OEt)(C₅H₃O)}]⁴⁸	235.8	220. 1	225. 6	146. 1	111. 8	112. 5	164. 3	316. 3	73. 7	15. 6	30. 7	28. 4	138.7 132.7 130.6 131.3
P^c: <i>Mer</i>- [W(CO)₃(DPPE)C{(OEt)(C₅H₃O)}]¹⁴		208. 1	217. 8	144. 9	112. 3	107. 3	170. 0	279. 1	74. 6	15. 5	30. 1	32. 5	137.3 132.2 128.8 130.2

^aSolvent: CDCl₃ (77 ppm)

^cSolvent: CD₂Cl₂ (53.5 ppm)

2.4.4 ^{31}P NMR spectroscopy

The data obtained from the ^{31}P NMR spectrum for **8** is summarised in Table 2.15, below.

Table 2.15: ^{31}P NMR assignments for **8**, including literature values

Complex	Chemical shift (δ , ppm)	
	P(<i>trans</i> to carbene)	P (<i>Trans</i> to CO)
8^c-<i>mer</i>	59.08	54.57
8^c-<i>fac</i>		55.24
3-<i>trans</i>^c	40.00	
3-<i>cis</i>^c		37.67
O^a: [Cr(CO)₃(DPPE)C{(OEt)(C₅H₃O)}]³²-<i>Mer</i>	83.4	78.6
P^c: [W(CO)₃(DPPE)C{(OEt)(C₅H₃O)}]¹⁴-<i>Mer</i>	40.51	41.66

^aSolvent: CDCl₃

^cSolvent: CD₂Cl₂

The data in Table 2.15 shows that when compared to complex **3**, there is significant deshielding in **8** which results in the chemical shifts moving downfield. In the case of the *fac* isomer, both phosphorus atoms are in the same environment which results in there being one intense peak on the NMR spectrum. In the case of the *mer* isomer, there is a significant difference in the electron environments in which the two phosphorous atoms find themselves. The phosphorous atom *trans* to the carbene will be in competition with the carbene for the electrons available for π -donation, whereas the phosphorous atom *trans* to a carbonyl will compete with the carbonyl. This means that the phosphorous atom *trans* to the carbene will have a higher chemical shift (be further downfield) than the other phosphorous atom. The data for **8** (Table 2.15) shows a very good correlation to the data that was found for **3**. The literature data shows that both phosphorus peaks should be in the same region (within ± 4.8 ppm) and the data for **8** is grouped to within 4.5ppm. The data for **8** lies between the data found for the chromium (**O**) and tungsten (**P**) analogues, that is to say the trend is $W > Mo > Cr$.

The ^{31}P NMR spectrum in Figure 2.28 proves that the dominant isomer in the sample was in fact the *fac* isomer since the *fac* peak is more intense than the *mer* peaks.

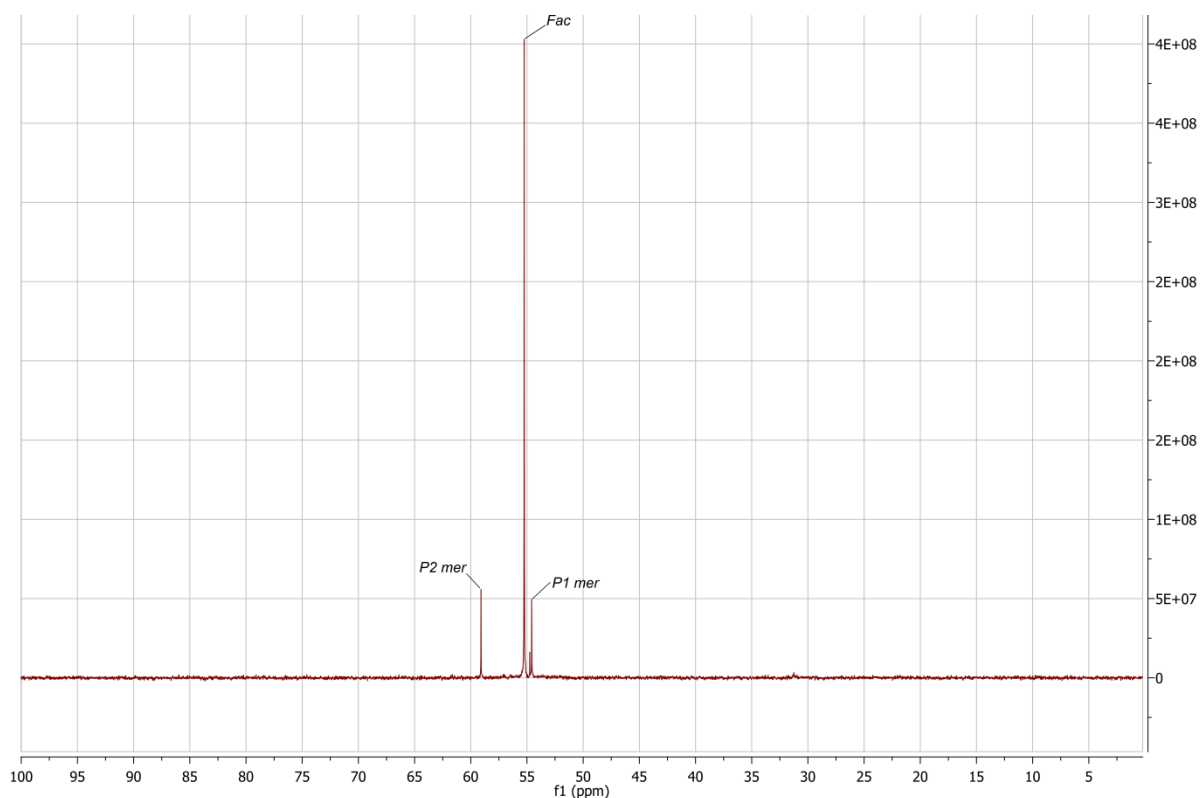


Figure 2.28: ^{31}P NMR spectrum of **8** (CD_2Cl_2)

2.4.5 X-ray crystallography

The crystal structure of **8-mer** was elucidated in full, and the ORTEP representation can be found in Figure 2.29, below.

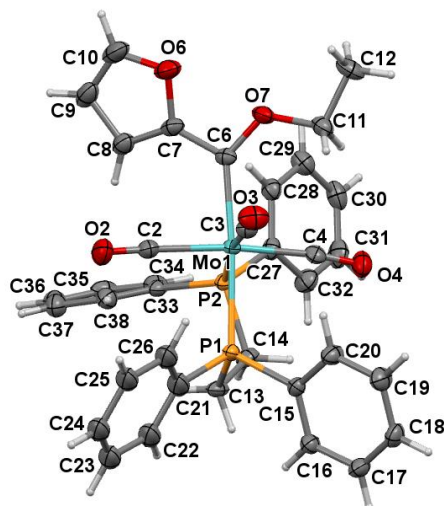


Figure 2.29: Crystal structure of **8-mer**

The crystal structure of **8-mer** adopted a *syn* conformation with respect to the oxygen atoms of the ethoxy and the furyl rings, as well as a *mer* isomeric configuration of the DPPE ligand. The same is true of the chromium DPPE structure synthesised by Fraser *et al.*⁴⁸ The crystal structure of **8-mer** is in contrast with the solution spectra of this molecule, which clearly favours the *fac* isomer. However, the tungsten DPPE analogue crystallised in the same form as **8-mer**.¹⁴

The crystal structure of **8-mer** shows that the furyl ring is rotated out of the plane of the ethoxy carbene carbon-metal plane by 19.3°. The two phenyl rings on P₁ are in an eclipsed conformation with the two carbene substituents. Defining the same plane as before (the two heteroatoms, C₆ and the metal), the furyl ring of **8-mer** is 25.5° out of this plane. A progression can be seen, in **1**, in addition to the carbene ligand, there were only unique carbonyl ligands (due to the symmetry of the space group) and the rotation of the furyl ring was 0° out of this plane. In **3-cis**, where there was one phosphine ligand, the rotation of the furyl ring was 7.6° out of this defined plane. Lastly, for **8-mer** where there are two phosphine ligands, the rotation of the furyl ring is 25.5° out of this plane. This indicates that as more carbonyl ligands are substituted, the complex becomes more distorted. For **8-mer**, the torsion angle between P₂-Mo-C₆-C₇ is 76.0°. This has also increased from **3-cis** (60.9°).

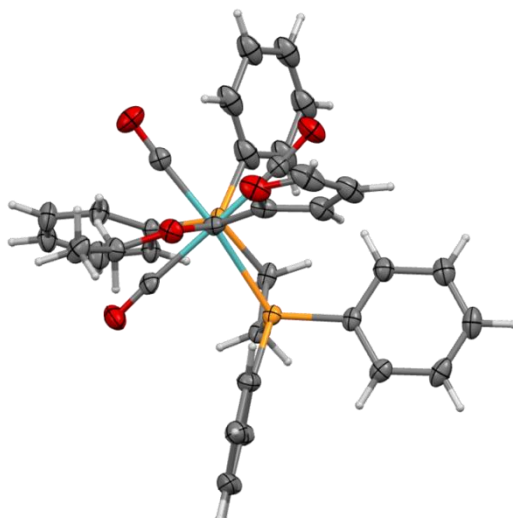


Figure 2.30: View down $C_6 \rightarrow Mo$ bond of *8-mer*

When looking along the $C_6 \rightarrow Mo$ bond of the molecule it is clear that the carbene's substituents will most likely always be eclipsed with some part of the molecule (Figure 2.30). In this case, the smaller ethoxy group is eclipsed with one of the *trans* phosphine's phenyl groups. This leaves the furyl moiety to be free of hindrance from the phosphine moiety and mostly staggered, albeit close to the planar phenyl belonging to the *cis* phosphine.

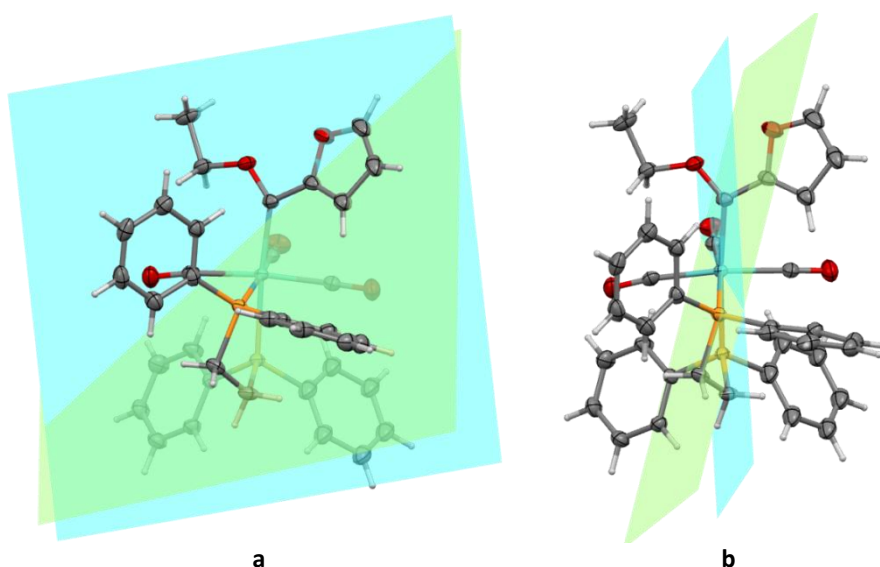


Figure 2.31: a) $C_7-C_8-C_9-C_{10}-O_6$ and $C_{12}-C_{11}-O_7$ planes; b) $Mo-P_1-C_{13}$ and $Mo-P_2-C_{14}$ planes through the molecule

The furyl ring is twisted 15.4° out of the ethoxy plane (Figure 2.31a). Although the *cis* phosphine is also closer to the furyl moiety, the angle of twist is smaller than what is observed for *3-cis* (refer to Figure 2.22). The ethane moiety of the DPPE group is twisted by 48.6° (Figure 2.31b).

The following table of data will make use of the numbering scheme shown below. Hydrogen atoms have been omitted for clarity.

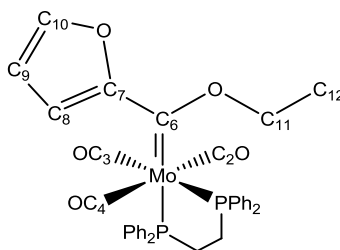


Table 2.16: Tabulated bond lengths of the crystal structure of **8-mer**, along with that for **3-cis**, **1** and literature values

Bond	Bond Length (Å)			
	8-mer	1	3-cis	O: [Cr(CO) ₃ (DPPE)C{(OEt)(C ₄ H ₃ O)}] ³²
O ₆ -C ₁₀	1.347(4)	1.45(2)	1.348(3)	
O ₆ -C ₇	1.383(3)	1.49(3)	1.376(3)	1.39(3)
C ₆ -C ₇	1.457(4)	1.41(4)	1.447(4)	1.46(7)
O ₇ -C ₆	1.336(3)	1.38(3)	1.329(4)	
C ₉ -C ₁₀	1.332(5)	1.23(2)	1.341(5)	1.32(8)
C ₈ -C ₉	1.429(4)	1.416(14)	1.403(4)	1.42(5)
C ₇ -C ₈	1.356(4)	1.32(2)	1.365(4)	1.35(7)
Mo-C ₆	2.133(3)	2.173(7)	2.180(3)	1.994(4)
Mo-C ₂	2.023(3)	2.147(12)	2.036(3)	1.881(5)
Mo-C ₄	2.018(3)		2.038(4)	
Mo-C ₃	1.985(3)	1.948(12)	1.982(3)	
Mo-P ₁ (<i>trans</i> to carbene)	2.287(1)			2.355(3)
Mo-P ₅ (<i>trans</i> to carbonyl)	2.522(7)		2.562(8)	2.378(1)

Upon addition of the DPPE ligand to **1**, the following differences were noted when comparing the crystal bond length data found in Table 2.16: the bond lengths that increased are the bonds between C₆-C₇, C₇-C₈, C₈-C₉, C₉-C₁₀, and Mo-C₃. The bond lengths that decreased are O₆-C₁₀, O₆-C₇, O₇-C₆, Mo-C₆ and Mo-C₂.

Both Powell *et al.*⁴⁹ and Barluenga *et al.*¹¹ found that both of the Mo-P bond lengths in their molecules were similar in size. This is not observed in the case of **8-mer**, however it must be noted that the diphosphine ligands used by Powell *et al.*⁴⁹ and Barluenga *et al.*¹¹ were not DPPE ligands, simply diphosphine ligands. It should also be noted that both of these complexes were *fac* complexes whereas **8-mer** is a *mer* isomer. There is a similarity between the Mo-C₆ bond lengths of **8-mer**, Barluenga *et al.*¹¹ and Powell *et al.*⁴⁹ (2.133(3) Å, 2.135 Å and 2.173 Å, respectively). There is a great similarity between the heteroatom-C₆ bond length observed for **8-mer** and Powell *et al.*⁴⁹ (1.336(3) Å and 1.333 Å, respectively), but this is not the case for the same bond in Barluenga *et al.*'s¹¹ complex (1.314 Å).

⁴⁹ Powell, J., Farrar, D.H., Smith, S.J., *Inorg. Chim. Acta.*, 85, 1984, L23

This data shows that the carbene-metal bond decreased in length from **3-cis** to **8-mer**, which means that there was an increase in back-bonding and the bond became stronger and increased in double bond character as a result of adding a DPPE ligand to the complex. This is expected because the triphenylphosphine ligand is not as good a π -acceptor as the carbonyls therefore there is increased back bonding to the carbene. This results in the expectation that the C₆-C₇ bond will increase, which was indeed the case. There was a negligible change in the bond lengths of the two carbonyls that are *trans* to each other indicating that there was no effect on the net bond strength or bond character. The carbonyl *trans* to the phosphine, however, had a large decrease in bond length, indicating that there was a large increase in back-bonding to this group, and that the bond has increased in strength - this reinforces the theory of the *trans* effect where one of two *trans* carbonyl ligands will be substituted by a weaker π -acceptor before any other carbonyls are substituted. The *mer* arrangement of this complex is expected since a carbonyl ligand *cis* to the carbene would be substituted first by one of the phosphine atoms (placing the phosphine in an equatorial position) to limit electron competition from its *trans* carbonyl (because the carbonyl is a stronger π -acceptor than both carbenes and phosphines). The second phosphine atom coordinates *trans* to the carbene (axial position) to limit steric strain. This can be said because the angle between the carbonyl plane and the carbonyl *trans* to the carbene is smaller in **1** than the angles between any of the planar carbonyls in **8-mer** (see Table 2.17, Table 2.5). After the addition of one phosphine (triphenylphosphine) moiety in **3-cis**, the adjacent carbonyls are pushed further away (larger angles as seen in Table 2.11), the same phenomenon should be observed with the addition of the first DPPE phosphine. This results in the *mer* isomer more sterically favourable. This is commonly observed with metals like tungsten and chromium.^{32, 14}

In the case of chromium, the *mer* isomer is not seen at all.⁴⁸ The tungsten analogue allows for stable *fac* and *mer* isomers, and both are isolable¹⁴. Barluenga found that the *fac* and the *mer* isomer can be interchanged depending on the temperatures the complexes are subjected to.¹¹ This means that in practice, thermodynamics can dominate which isomer is formed. As a result of this, it is not clear which isomer is more stable than the other and thus it is not unreasonable to observe one isomer in solution and another in the solid state.

The data in Table 2.17 shows that there is somewhat of a deviation from the ideal octahedral bond angle of 90 ° in complex **8-mer**, with the C₆-Mo-P₁ (*cis*) bond angle being 101.09(7) °. This is probably due to the bulkiness of the carbene moiety, the large phosphorous atom on the phosphine moiety and the cone angle of the diphenylphosphine which push each other apart. Additionally it could be

attributed to the bite angle of the bidentate ligand. The remainder of the angles shown in Table 2.17 draw a good comparison between **3-cis**, **8-mer** and the chromium analogue made by Fraser.³²

Table 2.17: Crystal structure bond angles of 8-mer, as well as that of 3-cis, 1 and literature values

Angle	Angle size (°)			
	8-mer	1	3-cis	O: [Cr(CO) ₃ (DPPE)C{(OEt)(C ₄ H ₃ O)}] ⁴⁸
O ₇ -C ₆ -C ₇	104.8(2)	102.6(7)	103.6(2)	103.33(14)
C ₆ -Mo-C ₂	89.46(11)	91.6(7)	95.99(12)	-
C ₆ -Mo-C ₄	96.81(11)		87.70(11)	-
C ₆ -Mo-C ₃	85.67(10)	92.6(7)	91.81(11)	-
C ₆ -Mo-P ₁ (<i>cis</i>)	101.09(7)		94.03(7)	98.6(2)
P ₂ (<i>trans</i>)-Mo-P ₁ (<i>cis</i>)	80.44(1)			83.38(4)

2.5 Computational analysis

It was not necessary to calculate all of the possible conformations discussed at the beginning of each section for the different complexes. The structural model used for the calculations in this chapter was based on a recent study of conformations of pentacarbonyl carbene complexes. Thompson *et al.*³² found that for pentacarbonyl carbene complexes substituted with ethoxy and furyl moieties, the *anti* conformation is more stable. The optimised conformations that were attained were similar to those of the crystal structures obtained for these complexes, in most cases. In the case where the crystal structure and the solution data was not in agreement, both isomers were computed and compared.

The numbering system adopted for the tables and figures in this section is the same as that used throughout the previous sections (the figures at Table 2.3, Table 2.14).

No imaginary frequencies were found for the computational data of any of the complexes presented.

The two isomers of the *anti*-conformation of **3** were computed, *cis* and *trans*. The *cis* isomer gave a lower total energy and is approximately 6.3 kJ/mol more stable than the *trans* isomer. The crystal obtained for **3** was a *cis* isomer.

The optimised structures of **8-fac** and **8-mer**, are shown in Figure 2.32; this shows that both the *fac* and the *mer* are in an *anti* conformation. The *fac* isomer gave a lower total energy and is approximately 0.5 kJ/mol more stable than the *mer* isomer. Since this is a very small difference in energy, this result explains the anomalies found in the solution data obtained and the x-ray diffraction studies. From this it is clear that both isomers are energetically feasible. It is not unexpected, then, to obtain solution data of one isomer and crystal data of the other isomer.

However differences may also be due to the fact that the x-ray diffraction studies confirmed the conformation to be *syn*.

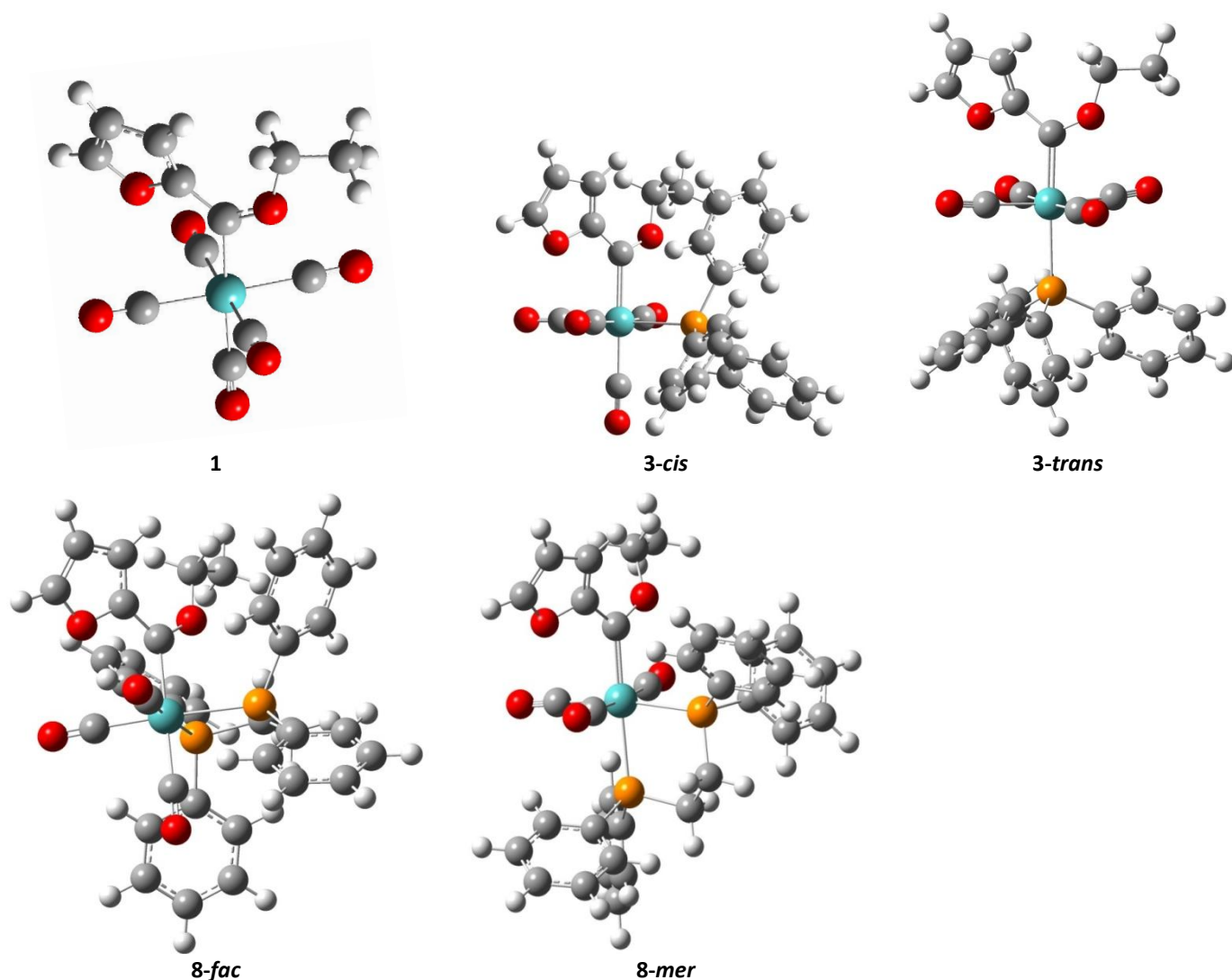


Figure 2.32: Optimised structures of **1**, **3-cis**, **3-trans**, **8-fac** and **8-mer**

The bond lengths that were found for **1**, **3** (*cis* and *trans*) and **8** (*fac* and *mer*) using the computational model are given and compared with the crystal structure's data in Table 2.18.

Table 2.18: Bond length comparison of **1**, **3** and **8**

Bond	Average Bond Length (Å)							
	Calculated					Crystal		
	1	3-cis	3-trans	8-fac	8-mer	1	3-cis	8-mer
Mo-C ₁	2.08	2.047	2.058	2.017	2.033	2.029(10)	2.021(4)	
Mo-C ₆	2.17	2.184	2.125	2.170	2.094	2.173(7)	2.180(3)	2.133(3)
C ₆ -C ₇	1.45	1.455	1.458	1.459	1.464	1.41(4)	1.447(4)	1.457(4)
O-C ₆	1.34	1.334	1.345	1.346	1.363	1.38(3)	1.329(4)	1.336(3)
Mo-P ₁		2.635	2.631	2.566	2.588		2.562(8)	2.522(7)
Mo-P ₂				2.567	2.590			2.287(1)

Upon comparison of the bond lengths of the crystal structure and the theoretical study as shown in Table 2.18, it can be seen that the correlation between the theoretical study and the actual crystal structure is superb. The computational study isolated a minimum for the complexes computed, the structures which were obtained from the crystals were in the same orientation. This data implies that the level of theory is adequate to accurately represent this system.

The theoretical data for **3-cis** correlates very well with the crystal data for **3-cis**. There is a very small difference in the M-P bond length between the *cis*- and *trans* isomers of **3**, but the *trans* bond length is shorter.

The bond lengths obtained for the *fac* isomer and the *mer* isomer show very little deviation in the Mo-CO, C₆-O and C₆-C₇ bond lengths. In the *fac* isomer, the bond lengths of the Mo-P bonds are almost identical in length, whereas for the *mer* isomer, there was a small difference. Also the Mo-C₆ bond is quite a bit longer in the *fac* than in the *mer* isomer. The bond lengths of the *mer* isomer correlate well with the crystal structure obtained. This was expected since the crystal structure that was obtained was in the *mer* isomeric form.

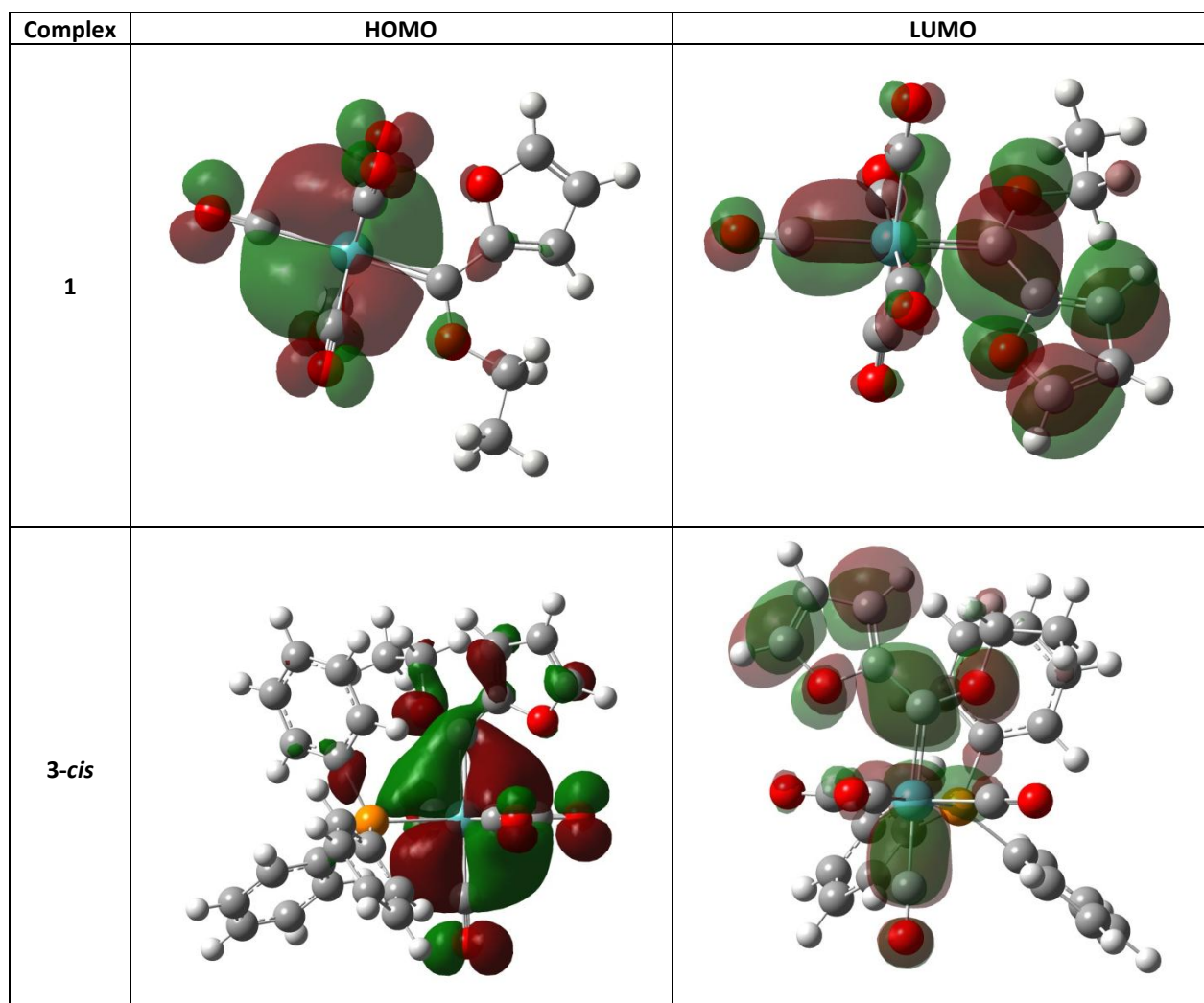
The calculations accurately predicted observations of the crystal data. One such observation was that the Mo-C₆ bond length increased from **1** to **3**, but decreased from **1** to **8**. Another such observation is that the M-phosphorous bond length decreased from **3** to **8**.

The calculated HOMO and LUMO plots for **1**, **3** (*cis* and *trans*) and **8** (*fac* and *mer*) are shown in Figure 2.33.

For **1**, the main contribution to the LUMO corresponds to a 3p_z orbital on the carbene carbon. The main contributions for **3-cis** and **3-trans** correspond to a 2p_z orbital on the carbene carbon in both isomers. Finally, those for the **8-fac** and **8-mer** isomers correspond to a 2p_x orbital and a 2p_z orbital, respectively on the carbene carbon. Upon visual inspection of the LUMO's in these complexes (Figure 2.33) they are found to be centred around the carbene moiety and the carbonyls, except in the case of **3-trans** and **8-mer**. Here, the LUMO is centred on the metal and the phosphorous atom which is *trans* to the carbene. The LUMO is the site where nucleophilic attack will occur on this molecule (from another molecule).

The main contributions to the HOMO of **1**, **3-cis**, **3-trans**, **8-fac** and **8-mer** all correspond to a d atomic orbital on the molybdenum atom of each complex. Since the HOMO of all the complexes computed was found to be most concentrated on the molybdenum atom, this means that this site is electron rich and nucleophilic attack will occur from the metal atom to another molecule. Since the

frontier orbitals determine the reactivity of the complex, computational articles focusing on the metathesis reaction catalysed by Fischer carbene complexes use frontier orbital considerations to assess the system.⁵⁰



⁵⁰ a) Nakatsuji, H., Ushio, J., Han, S., Yonezawa, T., *J. Am. Chem. Soc.*, 105, **1983**, 426; b) Tlenkopatchev, M., Fomine, S., *J. Organomet. Chem.*, 630, **2001**, 157; c) Du Toit, J.I., van Sittert, C.G.C.E., Vosloo, H.C.M., *J. Organomet. Chem.*, 738, **2013**, 76

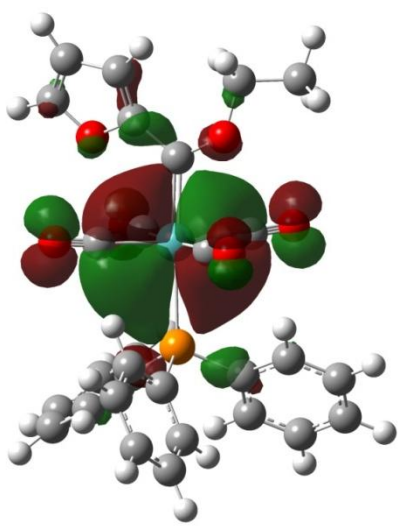
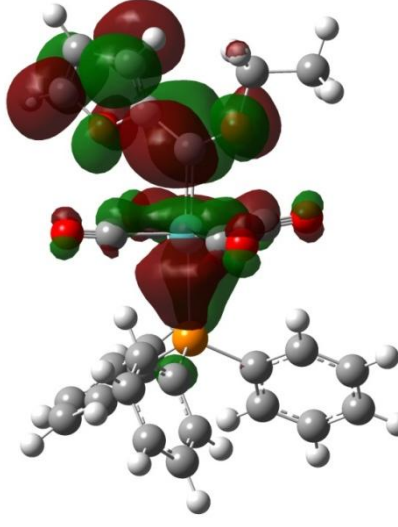
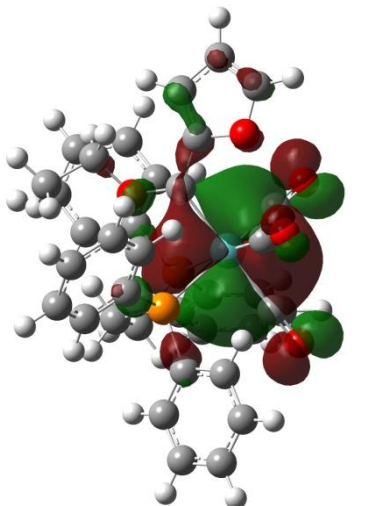
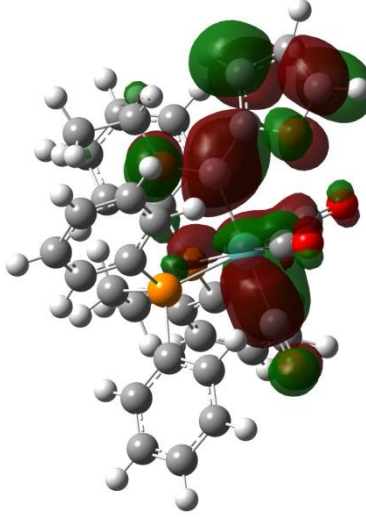
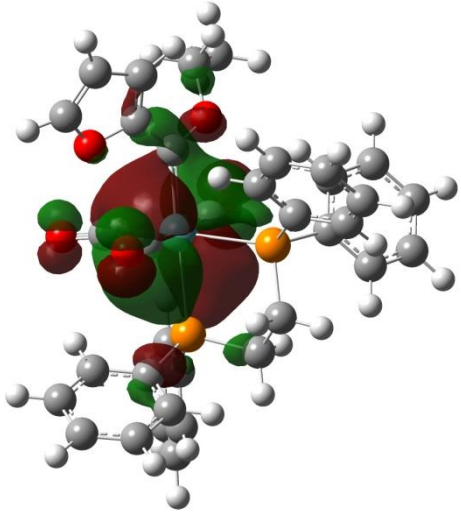
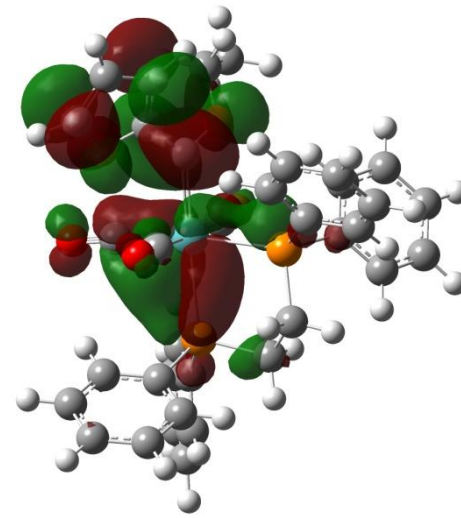
Complex	HOMO	LUMO
3-trans		
8-fac		
8-mer		

Figure 2.33: HOMO and LUMO illustrations of 1, 3-cis, 3-trans, 8-fac and 8-mer

Table 2.19: HOMO-LUMO gap in eV for 1, 3 and 8

Complex	HOMO-LUMO gap (eV)
1	+3.02
3-cis	+2.94
3-trans	+3.02
8-fac	+2.80
8-mer	+3.13

The reactivity of a complex can be measured, to an extent, by the HOMO-LUMO gap of the complex⁵¹. Upon substitution of Fischer carbene complexes with phosphine ligands, changes in reactivity during photocarbonylation reactions was determined using the HOMO-LUMO gap as a measure. The arylphosphine ligands have larger donor character than their alkylphosphine counterparts. As a result of this, monophosphinated complexes are expected to be the most reactive, while diphosphinated complexes are expected to be the least reactive because it becomes more difficult to substitute a carbonyl with each successive substitution. From the data in Table 2.19, it can be seen that **3-trans** will be the most reactive of the monophosphinated complexes and **8-fac** will be the most reactive of the diphosphinated complexes. However, the **8-fac** is predicted to be the most reactive (smallest gap) of the complexes in Table 2.19, and **8-mer** is predicted to be the least reactive (largest gap).

Figure 2.34 indicates that no region of exceptionally high electron density can be discerned for **1**, however the metal and the carbonyls hold the majority of the electron density, with the least amount of electron density being at the extremities of the carbene substituents. This figure shows that for both isomers of **3**, the carbonyls are somewhat electron rich. This change in the electron distribution (from **1**) is indicative of how the electron distribution has changed as a result of adding a weaker π -acceptor ligand to the molecule. The carbonyls have accepted more electrons from the metal, and one would expect that the metal-carbonyl bond will be stronger (and shorter) and in turn the carbon-oxygen bonds of the carbonyls will be weaker (and longer). The crystal data proves this hypothesis correct, and the data laid out in Table 2.18 shows that the carbon-oxygen bonds are longer and the carbon-metal bonds are, on average, shorter. There is a significant electron deficit in the region of the carbene carbon in **3-cis** and **3-trans**. This is shown to be the case by virtue of the fact that this is the site of the LUMO in these molecules. The electron deficit will facilitate the electrophilic attack in this region.

⁵¹ Arrieta, A., Cossío, F.P., Fernández, I., Gómez-Gallego, M., Lecea, B., Mancheño, M.J., Sierra, M.A., *J. Am. Chem. Soc.*, 122, **2000**, 11509

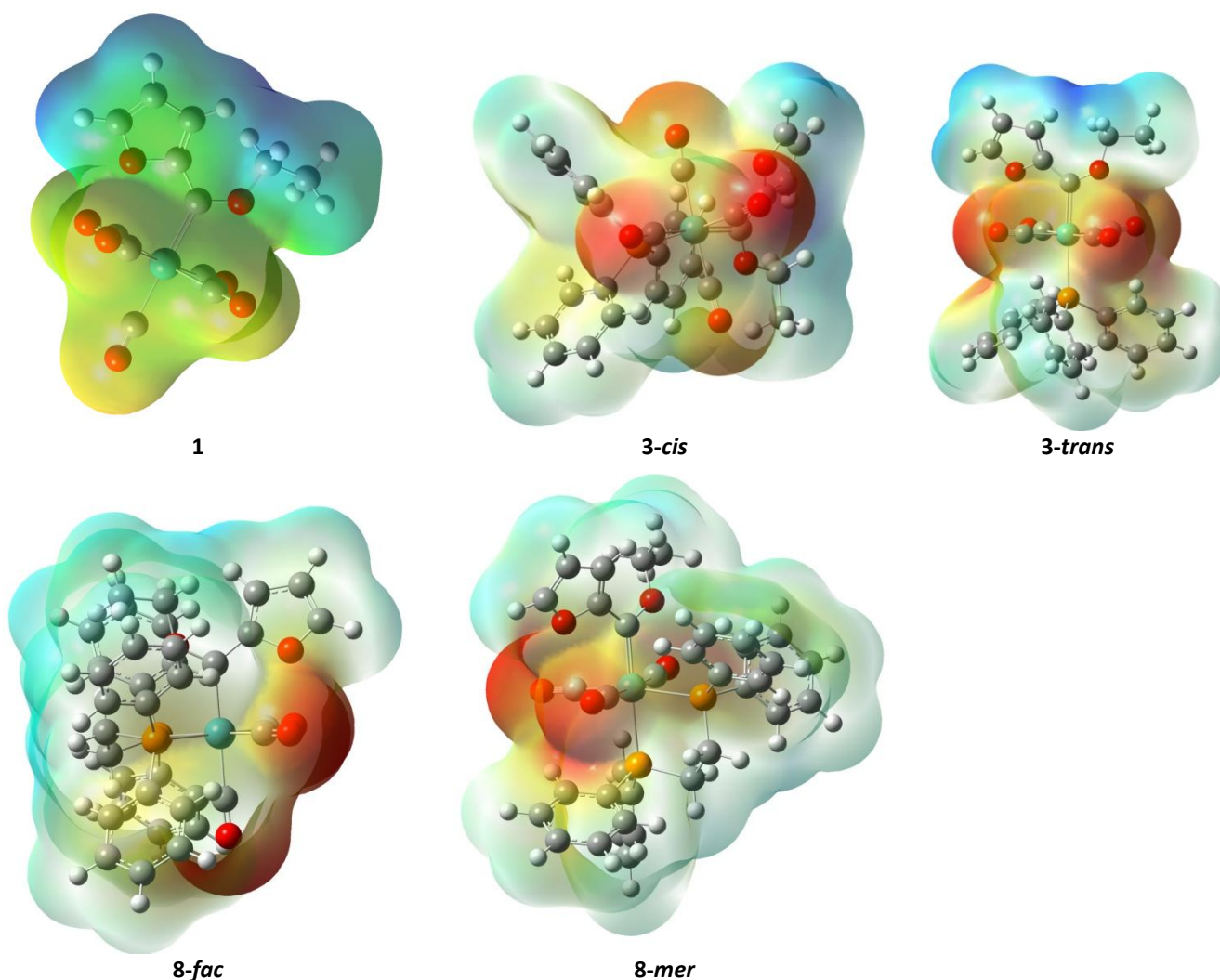


Figure 2.34: Electrostatic Potential Energy Map of 1, 3-*cis*, 3-*trans*, 8-*fac* and 8-*mer*

In the case of 8-*fac* and 8-*mer*, the electrostatic potential plots illustrate that the area of highest electron density is around the carbonyls. This is a somewhat interesting result since the HOMO does not lie there in either molecule.

There have been numerous analyses published regarding the IR spectra of complexes and compounds and how they correlate to those proposed by theoretical calculations. To correlate the theoretical IR frequencies with the experimental frequencies, most often a scaling factor is presented; these scaling factors change depending on which functional is used in the particular calculations. In this study, the computations were completed using B3LYP/Gen (6-31G* and LANL2DZ) method, while Rauhut and Pulay⁵² proposed a scaling factor of 0.963 when using B3LYP/6-31G*. This scaling factor gave an rms deviation of 19 cm⁻¹. Finlay and Stephens⁵³ obtained

⁵² Rauhut, G., Pulay, R., *J. Phys. Chem.*, 99, 1995, 3093

⁵³ Finlay, J.W., Stephens, P.J., *Mol. Struct. (Theochem)*, 357, 1995, 225

the same result. Scott and Radom⁵⁴ obtained a result of 0.9614 with an rms deviation of 34 cm⁻¹. In 2002, Zhang *et al*⁵⁵ proposed a formula for the scaling factor; this formula was $\alpha = v_{exp}/v_{calc}$; where v_{exp} represents the experimental data and v_{calc} represents the calculated data. A variation of this formula is used in the pages that follow since it gives the smallest rms value and is designed for the B3LYP/6-31G* method.

The generated IR plot shown in Figure 2.35 is good approximation of the shape of the recorded IR spectrum for **1**. This general shape follows for all monocarbene complexes of the type M(CO)₅L. In the recorded spectrum there are two strong, obvious peaks (assigned as A₁⁽¹⁾ and E bands) and the E band has two more discernible peaks (assigned as A₁⁽²⁾ and B₁). The experimental IR spectrum of **3** corresponds in shape to the generated IR, the only exception being that the B₂ band in the experimental spectrum is more obvious. The carbonyl region of the *trans*-isomer of **3** is shown in Figure 2.35.

Table 2.20: Comparison of theoretical IR frequencies and observed IR frequencies

Complex	Assignments	CO stretching frequencies (cm ⁻¹)			
		A ₁ ⁽¹⁾	B ₁	E	A ₁ ⁽²⁾
1	Observed	2068 (m)	1988 (m)	1923 (vs)	1942 (s)
	Calculated ^a	2031	1976	1954	1958
	Assignments	A ₁ ⁽¹⁾	B ₁	E	A ₁ ⁽²⁾
3-cis	Observed	2013 (m)	1890 (vs)	1865 (s)	1924 (m)
	Calculated ^a	1981	1898	1898	1913
	Assignments	A ₁	B ₁	E	
3-trans	Observed	2018	1944	1889	
	Calculated ^a	1995	1941	1914	
	Assignments	A ₁	B ₁	E	

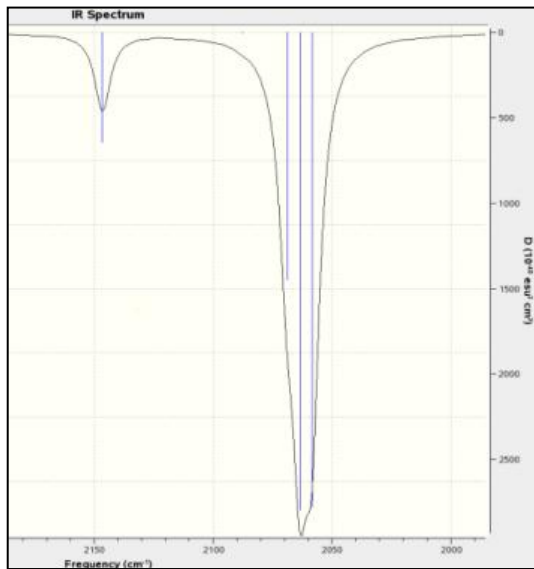
^aScaled calculated data

The data in Table 2.20 shows that the scaled calculated frequencies are consistently higher than the experimental values. This may be due to the experimental values being recorded in a matrix (KBr), whereas the calculated values are calculated assuming the sample is in the gas phase. The correlation between the experimental values observed and the calculated and scaled values is very good.

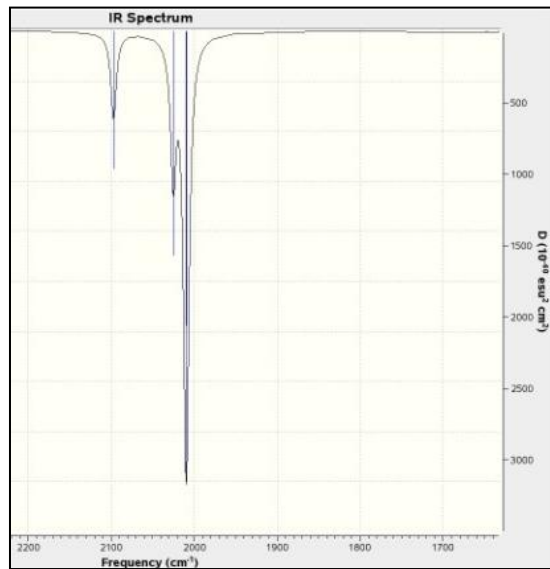
Due to the fact that the experimental IR was taken using a mixture of the two isomers of **8**, no comparisons could be drawn from the calculated IR data.

⁵⁴ Scott, A.P., Radom, L., *J. Phys. Chem.*, 100, **1996**, 16502

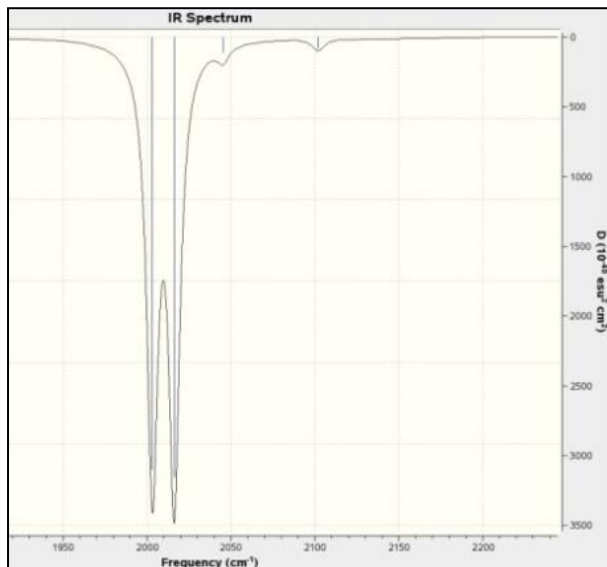
⁵⁵ Zhang, L., Zhang, Y., Tao, H., Sun, X., Guo, Z., Zhu, L., *J. Mol. Struct. (Theochem)*, 617, **2002**, 87



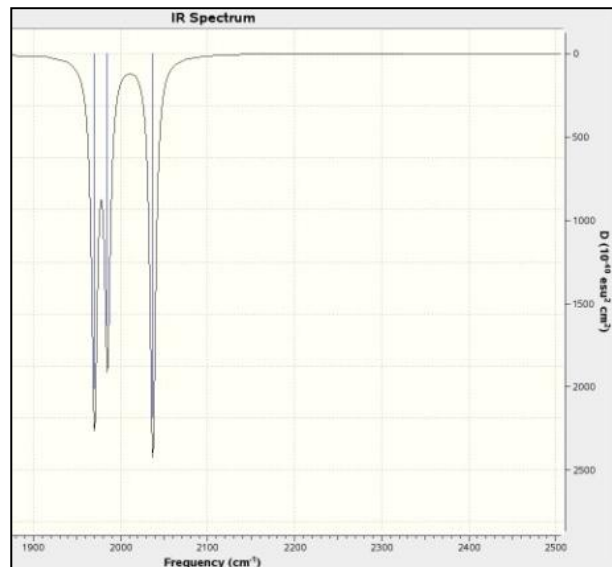
1



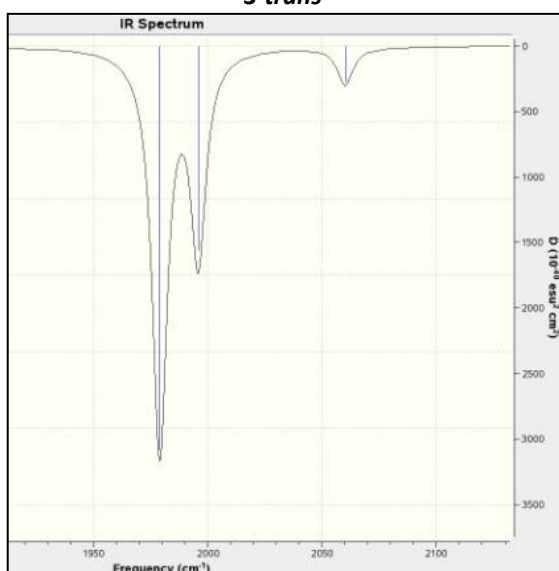
3-cis



3-trans



8-fac



8-mer

Figure 2.35: Carbonyl regions of the generated IR of 1, 3-cis, 3-trans, 8-fac and 8-mer

Chapter 3:

Amino Carbene Complexes

“The most beautiful experience we can have is the
mysterious – the fundamental emotion which
stands at the cradle of true art
and true science.”

– Albert Einstein

3.1 Introduction

Aminolysis reaction

Amino carbene complexes are readily formed by nucleophilic attack at the carbene carbon resulting in a substitution of the alkoxy carbonyl substituent for an amino one.¹ In a similar manner, thiocarbenes and arylcarbenes can be achieved.¹ The aminolysis reaction is incredibly simple and results in stable complexes and thus, unsurprisingly, has been used the most.² Amino carbene complexes were first synthesised in 1968 by Heckl, Werner and Fischer.³ Amino carbene complexes can be made in a variety of different ways. Examples include base catalysed substitution,⁴ Hegedus synthesis⁵ and nucleophilic attack.⁶ Amino carbene complexes frequently find application in Pauson-Khand cyclisation reactions.⁷ The catalyst shown in Figure 3.1 is the original catalyst used by Pauson and Khand.⁸ Amino carbene complexes have since been used for this reaction.⁷

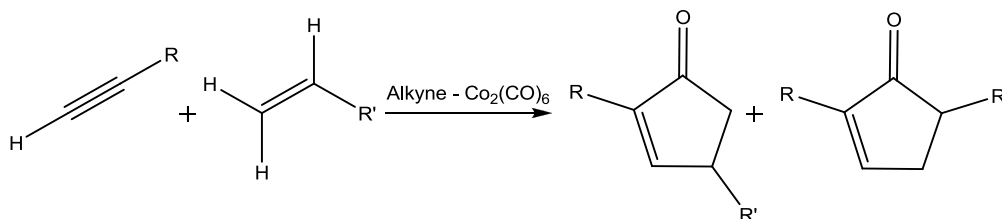


Figure 3.1: General Pauson-Khand cyclisation reaction⁸

Heteroaromatic rings

It has been found that the most reactive positions on a five-membered heteroaromatic ring are positions 2 and 5, which are those adjacent to the heteroatom.⁹ These positions have been shown to be more acidic than the 3 and 4 positions.¹⁰ This means that proton removal will preferentially occur at positions 2 and/or 5. In the case of thiophene, the heteroatom can accommodate both a positive charge or a negative charge; whereas furan can only accommodate a negative charge.^{11,12,13}

¹ Dötz, K.H., Tomuschat, P., *Chem. Soc. Rev.*, 28, **1999**, 187

² Andrada, D.M., Jimenez-Halla, J.O.C., Solá, M.J., *J. Org. Chem.*, 75, **2010**, 5821

³ Heckl, B., Werner, H., Fischer, E.O., *Angew. Chem. Int. Ed. Engl.*, 7, **1968**, 817

⁴ Bernsoni, C.F., Stronach, M.W., *J. Am. Chem. Soc.*, 115, **1993**, 1341

⁵ Imwinkelried, R., Hegedus, L. S. *Organometallics*, 7, **1988**, 702

⁶ Fischer, E. O., Winkler, E., Kreiter, C. G., Huttner, G., Krieg, B., *Angew. Chem., Int. Ed. Engl.*, 10, **1971**, 922.

⁷ Sabaté, R., Schick, U., Moreto, J.M., Ricart, S., *Organometallics*, 15, **1996**, 3611

⁸ a) Khand, I.U., Knox, G.R., Pauson, P.L., Watts, W.E., *J. Chem. Soc.*, **1971**, 36. b) Khand, I.U., Knox, G.R., Pauson, P.L., Watts, W.E., Foreman, M.I., *J. Chem. Soc.*, **1973**, 977.

⁹ Lotz, S., van Jaarsveld, N.A., Liles, D.C., Crause, C., Görls, H., Terblans, Y.M., *Organometallics*, 31, **2012**, 5371

¹⁰ Shatenstein, A.I., Kamrad, A.G., Shapiro, I.O., Ranneva, Y.I., Zvyagintseva, E.N., *Dokl. Kd. Nauk. SSSR.*, 168, **1966**, 364

¹¹ Abarca, B., Asensio, G., Ballesteros, R., Varea, T., *J. Org. Chem.*, 56, **1991**, 3224

¹² Kawase, T., Ueno, N., Oda, M., *Tetrahedron Lett.*, 33, **1992**, 5405

Barluenga *et al.*¹⁴ published a review detailing methods to produce heterocycles containing nitrogen, oxygen and both nitrogen and oxygen (Figure 3.2a, b and c, respectively) using amino and ethoxy carbene complexes of group VI metals. It was shown that group VI metals are versatile in their reactivity.

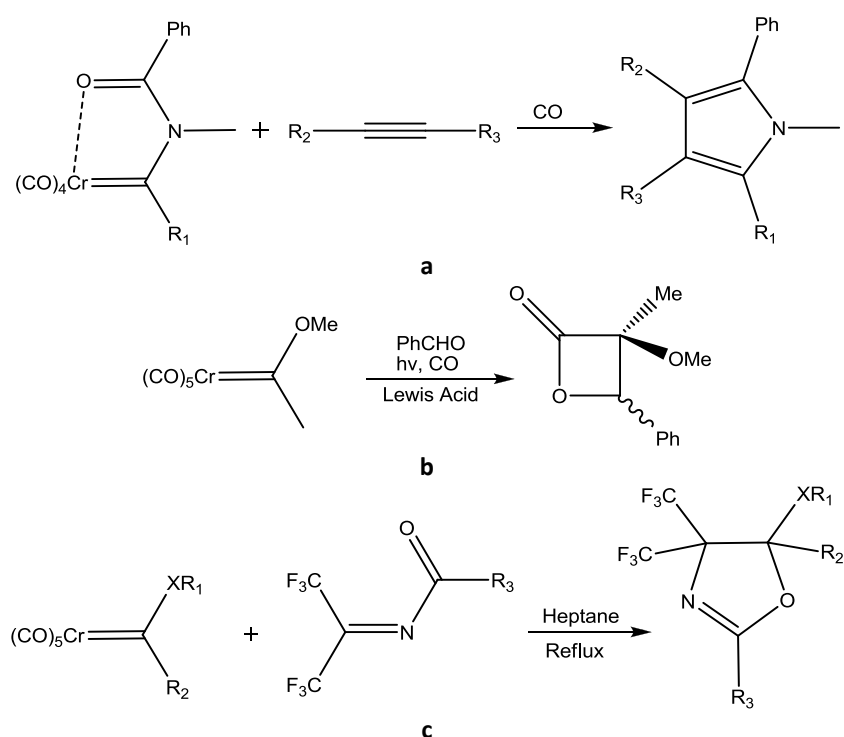


Figure 3.2: a) Synthesis of nitrogen-containing heterocycle; b) Synthesis of oxygen-containing heterocycle; c) Synthesis of mixed heterocyclic ring.¹⁴

Hong Ng *et al.*,¹⁵ synthesised Fischer carbene complexes containing a phosphole (Figure 3.3) as the five-membered ring, rather than the much more common furan, thiophene and pyrrole five-membered rings. It was found that these types of complexes induced greater conjugation between the carbene moiety and the heteroarene. This came as a result of the phosphole being less aromatic in nature than the other heteroarenes mentioned.¹⁵

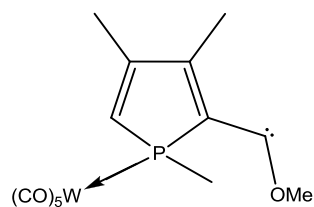


Figure 3.3: Representative phosphole¹⁵

¹³ Kawase, T., Muro, S., Kurat, H., Oda, M.J., *J. Chem. Soc. Chem. Commun.*, 23, **1992**, 778

¹⁴ Barluenga, J., Santamaria, J., Tomás, M., *Chem. Rev.*, 104, **2004**, 2259

¹⁵ Hong Ng, K., Li, Y., Ganguly, R., Mathey, F., *Organometallics*, 32, **2013**, 2287

Ferrocene as a substituent

López-Cortés *et al.*¹⁶ synthesised ferrocenyl-N-pentylamino carbene complexes of all the group VI metals which contained bidentate allene-amino carbene substituents. Their aim was to introduce chirality into the ferrocene complexes using an additional transition metal because it was suggested that such complexes could have significant reactivity and industrial applications.¹⁷ Carbene complexes of molybdenum, chromium and tungsten have been synthesised whereby one of the substituents on the carbene carbon is a pentylamine moiety and the other is a ferrocene moiety (Figure 3.4).¹⁸ The same complexes using allylamine have also been synthesised.¹⁸

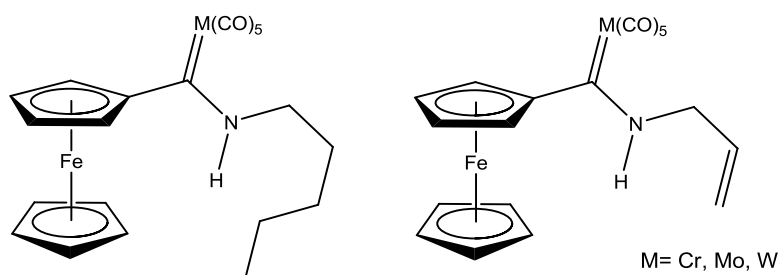


Figure 3.4: Complexes synthesised by López-Cortés *et al.*¹⁸

Application of amino carbene complexes

Phenol formation using amino stabilised α , β -unsaturated Fischer carbene complexes of chromium, using alkynes as a substrate was first reported by Wulff *et al.*¹⁹ in 1995. Before this, it was thought that complexes stabilised by alkoxy substituents would produce six-membered ring products, and those stabilised by amino substituents would produce five-membered ring products. The reactions that gave rise to these notions were performed using alkoxy stabilised Fischer carbene complexes and were reported in 1975 by Dötz.²⁰ These reactions produced valuable phenol products. The solvent seems to be the major factor which determines which ring is the product in these reactions. In general, polar solvents give rise to five-membered rings, and apolar solvents give rise to six-membered rings.¹⁹ An amino substituent has a greater donating ability than the alkoxy substituent.⁴² This would result in more electron density on the metal centre as well as stronger metal-carbonyl bonds.¹⁹ With these in mind, Wulff *et al.*¹⁹ found that the alkenyl amino-substituted chromium complexes give 4-aminophenol products after a benzannulation reaction with terminal

¹⁶ López-Cortés, J.G., Samano-Galindo, A., Ortega-Alfaro, M.C., Toscano, A., Rudler, H., Parlier, A., Alvarez-Toledano, C., *J. Organomet. Chem.*, 690, **2005**, 3664

¹⁷ a) Colacot, T.J., *Chem. Rev.*, 103, **2003**, 3101. b) Richards, C.J., Locke, A.J., *Tetrahedron: Asymm.*, 9, **1998**, 2377. c) Dai, T., Tu, T., You, S., Deng, W., Hou, X., *Acc. Chem. Res.*, 36, **2003**, 659

¹⁸ López-Cortés, J.G., de la Cruz, L.F.C., Ortega-Alfaro, M.C., Toscano, R.A., Alvarez-Toledano, C., Rudler, H., *J. Organomet. Chem.*, 690, **2005**, 2229

¹⁹ Wulff, W.D., Gilbert, A.M., Hsung, R.P., Rahm, A., *J. Org. Chem.*, 60, **1995**, 4566

²⁰ Dötz, K.H., *Dietz. R., Chem. Ber.*, 111, **1978**, 2517

alkenes. However, it was found that no benzannulated products were found with aryl amino complexes with terminal alkenes as a substrate.

Phosphine and nitrogen-containing ligands have greatly advanced researchers' quest for faster and more efficient catalysts.²¹ These catalysts stabilise the active species and accelerate various steps in the catalytic process. There is a disadvantage, however; the more bulky the substituents, the slower the coupling of the complex becomes to these bulkier substrates.²² In 2004, Altenhoff *et al.*²³ developed the notion of "flexible steric bulk". The ligands that were used in this study were cyclohexane ligands. Lavallo *et al.*²⁴ show that cyclic alkyl amino carbene (CAAC) complexes can be stable and that replacing an amino substituent of an NHC with a σ -donor, makes these complexes more electron rich (Figure 3.5).

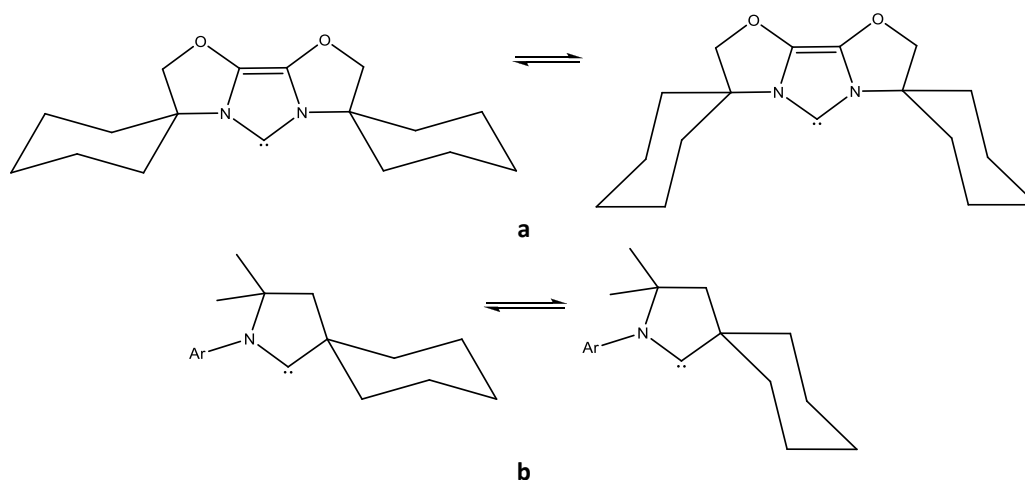


Figure 3.5: Flexible steric bulk illustrated on an a) NHC, b) CAAC²⁴

It is shown that a tertiary alkyl group which is bonded to the carbene carbon imbues the alkyl amino carbene complexes with stability and σ -donor properties toward transition metals.²⁴

Focus of this study

In this study, amino carbene complexes of molybdenum are presented. The amine reagents used in the aminolysis reactions are cyclohexylamine and ammonia. The heterocyclic rings used are thiophene and furan rings. There are no other comparable examples of phosphine-substituted

²¹ a) Littke, A.F., Fu, G.C., *Angew. Chem.*, 114, **2002**, 4350; *Angew. Chem. Int. Ed.*, 41, **2002**, 4176. b) Zapf, A., Beller, M., *Chem. Commun.*, **2005**, 431. c) Muira, M., *Angew. Chem.*, 116, **2004**, 2251; *Angew. Chem. Int. Ed.*, 43, **2004**, 2201.

²² Gstöttmayr, C.W.K., Böhm, V.P.W., Herdtweck, E., Grosche, M., Herrmann, W.A., *Angew. Chem.*, 114, **2002**, 1421; *Angew. Chem. Int. Ed.*, 41, **2002**, 1363.

²³ a) Altenhoff, G., Goddard, R., Lehmann, C.W., Glorius, F., *J. Am. Chem. Soc.*, 126, **2004**, 15195. b) Altenhoff, G., Goddard, R., Lehmann, C.W., Glorius, F., *Angew. Chem.*, 115, **2003**, 3818; *Angew. Chem. Int. Ed.*, 42, **2003**, 3690.

²⁴ Lavallo, V., Canac, Y., Präsang, C., Donnadieu, B., Bertrand, G., *Angew. Chem.*, 117, **2003**, 5851

aminolysed carbene complexes available in the literature, save for those published by our own laboratories.²⁵

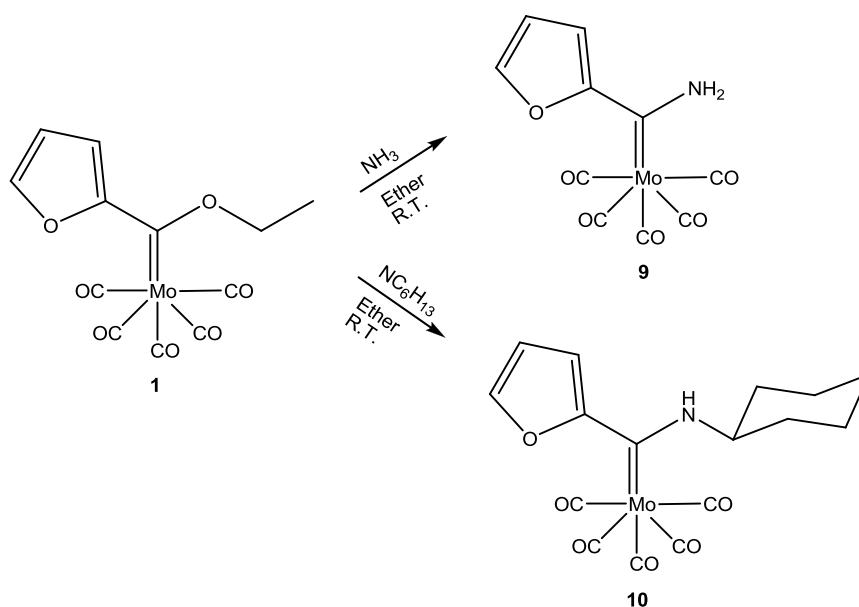
This chapter will focus on the synthesis, characterisation data and theoretical properties of six novel complexes (**9-14**). Crystal structures of five of these complexes (**9-13**) will be discussed.

Known complexes (**S-AD**) obtained from literature will be utilised for comparison with the novel complexes. The literature references pertinent to each will be displayed during the chapter where the data for each complex is first presented.

3.2 Molybdenum pentacarbonyl amino carbene complexes

The complexes that will be discussed in this section are $[\text{Mo}(\text{CO})_5\text{C}\{(\text{NH}_2)(\text{C}_4\text{H}_3\text{O})\}]$ (**9**) as well as $[\text{Mo}(\text{CO})_5\text{C}\{(\text{NC}_6\text{H}_{12})(\text{C}_4\text{H}_3\text{O})\}]$ (**10**).

The following reaction scheme was followed for the synthesis of complexes **9** and **10**.



Scheme 3.1: The synthetic route to obtain **9** and **10**

The amino carbene complexes presented in this chapter were synthesised using the procedure laid out by Klabunde and Fischer.²⁶ Complex **1** was dissolved in ether and was reacted either with

²⁵ a) Landman, M., Pretorius, R., Buitendach, B.E., van Rooyen, P.H., Conradie, J., *Organometallics*, 32, **2013**, 5491; b) Landman, M., Fraser, R., Pretorius, R., Prinsloo, R., Liles, D.C., van Rooyen, P.H., *Acta Cryst.*, E68, **2012**, m930; c) Landman, M., Pretorius, R., Fraser, R., Buitendach, B.E., Conradie, M.M., van Rooyen, P.H., Conradie, J., *Electrochim. Acta*, 130, **2014**, 104; d) Landman, M., Liu, R., Fraser, R., van Rooyen, P.H., Conradie, J., *J. Organomet. Chem.*, 752, **2014**, 171

²⁶ Klabunde, U., Fischer, E.O., *J. Am. Chem. Soc.*, 89, **1967**, 7141

ammonia gas at room temperature to form **9** or with cyclohexylamine overnight at room temperature to form **10**. The colour of both of the solutions changed from red to yellow. These reactions were followed using thin layer chromatography. Prior to reaction completion, two bands were observed in each case - an unreacted starting material band and a product band. Upon reaction completion of the synthesis of **9**, excess ammonia gas was removed *in vacuo*. This inevitably lead to the solvent being removed as well. This reaction produced **9** with 100% yield. The reaction mixture which resulted in the synthesis of **10** was purified using silica gel column chromatography. This reaction produced **10** with 64% yield.

The resonance structures that can be found in **9** are shown in the figure below. These are similar for those which can be found for **10**.

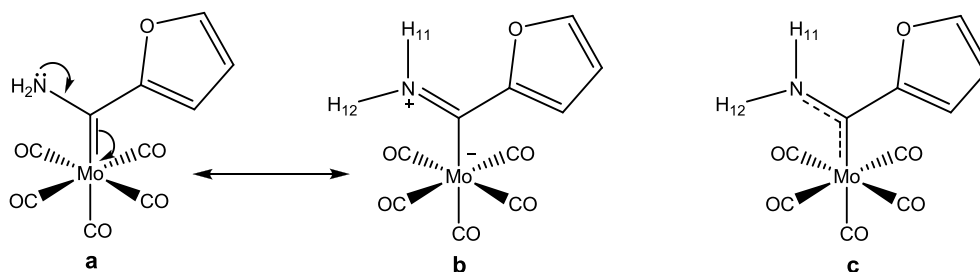


Figure 3.6: a and b: Resonance structures of **9**; c: Resonance hybrid

In resonance structure (a), there is a double bond between the metal and the carbene carbon. This means that there is free rotation around the carbene carbon-nitrogen bond. However, due to the free rotation in (a), these two protons will be equivalent in solution. The other resonance structure (b) can be seen to show a double bond between the nitrogen and the carbene carbon. This essentially locks the rotation of the amino group. The proton H_{12} , will be largely influenced by the metal and carbonyls because of its proximity. This interaction will deshield H_{12} , causing it to be more downfield than H_{11} . As a result of the double bond, the two protons can be differentiated and specific shifts can be assigned to each, even in solution spectra.

While **9** can again be found in two possible conformations, as discussed in the previous chapter, **10** on the other hand, has two possible sets of conformers - meaning four possible conformers in the solid state, which are depicted in Figure 3.7.

The crystal structures obtained from **9** and **10** both crystallized with the two heteroatoms in a *syn* conformation (Figure 3.11).

The obvious consequence of the resonance structures, discussed above, will be found in the ^{13}C NMR spectra. Two different structures results in the opportunity for two, three or four carbonyl signal

patterns in the ^{13}C NMR to exist. If the metal-carbon bond is rigidly fixed - as would be observed in the conventional drawings of these structures - where this bond is depicted as a double bond, two of the three signal patterns can arise.

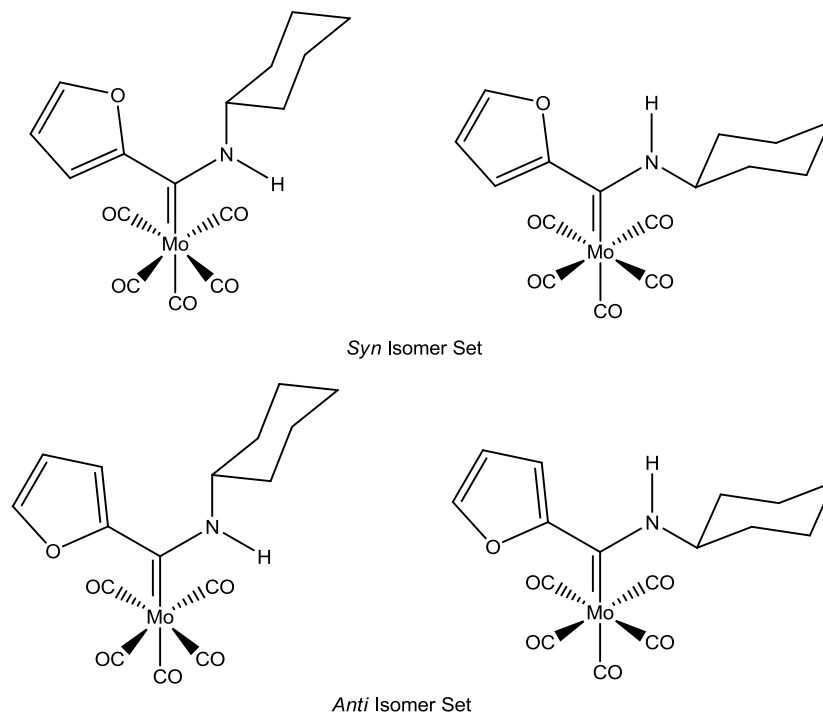


Figure 3.7: The possible conformations of **10**

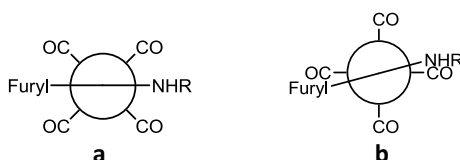


Figure 3.8: Newman projections viewed down the C₆=M bond in a) Three carbonyl peak scenario; b) Four carbonyl peak scenario

The three carbonyl signals scenario arises as a result of the double bond being fixed in the manner depicted above - with the carbene substituents staggered with respect to the carbonyls when looking down the carbene-molybdenum double bond (Figure 3.8a). This results in the axial carbonyl (which cannot be seen in Figure 3.8a) showing one signal on the NMR spectrum, the two carbonyls adjacent to the furfuryl giving rise to another signal and the two carbonyls adjacent to the amino group presenting as the third signal.

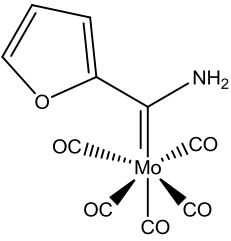
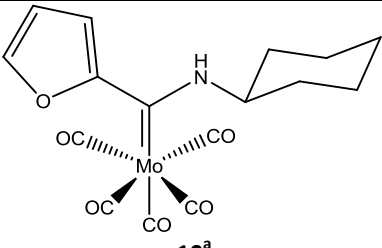
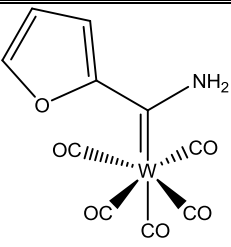
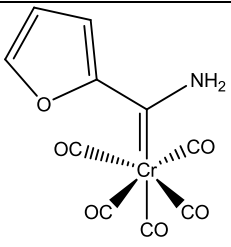
The four carbonyl signals scenario arises as a result of the double bond being fixed in such a manner that the carbene substituents are laid directly over two of the carbonyls (Figure 3.8b). This will result in one signal each for the eclipsed carbonyls, one for the axial carbonyl and one for the two remaining carbonyls (they are equivalent) on the NMR spectrum.

However, if the double bond lies between the carbene carbon and the nitrogen atom, the Mo-C₆ bond can rotate freely. Therefore only two signals due to the four equatorial carbonyls being in an equivalent environment would be expected on the NMR spectrum.

3.2.1 Infrared spectroscopy

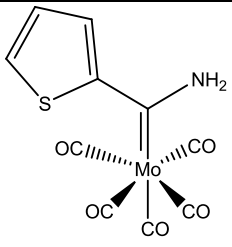
The data obtained from the IR spectra of **9** and **10**, are summarised in Table 3.1, below.

Table 3.1: IR frequency assignments for **9** and **10**, including literature values

Complexes	Carbonyl Stretching Frequency (cm ⁻¹)			
	A ₁ ⁽¹⁾	B ₁	E	A ₁ ⁽²⁾
 9^a	2064 (m)	1979 (m)	1933 (vs)	1898 (s)
 10^a	2061(m)	1977 (m)	1928 (vs)	1890 (m)
 S^a: [W(CO)₅C{(NH₂)(C₄H₃O)}] ²⁷	2064(m)	1976(m)	1928(vs)	1888(m)
 T^b: [Cr(CO)₅C{(NH₂)(C₄H₃O)}] ²⁸	2060(m)	1991(m)	1961(vs)	1946(m)

²⁷ Streubel, R., Priemer, S., Ruthe, F., Jones, P.G., Gudat, D., *Eur. J. Inorg. Chem.*, **1998**, 575

²⁸ Connor, J. A., Jones, E. M., *J. Chem. Soc., Part A*, **1971**, 1974

Complexes	Carbonyl Stretching Frequency (cm ⁻¹)			
	A ₁ ⁽¹⁾	B ₁	E	A ₁ ⁽²⁾
 U^b: [Mo(CO)₅C{(NH₂)(C₄H₃S)}]²⁹	2066(m)	1981(m)	1931(vs)	1931(m)
V^a: [W(CO)₅C{(NHCy)(C₄H₃O)}]³⁰	2059 (m)	1996 (vw)	1908 (s)	1882 (vs)
W^a: [W(CO)₅C{(NHCy)(C₄H₃S)}]³⁰	2061 (m)	1972(vw)	1950 (s)	1906(vs)

^aMedium: KBr

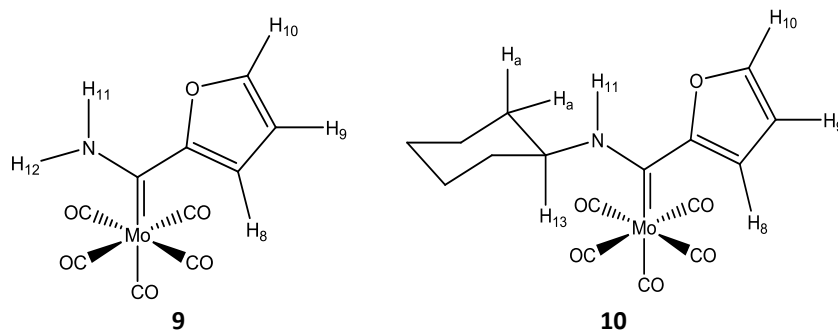
^bMedium: Hexane

Complex **9** and **10** have the same symmetry as **S**, **T** and **U** (C_{4v}), since they are all pentacarbonyl complexes.³¹ There is very good correlation between **9**, **10** and **U** with all the values observed for **9**, although Landman²⁹ observed overlap in the E and A₁⁽²⁾ bands. This correlation shows that the aromatic substituent, whether it is thienyl or furyl, does not greatly affect the carbonyl's stretching frequencies.

The A₁⁽¹⁾ band shows good correlation between **9**, **10**, **T** and **S**. Bands B₁, E and A₁⁽²⁾ all show better correlation with **S** and little correlation to **T**. Despite this, it can be seen that the same trend observed in the previous chapter recurs here. The trend being that the stretching frequencies of the molybdenum complex are found to be of intermediate value.

3.2.2 ¹H NMR spectroscopy

The data obtained from the ¹H NMR spectra of **9** and **10** is summarised below. The data displayed in the table are all given using the numbering system that follows, regardless of the identity of the metal centre.



²⁹ Landman, M. PhD thesis: Synthesis of Metal Complexes with Thiophene Ligands, **2000**, 47

³⁰ Landman, M., Pretorius, R., Buitendach, B.E., van Rooyen, P.H., Conradie, J., *Organometallics*, **2013**, 5491

³¹ A. Salzer, C. H. Elschenbroich, *Organometallics: A Concise Introduction.*, Second Ed., VCH Verlag, Weinheim, **1992**, 210-241

H₁₁ and H₁₂ are found to be very broad singlets, as is common for amino group protons. They are not found to be in the same environment. This can be explained by the actual structure, which is a resonance hybrid, as shown in Figure 3.6. The proton H₁₂, will be largely influenced by the metal and carbonyls because of its proximity. This interaction will deshield H₁₂, causing it to be more downfield than H₁₁. Protons 11 and 12 of **9** show good correlation to the same protons of **S**. In these complexes, the shift values of these protons are 0.71 ppm apart.

Table 3.2: ¹H NMR assignments for **9** and **10**, including literature values

Complexes	Chemical Shift (δ, ppm), Multiplicity and Coupling constant (J, Hz)							
	H ₁₀	H ₉	H ₈	N-H ₁₁	N-H ₁₂	H ₁₃	H _a	H _b
9 ^a	7.54 d J = 1.7	6.16 dd J = 1.8, 3.7	7.5 d J = 3.7	8.05 s	8.76 s			
10 ^a	7.36 d J = 1.6	6.46 dd J = 1.8, 3.6	7.30 d J = 3.6	8.91 s		2.20 dd J = 5.1, 10.6	1.38 dt J = 11.2, 15.5	1.14 m
S ^a : [W(CO) ₅ C{(NH ₂)(C ₄ H ₃ O)}] ²⁷	7.54 - 7.55 m	6.56 dd J = 1.8, 3.7	7.45 - 7.47 m	7.91 s	8.94 s			
T ^a : [Cr(CO) ₅ C{(NH ₂)(C ₄ H ₃ O)}] ²⁸	7.55 d J = 3.7	6.61 dd J = 1.8, 3.7	7.51 s	8.16 s	8.73 s			
X ^a : [Cr(CO) ₅ C{(NH ₂)(C ₄ H ₃ S)}] ³²	7.62 d J = 4.5	7.19 dd J = 3.9	7.69 d J = 3.9	8.20 s				
U ^a : [Mo(CO) ₅ C{(NH ₂)(C ₄ H ₃ S)}] ²⁹	7.71 d J = 4.5	7.24 dd J = 4.5, 4.5	7.72 d J = 4.5	8.21 s	8.36 s			
V ^a : [W(CO) ₅ C{(NH ₂)(C ₄ H ₃ O)}] ³⁰	7.51 d J = 1.4	6.57 dd J = 0.5, 3.6	7.38 dd J = 0.5, 3.6	8.93 s		4.31- 4.42 m	1.12-2.15 m	
W ^a : [W(CO) ₅ C{(NH ₂)(C ₄ H ₃ S)}] ³⁰	7.46 dd J = 1.1, 5.0	7.07 dd J = 3.7, 5.0	6.93 dd J = 1.1, 3.7	8.64 s		3.73- 3.86 m	1.10-2.20 m	

^aSolvent: CDCl₃(7.24ppm).

There is a good correlation between H₈, H₉ and H₁₀ of **10** and **9**, **S**, **T** and **U**. The change in the amino substituent on the carbene moiety changed the NH₁₁ shift quite substantially. Rather interestingly there are only two signals for the cyclohexylamine ring, apart from H₁₃. This is unexpected, yet

³² Thompson, S., Wessels, H.R., Fraser, R., van Rooyen, P.H., Liles, D.C., Landman, M., *J. Mol. Struct.*, 1060, 2014, 111

explainable. The cyclohexylamine ring is diastereotopic due to the presence of the nitrogen and the rest of the molecule. As a result of its diastereotopicity, the axial-equatorial interaction becomes more prevalent than the protons on the ring being simply unequivalent.³³ For this reason, only two signals are observed. Geminal couplings in these systems have absolute values of 10 to 15 Hz.³³ Vicinal couplings are 6-14 Hz for axial-axial interactions, 3-5 Hz for axial-equatorial interactions and 0-5 Hz for equatorial-equatorial interactions.³³ The larger axial-axial coupling constant is due to the dihedral angle being larger (180°) than that for axial-equatorial or equatorial-equatorial (60°).³³ The coupling constants observed at H_{13} are indicative of vicinal axial-axial coupling (10.6 Hz) and axial-equatorial coupling (5.1 Hz). This indicates that the chair conformation where H_{13} is in the axial position and the amino carbene moiety is in the equatorial position, is the prevalent conformation in solution. This is supportive of the conventional theory that indicates that the large substituent groups on a cyclohexane ring will be favoured in the equatorial position.³⁴ The coupling constants at H_a are indicative of vicinal axial-axial couplings (11.2 Hz) and geminal coupling constants (15.5 Hz).

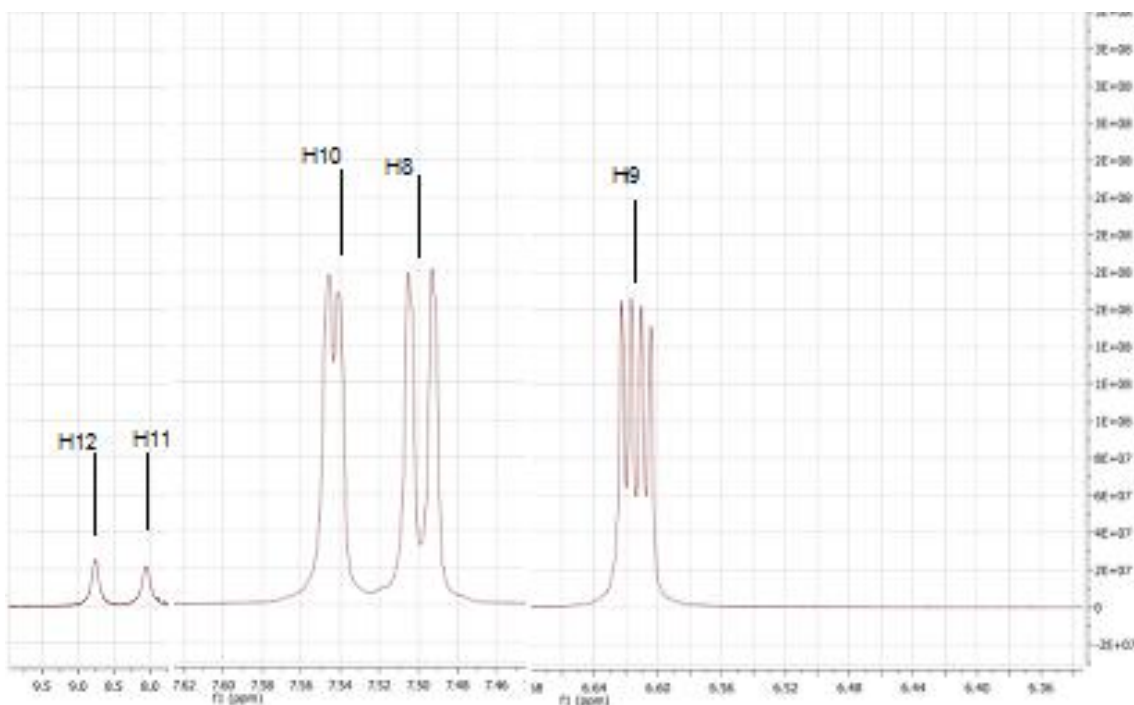


Figure 3.9: Experimental ^1H NMR spectrum of **9 (CDCl_3)**

The only protons which are found on the ^1H NMR spectrum of **9** are the protons of the amine and those of the furyl ring. This simplifies the ^1H NMR spectrum greatly, as can be seen in Figure 3.9. Please note the x-axis of the figure has been cut. There is coupling exhibited by H_8 , H_9 and H_{10} . Each of H_8 and H_{10} have only one adjacent proton, which results in doublets for each of these protons. In

³³ Friebolin, H., Basic one- and two-dimensional NMR Spectroscopy, VCH verlag, Weinheim **1991**

³⁴ Gorzynski Smith, J., Organic Chemistry, McGraw Hill, Second Edition, **2007**

the case of H₉, however, there are two non-equivalent protons, which results in a doublet of doublets splitting pattern.

3.2.3 ¹³C NMR spectroscopy

The ¹³C NMR spectrum data of **9**, **10** and selected literature values is summarised in Table 3.3. The following numbering system was used for all of the data presented.

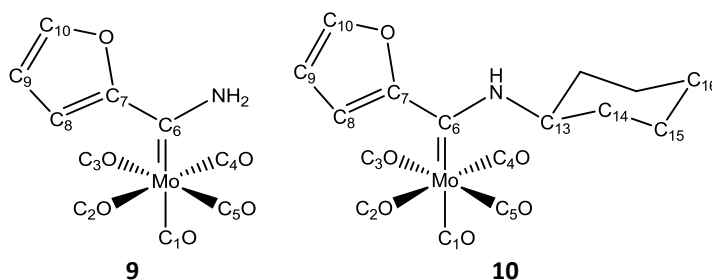


Table 3.3: ¹³C NMR assignments for **9** and **10**, including literature values

Complexes	Chemical Shift (δ, ppm)										
	C ₁ O (<i>trans</i>) [#]	C ₂ O, C ₃ O, C ₄ O, C ₅ O (<i>cis</i>) [#]	C ₆	C ₇	C ₈	C ₉	C ₁₀	C ₁₃	C ₁₄	C ₁₅	C ₁₆
9 ^a	212.5	206.6	243.0	157.5	129.3	114.3	145.3				
10 ^a	212.6	206.6	237.3	157.8	126.1	113.7	144.0	63.7	33.2	24.6	25.0
S ^a : [W(CO) ₅ C{(NH ₂)(C ₄ H ₃ O)}] ²⁷	202.6	198.4	229.8	159.0	129.4	114.5	145.6				
T ^b : [Cr(CO) ₅ C{(NH ₂)(C ₄ H ₃ O)}] ³⁵	224.7	219.5	255.6	158.5	129.0	115.2	146.0				
X ^b : [Cr(CO) ₅ C{(NH ₂)(C ₄ H ₃ S)}] ³⁵	226.2	220.8	271.8	154.8	134.4	134.4	135.0				
U ^a : [Mo(CO) ₅ C{(NH ₂)(C ₄ H ₃ S)}] ²⁹	213.0	206.7	257.5	152.2	133.1	129.1	133.1				
V ^a : [W(CO) ₅ C{(NHCy)(C ₄ H ₃ O)}] ³⁰	202.4	198.4	219.3	159.1	126.3	113.7	144.1	64.3	33.1	24.5	25.3
W ^a : [W(CO) ₅ C{(NHCy)(C ₄ H ₃ S)}] ³⁰	203.5	198.7	245.7	150.2	127.3	124.2	127.8	59.5	33.3	24.7	24.2

^aSolvent: CDCl₃ (77 ppm)

^bSolvent: (CD₃)₂O (29.8 ppm)

[#]Position relative to carbene ligand

The data obtained for **9** and **10** are in agreement with the data for furyl-substituted complexes found in literature (**S** and **T**). Additionally, comparison of the shifts for C₆ of **9**, **10** and **U**, shows that the influence of the sulfur in the thienyl moiety is more withdrawing than the oxygen of the furyl moiety (δ = 257.5 ppm for thienyl, and δ = 243.0 ppm for furyl). Since the carbene carbon shift for thienyl is more downfield, the carbene carbon is more deshielded.

As expected, the change in the amino substituent on the carbene moiety has had very little effect on the shifts of the furyl ring or the carbonyl ligands.

³⁵ Connor, J.A., Jones, E.M., Randall, E.W., Rosenberg, E., *J. Chem. Soc. A.*, **1972**, 2419

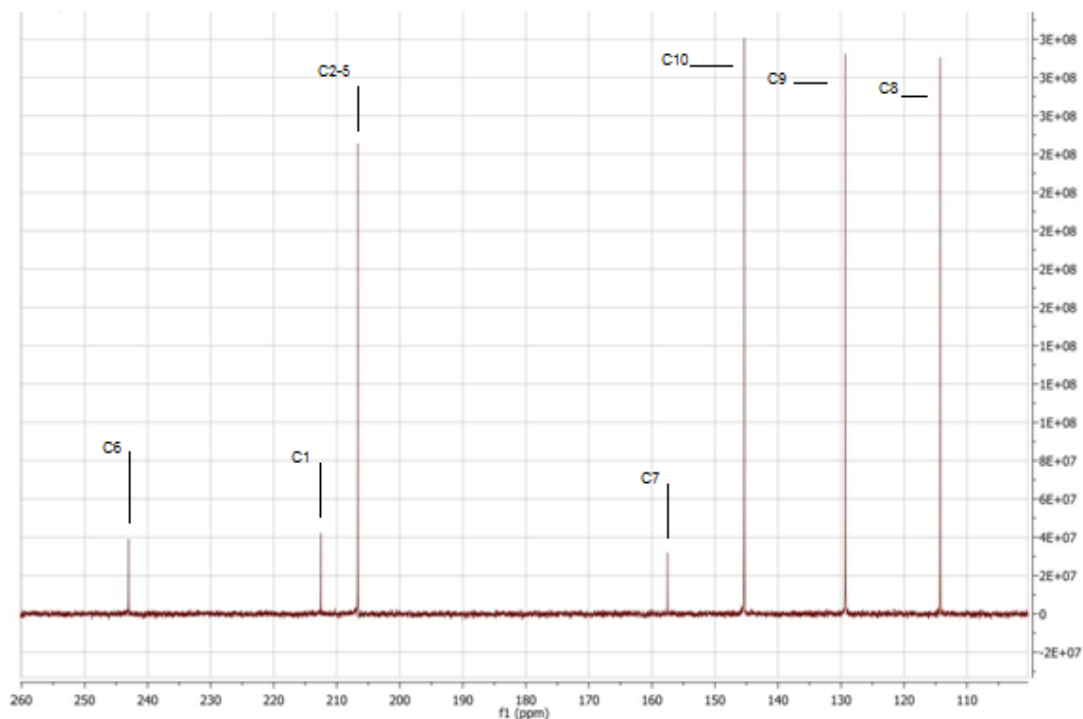


Figure 3.10: ^{13}C NMR spectrum of **9** (CDCl_3)

Figure 3.10 shows the ^{13}C NMR spectrum of **9**.

3.2.4 X-Ray crystallography

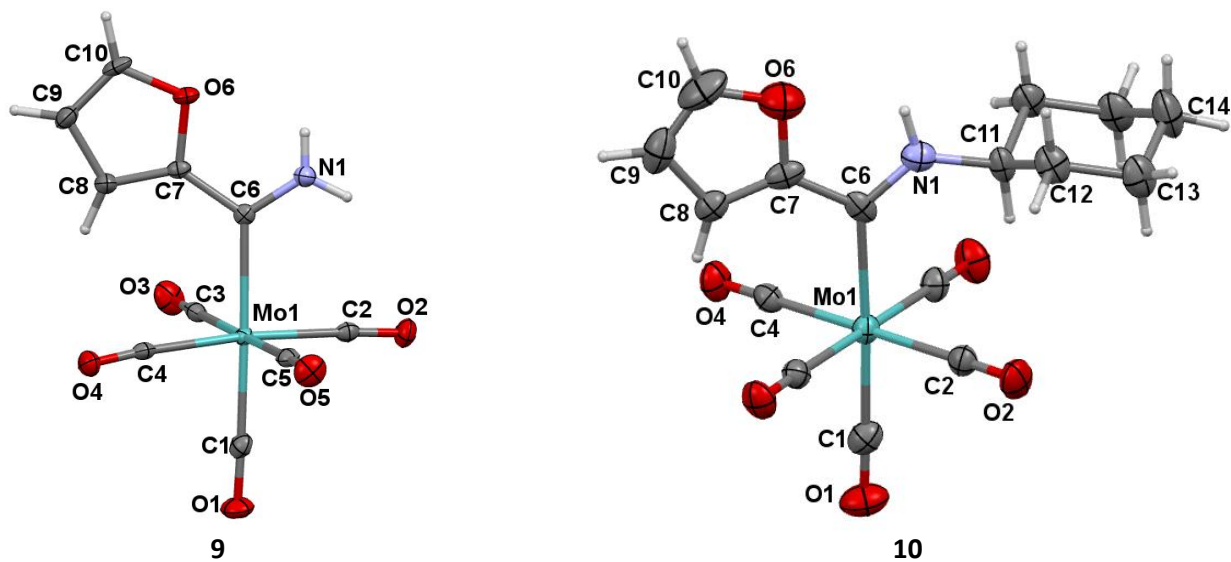


Figure 3.11: Crystal structures of **9** and **10** (ORTEP representation)

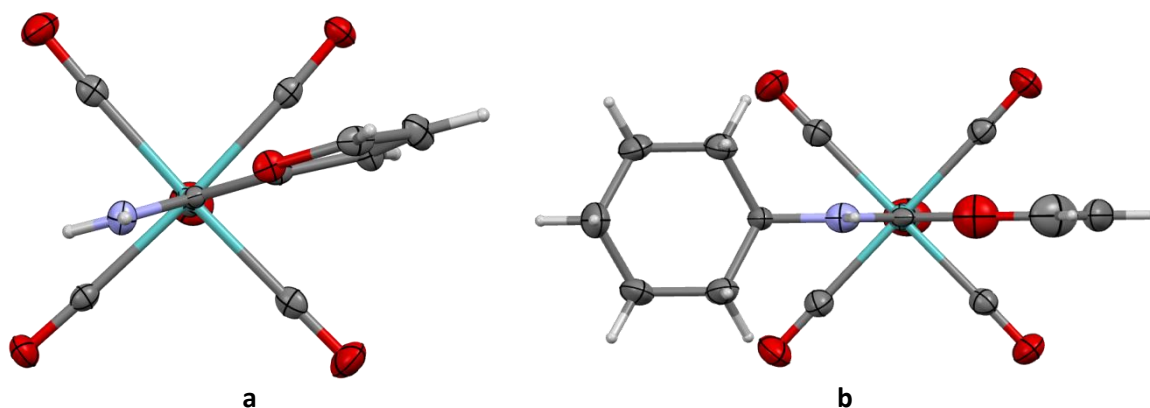


Figure 3.12: View down M→C₆ bond of a) **9** and b) **10**

The amino group and the furyl group are in the same plane with the metal and the *trans* carbonyl (Figure 3.12a and b). In both structures, the furyl oxygen atom and the amino moiety nitrogen atom are *syn* in conformation (Figure 3.12a and b).

Table 3.4: Bond lengths obtained from the crystal structure of **9** and **10**

Bond	Bond Length (Å)	Bond Length (Å)
O ₆ -C ₁₀	1.358(3)	1.377(6)
O ₆ -C ₇	1.386(3)	1.372(5)
C ₇ -C ₈	1.366(3)	1.336(5)
C ₈ -C ₉	1.416(4)	1.413(6)
C ₉ -C ₁₀	1.343(4)	1.301(7)
C ₇ -C ₆	1.444(3)	1.461(5)
N-C ₆	1.316(3)	1.311(4)
Mo-C ₆	2.233(3)	2.264(4)
Mo-C ₁	2.022(3)	2.010(4)
Mo-C ₂	2.033(2)	2.050(2)
Mo-C ₃	2.059(2)	-
Mo-C ₄	2.046(2)	2.056(2)
Mo-C ₅	2.047(2)	-
N-H ₁₁	0.79(3)	0.881 ^a
N-H ₁₂	0.84(3)	
N-C ₁₁		1.447(4)

^aCalculated value

There are negligible differences to be seen between the bond lengths of **9** and **10**.

There is no difference between the N-C₆ bond of **9** and that of **10**, but the N-C₁₁ is longer than the N-C₆ bond. This means that the N-C₁₃ bond has more single bond character than the N-C₆ bond in

these molecules. The fact that the N-C₆ bond has more of a double bond character in both **9** and **10** than the other N-C bond, reiterates the resonance structure shown in Figure 3.6. The N-C₆ bond length of these is comparable to the same bond length found by Sandoval-Chávez (1.301(4) Å).³⁶ The bond length of **10** is very slightly shorter than that of **9**. Both of these are comparable to the Mo-C₆ bond length of Sandoval-Chavez *et al.* (2.278(3) Å)³⁶ and Erker *et al.* (2.195(6) Å).³⁷

There are negligible differences between the carbonyl bond lengths of **9** and **10**. These bond lengths are longer than those found for (η⁶-ArNH₂)Mo(CO)₃, by Lorber and Vendier (1.935(3) Å, 1.944(3) Å and 1.946(4) Å).³⁸ The length of the carbonyl *trans* to the carbene moiety, in **9** and **10**, is slightly shorter than the other carbonyl bond lengths, this is because this carbonyl is *trans* to a weaker π-acceptor ligand.

Table 3.5: Bond angles obtained from the crystal structure of **9** and **10**

Angle	Angle size (°)	
	9	10
N-C ₆ -C ₇	112.7(2)	110.6(3)
C ₄ -Mo-C ₅	85.71(9)	-
C ₂ -Mo-C ₃	91.82(9)	-
C ₃ -Mo-C ₄	92.00(9)	-
C ₂ -Mo-C ₅	90.60(9)	-
C ₆ -Mo-C ₄	92.78(9)	89.06(9)
C ₆ -Mo-C ₅	90.79(9)	-
C ₆ -Mo-C ₂	92.03(9)	91.21(9)
C ₆ -Mo-C ₃	87.62(9)	-
H ₁₁ -N-H ₁₂	116(3)	
C ₆ -N-C ₁₁		128.5(3)

From the data in Table 3.5, it can be seen that there is no significant deviation from the ideal octahedral angle of 90° around the metal in neither **9** nor **10**.

The angles N-C₆-C₇ and H₁₁-N-H₁₂ in **9** are 112.7(2)° and 116(3)°, respectively. These are angles which would be expected for trigonal planar geometry. Trigonal planar geometry around C₆ is not a surprise - it is expected to be trigonal planar. Trigonal planar geometry around the NH₂ is interesting because conventional drawing of Fischer carbene complexes implies a pyramidal geometry for the nitrogen atom. This result, as well as that of the bond length data, provides a small piece of evidence in favour of the resonance structure in Figure 3.6b. The C₆-N-C₁₁ angle of **10** is 128.5(3)° which indicates a trigonal planar or trigonal pyramidal geometry around the nitrogen atom.

³⁶ Sandoval-Chávez, C., López-Cortés, J.G., Gutiérrez-Hernández, A.I., Ortega-Alfaro, M.C., Toscano, A., Alvarez-Toledano, C., *J. Organomet. Chem.*, 694, **2009**, 3692

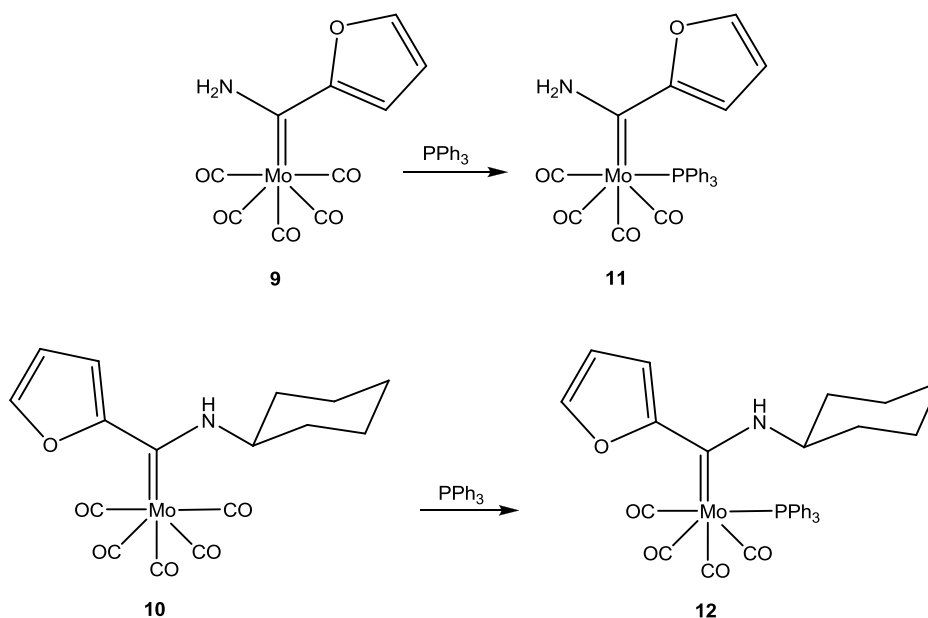
³⁷ Erker, G., Dorf, U., Kruger, C., Tsay, Y., *Organometallics*, 6, **1987**, 682

³⁸ Lorber, C., Vendier, L., *Organometallics*, 29, **2010**, 5

3.3 Molybdenum tetracarbonyl phosphine-substituted amino carbene complexes

The complexes that will be discussed in this section are $[\text{Mo}(\text{CO})_4(\text{PPh}_3)\text{C}\{(\text{NH}_2)(\text{C}_4\text{H}_3\text{O})\}]$ (**11**) as well as $[\text{Mo}(\text{CO})_4(\text{PPh}_3)\text{C}\{(\text{NC}_6\text{H}_{12})(\text{C}_4\text{H}_3\text{O})\}]$ (**12**).

The following is a reaction scheme for complexes **11** and **12**.



Scheme 3.2: The synthetic route to obtain **11** and **12**

The synthesis of **11** and **12** was achieved following Barluenga's synthetic strategy.³⁹ Amino carbene product **9** and triphenylphosphine was dissolved in toluene and was allowed to react under reflux for five hours. The colour of the solution changed from yellow to brown. Amino carbene product **10** and triphenylphosphine was dissolved in toluene and was allowed to react under reflux for two hours. The colour of the solution changed from yellow to dark red.

The reactions were followed using thin layer chromatography where only one product band could be seen in both cases. Both mixtures were purified using silica gel column chromatography. These reactions produced **11** with 80 % yield and **12** with 43 % yield.

Complex **11** only has four possible isomers that can be produced; **12** can have additional isomers in the set, which arise due to the flip of the chair conformation in the cyclohexyl ring. All isomers can be seen below save for the isomers that result from the ring flip.

³⁹ Barluenga, J., Muñiz, K., Tomás, M., Ballesteros, A., Garcia-Granda, S., *Organometallics*, 22, **2003**, 1756-1760

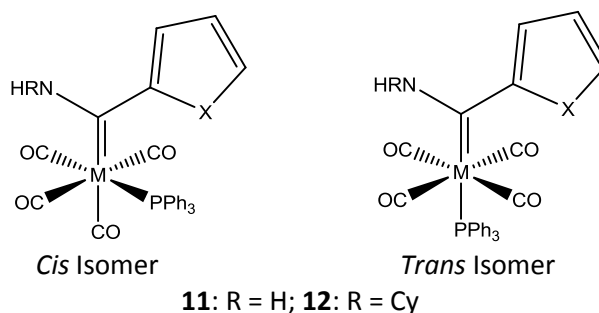


Figure 3.13: The possible isomers for **11** and **12**

Similarly to section 2.4, complexes **11** and **12** can have different conformers, *syn* and *anti*, as well as different isomers, *cis* and *trans* (Figure 3.13). From the crystal structure obtained for **11**, it can be seen that this structure crystallises in a *syn* conformation (Figure 3.16). It is plausible to obtain both *cis* and *trans* isomers of **11**, however it is difficult to isolate both on molybdenum. This may be due to thermodynamic stability during crystallisation. On the other hand, for tungsten it is possible to isolate both products.⁴⁰ The mechanism used to substitute a carbonyl for the phosphine ligand will be the dissociative mechanism due to the identity of the phosphine ligand being triphenylphosphine.⁴¹ More literature on the history of phosphine as a ligand can be found in section 2.1.

3.3.1 Infrared spectroscopy

The IR frequency assignments for **11-cis**, **12-cis** and selected literature complexes are summarised in Table 3.6.

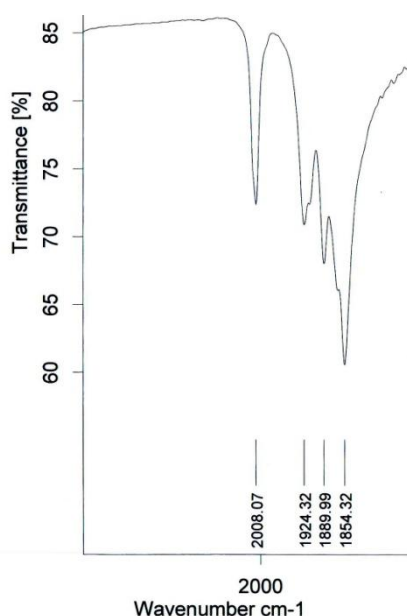
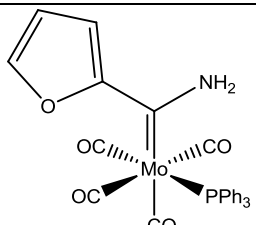
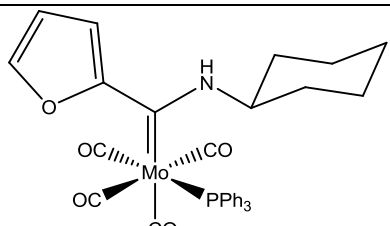


Figure 3.14: Carbonyl region on the IR spectrum of **11** (KBr)

⁴⁰ Landman, M., Levell, T., van Rooyen, P.H., Conradie, J., *J. Mol. Struct.*, 29, **2014**, 1065

⁴¹ Arndtsen, B.A., Schoch, T.K., McElwee-White, L., *J. Am. Chem. Soc.*, 114, **1992**, 7041

Table 3.6: IR frequency assignments for **11** and **12**

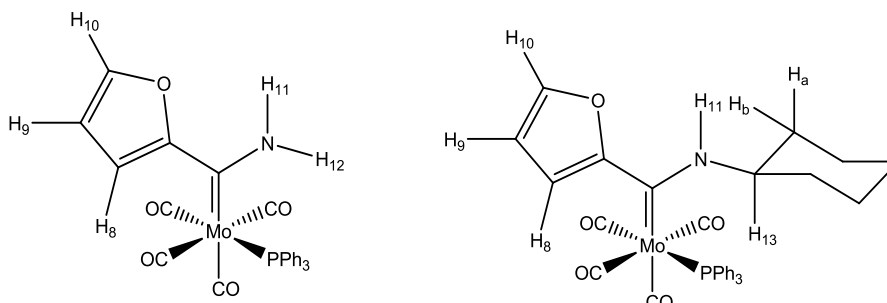
Complexes	Carbonyl Stretching Frequency (cm ⁻¹)			
	A ₁ ⁽¹⁾	B ₁	B ₂	A ₁ ⁽²⁾
 11^a	2008 (w)	1890 (s)	1854 (vs)	1924 (m)
 12^a	2006 (s)	1887 (vs)		
Y^a: cis-[W(CO)₄(PPh₃)C{(NHCy)(C₄H₃O)}] ⁴²	2001 (s)	1875 (s)		
Z^a: cis-[W(CO)₄(PPh₃)C{(NHCy)(C₄H₃S)}] ⁴²	2002 (s)	1870 (s)	1860 (s)	1894 (s)
9^a	2064 (m)	1979 (m)		1898 (s)
10^a	2061 (m)	1979 (m)		1890 (m)

^aMedium: KBr

The data in Table 3.6 illustrates that substituting a carbonyl can change the position of the IR carbonyl stretching peaks quite substantially. There is significant overlap of the B₁, B₂ and A₁⁽²⁾ bands in **12-cis**, resulting in the observation of only one peak. The correlation between **11-cis** and **12-cis** is excellent. Both **11-cis** and **12-cis** have C_{2v} symmetry.

3.3.2 ¹H NMR spectroscopy

The ¹H NMR assignments of **11-cis** and **12-cis** is summarised in Table 3.7. The following numbering system is used for all the data displayed in the table.



⁴² Landman, M., Pretorius, R., Fraser, R., Buitendach, B.E., Conradie, M.M., van Rooyen, P.H., Conradie, J., *Electrochim. Acta*, 130, **2014**, 104

Table 3.7: ^1H NMR assignments for **11-cis** and **12-cis**

Complexes	Chemical Shift (δ , ppm), Multiplicity and Coupling constant (J, Hz)								
	H ₁₀	H ₉	H ₈	N-H ₁₁	N-H ₁₂	H ₁₃	H _a	H _b	PPh ₃
11-cis ^c	7.45 dd J = 1.7, 3.6	6.52 dd J = 1.8, 3.6	7.29 dd J = 2.6, 3.0	7.13 s	8.20 s				7.34- 7.33 m
12-cis ^c	7.55 d J = 1.5	6.25 dd J = 1.8, 3.6	6.82 d J = 3.4	8.82 s		2.30 dd J = 11.4, 14.7	1.27 s	1.54 s	7.37- 7.31 m
Y^b: cis- [W(CO) ₄ (PPh ₃)C{(NHCy)(C ₄ H ₃ O)}] ⁴²	7.21- 7.46 m	6.26 dd J = 1.7, 3.6	6.82 d J = 3.6	8.75 s		4.15- 4.32 m	1.10-1.35 1.55-1.80 m		7.21- 7.46 m
Z^b: cis- [W(CO) ₄ (PPh ₃)C{(NHCy)(C ₄ H ₃ S)}] ⁴²	7.33- 7.43 m	6.97 dd J = 3.7, 5.0	7.12 dd J = 1.2, 3.7	8.10 s		4.02- 4.13 m	1.06-1.30 1.58-1.75 m		7.33- 7.43 m
9^a	7.54 d J = 1.7	6.16 dd J = 1.8, 3.7	7.5 d 3.7	8.05 s	8.76 s				
10^a	7.36 d J = 1.6	6.46 dd J = 1.8, 3.6	7.30 d J = 3.6	8.91 s		2.20 dd J = 5.1, 10.6	1.14 m	1.38 dt J = 11.2, 15.5	

^aSolvent: CDCl₃ (7.24 ppm)

^bSolvent: CD₂Cl₂ (5.32 ppm)

^cSolvent: C₆D₆ (7.2ppm)

Complex **11-cis** shows a larger difference in the shift values for H₁₁ and H₁₂ than **9** does. This may come as a result of the carbonyl substitution for the triphenylphosphine ligand. The triphenylphosphine ligand is not as good a π -acceptor as a carbonyl, so the carbonyl *trans* to it (and nearest to H₁₂) will have more electron density in **11-cis** than in **9**. This results in H₁₂ being more deshielded in **11-cis** than in **9** and hence results in it shifting more downfield.

As with **9**, it can be seen that the one proton (H₁₂) on the amino group of **11-cis** is shifted far upfield and away from the other proton in the amino group this again can be explained by the concept of the alternative resonance structure that gives nitrogen a double bond and the metal a negative charge. Thus H₁₂ is deshielded and shifts downfield, away from H₁₁. Interestingly the shift of H₁₁ is much more upfield when compared to **9**. Additionally, as with **3-cis**, H₈ is shifted downfield to a position close to H₁₀, again due to the above mentioned *anti*-conformation preference which results in the metal-H₈ interaction. This shift puts H₈ amongst the aromatic protons as well. All of the peaks are shifted upfield relative to **9**.

The chemical shift for **12-cis** - with regard to the furyl moiety - parallels that for **9**, **10** and **11-cis**. The shift for H₁₁ parallels that for **10**, but both are significantly further downfield than **9** and **11-cis**.

3.3.3 ¹³C NMR spectroscopy

The tabulated data is reported using the following numbering system:

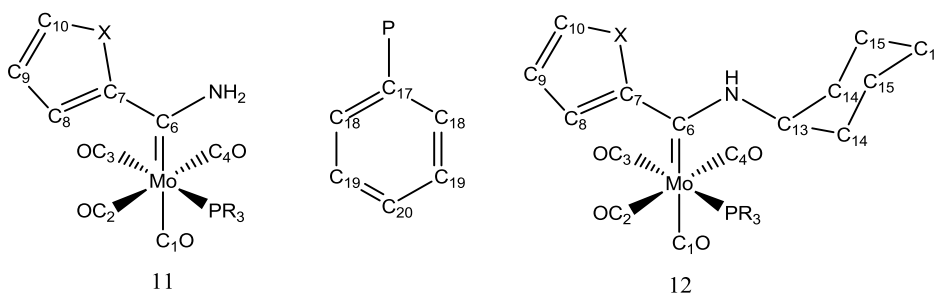


Table 3.8: ¹³C NMR assignments for **11-cis** and **12-cis**

Complexes	Chemical Shift (δ , ppm)												Aromatic
	C ₁ O (<i>trans</i>) [#]	C ₃ O	C ₂ O, C ₄ O, (<i>cis</i>) [#]	C ₆	C ₇	C ₈	C ₉	C ₁₀	C ₁₃	C ₁₄	C ₁₅	C ₁₆	
11-cis ^c	218.3	215.5	210.5	250.4	158.1	127.9	114.0	144.1					128.3- 136.0
12-cis ^c	218.8	214.6	211.7	238.6	159.1	126.5	113.4	144.0	66.2	33.5	25.0	25.6	337.0- 128.7
Y^b: cis- [W(CO)₄(PPh₃) C{(NHCy)(C₄H₃O)}] ⁴²	210.1	208.4	204.9	228.8	160.6	123.8	113.4	145.0	63.4	33.5	25.0	25.6	136.5 134.0 130.3 128.7
Z^b: cis- [W(CO)₄(PPh₃) C{(NHCy)(C₄H₃S)}] ⁴²	210.6	208.2	204.6	245.2	159.0	127.6	127.3	128.2	64.0	33.5	25.1	25.7	137.0 134.1 130.6 128.9
9^a	212.5	206.6		243.0	157.5	129.3	114.3	145.3					
10^a	212.6	206.6		237.3	157.8	126.1	113.7	144.0					

^aSolvent: CDCl₃ (77 ppm)

^bSolvent: CD₂Cl₂ (54.0 ppm)

^cSolvent: C₆D₆ (128.0ppm)

[#]Position relative to carbene ligand

Upon comparison of the chemical shifts of **11-cis** to **9**, it can be seen that there is not a significant change in the shifts of the carbons. Neither is there a significant change when comparing **10** and **12-cis**. With the exception of the shift for C₆, there is a good correlation between the data of **11-cis** and **12-cis**. In **12-cis**, the shift for C₆ is more upfield. This is due to the electron-donating nature of the cyclohexyl group. This means that electron density is pushed on to the carbene moiety, making it more shielded and shift appears more upfield.

3.3.4 ³¹P NMR spectroscopy

Table 3.9: ³¹P NMR assignments for **11-cis** and **12-cis**

Complex	Chemical shift (δ, ppm)
	<i>Cis</i>
11-cis ^a	42.1
12-cis ^a	41.4
Y ^b : <i>cis</i> -[W(CO) ₄ (PPh ₃)C{(NHCy)(C ₄ H ₃ O)}] ⁴²	24.10
Z ^b : <i>cis</i> -[W(CO) ₄ (PPh ₃)C{(NHCy)(C ₄ H ₃ S)}] ⁴²	24.30

^aSolvent: C₆D₆

^bSolvent: CD₂Cl₂

There is a good correlation in the chemical shift values of **11-cis** and **12-cis**, in spite of a change in the amine moiety. Complexes **11-cis** and **12-cis** are identical in the atoms bonded to the metal. Since the chemical shifts of **Y** and **Z** are clearly not comparable to those of the molybdenum, alternative molybdenum complexes were sought. Lindner *et al.*⁴³ synthesised [Cp(CO)₂MoPPh₂(CH₂)₃] and [Cp(CO)₂MoPPh₂(CH₂)₄], and obtained ³¹P NMR spectra, in solution. The chemical shifts for these complexes were 91.8 and 47.3 ppm, respectively. Diel *et al.*⁴⁴ synthesised *fac*-[(CO)₃Mo(PhC₃H₆)₃] and reported an ³¹P NMR chemical shift of 59.1 ppm. All of these, although they are all bound to a molybdenum metal centre, show very disparate chemical shift values for the ³¹P NMR.

Further comparison of these chemical shifts to those found in chapter 2 will be done in the next chapter.

One signal is found on the ³¹P NMR spectrum of **11-cis**. This is expected since there is only one phosphorous present in the molecule.

⁴³ Lindner, E., Fawzi, R., Mayer, H.A., Eichele, K., Pohmer, K., *Inorg. Chem.*, 30, 5, **1991**, 1103

⁴⁴ Diel, B.N., Haltiwanger, R.C., Norman, A.D., *J. Am. Chem. Soc.*, 104, **1982**, 4701



Figure 3.15: Experimental ^{31}P NMR spectrum of 11-*cis* (C_6D_6)

3.3.5 X-Ray crystallography

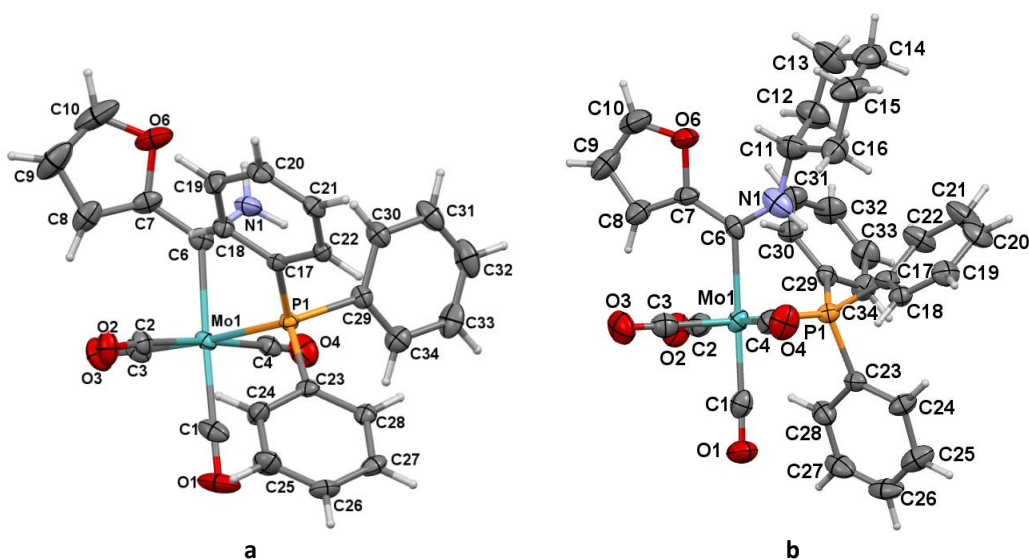


Figure 3.16: Crystal structures of a) 11-*cis* and b) 12-*cis* (ORTEP representation)

The amino group and the furyl group are in the same plane as the metal and C_1 , as well as in a *syn* conformation with each other.

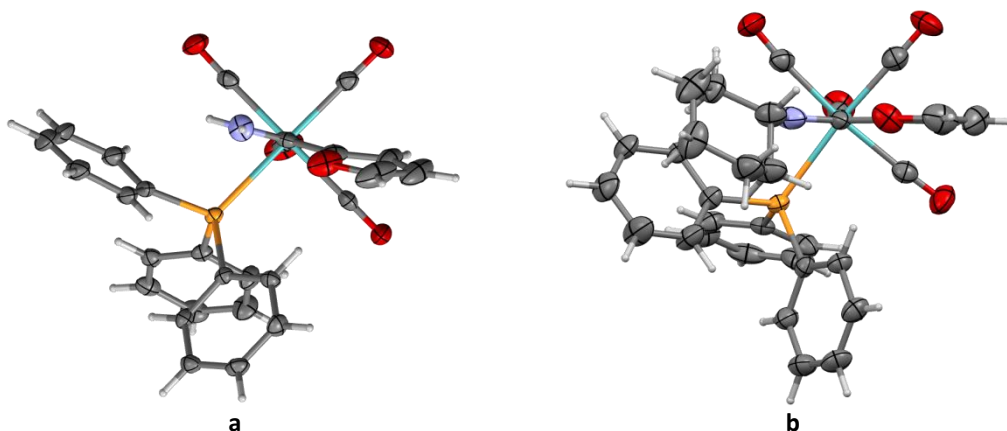
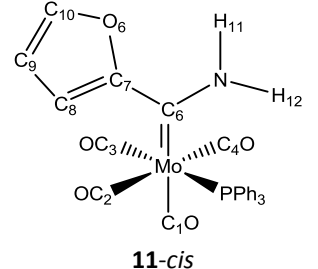
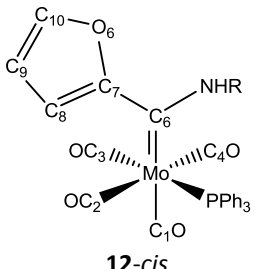
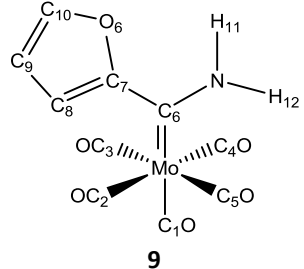
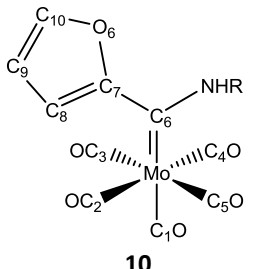


Figure 3.17: View down the $C_6 \rightarrow M$ bond of a) **11-cis**, and b) **12-cis**

Figure 3.17a shows that **11-cis** crystallised with the carbene moiety and the carbonyls on the metal in an eclipsed conformation when the structure is viewed down the $C_6 \rightarrow M$ bond. The NH_2 is closer to the phosphine moiety than the furyl ring. Figure 3.17b shows that **12-cis** is in more of a staggered conformation and the cyclohexylamine moiety, although more bulky, is closer to the phosphine moiety than the furyl ring.

Table 3.10: Bond lengths for the crystal structures of **11-cis** and **12-cis**, along with **9** and **10** for comparison

				
	11-cis	12-cis	9	10
Bond	Bond Length (Å)	Bond Length (Å)	Bond Length (Å)	Bond Length (Å)
O_6-C_{10}	1.363(3)	1.345(7)	1.358(3)	1.377(6)
O_6-C_7	1.388(3)	1.392(5)	1.386(3)	1.372(5)
C_7-C_8	1.349(4)	1.359(7)	1.366(3)	1.336(5)
C_8-C_9	1.416(4)	1.408(7)	1.416(4)	1.413(6)
C_9-C_{10}	1.333(5)	1.341(8)	1.343(4)	1.301(7)
C_6-C_7	1.454(3)	1.439(6)	1.446(3)	1.461(5)
$N-C_6$	1.314(3)	1.324(6)	1.316(3)	1.311(4)
$Mo-C_6$	2.225(2)	2.257(4)	2.231(3)	2.264(4)
$Mo-C_1$	1.987(3)	2.001(5)	2.022(3)	2.010(4)
$Mo-C_2$	2.048(3)	2.028(5)	2.033(2)	2.050(2)
$Mo-C_3$	1.993(3)	1.978(5)	2.059(2)	-
$Mo-C_4$	2.022(3)	2.027(5)	2.046(2)	2.056(2)
$N-H_{11}$	0.880	0.879	0.79(3)	0.881
$N-H_{12}$	0.880		0.84(3)	
$N-C_{11}$		1.424(6)		1.447(4)
$Mo-P$	2.523(1)	2.5570(12)		

Where R = Cyclohexyl

There are negligible differences between the bond lengths that are presented in Table 3.10. Mo-C₃ is shorter in **11-cis** and **12-cis** than in their non-phosphinated counterparts. This observation is directly resultant from the fact that the triphenylphosphine ligand is not as good a π-acceptor as the carbonyl ligand. Therefore there is an increase in back-bonding to the carbonyl *trans* to the triphenylphosphine, thereby decreasing the bond length. The Mo-C₆ bond is consistently shorter in the **11-cis** and **12-cis** compared to the pentacarbonyl complexes. The same is true for the *trans* Mo-carbonyl bond, as well as the Mo-C₃ bond. The Mo-C₆ bond of **12-cis** shows excellent correlation to that of the complex made by Fuss *et al.* (2.258(3) Å).⁴⁵ Complex **11-cis** shows excellent correlation to the N-C₆ bond of the same complex by Fuss *et al.* (1.316(4) Å).

Table 3.11: Bond angles for the crystal structures of **11-cis** and **12-cis**, along with selected bond angle data of **9** and **10**

Angle	Angle size (°)			
	11-cis	12-cis	9	10
N-C ₆ -C ₇	112.7(2)	120.9(4)	112.7(2)	110.6(3)
C ₄ -Mo-C ₅			85.71(9)	-
C ₄ -Mo-P	91.26(7)	98.27(14)		
C ₂ -Mo-C ₃	90.315(10)	87.8(2)	91.82(9)	-
C ₃ -Mo-C ₄	88.75(10)	86.9(2)	92.00(9)	-
C ₂ -Mo-C ₅			90.60(9)	-
C ₂ -Mo-P	90.58(7)	87.10(13)		
C ₆ -Mo-C ₄	93.42(9)	87.35(18)	92.78(9)	89.06(9)
C ₆ -Mo-C ₅			90.79(9)	-
C ₆ -Mo-P	87.56(6)	89.90(11)		
C ₆ -Mo-C ₂	91.98(9)	95.64(17)	92.03(9)	91.21(9)
C ₆ -Mo-C ₃	89.12(9)	89.45(18)	87.62(9)	-
H ₁₁ -N-H ₁₂	119.96		116(3)	
H ₁₁ -N-C ₁₁		112.08		128.5(3)

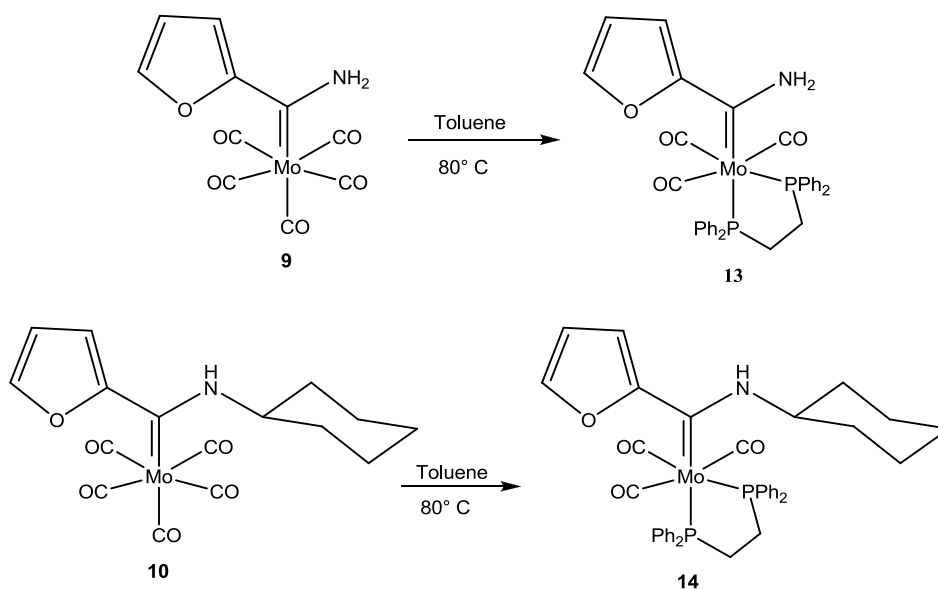
The data in Table 3.11 shows that around the metal centre, there is no significant deviation from the ideal octahedral angle of 90° in either **11-cis** or **12-cis**. Upon addition of the triphenylphosphine ligand, the angles between H₁₁ and H₁₂ increase from 116(3)° in **9** to 120.0° in **11-cis**.

3.4 Molybdenum tricarbonyl diphosphine-substituted amino carbene complexes

The complexes that will be addressed in this section are [Mo(CO)₃(DPPE)C{(NH₂)(C₄H₃O)}] (**13**), as well as [Mo(CO)₃(DPPE)C{(C₆H₁₂N)(C₄H₃O)}] (**14**).

The following reaction schemes show the synthetic routes used to synthesise the products.

⁴⁵ Fuss, B., Dede, M., Weibert, B., Fischer, H., *Organometallics*, 21, **2002**, 21



Scheme 3.3: The synthetic route to obtain **13** and **14**

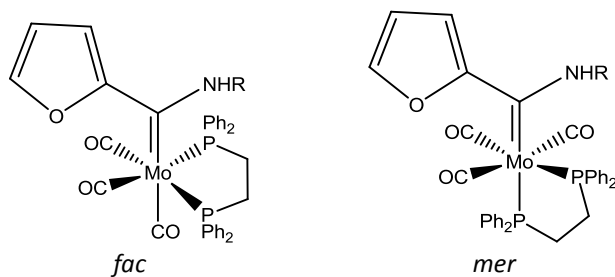
Complexes **13** and **14** were synthesised following the strategy laid out by Reinheimer.⁴⁶ Amino carbene product **9** and diphenylphosphinoethane (DPPE) was dissolved in toluene and was allowed to react under reflux for two hours. The same reaction was repeated with **10**. The colour of both solutions changed from yellow to dark purple. The reactions were followed using thin layer chromatography. Three bands were seen on TLC; un-reacted starting material, *fac*- and *mer* isomers of the reaction product. The mixture was purified using silica gel column chromatography. This reaction produced **13** with 47 % yield and **14** with 69 % yield.

Although the solid state structure of **13** crystallised as the *fac* isomer, solution spectra of **13** and **14** seem to indicate the presence of both isomers to varying amounts. Fraser *et al.*⁴⁸ only isolated and completely characterised the *mer* isomer of the chromium carbene analogue of **14**, but were able to identify peaks belonging to both isomers on IR and ³¹P NMR spectra. This indicates that the DPPE substituted amino carbene complexes forms the *mer* isomer by preference.

The molecular structures of the two possible isomers that can arise in terms of the attachment of the DPPE ligand - *fac* and *mer* are shown in Figure 3.18.⁴⁷

⁴⁶ Reinheimer, E.W., Kantardjieff, K.A., Herron, S.R., Tisserat, C.G., Casalnuovo, J.A., *J. Chem. Crystallogr.*, **33**, **2003**, 503

⁴⁷ Atkins, P., Overton, T., Rourke, J., Weller, M., Armstrong, F., Shriver and Atkins Inorganic Chemistry, Fourth Edition, Oxford University Press, **2006**



13: R = H; **14:** R = cyclohexyl

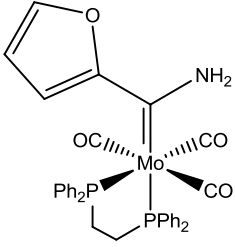
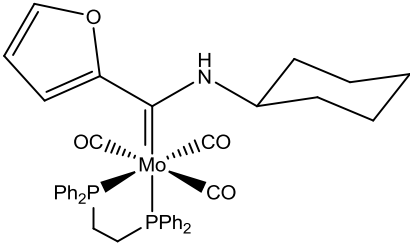
Figure 3.18: Possible isomers of DPPE substituted amino carbene complexes.

There are an additional two isomers possible for **14**, which arise due to the ring flip that is possible on the cyclohexylamine substituent, but these are not shown.

3.4.1 Infrared spectroscopy

The data from the IR frequency assignments of **13-mer** and **14-mer** is displayed in Table 3.12.

Table 3.12: IR frequency assignments for **13-mer** and **14-mer**

Complexes	Carbonyl stretching frequency (cm ⁻¹)		
	A ₁ ⁽¹⁾	B ₁	A ₁ ⁽²⁾
 13-mer^a	2006 (w)	1921 (s)	1828 (vs)
 14-mer^a	2018 (w)	1920 (vs)	1828 (vs)
AA^a: [W(CO)₃(DPPE)C{(NHCy)(C₄H₃O)}]⁴²		1914 (s)	1821 (s)
AB^a: [W(CO)₃(DPPE)C{(NHCy)(C₄H₃S)}]⁴²		1916 (s)	1829 (s)
AC^a: [Cr(CO)₃(DPPE)C{(NHCy)(C₄H₃O)}]⁴⁸	2005 (w)	1911 (s)	1825 (s)
AD^a: [Cr(CO)₃(DPPE)C{(NHCy)(C₄H₃S)}]⁴⁸	2005 (w)	1909 (s)	1805 (s)
9^a	2064 (m)	1979 (m)	1898 (s)
10^a	2061 (m)	1977 (m)	1890 (m)

^aMedium: KBr

Tricarbonyl complexes exhibit C_{2v} symmetry in the *mer* isomeric form. This means a maximum of three carbonyl stretching peaks are expected on the IR spectrum, but often only two are observed

⁴⁸ Landman, M., Liu, R., Fraser, R., van Rooyen, P.H., Conradie, J., *J. Organomet. Chem.*, 752, **2014**, 171

(section 2.5.1).⁴⁹ Complexes **13-mer** and **14-mer** show good correlation to the symmetry and the *mer* isomer seems to dominate in solution of each complex. The data of **13-mer** and **14-mer** shows a good correlation to each other.

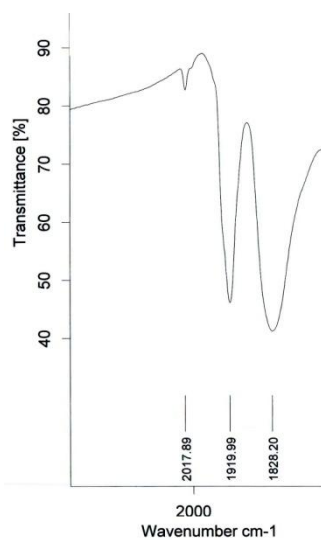
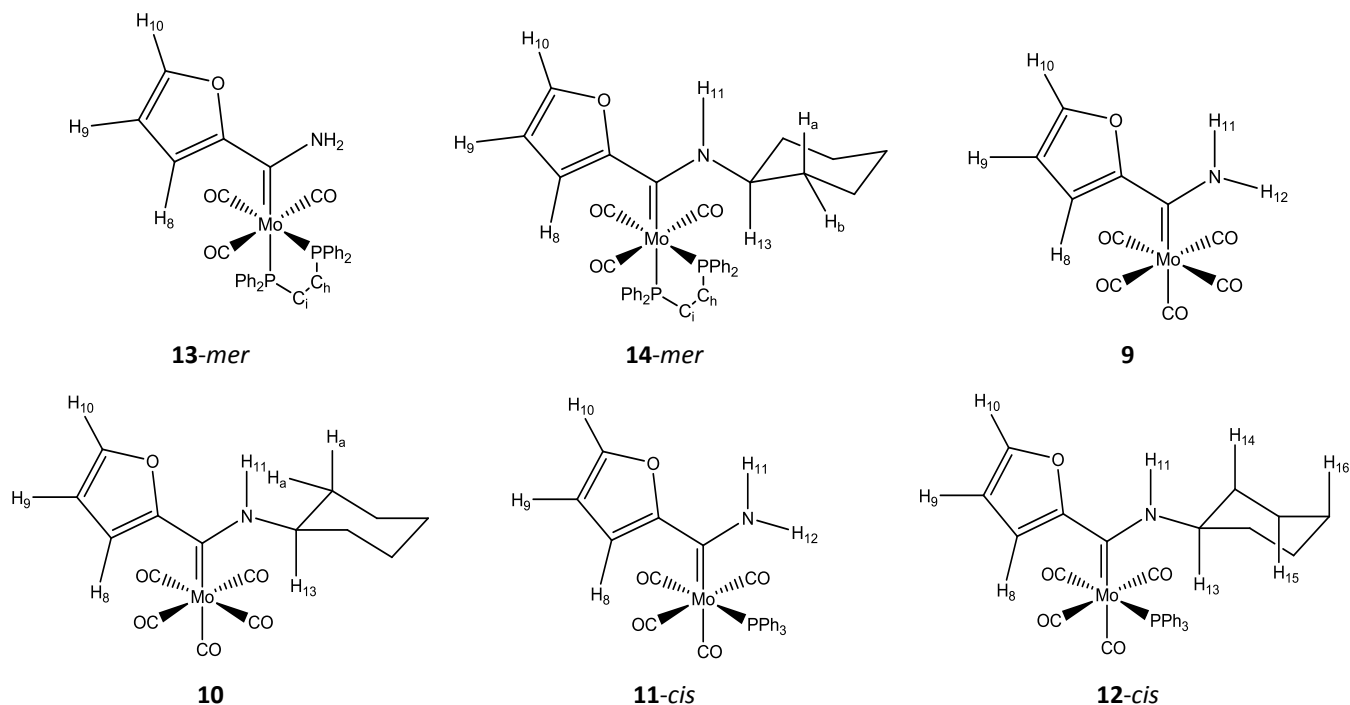


Figure 3.19: Carbonyl region on the experimental IR spectrum of **14-mer** (KBr)

3.4.2 ¹HNMR spectroscopy

The data in Table 13 is assigned based on the numbering system which follows.



⁴⁹ Braterman, P.S., Metal Carbonyl Spectra, Academic Press, 1975

Table 3.13: ¹H NMR assignments for 13-mer and 14-mer

Complex No.	Chemical Shift (δ , ppm), Multiplicity and Coupling constant (J, Hz)										
	H ₁₀	H ₉	H ₈	N-H ₁₁	N-H ₁₂	H ₁₃	H _a	H _b	PPh ₂	C _H H ₂	C _I H ₂
13-mer ^c	7.01 d J = 1.6	5.90 dd J = 1.8, 3.6	6.62 dd J = 4.3, 3.1	8.13 s	9.33 s				7.38- 7.34 m 7.07- 7.04 m	3.30 q J = 7.0	2.25 m
14-mer ^c	6.96 d J = 1.8	6.62 dd J = 1.7, 3.6	6.89 d J = 3.6	8.72 s		2.08 m	1.25 m	1.52 m	7.47- 6.83 m	3.44 m	2.62 dt J = 9.4, 14.0
AA ^b : [W(CO) ₃ (DPPE) C{(NHCy)(C ₄ H ₃ O)}] ⁴²	7.30 s	6.26 dd J = 1.5, 3.2	6.65 s	8.59 s		4.15- 4.30 m	1.12-1.90		7.25- 7.45 7.55- 7.75 m	2.22-2.50 m	
AB ^b : [W(CO) ₃ (DPPE) C{(NHCy)(C ₄ H ₃ S)}] ⁴²	7.02- 7.45 m	6.91 dd J = 4.9, 3.6	6.52 dd J = 1.2, 3.5	8.40 s		3.90- 4.05	1.15-1.90 m		7.02- 7.45 7.57- 7.72	2.55- 2.85 m	2.20- 2.50 m
AC ^d : [Cr(CO) ₃ (DPPE) C{(NHCy)(C ₄ H ₃ O)}] ⁴⁸	7.45 dd J = 0.9, 1.8	6.50 dd J = 1.8, 3.5	7.01 dd J = 0.8, 3.5	8.65 s		3.70- 3.83 m	1.20-1.60 m		7.25- 7.70 7.44- 7.72 m	2.65 m	2.41- 2.53 m
AD ^d : [Cr(CO) ₃ (DPPE) C{(NHCy)(C ₄ H ₃ S)}] ⁴⁸	7.42 dd J = 1.1, 5.0	7.03 dd J = 3.7, 5.0	7.46 dd J = 1.2, 3.7	8.40 s		3.93 m	1.20-2.10 m		7.20- 7.40 7.55- 7.70 m	2.85- 2.96 m	2.53- 2.70 m
9 ^a	7.54 d J = 1.7	6.16 dd J = 1.8, 3.7	7.5 d J = 3.7	8.05 s	8.76 s						
10 ^a	7.36 d J = 1.6	6.46 dd J = 1.8, 3.6	7.30 d J = 3.6	8.91 s		2.20 dd J = 5.1, 10.6	1.14 m	1.38 dt J = 11.2, 15.5			
11-cis ^c	7.45 dd J = 1.7, 3.6	6.52 dd J = 1.8, 3.6	7.29 dd J = 2.6, 3.0	7.13 s	8.20 s				7.34- 7.33 m		
12-cis ^c	7.55 d J = 1.5	6.25 dd J = 1.8, 3.6	6.82 d J = 3.4	8.82 s		2.30 dd J = 11.4, 14.7	1.27 s	1.54 s	7.37- 7.31 m		

^aSolvent: CDCl₃ (7.24ppm)

^bSolvent: CD₂Cl₂ (5.32 ppm)

^cSolvent: C₆D₆ (7.2ppm)

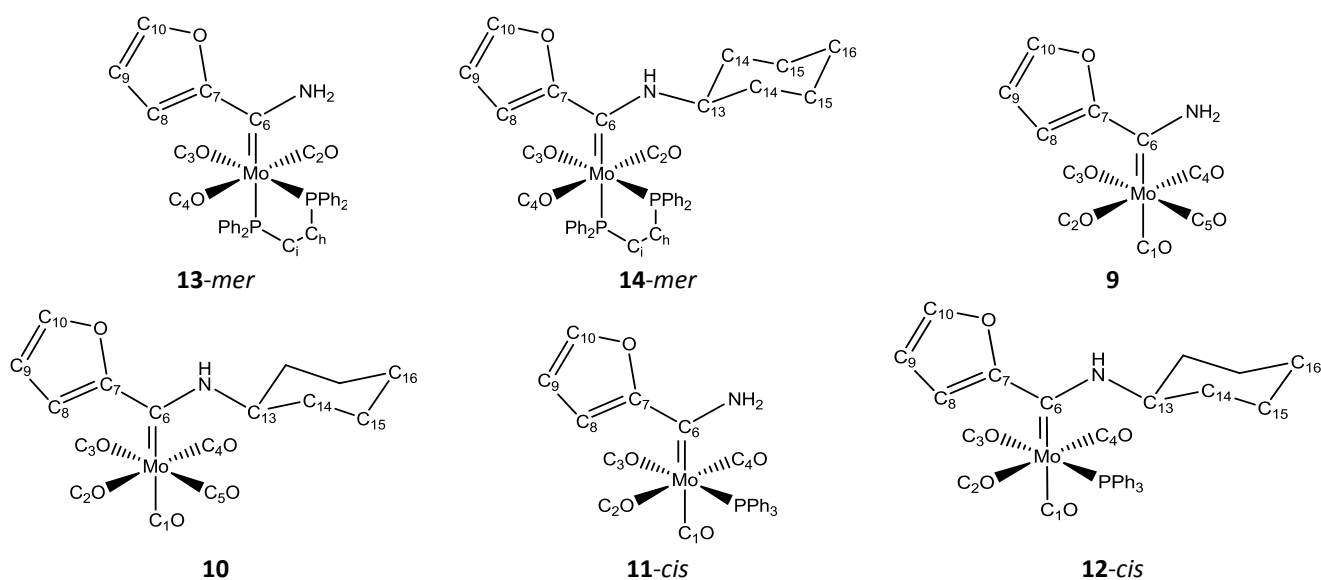
^dSolvent: CD₃CN (1.93ppm)

In general, H₈, H₉ and H₁₀ are more upfield in **13-mer** and **14-mer** than in **9**, **10**, **11-cis** and **12-cis**. This indicates that in these complexes, these protons have become more shielded. This can have its roots in the fact that the DPPE ligand consists of two diphenyl phosphine moieties - which are not as good π -acceptors as the carbonyls - and an ethyl moiety. The ethyl moiety of the DPPE will donate electron density to the phosphine moieties, since alkyl moieties are electron donors.³⁴ As a result of this, the phosphine moieties will be a weaker acceptor of electron density from the metal. This means that there will be more electron density to distribute over the rest of the molecule.

The set of **13-mer** and **14-mer** follows the trends of the previous sets (**9** and **10**, and **11-cis** and **12-cis**) in that the proton on the cyclohexylamine is observed more downfield than the same proton on the amino group. Again it can be seen that only three signals are present for all the protons of the cyclohexyl ring moiety. Two of these three signals represent the axial protons (1.25 ppm) and the equatorial protons (1.52 ppm). The third signal represents the proton on the *ipso* carbon (2.08 ppm).

3.4.3 ¹³C NMR spectroscopy

The data in Table 14 is assigned based on the following atom numbering system:



With regard to Table 3.14, the following legend is necessary to state.

AA^b: [W(CO)₃(DPPE)C{(NHCy)(C₄H₃O)}]⁴²

AB^b: [W(CO)₃(DPPE)C{(NHCy)(C₄H₃S)}]⁴²

AC^d: [Cr(CO)₃(DPPE)C{(NHCy)(C₄H₃O)}]⁴⁸

AD^d: [Cr(CO)₃(DPPE)C{(NHCy)(C₄H₃S)}]⁴⁸

Table 3.14: ^{13}C NMR assignments for 13-mer and 14-mer

Complex	Chemical Shift (δ , ppm)														
	C_1O (<i>trans</i>) [#]	C_3O	$\text{C}_2\text{O},$ $\text{C}_4\text{O},$ (<i>cis</i>) [#]	C_6	C_7	C_8	C_9	C_{10}	C_{13}	C_{14}	C_{15}	C_{16}	C_i	C_h	Aro- matic
13- mer ^c		224.7	253.1	300.9	159.3	114.7	113.8	142.3					30.1	28.7	139.4- 138.8 m 133.5- 132.3 m 129.1- 128.5 m
14- mer ^c		300.7	n.o	306.9	158.4	128.2	113.1	143.3	66.2	32.3	24.3	25.0	34.0	25.4	133.5- 132.9 m 130.2- 128.0 m
AA ^b		218.5	202.9	n.o	161.7	113.5	108.3	145.2	55.7	34.0	26.2	25.6	35.7	32.6	131.2- 139.2
AB ^b		216.9	208.7	n.o	159.5	121.0	113.7	126.5	58.7	32.0	25.3	24.4	33.4	30.9	140.1 132.2 128.8 130.6
AC ^d		235.5	220.1 229.0	262.6	157.8	129.7	118.7	143.5	59.8	30.7	24.4	25.5	33.2	31.5	138.5 131.8 129.1 131.3
AD ^d		234.4	220.1 229.0	277.7	150.6	123.0	119.2	126.1	58.1	30.3	25.0	25.6	33.1	31.7	138.0 132.7 129.2 131.4
9 ^a	212.5	206.6		243.0	157.5	129.3	114.3	145.3							
10 ^a	121.6	206.6		237.3	157.8	126.1	113.7	144.0	63.7	33.2	24.6	25.0			
11- cis ^c	218.3	215.5	210.5	250.4	158.1	127.9	114.0	144.1							128.3- 136.0

Complex	Chemical Shift (δ , ppm)														
	C ₁ O (<i>trans</i>) [#]	C ₃ O	C ₂ O, C ₄ O, (<i>cis</i>) [#]	C ₆	C ₇	C ₈	C ₉	C ₁₀	C ₁₃	C ₁₄	C ₁₅	C ₁₆	C _i	C _h	Aro- matic
12-<i>cis</i> ^c	218.8	214.6	211.7	238.6	159.1	126.5	113.4	144.0	66.2	33.3	25.0	25.6			337.0- 128.7

^aSolvent: CDCl₃ (77 ppm)

^bSolvent: CD₂Cl₂ (54.0 ppm)

^cSolvent: C₆D₆ (128.0 ppm)

^dSolvent: CD₃CN (1.4, 118.7 ppm)

[#]Position relative to carbene ligand

There is no significant variation between the data obtained for any of the carbon spectra studied in this chapter. The only variation is in the carbonyl region and the carbene carbon. In **13-mer** all the carbonyl signals, as well as the carbene carbon, are more down field than in **9**, **10**, **11-*cis*** and **12-*cis***. This reiterates what was found at the analysis of the ¹H NMR spectrum. There is more electron density to distribute over the rest of the molecule when there are two phosphine ligands bound to the same metal.

3.4.4 ³¹P NMR spectroscopy

Table 3.15: ³¹P NMR assignments for **13-mer** and **14-mer**, including literature values

Complex	Chemical Shift (δ , ppm)	
	<i>Trans</i> to C ₃ O	<i>Trans</i> to C ₆
13-mer ^c	58.0	56.2
14-mer ^c	52.1	47.6
AA ^b : [W(CO) ₃ (DPPE)C{(NHCy)(C ₄ H ₃ O)}] ⁴²	46.4	39.1
AB ^b : [W(CO) ₃ (DPPE)C{(NHCy)(C ₄ H ₃ S)}] ⁴²	45.6	40.2
AC ^d : [Cr(CO) ₃ (DPPE)C{(NHCy)(C ₄ H ₃ O)}] ⁴⁸	78.9	77.6
AD ^d : [Cr(CO) ₃ (DPPE)C{(NHCy)(C ₄ H ₃ S)}] ⁴⁸	79.4	77.3
11-<i>cis</i> ^c	42.1	
12-<i>cis</i> ^c	41.4	

^bSolvent: CD₂Cl₂

^cSolvent: C₆D₆

^dSolvent: CD₃CN

Both of the phosphine signals in **13** and **14** are more downfield than in the complexes where there was only one phosphine on the molecule (**11-*cis*** and **12-*cis***). The phosphine *trans* to the carbonyl is more downfield than the phosphine *trans* to the carbene carbon. This is due to the carbonyl being a better π -acceptor than the carbene ligand, which would withdraw electron density making the phosphine more deshielded.

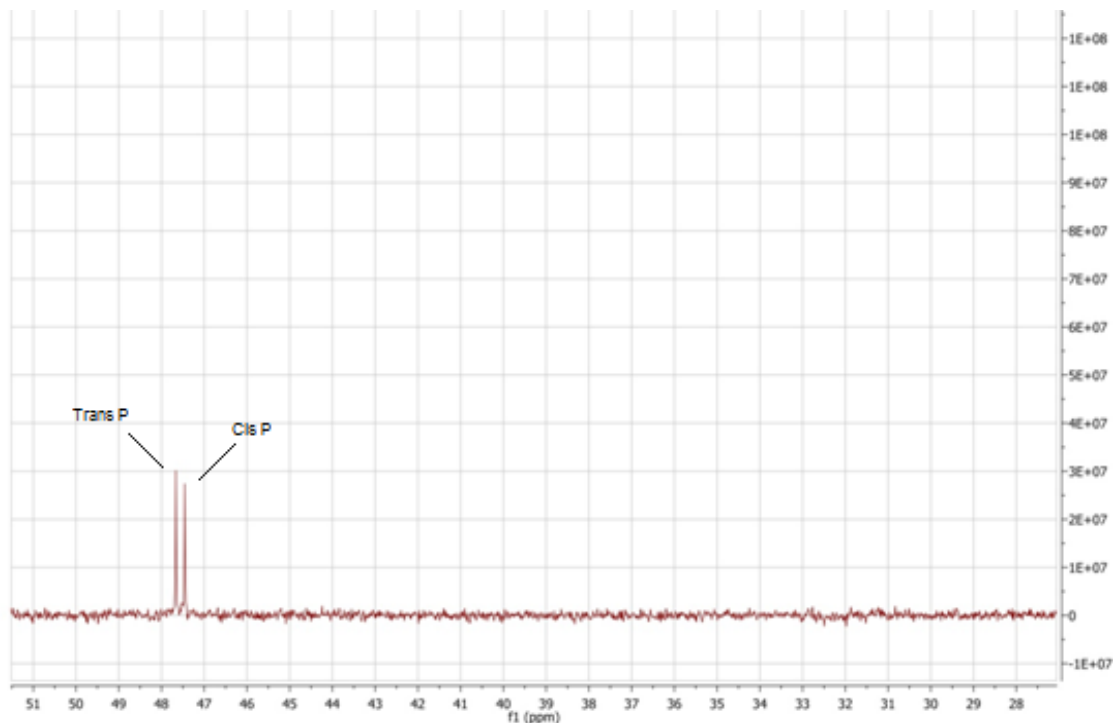


Figure 3.20: ^{31}P NMR spectrum of **14-mer** (C_6D_6)

The spectrum shown in Figure 3.20 shows the ^{31}P NMR of **14-mer**, the signals are both singlets. The signal on the left is the phosphine *trans* to the carbonyl and the signal on the right is the phosphine *trans* to the carbene carbon.

3.4.5 X-Ray crystallography

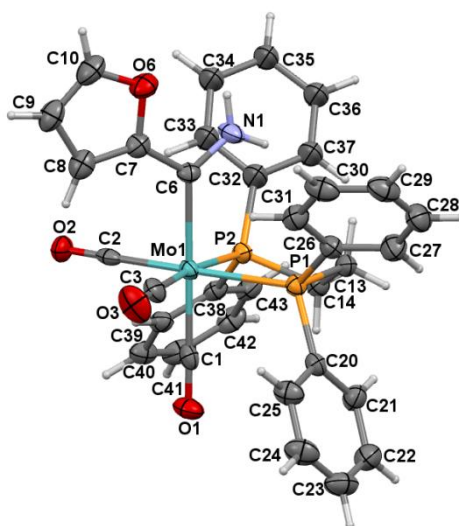


Figure 3.21: Crystal structure of **13-fac** (ORTEP representation)

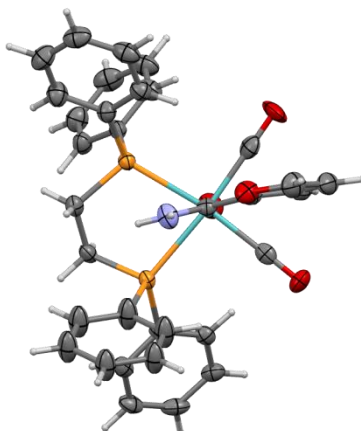


Figure 3.22: View down $C_6 \rightarrow Mo$ bond

It can be seen from Figure 3.22 that the amino group and the furfuryl group are in the same plane. The $P_1-C_{13}-C_{14}-P_2$ dihedral angle is $55.0(6)^\circ$.

Table 3.16: Bond lengths obtained for the crystal structure of **13-fac**

Bond	Bond Length (Å)
O_6-C_{10}	1.357(14)
O_6-C_7	1.389(13)
C_6-C_7	1.449(14)
$N-C_6$	1.323(11)
C_9-C_{10}	1.333(14)
C_8-C_9	1.413(14)
C_7-C_8	1.357(17)
$Mo-C_6$	2.218(8)
$Mo-C_1$	1.996(9)
$Mo-C_2$	1.971(8)
$Mo-C_3$	1.972(9)
$Mo-P_1$	2.502(2)
$Mo-P_2$	2.514(2)

When compared to the crystal bond length data obtained for **9** and **10**, the data in Table 3.16 has no significant differences. There is a small difference in the metal-carbonyl bond length, however. This slight difference can be attributed to the two phosphine moieties which replaced two carbonyl ligands.

Upon comparison to **11-cis**, a trend can be seen to be emerging - the M-C bond length of the carbonyl *trans* to the phosphine is smaller than the bond lengths of all the other carbonyls. The carbonyl *trans* to the carbene moiety has the second shortest bond length. The comparison to **11-cis** also shows that none of the other bond lengths in the molecule differs significantly.

The Mo-P bond lengths are similar to those found in the study by Powell *et al.* (2.496(2) Å and 2.485(2) Å).⁵⁰ The Mo- C_6 bond length of **13-fac** is similar to that found by Schobert *et al.*

⁵⁰ Powell, J., Rarrar, D.H., Smith, S.J., *Inorg. Chim. Acta*, 85, **1984**, L23

(2.226(3) Å).⁵¹ Finally, the N-C₆ bond length of **13-fac** correlates very well to that of Schobert *et al.*⁵¹ (1.309(4) Å) and to that of Streubel *et al.* (1.303(3) Å).⁵²

Table 3.17: Bond angles for the crystal structure of 13-fac

Angle	Angle size (°)
N-C ₆ -C ₇	112.3(8)
H-N-H	119.96
C ₆ -Mo-C ₂	88.90(3)
C ₆ -Mo-C ₃	90.90(3)
C ₆ -Mo-P ₁	93.95(19)
C ₆ -Mo-P ₂	93.78(18)
P ₁ -Mo-P ₂	79.75(7)
C ₂ -Mo-P ₂	95.7(3)

The bond angles around the metal show no significant deviation from the ideal octahedral geometry angles, for the most part. The only exception to this is the angle between the phosphine moieties. This is a consequence of the bite angle of the bidentate ligand. The angle between the protons on the nitrogen moiety is congruent with the perfect trigonal planar geometry. This points to the probability of the resonance structure showing a double bond between C₆ and the heteroatom to be the dominant resonance structure.

3.2.5 Computational analysis

It was not necessary to calculate all of the possible conformations discussed at the beginning of each section for the different complexes. The structural model used for the calculations in this chapter was based on a recent study of conformations of pentacarbonyl carbene complexes. Thompson *et al.*³² found that for carbene complexes substituted with amino and furyl moieties, the *syn* conformation is more stable. The optimised conformations that were attained were similar to those of the crystal structures obtained for these complexes. In the case where the crystal structure data and the solution data was not in agreement, both isomers were computed and compared.

Note: the numbering system adopted for the tables and figures in this section is the same as that used throughout the previous sections.

⁵¹ Schobert, R., Kempe, R., Schmalz, T., Gmeiner, A., *J. Organomet. Chem.*, 691, **2006**, 859

⁵² Streubel, R., Hobbold, M., Jeske, J., Ruhte, F., Jones, P.G., *J. Organomet. Chem.*, 529, **1997**, 351

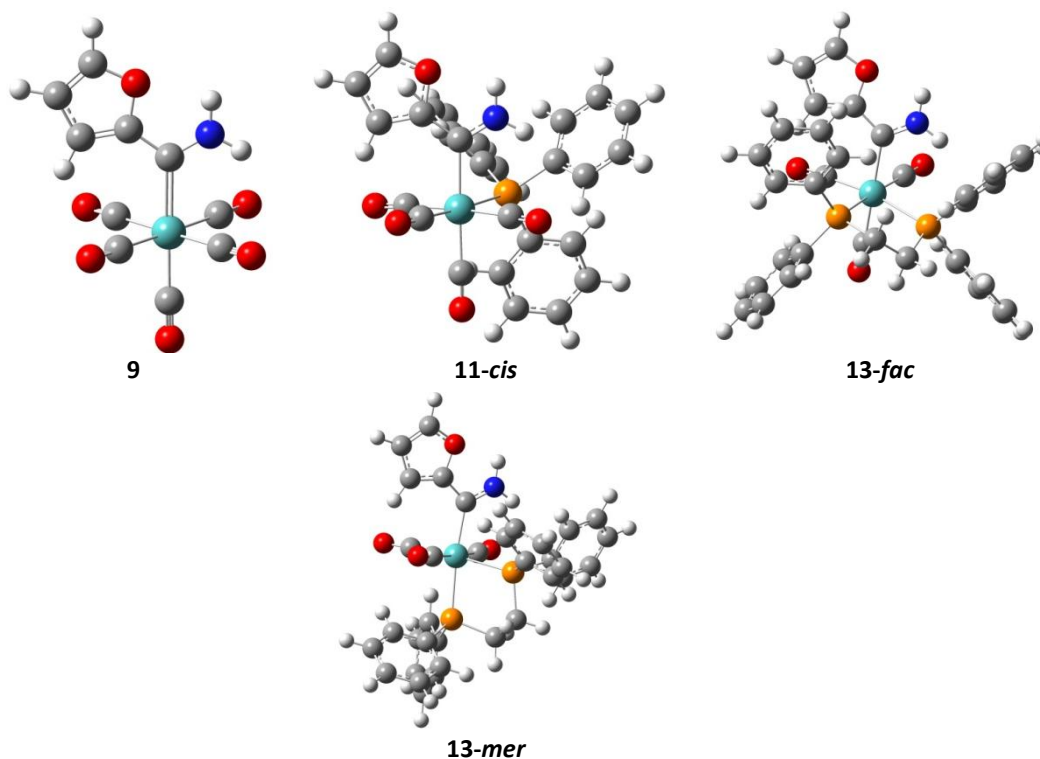


Figure 3.23: Optimised structures of **9**, **11-cis**, **13-fac** and **13-mer**

The optimised structures are similar in conformation to the crystal complexes.

It was found that the *mer* isomer of **13** was 2.95 kJ/mol lower in energy than the *fac* isomer. This does not parallel the crystal that was found. The data for **9**, **11-cis** and both the *fac* and *mer* isomers of **13** will be presented here.

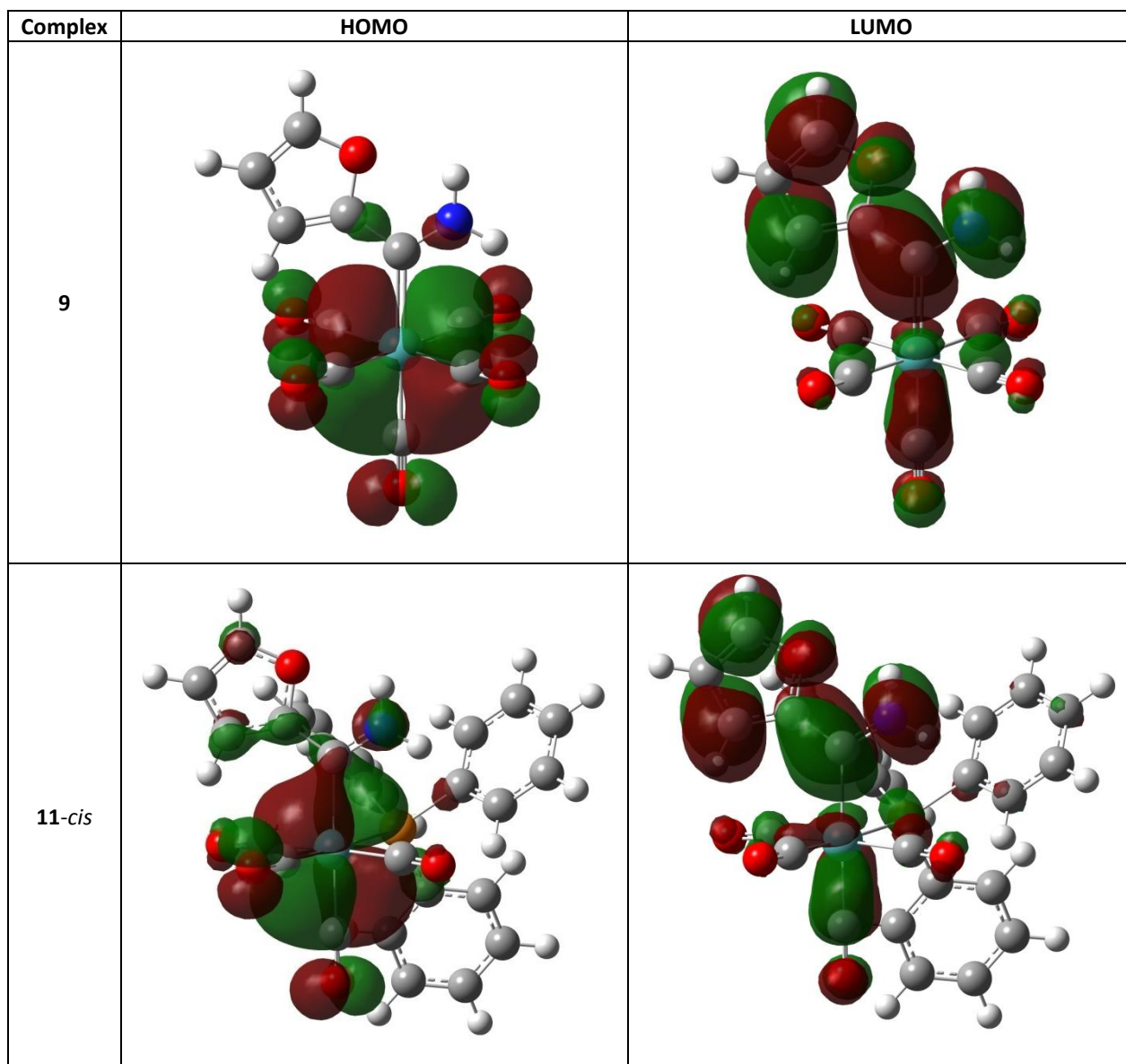
From the optimised structures in Figure 3.23, it can be seen that it is predicted that the phosphine will substitute on the amino side of the molecule. This is what is observed in the crystal structures presented in previous sections.

The bond lengths are given by the following:

Table 3.18: Bond length comparison of **9**, **11-cis** and **13**

Bond Type	Average Bond Lengths (Å)						
	Calculated				Crystal		
	9	11-cis	13-fac	13-mer	9	11-cis	13-fac
Mo-CO	2.08	2.04	2.00	2.03	2.041(3)	2.013(3)	1.980(9)
Mo-C ₆	2.22	2.25	2.26	2.18	2.233(3)	2.225(2)	2.218(8)
C ₆ -C ₇	1.45	1.45	1.45	1.46	1.444(3)	1.454(3)	1.449(14)
N-C ₆	1.33	1.33	1.33	1.34	1.316(3)	1.314(3)	1.323(11)
Mo-P ₁		2.64	2.58	2.53		2.523(1)	2.514(2)
Mo-P ₂			2.58	2.57			2.502(2)

The bond lengths of **9**, **11-cis** and **13** show, in general, a very good correlation between the calculated structure data and the crystal structure data. This indicates that the computational model is an adequate representation of the crystal structures presented in previous sections, in terms of the bond length data. The calculated Mo-C₆ bond length and both of the P-Mo bond lengths are shorter in the *mer* isomer of **13**. Both of the Mo-P bonds are calculated to be somewhat longer than that which is found in the crystal structure. Crystal packing features may lead to this observation since the calculation was done assuming gas phase.



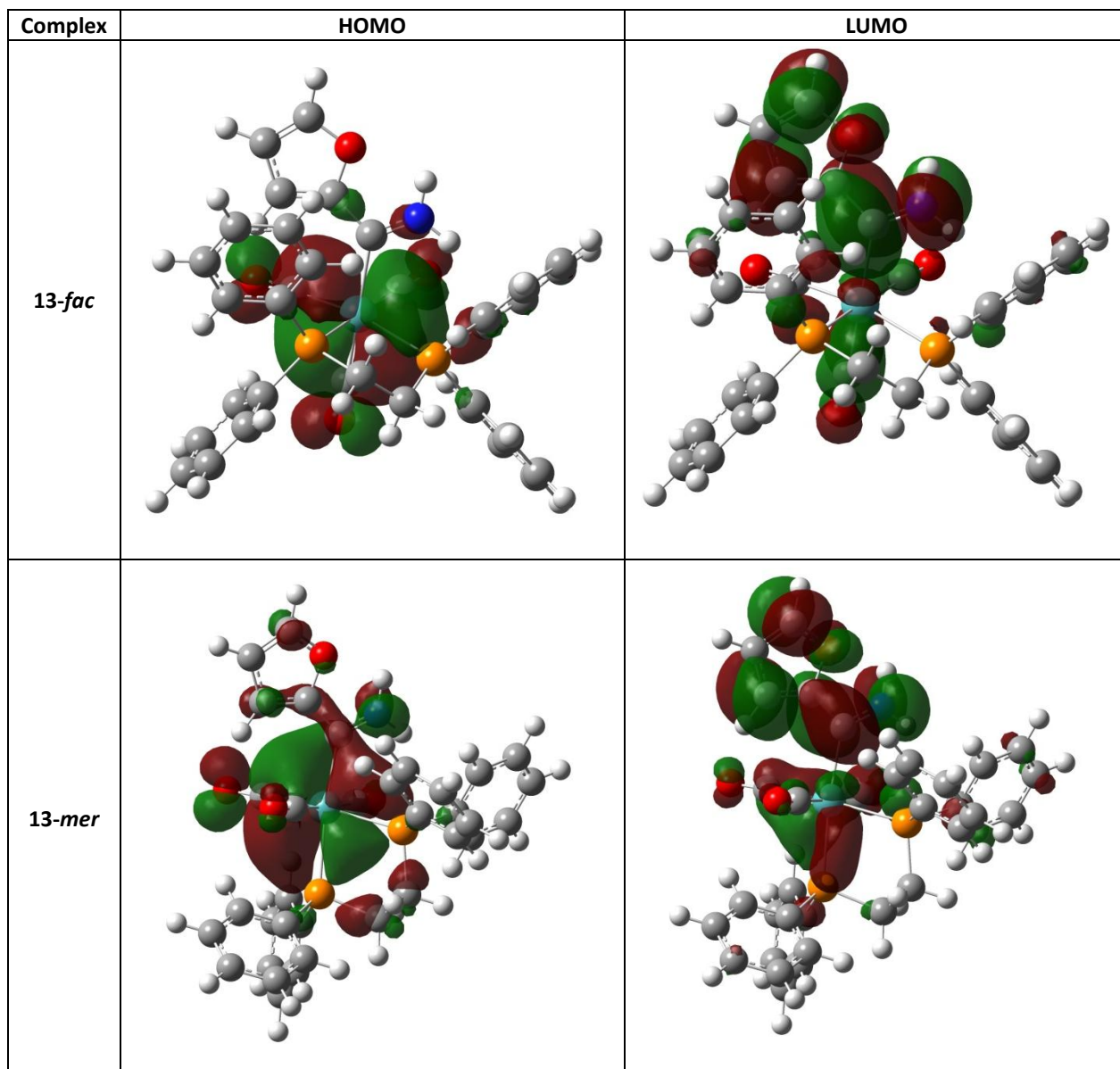


Figure 3.24: a) HOMO and LUMO illustrations of **9**, **11-*cis***, **13-*fac*** and **13-*mer***

The highest contribution to the LUMO of **9**, **11-*cis***, **13-*fac*** and **13-*mer*** corresponds to a $2p_z$ orbital, a $2p_y$ orbital, a $2p_z$ orbital and a $2p_z$ orbital, respectively, on the carbene carbon. The LUMO is found most concentrated on the carbene carbon (nucleophilic attack will be directed to here) for all of the complexes calculated.

The highest contribution to the HOMO of **9**, **11-*cis***, **13-*fac*** and **13-*mer*** corresponds to the d atomic orbital on the molybdenum atom. Once again the HOMO is found on the molybdenum atom (nucleophilic attack will come from here) for all the complexes investigated.

Table 3.19: HOMO-LUMO gap in eV for **9**, **11-cis**, **13-fac** and **13-mer**

Complex	HOMO-LUMO gap (eV)
9	+3.47
11-cis	+3.16
13-fac	+3.07
13-mer	+3.11

Although the monophosphinated complexes were predicted to be the most reactive, and the diphosphinated complexes the least reactive⁵³, this is not observed here. The data in Table 3.19 shows that **13-fac** should be the most reactive complex, and **9** should be the least reactive.

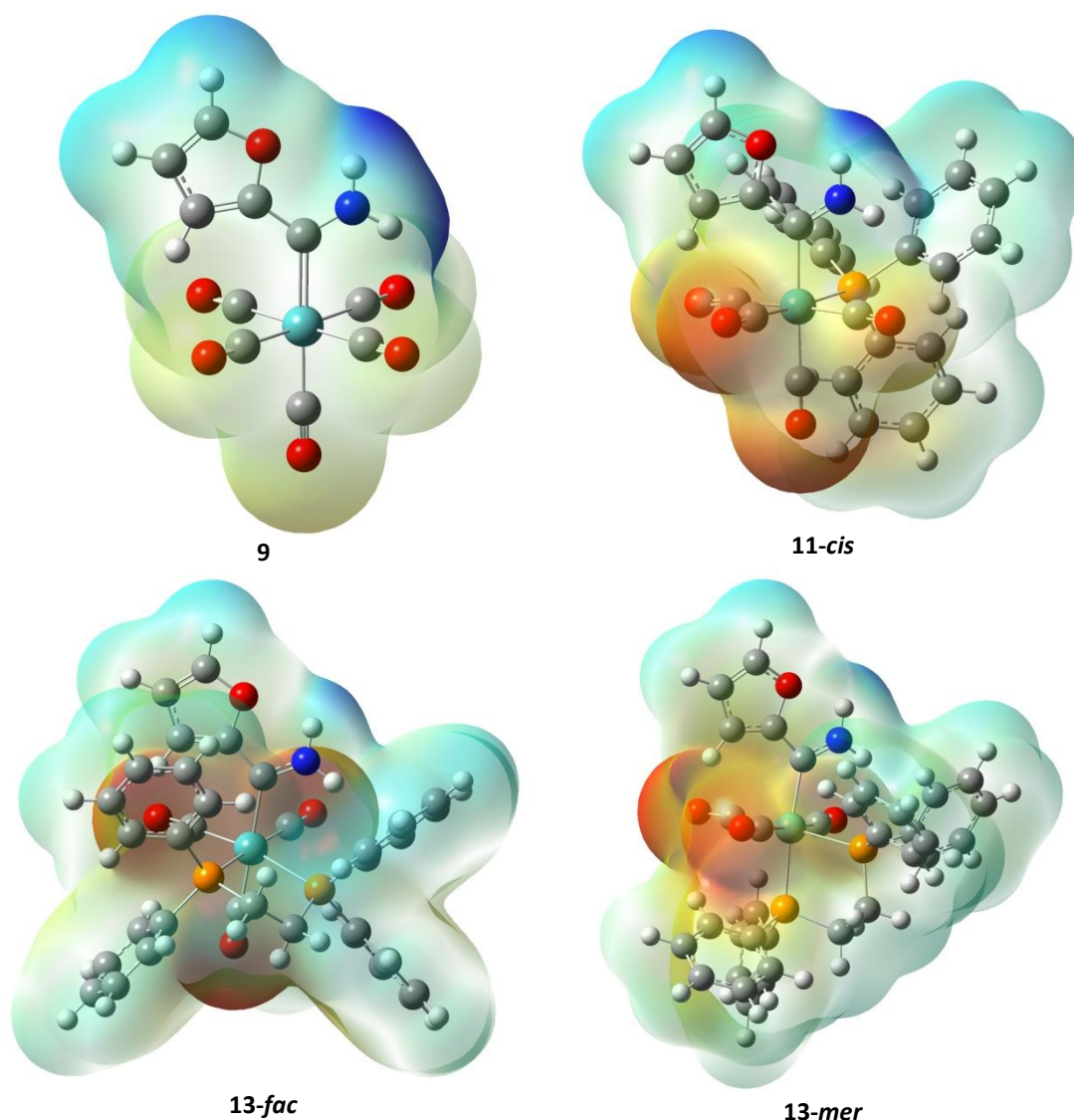


Figure 3.25: Electrostatic Potential energy map of **9**, **11-cis**, **13-fac** and **13-mer**

It can be seen from Figure 3.25, that there is no notable high electron density area in **9**, rather it is delocalised over the metal and its carbonyls. There is a very electron poor region around the amino

⁵³ Arrieta, A., Cossío, F.P., Fernández, I., Gómez-Gallego, M., Lecea, B., Mancheño, M.J., Sierra, M.A., *J. Am. Chem. Soc.*, 122, **2000**, 11509

group and the carbene carbon and a little more density around the furyl ring, however is still electron deficient. In the case of **11-cis**, the regions of highest electron density lie on the carbonyls. There is little available electron density elsewhere in the molecule. The electrostatic map of both isomers of **13** (Figure 3.25) shows that the regions of high electron density on both molecules lie on the carbonyls. In both isomers of **13**, there is an electron deficient region around the NH₂ moiety but this is not as great as in the case of **9**. This is due to the fact that the phosphorous molecules are pushing more electron density into the molecule forcing the NH₂ to become less electron poor as more phosphine moieties are added to the molecule.

The generated IR spectra are good approximations to the general shape of the experimental IR spectra (Figure 3.26). There are no observed differences between the shape and/or order of peaks found in the spectra of the ethoxy-containing *mer* complexes and the amino-containing *mer* complexes.

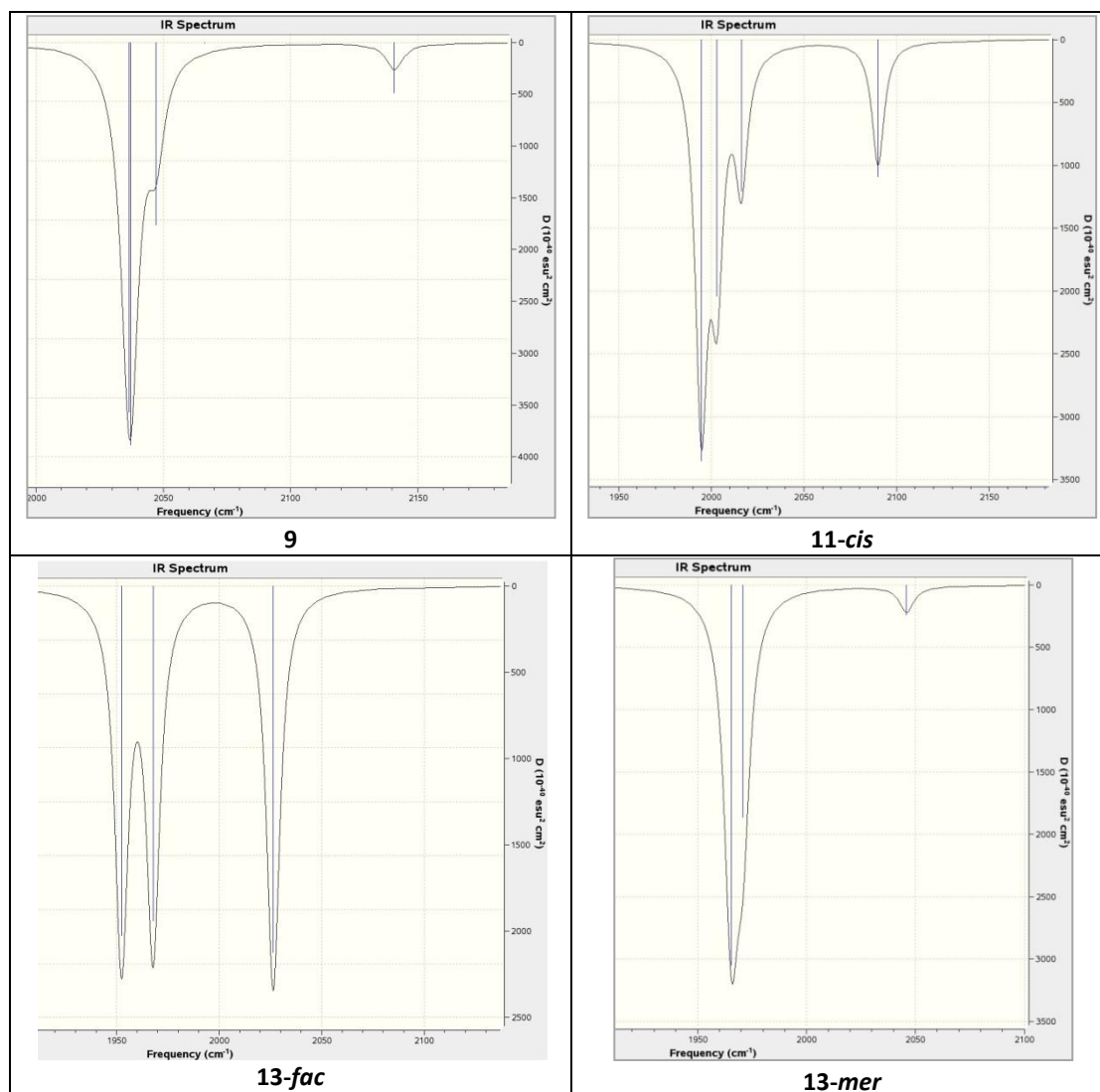


Figure 3.26: Theoretically calculated carbonyl regions of the IR spectra of **9**, **11-cis**, **13-fac** and **13-mer**

The method outlined by Zhang⁵⁴ (modified) is used to perform the scaling on the theoretical data. This is because the method was developed for the B3LYP/6-31G* method, and it gave the lowest rms value of those investigated.

Table 3.20: Comparison of theoretical and observed IR carbonyl stretching frequencies for **9, **11-cis**, **13-fac** and **13-mer****

Complex		CO stretching frequencies (cm ⁻¹)			
		A ₁ ⁽¹⁾	B ₁	E	A ₁ ⁽²⁾
9	Assignments	A ₁ ⁽¹⁾	B ₁	E	A ₁ ⁽²⁾
	Observed	2064	1979	1933	1898
	Calculated ^a	2033	1962	1934	1944
11-cis	Assignments	A ₁ ⁽¹⁾	B ₁	B ₂	A ₁ ⁽²⁾
	Observed	2008	1890	1854	1924
	Calculated ^a	1979	1897	1889	1909
13-mer	Assignments	A ₁ ⁽¹⁾	B ₁	A ₁ ⁽²⁾	
	Observed	2006	1921	1828	
	Calculated ^a	1967	1895	1891	

^aScaled calculated value

The raw data obtained from the calculations, is not a very good approximation of the actual data obtained experimentally. This is due to matrix effects as discussed previously. The scaling of the raw data using the modified Zhang method greatly improved the rms of the calculated values.

Comparison of the generated IR data of **9** to the recorded IR spectral data of **9** presented in Table 3.20, shows a good correlation on the whole. A slight discrepancy is seen in that the A₁⁽²⁾ band is found to the right of the E band in the recorded spectrum, not to the left as shown in the ethoxy carbene complex spectrum (section 2.3.6). There is excellent agreement between the scaled and the experimental values of the A₁⁽¹⁾ and A₁⁽²⁾ bands in **11-cis** (Table 3.20). In the case of **13-mer**, IR spectral data obtained from the generated IR, in Table 3.20, does not approximate the experimental data obtained. The rms was greatly improved by the scaling of the calculated data. There is no significant correlation between the experimental and the calculated data.

⁵⁴ Zhang, L., Zhang, Y., Tao, H., Sun, X., Guo, Z., Zhu, L., *J. Mol. Struct. (Theochem)*, 617, **2002**, 87

Chapter 4:

Comparisons and Conclusions

“It is a popular delusion that the scientific enquirer is under an obligation not to go beyond generalisation of observed facts... but anyone who is practically acquainted with scientific work is aware that those who refuse to go beyond the fact, rarely get as far.”

– Thomas Henry Huxley (1825 – 95)

4.1 Introduction

Within the pages of this chapter, comparisons will be made between the data presented in the previous chapters. These comparisons will include those between the individual analysis methods, with the aim of establishing whether there is a correlation between one property observable using one technique and another property observable with a different technique. These will be addressed in the general section of this chapter.

This chapter will also serve as a conclusion for this dissertation.

4.2 Comparisons

4.2.1 Infrared spectroscopy

The data used for the comparisons in this section can be found at sections 2.3.1, 2.4.1, 2.5.1, 3.3.1, 3.4.1 and 3.5.1.

Upon comparing the amino-substituted pentacarbonyl complexes with the ethoxy-substituted pentacarbonyl complexes, it is found that the intensity of the respective peaks is the same or very similar and the $A_1^{(1)}$ and B_1 bands are similar in frequency. In the case of the $A_1^{(2)}$ and E bands, however, the E band had the lowest frequency in the ethoxy-substituted complexes, while the $A_1^{(2)}$ band had the lowest stretching frequency in the amino-substituted complexes. This is as a result of the substitution of the ethoxy group for the amino group. The nitrogen is less electronegative than the oxygen in the ethoxy group, so charge that has been withdrawn from the metal is not able to be accommodated as well on the amino group compared to the ethoxy group. This makes this carbene ligand (amino analogue) a worse π -acceptor ligand which will cause the $A_1^{(2)}$ band to drop below the E band in frequency¹. This is found to be commonly the case in literature².

In the tetracarbonyl complexes, there is little difference between the stretching frequencies of the ethoxy-substituted complexes and the amino-substituted complexes. From this, it could be inferred that because of the presence of the triphenylphosphine ligand, the change in the heteroatom on the carbene has little effect on the electron density available for the carbonyls and thus there is little change in their IR stretching frequencies.

¹ A. Salzer, C. H. Elschenbroich, *Organometallics: A Concise Intro.*, Second Ed., **1992**, VCH Verlag, Weinheim, 210-241

² R. Fraser, MSc Thesis, Fischer and N-Heterocyclic carbene complexes of Chromium (0), **2012**

In the IR spectra of each complex observed during this study, all exhibited an $A_1^{(1)}$ band. The figure below shows graphically the trends observed in the carbonyl stretching frequencies of these complexes.

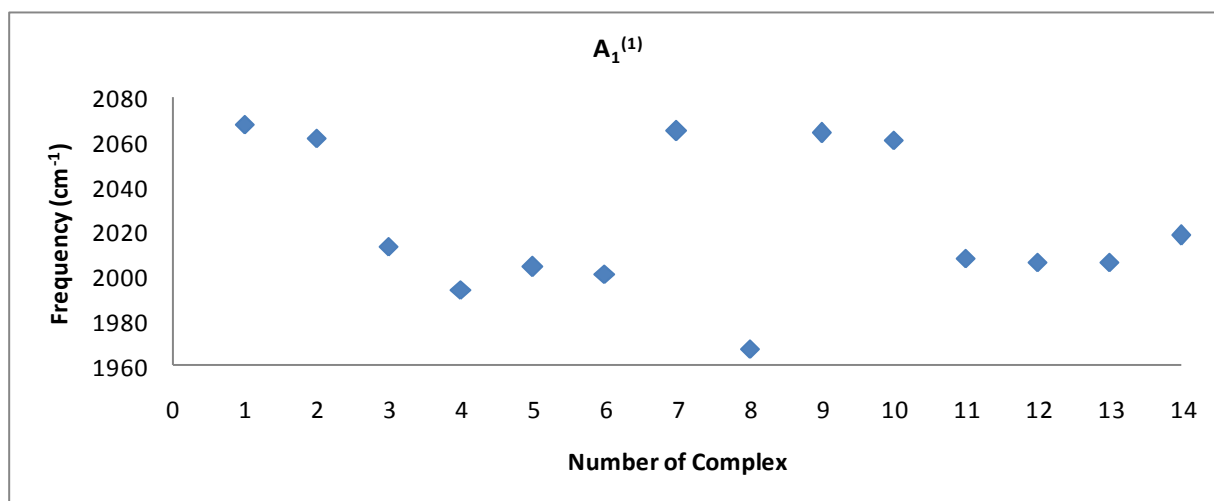


Figure 4.1: Graphical representations of the $A_1^{(1)}$ bands of the complexes observed in this thesis

It can be seen in Figure 4.1 that upon addition of the phosphine ligand, PR_3 , (irrespective of the R groups on the phosphine) to **1**, there is a decrease in the $A_1^{(1)}$ band (**3-cis** and **7**). The chromium ethoxy-substituted complexes (**5**, **6**) exhibit a lower $A_1^{(1)}$ stretching frequency than the molybdenum analogue (**3-cis**). There is not a large change in the frequencies upon exchange of the furyl moiety for a thienyl one.

Upon addition of the DPPE ligand (**8-mer**), there is also a drop in the frequency of this band. This means that the trend observed in the $A_1^{(1)}$ band of the ethoxy-substituted carbene complexes is as follows:



The aminolysed complexes follow the same trend and maintain approximately the same frequencies as observed for the ethoxy-substituted carbene complexes.

4.2.2 NMR spectroscopy

In the proton spectra of the amino-substituted complexes under study, H_{11} and H_{12} are found to be very broad singlets, as is common for amino group protons. They are not found to be in the same environment due to resonance structures that can be drawn (section 3.3.2).

In general, there is very little variation in the chemical shifts of the protons in the complexes under study. The data for this comes from sections 2.3.2, 2.4.2, 2.5.2, 3.3.2, 3.4.2 and 3.5.2.

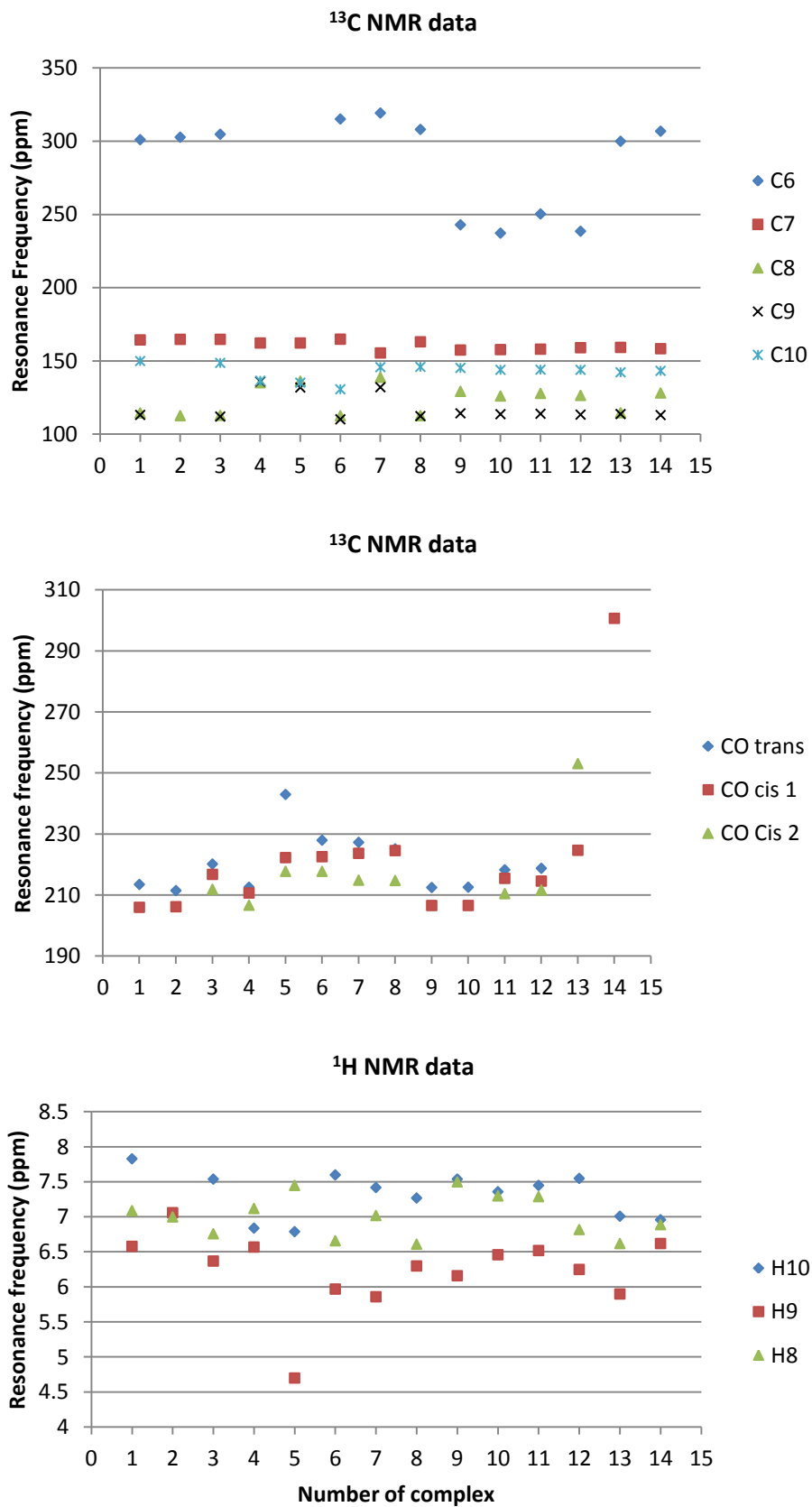


Figure 4.2: Summary of the NMR data obtained

In the carbon spectra, upon comparing the ethoxy-substituted complexes to the amino-substituted complexes, it can be seen that there is not a large variation in the chemical shifts of the carbonyls. This suggests that the change of the carbene substituents does not have a great effect on the electronic environment of the carbonyls.

For the amino-substituted pentacarbonyl- and the tetracarbonyl complexes, the carbene carbon is shifted quite further upfield than in the ethoxy-substituted complexes. This suggests that in changing the carbene substituent to an amino group, the carbene becomes more shielded since an amino group is not as good a π -acceptor as the ethoxy group and thus there is more electron density on the carbene carbon. The same trend is not observed in the tricarbonyl complexes.

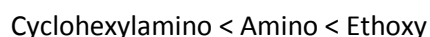
The phosphorous NMR spectra shows that the chemical shift observed for the tricarbonyl complexes have higher ppm values (more downfield) and thus shows that the phosphorous is deshielded in these complexes, when compared to the tetracarbonyl complexes.

The ^1H and ^{13}C NMR data is summarised in Figure 4.2; however conclusions cannot be drawn with respect to trends since the NMR experiments were performed in different solvents.

4.2.3 X-Ray crystallography

All the complexes with furyl and ethoxy carbene substituents crystallised in an *anti* conformation for the pentacarbonyl and tetracarbonyl carbene complexes. In the tricarbonyl case, the crystal was in a *syn* conformation. The complex whose carbene carbon was substituted with thienyl and ethoxy moieties crystallised in a *syn* conformation regardless of the number of carbonyl ligands attached to the metal centre. All the complexes with furyl and either amino or cyclohexylamino carbene substituents crystallised in the *syn* conformation, regardless of the identity of the other ligands attached to the metal centre.

The normal average hexacarbonyl molybdenum bond length is approximately 2.055 Å.³ Upon addition of the carbene ligand, this average carbonyl bond length decreases to 2.044(12) Å, 2.0414(3) Å and 2.039(4) Å in the ethoxy-, amino- and cyclohexylamino-substituted carbene complexes, respectively. The trend that is observed is the following:



This observation indicates that resonance plays a larger role in the amino complexes than the ethoxy complexes.

³ Mak, T.C.W., *Z. Kristallogr.*, 166, **1984**, 277

The fact that the Mo-C₆ bond increases indicates that the replacement of the ethoxy group with the smaller, less electronegative amino group, decreases the amount of back bonding (and therefore the bond strength) to the carbene carbon, not by much, but it is still noteworthy. The CO bond *trans* to the carbene carbon decreased in length upon addition of the amino group, indicating a stronger metal-carbon bond and more back bonding. Interestingly the bond lengths of the two carbonyls on the amino side increase in bond length while the other two decrease in bond length, this may be due to less steric hindrance on the amino side of the complex.

There is not a large change in the bond length of the N-C₆ bond of the amino-substituted complexes when compared to the O₇-C₆ bond of the ethoxy-complexes. The N-C₆ bond length is a little larger than O₇-C₆ which is to be expected since nitrogen is less electronegative than oxygen. This is supported by the organic structures obtained by Knighton *et al.*⁴ where the N-C bond is 1.4655(3) Å, and that obtained by Guo *et al.*⁵ where the N-O bond length is 1.435(3) Å.

The carbene-molybdenum bond is shorter in the ethoxy-substituted complexes, indicating that there is more double bond character in the carbene-metal bond. The carbene-molybdenum bond is less double bond in nature in the amino-substituted complexes. The N-C₆ bond is more double bond in nature, as evidenced by the NMR analysis; however this is not so clearly reflected in the crystal data. The phosphine metal bond is very slightly smaller in the amino-substituted- than in the ethoxy-substituted complexes.

The angles between C₆-Mo-CO (carbonyls) have increased significantly in the penta- and tetracarbonyl amino-substituted complexes when compared to the penta- and tetracarbonyl ethoxy-substituted complexes. The C₄-Mo-P bond angle (on the amino side of the molecule) in tetracarbonyl complex, is smaller by approximately 3.74 ° than the same angle in the ethoxy-substituted case. This is because C₄ can get closer to the triphenylphosphine ligand when there is only a hydrogen to serve as steric hindrance (as in the amino-substituted complex), rather than a carbon as well as a hydrogen (as in the case of the ethoxy-substituted complex).

The figures below show, graphically, selected bond lengths (Mo-C₁/P and Mo-C₅/P) from each of the crystals obtained. The numbering system is the same as that used in the previous chapters and is shown here for convenience.

As expected, one can see overlap of some of the bond lengths for Mo-C₁/P and Mo-C₅/P. These are due to the ligands at Mo-C₁/P and Mo-C₅/P both being carbonyls, and therefore pentacarbonyl

⁴ Knighton, R.C., Sambrook, M.R., Vincent, J.C., Smith, S.A., Serpell, C.J., Cookson, J., Vickers, M.S., Beer, P.D, *Chem. Commun.*, 49, **2013**, 2293

⁵ Guo, Z., Wang, S., Tong, H., Chao, J., Wei, X., *Inorg. Chem. Commun.*, 33, **2013**, 68

complexes (**1**, **9** and **10**) or both being phosphines (tricarbonyl complex, **8-mer**). In the remaining tetracarbonyl complexes (**3-cis**, **5**, **11-13**), it is found that the ligand at Mo-C₅/P is consistently higher than those at Mo-C₁/P - due to there being a less π -accepting phosphine at Mo-C₅/P. This means that the phosphine bond is more single bond in nature, and the carbonyl bond is more double bond in nature upon addition of the phosphine ligand. The bond length between C₆ and the heteroatom does not fluctuate with the identity of the hetero-atom. The only notable fluctuation in the metal-C₆ bond length is when there is a change in the metal centre (**5**), this is not a surprising result.

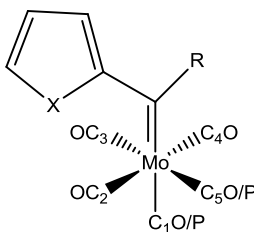


Figure 4.3: Depiction of the atom labels for use in Figure 4.4

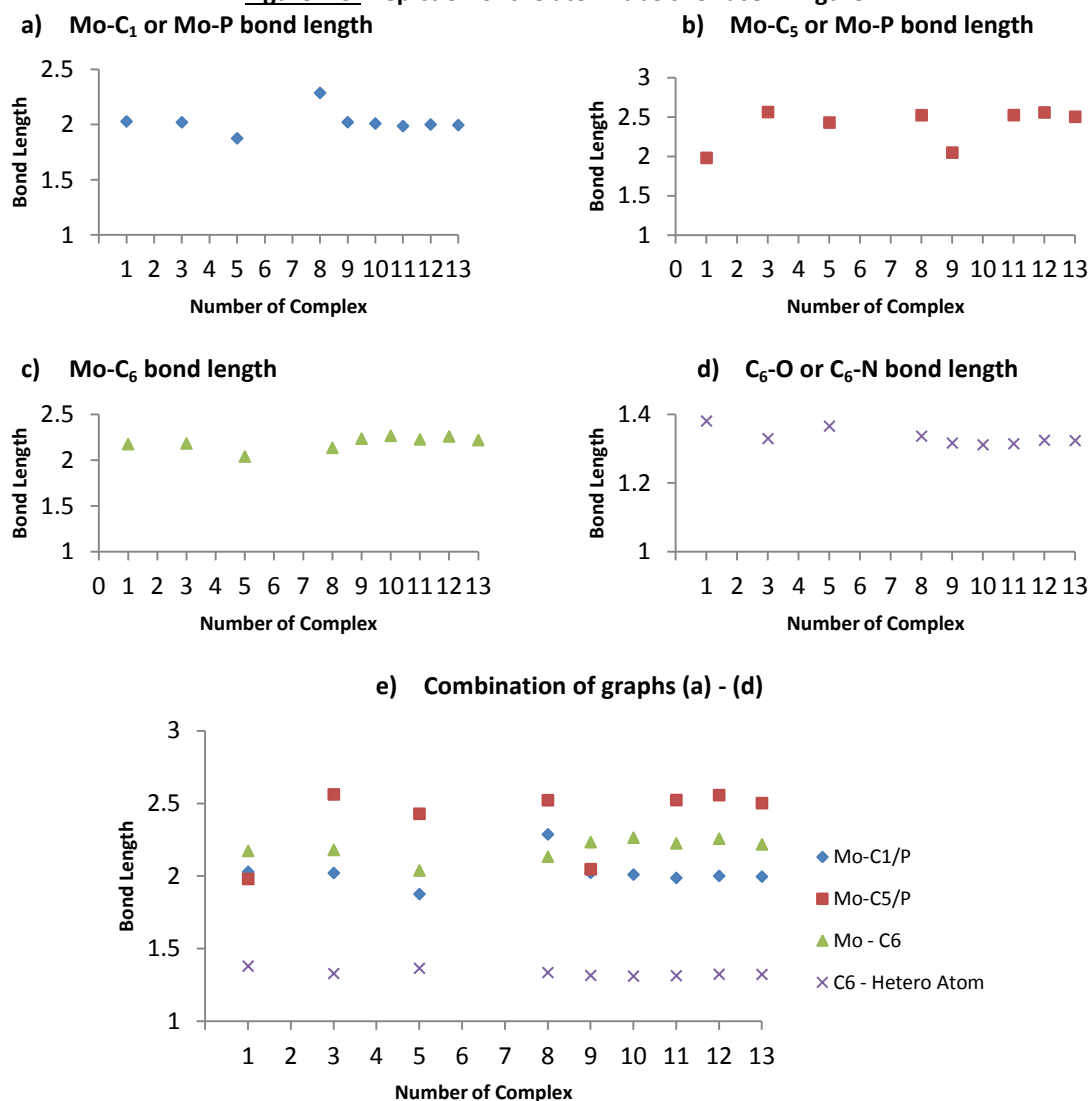


Figure 4.4: Graphical representation of the bond lengths of selected bonds for all crystals obtained in chapters 2 and 3, both individually and superimposed.

Table 4.1: Comparison of average bond lengths and the effects of metal centre and extent of carbonyl substitution

Metal	Bond lengths	Pentacarbonyl		Tetracarbonyl		Tricarbonyl	
		Amino	Ethoxy	Amino	Ethoxy	Amino	Ethoxy
Mo	Mo-C ₆	2.249(4)	2.173(7)	2.241(4)	2.180(3)	2.218(8)	2.133(3)
	C ₆ -C ₇	1.453(5)	1.41(4)	1.447(6)	1.447(4)	1.449(14)	1.457(4)
	C ₆ -X	1.314(4)	1.38(3)	1.319(6)	1.329(4)	1.323(11)	1.336(3)
Cr	Mo-C ₆	2.0912(13)	-	-	2.038(6)	2.035(5)	1.992(17)
	C ₆ -C ₇	1.772(18)	-	-	1.457(9)	1.498(8)	1.473(8)
	C ₆ -X	1.316(17)	-	-	1.365(7)	-	-
W	Mo-C ₆	2.26	-	2.246	-	-	2.118
	C ₆ -C ₇	1.47	-	1.493	-	-	1.457
	C ₆ -X	1.33	-	1.315	-	-	-

In both the ethoxy and the amino-substituted complexes, there is a small decrease in the bond lengths in the tricarbonyl complexes, but there is not a drastic change between the penta- and the tetracarbonyl complexes. There is very little difference between the amino carbene complexes' bond lengths and the ethoxy carbene complexes'. Although the values are relatively similar, two trends can be seen to be emerging:



4.2.4 Computational analysis

The outcomes of the computational analyses of the complexes presented previously are all very similar. The HOMO lies on the metal, and the LUMO lies on the carbene carbon (C₆) in these complexes. This implies that nucleophilic attack will occur on the carbene carbon, and electrophilic attack will occur on the metal. There is never a region of extensively high electron density. The bond lengths generated were excellent approximations to the crystalline bond lengths, and the generated IR spectra approximated the shape of the experimental IR spectra very well.

Below is a graphical representation of the energies of the HOMO's and LUMO's of the complexes computed. It shows that there is an energy dip of both the HOMO and the LUMO of the biscarbene, while there is negligible energy difference observed between the phosphinated and non-phosphinated complexes. There is negligible difference between the energies when the carbene substituent is ethoxy or amine. There is a slight rise in HOMO and LUMO energy when removing carbonyl ligands and adding phosphine ligands.

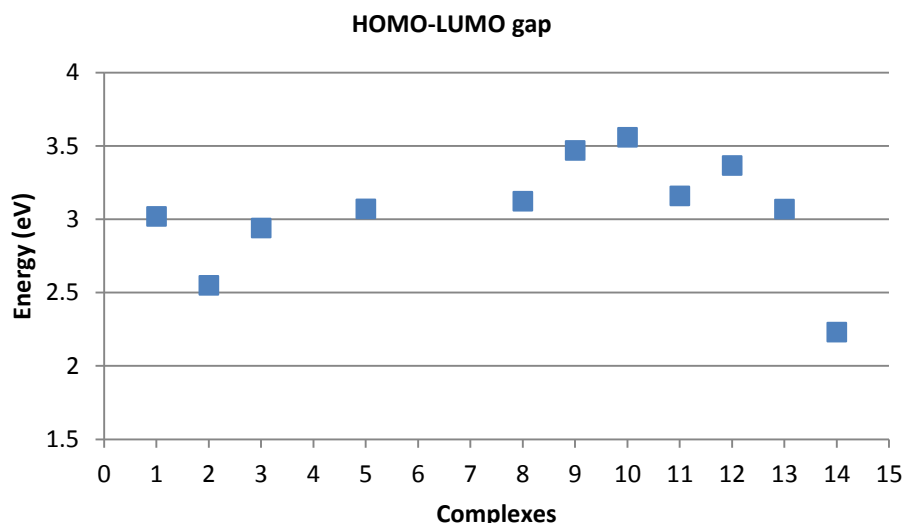


Figure 4.5: Graphical representation of the HOMO energies and the LUMO energies of the computed complexes

Due to the HOMO being found on the metal and the LUMO being on the carbene carbon, Du Toit *et al.* predicts that these complexes will probably be catalytic for alkene cyclopropanation, C-H insertion and ylide forming types of reactions⁶. Overall, in terms of the size of the HOMO-LUMO gap, Arrieta *et al.*⁷ predicts that **14-mer** will be the most reactive of the complexes presented, and **10** should be the least reactive, although in terms of the substitution of the metal centre, this does not parallel the predictions laid out by Arrieta *et al.* After each subsequent carbonyl substitution, the reactivity of the complex lessens toward further carbonyl substitutions.

Table 4.2: AO contributions to the HOMO and LUMO

Complex	HOMO			LUMO		
	Mo	C ₆	Trans-CO	Mo	C ₆	Trans-CO
1	67%	1%	10%	13%	27%	14%
3-cis	58%	2%	12%	7%	34%	11%
3-trans	68%	1%		11%	27%	
8-mer	69%	1%		15%	32%	
8-fac	67%	0%	12%	9%	31%	8%
9	68%	0%	11%	4%	31%	4%
11-mer	65%	2%	12%	5%	30%	5%
13-mer	67%	3%		7%	27%	
13-fac	66%	0%	13%	4%	29%	5%

It has been shown that in order for a complex to be metathesis active, the LUMO must be centred on the metal atom, while the HOMO should be centred on the carbene carbon. The computational analysis of the HOMO-LUMO contributions from atomic orbitals calculations shows very little difference in contributions upon substitution of the pentacarbonyl carbene complexes for tetra- or

⁶ Du Toit, J.I., van Sittert, C.G.C.E., Vosloo, H.C.M., *J. Organomet. Chem.*, **738**, **2013**, 76-91

⁷ Arrieta, A., Cossío, F.P., Fernández, I., Gómez-Gallego, M., Lecea, B., Mancheño, M.J., Sierra, M.A., *J. Am. Chem. Soc.*, **2000**, **122**, 11509

tricarbonyl complexes. Changing the carbene, furyl to thienyl and ethoxy to amino, did not affect the contributions substantially.

4.3 Conclusions

This study has begun to fill the gap between the abundance of data available for chromium- and tungsten carbene complexes and the lack of data available for molybdenum. Fourteen novel complexes have been synthesised in this study. Comparisons between these novel molybdenum carbene complexes and their chromium and tungsten analogues have revealed specific trends for this series of group VI phosphine substituted carbene complexes. The additional information obtained from structural data as well as theoretical studies will now enable a more thorough study in the application of these complexes in catalysis. There is great potential for these complexes to be catalytically active if work that has been done previously is used as an indicator.

A trend that was made apparent during the study is the strength of the π -acceptors. This trend is carbonyl > phosphine > carbene. This trend became apparent as a result of the bond lengths obtained from X-ray crystallography data as well as isomer stability. It was also noted that the resonance structures of the Fischer carbenes play a large role in the chemical shifts of the furyl protons and carbons in NMR spectra.

When the ethoxy group is substituted for an amino group, there is a large shift in the position of the proton and carbon adjacent to the carbene attachment carbon on the ^{13}C NMR spectrum. This is as a result of the compound preferring a conformation where the metal is close to the oxygen of the furyl (*anti*) in the case of an ethoxy substituent. In the event where there is an amino substituent, it prefers a conformation where the amino is close to the oxygen on the furyl (*syn*). This is substantiated by crystal data. It was found that the *cis* isomer is more stable when substituting a carbonyl with a weaker π -acceptor.

In the theoretical studies, the HOMO of the molecule was distributed around the metal atom, which implies that nucleophilic attack by this molecule will originate from here. The LUMO was found to be concentrated around the carbene carbon, which indicates that any nucleophilic attack on this molecule will be primarily on this atom - this is what is found in experimental observation. The theoretical studies did not consistently parallel the energy conformers (i.e. crystal structures) found in experiments. From the analyses of the computational data, it has become clear that varying of the carbene substituents and ligand substitution seemed to have had very little effect on changing the reactivity patterns of the Fischer carbene complexes, as far as the metathesis reaction is concerned.

Future work will focus on employing the results of this study in designing catalytic processes most suitable to this type of complex, for example alkene cyclopropanation reactions, C-H insertion reactions and ylide forming reactions to test the viability of these complexes as catalysts. Electrochemical studies will be conducted to aid in obtaining this outcome.

Chapter 5:

Experimental

“If we knew what it was we were doing,

it would not be called research,

would it? –Albert Einstein

The overall synthetic routes that were to be achieved are outlined in figure 7.1.

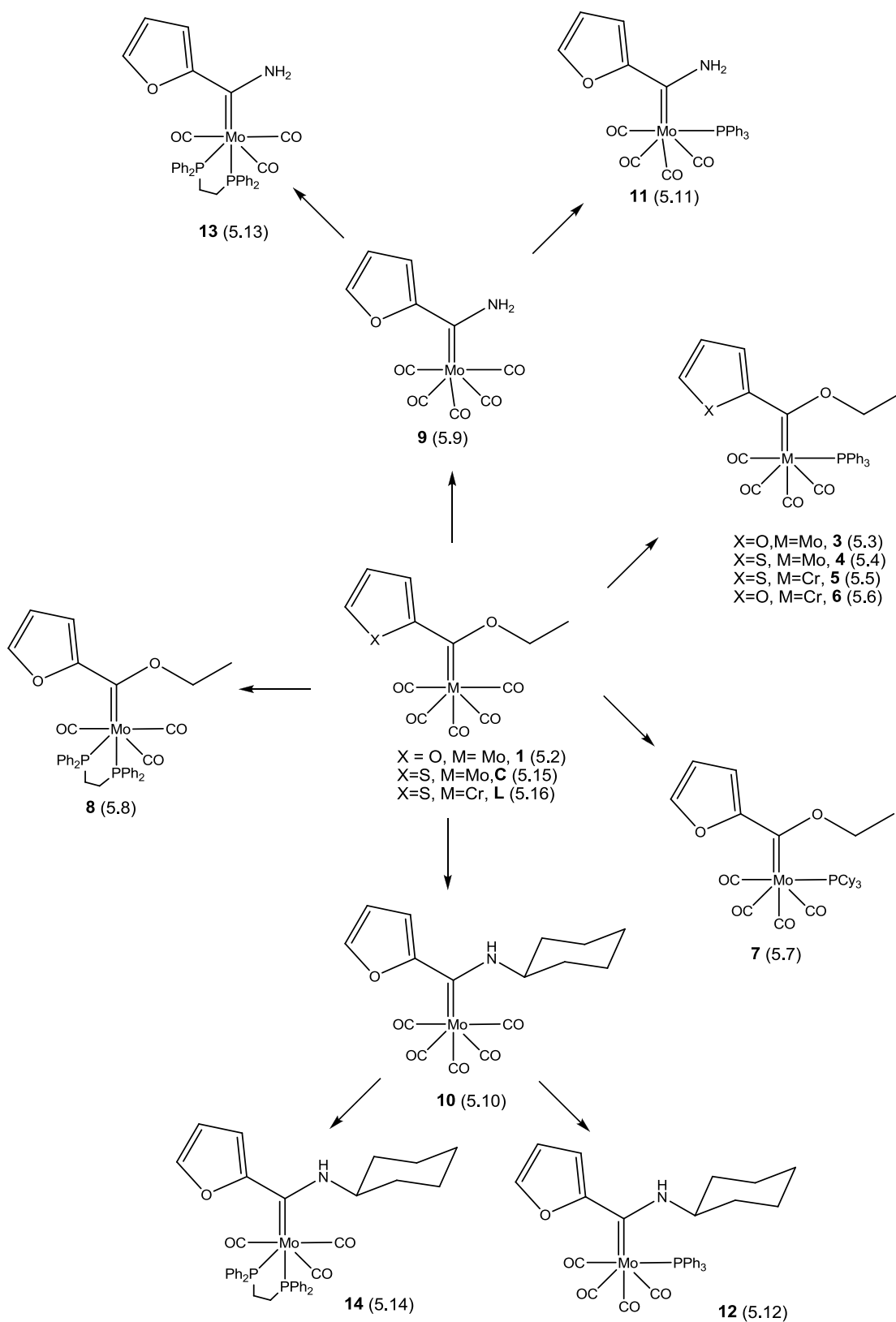


Figure 7.1: Synthesis of the molybdenum(0) and chromium(0) carbene complexes

5.1 General comments

All reactions attempted in this study utilised classical Fischer and Schlenk methodology as well as synthetic procedures described in literature. All reactions were carried out in inert conditions using nitrogen gas and/or argon gas and oven dried glassware. Solvents used were distilled/dried and used under inert conditions and removed *in vacuo*. The progress reactions were monitored using TLC plates consisting of silica gel on TLC-PET foils. Multiple TLC analyses were performed on each reaction using hexane, DCM and hexane:DCM (1:1) as eluents. TLC analysis was not used for identification purposes. The products of these reactions were purified, unless otherwise stated, using column chromatography with silica gel 60 (0.063-0.0200 mm) as a stationary phase and incorporating dry loading as a sample introduction method. Low temperatures were achieved using an acetone bath.

A Perkin-Elmer Spectrum RX IFT-IR spectrometer as well as a Bruker Alpha spectrometer was used to record infrared spectra. All spectra were recorded using KBr pellets.

A Bruker ARX-300, Bruker Ultrashield plus 400 AVANCE III and a Bruker DRX 500 AVANCE spectrometer were used to record ^1H NMR spectra at 300.1, 400.21 and 500.13 MHz respectively. The same machines were used to record ^{13}C NMR spectra at 75.5, 100.6 and 125.8 MHz respectively, as well as the ^{31}P NMR spectra at 121.495 MHz. The solvent, unless otherwise stated was deuterated chloroform (Proton NMR (CDCl_3): 7.24 ppm).

The X-ray crystallography data was recorded at the University of Johannesburg, the University of Stellenbosch and the University of Pretoria. The specifications of the machines used are available on request. All of the crystallographic data including the cif and checkcif files are included on the accompanying CD.

The mass spectra were recorded on a SYNAPT G2 HDMS. The data was acquired using direct flow injection using both ESI and APCI over 3 minutes. This allowed at least 50 scans to be collected. Data was acquired in the positive mode over the mass range of 100-1000 Da. The following additional parameters were used:

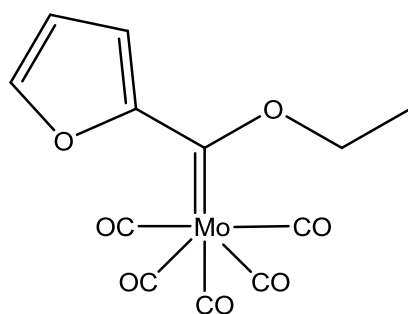
- Corona current (μA): 7
- Capillary (kV): 2.8000
- Source temperature ($^{\circ}\text{C}$): 120
- Sampling cone: 40.0000

- Extraction cone: 5.0000
- Source gas flow (mL/min): 0.00
- Desolvation temperature (°C): 350
- Cone gas flow (L/hr): 50.0
- Desolvation gas flow (L/hr): 600.0

Theoretical calculations were executed using GAUSSIAN 03 software.¹ All calculations were done using ground state DFT calculations with the B3LYP functional and the GEN basis set (6-31G* for C, H, O, P, N and LANL2DZ for Mo and Cr), the charge was set to neutral the spin state set to singlet. Frequencies were calculated and no imaginary frequencies were observed. All input and output files for the DFT calculations of the complexes have been included on the accompanying CD. The contributions to the HOMO and the LUMO were estimated using the Mulliken contribution method in the Chemissian software package.

Complex **1** was synthesised using classical Fischer methods.^{2,3} Complex **2** was a side product of the methods just stated. Complexes **9** and **10** were made using the method laid out by Klabunde and Fischer⁴ as well as that laid out by Connor.⁵ Complexes **3** through **8** and **11** through **14** were synthesised using methods described by Barluenga⁶ and Reinheimer.⁷

5.2 Synthesis of $[Mo(CO)_5\{C(OEt)(C_4H_3O)\}]$ (**1**) and $[{(CO)_5MoC}_2(C_4H_3O)]$ (**2**)



THF (20 mL) was placed in a prepared, inert and oven dried schlenk tube flask. This reaction flask was cooled to -30 °C and furan (0.22 mL, 3 mmol) was added. Deprotonation was achieved by drop-

¹ Frisch, M. J., Trucks, G. W., and Schlegel, H. B., *et al.*, *Gaussian 03*, revision D.01 Gaussian, Inc., Wallingford CT, **2004**.

² Fischer, E.O., Maasböl, A., *Angew. Chem. Int. Ed. Engl.*, **3**, **1964**, 580

³ Aoki, S., Fujimura, T., Nakamura, E., *J. Am. Chem. Soc.*, **114**, **1992**, 2985

⁴ Klabunde, U., Fischer, E.O., *J. Am. Chem. Soc.*, **89**, **1967**, 7141

⁵ Connor, J.A., Fischer, E.O., *J. Chem. Soc. (A)*, **1969**, 578

⁶ Barluenga, J., Muñiz, K., Tomás, M., Ballesteros, A., Garcia-Granda, S., *Organometallics*, **22**, **2003**, 1756

⁷ Reinheimer, E.W., Kantardjieff, K.A., Herron, S.R., Tisserat, C.G., Casalnuovo, J.A., *J. Chem. Crystallogr.*, **33**, **2003**, 503

wise addition of n-butyl lithium (ⁿBuLi) (2 mL, 3 mmol). The reaction mixture was allowed to react in the cold bath for 30 minutes. A light yellow solution resulted.

The above mixture was cooled to approximately -78 °C and hexacarbonyl molybdenum(0) (0.794 g, 3 mmol) was added, this was stirred in the cold for 20 minutes and then allowed to warm to room temperature and stirred for a further 40 minutes. A red mixture resulted.

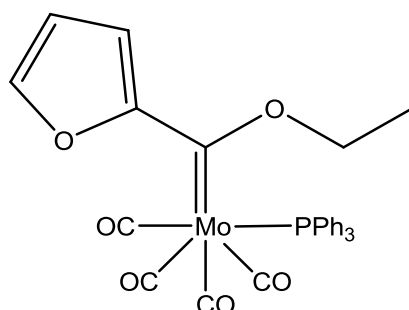
The solvent on the above mixture was removed in *vacuo*. The remaining solids were re-dissolved in approximately 10 mL dichloromethane. This was cooled to approximately -30 °C. To this triethyloxonium tetrafluoroborate (0.56938 g, 2.997 mmol) was added slowly. The mixture became darker, almost brown after 30 minutes. Thin Layer Chromatography (TLC) was used to determine whether the reaction had gone to completion. The solvent was removed in *vacuo*.

The impurities were removed using silica gel column chromatography (eluent: gradients of hexane and DCM). There was no observable butyl-carbene. The unreacted metal eluted in the first fraction, the monocarbene in the second fraction, and a biscarbene in the third fraction; these were all collected separately. The solvent was removed from the mono- and biscarbene fractions, affording a red solid from the monocarbene fraction and a purple solid from the biscarbene fraction.

The solids were characterised using IR- and NMR spectroscopy. Crystals were obtained by the solvent exchange method using DCM and hexane; the resulting crystals were analysed using X-ray crystallography. (Yield 40% monocarbene, 0.6% biscarbene)

*yield calculated assuming that each product should be the only product of the reaction (i.e. in the method given above the theoretical yield would be taken as 3mmol). For **1**: MS (ESI): m/z [M]⁺ - 5CO 222.9738, [M]⁺ - Furan - 3 CO 211.9579. For **2**: MS (ESI): m/z [M]⁺ - MoCO₅{C(OEt)} 362.0712.

5.3 Synthesis of $[Mo(CO)_4(PPh_3)\{C(OEt)(C_4H_3O)\}]$ (**3**)

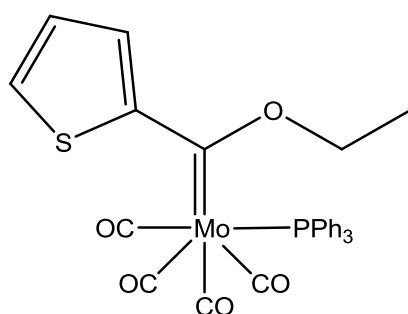


[Mo(CO)₅{C(OEt)(C₄H₃O)}] (0.18 g, 0.5 mmol) and triphenylphosphine (0.132 g, 0.6 mmol) was added to 20 mL toluene and refluxed at 77 °C for one hour only. TLC analysis (eluent DCM and Hexane (1:1)) showed the presence of two brown products, as well as remaining red starting material (approximately 60%). Decomposition products begin to form if the reaction is allowed to continue for longer than one hour. The solution turned from red to brown with a yellow ‘halo’.

The solvent was removed and the products were purified using silica gel column chromatography (eluent: gradients ranging from pure hexane to pure DCM). The UV-active triphenylphosphine eluted first, red [Mo(CO)₅{C(OEt)(C₄H₃O)}] eluted second, a yellow brown elution band in third and finally a red brown elution band was collected. The solvents were removed from the two product elution bands; which resulted in a yellow-brown solid and a red-brown solid. Both solids were analysed using IR spectroscopy.

Upon solvation, the yellow-brown *trans* complex converted quickly (± 90 seconds) to the red-brown *cis* complex, and thus no NMR spectrum could be obtained of the *trans* isomer. The red brown solid was characterised using NMR spectroscopy and X-ray crystallography as well. (Yield 60% *cis* isomer, 40% *trans* isomer)

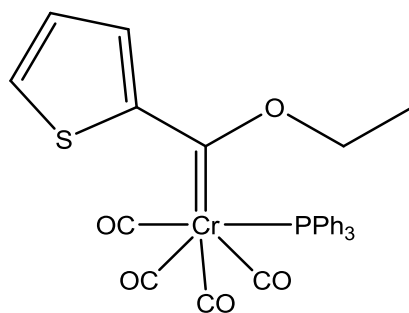
5.4 Synthesis of [Mo(CO)₄(PPh₃){C(OEt)(C₄H₃S)}] (4)



Triphenylphosphine (0.196 g, 0.75 mmol) and [Mo(CO)₅{C(OEt)(C₄H₃S)}] (0.178 g, 0.47 mmol) were dissolved in ± 20 mL toluene and refluxed at 70 °C for one hour.

The above was purified using silica gel column chromatography (eluent: gradients ranging from pure hexane to pure DCM). Only a short column was necessary. Characterisation was done using IR- and NMR spectroscopy, as well as X-ray crystallography. (Yield 56%)

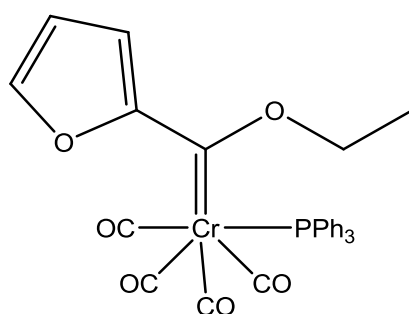
5.5 Synthesis of $[Cr(CO)_4(PPh_3)\{C(OEt)(C_4H_3S)\}]$ (5)



$[Cr(CO)_5\{C(OEt)(C_4H_3S)\}]$ (0.332 g, 1 mmol) and triphenylphosphine (0.268 g, 1 mmol) were added to \pm 20 mL toluene. This was refluxed at 90 °C for two hours. Triphenylphosphine (0.131 g, 1.5 mmol) was added and the reaction was left under reflux for another 17 hours. At this time the reaction was stopped.

The toluene was removed and the product was purified using silica gel column chromatography (eluent: gradients ranging from pure hexane to pure DCM). Separation was achieved in pure hexane; the first fraction was un-reacted $[Cr(CO)_5\{C(OEt)(C_4H_3S)\}]$. Subsequent elution bands were the yellow *trans* isomer product and the red-brown *cis* isomer product. Characterisation was done using IR- and NMR spectroscopy, as well as X-ray crystallography. (Yield 62%)

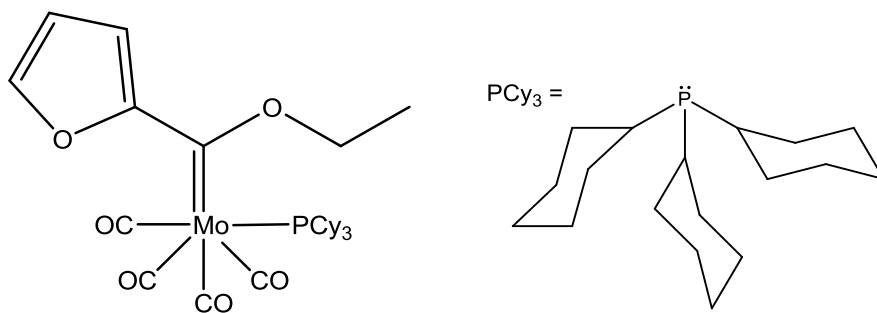
5.6 Synthesis of $[Cr(CO)_4(PPh_3)\{C(OEt)(C_4H_3O)\}]$ (6)



Triphenylphosphine (0.197 g, 0.75 mmol) and $[Cr(CO)_5\{C(OEt)(C_4H_3O)\}]$ (0.196 g, 0.59 mmol) were dissolved in \pm 20 mL toluene and reacted under reflux at 70 °C for two hours.

The above was purified by washing the solid product mixture with cold hexane. This afforded a brown solid. Characterisation was done using IR- and NMR spectroscopy, as well as X-ray crystallography. (Yield 54%)

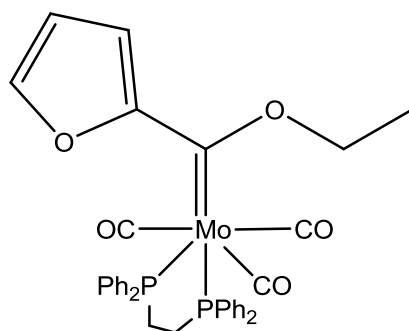
5.7 Synthesis of $[Mo(CO)_4(P(C_6H_{11})_3)\{C(OEt)(C_4H_3O)\}]$ (7)



Tricyclohexylphosphine (0.340 g, 1.21 mmol) and $[Mo(CO)_5\{C(OEt)(C_4H_3O)\}]$ (0.414 g, 1.149 mmol) was dissolved in ± 20 mL toluene. This was stirred at room temperature for 48 hours. TLC analysis shows the presence of two products in addition to un-reacted starting material.

The product was purified using aluminium oxide column chromatography; adequate separation of the two products was achieved using only hexane. This afforded the products as an orange brown solid and a purple solid. Characterisation was done using IR- and NMR spectroscopy, as well as X-ray crystallography. (Yield 7%)

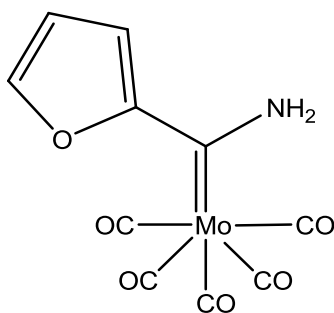
5.8 Synthesis of $[Mo(CO)_3(DPPE)\{C(OEt)(C_4H_3O)\}]$ (8)



$[Mo(CO)_5\{C(OEt)(C_4H_3O)\}]$ (0.180 g, 0.5 mmol) and 1,2-bis(diphenylphosphino)ethane (0.200 g, 0.5 mmol) was added to 20 mL toluene and refluxed at 82 °C for one hour. The reaction mixture turned from red to deep brown.

Purification was achieved through re-crystallisation using solvent diffusion of DCM and hexane. Deep purple crystals were obtained. Characterisation was done using IR- and NMR spectroscopy, as well as X-ray crystallography. (Yield 65%) MS (ESI): m/z $[M]^+$ - CO 677.0865, $[M]^+$ - 2CO 649.0812, $[M]^+$ - 3CO 620.0928, $[M]^+$ - OEt - 2CO 603.0530, $[M]^+$ - Et - 3CO 592.0536, $[M]^+$ - Carbene - CO 553.0362

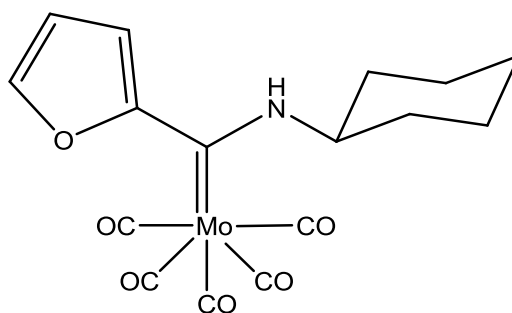
5.9 Synthesis of $[Mo(CO)_5\{C(NH_2)(C_4H_3O)\}]$ (9)



$[Mo(CO)_5\{C(OEt)(C_4H_3O)\}]$ (0.180 g, 0.5 mmol) was dissolved in 20 mL ether. Ammonia gas was bubbled through the mixture for approximately one minute. The mixture turned from red to yellow. Complete conversion was determined using TLC analysis. Once all the starting material was converted to product, the ether and excess ammonia was removed in *vacuo*. This afforded a bright yellow solid complex.

No further purification was required. There were no side products of this reaction. Characterisation was done using IR- and NMR spectroscopy, as well as X-ray crystallography. (Yield 100%)

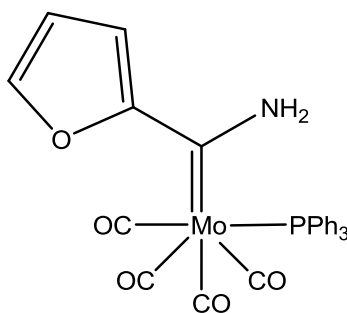
5.10 Synthesis of $[Mo(CO)_5\{C(C_6H_{12}N)(C_4H_3O)\}]$ (10)



$[Mo(CO)_5\{C(OEt)(C_4H_3O)\}]$ (0.735 g, 2.04 mmol) was dissolved in ± 20 mL diethyl ether. Cyclohexylamine (0.25 mL, 2.17 mmol) was added to the above. The mixture was allowed to react at room temperature overnight.

The above was purified using column chromatography (eluent Hexane, Hexane and DCM (1:1)). Characterisation was done using IR- and NMR spectroscopy, as well as X-ray crystallography. Crystals for x-ray crystallography were grown using the solvent exchange method using diethyl ether and hexane. The product is a yellow crystalline solid. (Yield 64%)

5.11 Synthesis of $[Mo(CO)_4(PPh_3)\{C(NH_2)(C_4H_3O)\}]$ (11)

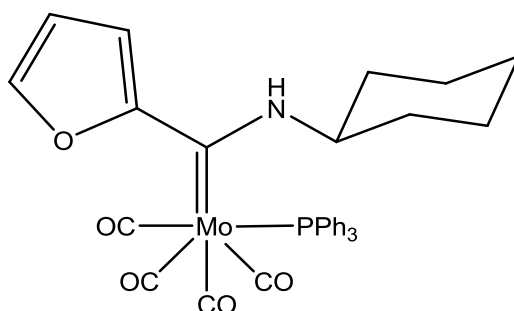


$[Mo(CO)_5\{C(NH_2)(C_4H_3O)\}]$ (0.056 g, 0.169 mmol) and triphenylphosphine (0.1 g, 0.381 mmol) was added to 10 mL toluene and refluxed at 80 °C for five hours. The solution underwent a colour change from yellow to brown.

The mixture was purified using silica gel column chromatography (eluent hexane, hexane and DCM (10:1)), and although inadequate separation of the starting materials and the product was seen in a TLC analysis, a column of no more than 15 cm (of silica) was required to achieve separation at a solvent ratio of hexane and DCM (10:1). The solvent was removed in *vacuo* which afforded a brown-orange solid.

The brown-orange product was characterised using IR- and NMR spectroscopy, as well as X-ray crystallography. (Yield 100% *cis* isomer) MS (ESI): m/z $[M]^+$ - NH_2 549.9879, $[M]^+$ - 2CO 512.0334, $[M]^+$ - Phenyl 490.0056, $[M]^+$ - 3CO 484.0200, $[M]^+$ - 4CO 456.0448, $[M]^+$ - furan - 3CO 416.9988, $[M]^+$ - PPh_3 263.1078

5.12 Synthesis of $[Mo(CO)_4(PPh_3)\{C(C_6H_{12}N)(C_4H_3O)\}]$ (12)

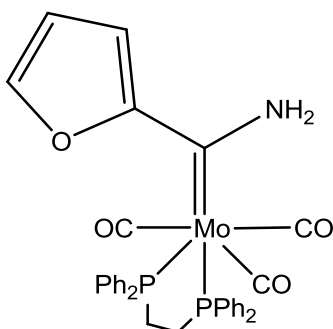


Triphenylphosphine (0.393 g, 1.5 mmol) was dissolved in \pm 20 mL toluene. Excess $[Mo(CO)_5\{C(C_6H_{12}N)(C_4H_3O)\}]$ was dissolved in toluene and added to the above. This was reacted

under reflux for two hours and the solvent was removed. The solution mixture went from yellow to a very dark colour.

This was purified using silica gel column chromatography (eluent: gradients ranging from pure hexane to pure DCM). Only a very short column was necessary. Characterisation was done using IR- and NMR spectroscopy, as well as X-ray crystallography. (Yield 43%) MS (ESI): m/z $[M]^+$ - PPh_3 263.1076

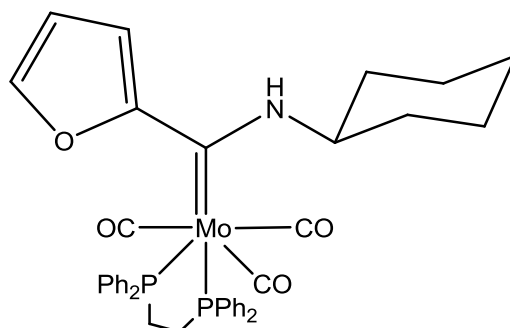
5.13 Synthesis of $[Mo(CO)_3(DPPE)\{C(NH_2)(C_4H_3O)\}]$ (13)



$[Mo(CO)_5\{C(NH_2)(C_4H_3O)\}]$ (0.165 g, 0.4983 mmol) and bis(diphenylphosphino)ethane (0.19 g, 0.477 mmol) was added to ± 20 mL toluene and refluxed at 80 °C for two hours. Another equivalent of bis(diphenylphosphino)ethane (0.204 g, 0.512 mmol) was added to the reaction mixture. The mixture was allowed to react for a further 17 hours. The solution mixture turned from yellow to red. TLC analysis indicated the presence of two products (dark orange/purple and orange) in addition to un-reacted starting material.

The products were purified using crystallisation, yielding a dark purple solid. Characterisation was done using IR- and NMR spectroscopy, as well as X-ray crystallography. (Yield 47%) MS (ESI): m/z $[M]^+$ - CO 648.0714, $[M]^+$ - 2CO 619.0716, $[M]^+$ - furan - H_2 606.0639, $[M]^+$ - 3CO 591.0793, $[M]^+$ - furan - 2CO 553.0383, $[M]^+$ - furan - 3CO 525.0381, $[M]^+$ - DPPE - CO 248.0283

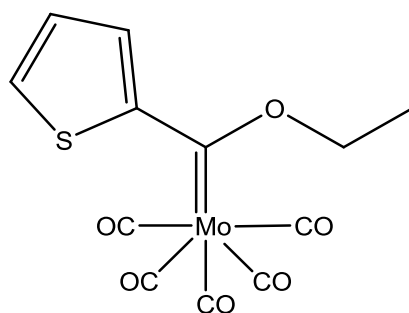
5.14 Synthesis of $[Mo(CO)_3(DPPE)\{C(C_6H_5O)\}(C_6H_{12}N)\}]$ (14)



$[Mo(CO)_5\{C(C_6H_5O)\}(C_6H_{12}N)\}]$ (0.408 g, 0.99 mmol) was dissolved in \pm 20 mL toluene. To this 1,2-bis(diphenylphosphino)ethane (0.797 g, 2 mmol) was added and dissolved. This reaction mixture was reacted under reflux at 78 °C for two hours.

The product was purified using silica gel column chromatography (eluent: gradients from pure hexane to pure DCM). Only a very short column was necessary. Characterisation was done using IR- and NMR spectroscopy, as well as X-ray crystallography. (Yield 69%) MS (ESI): m/z $[M]^+$ 758.133, $[M]^+$ - carbene - 2CO 524.0375

5.15 Synthesis of $[Mo(CO)_5\{C(OEt)\}(C_4H_3S)\}]$ (C)

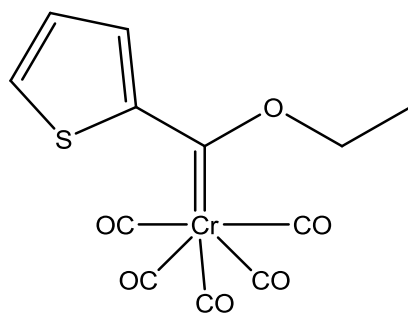


The method outlined by Landman⁸ was used to synthesise this starting material.

Thiophene (0.4 mL, 4.99 mmol) was deprotonated at -35 °C using ⁿBuLi (3.33 mL, 4.99 mmol). The mixture was then metallated using hexacarbonyl molybdenum(0) (1.355 g, 5.13 mmol) at -78 °C. This was alkylated using triethyloxonium tetrafluoroborate (0.95 g, 4.99 mmol) at -35 °C. This yielded a red solid which was used as starting material for **4**.

⁸ M. Landman, PhD thesis: Synthesis of Metal Complexes with Thiophene Ligands, **2000**, 150

5.16 Synthesis of $[Cr(CO)_5\{C(OEt)(C_4H_3S)\}] (L)$



The method outlined by Connor⁵ was used to synthesise this starting material.

Thiophene (0.4 mL, 4.99 mmol) was deprotonated at -35 °C using ⁿBuLi (3.33 mL, 4.99 mmol). The mixture was then metallated using hexacarbonyl chromium(0) (1.1 g, 5 mmol) at -78 °C. This was alkylated using triethyloxonium tetrafluoroborate (0.95 g, 4.99 mmol) at -35 °C. This yielded a red solid which was used as starting material for **5**.

Appendices

Appendix A

Table 1. Crystal data and structure refinement for Complex 1.

Identification code	Complex 1	
Empirical formula	C ₁₂ H ₈ Mo O ₇	
Formula weight	360.12	
Temperature	100(2) K	
Wavelength	0.71073 Å	
Crystal system	Orthorhombic	
Space group	A m a 2	
Unit cell dimensions	a = 7.5881(15) Å	α = 90°.
	b = 12.055(2) Å	β = 90°.
	c = 14.800(3) Å	γ = 90°.
Volume	1353.9(5) Å ³	
Z	4	
Density (calculated)	1.767 Mg/m ³	
Absorption coefficient	0.996 mm ⁻¹	
F(000)	712	
Crystal size	0.120 x 0.100 x 0.060 mm ³	
Theta range for data collection	2.179 to 26.358°.	
Index ranges	-9<=h<=9, -15<=k<=15, -9<=l<=18	
Reflections collected	3827	
Independent reflections	1082 [R(int) = 0.0360]	
Completeness to theta = 25.240°	99.9 %	
Absorption correction	Semi-empirical from equivalents	
Max. and min. transmission	0.9427 and 0.8898	
Refinement method	Full-matrix least-squares on F ²	
Data / restraints / parameters	1082 / 1 / 91	
Goodness-of-fit on F ²	1.068	
Final R indices [I>2σ(I)]	R1 = 0.0310, wR2 = 0.0606	
R indices (all data)	R1 = 0.0384, wR2 = 0.0646	
Absolute structure parameter	0.5	
Extinction coefficient	n/a	
Largest diff. peak and hole	0.547 and -0.479 e.Å ⁻³	

Appendix B

Table 2. Crystal data and structure refinement for Complex 3.

Identification code	Complex 3
Empirical formula	C ₂₉ H ₂₃ Mo O ₆ P
Formula weight	594.38
Temperature	150(2) K
Wavelength	0.71073 Å
Crystal system	Monoclinic
Space group	<i>P</i> 2 ₁ / <i>c</i>
Unit cell dimensions	<i>a</i> = 10.5978(9) Å <i>b</i> = 12.6167(11) Å <i>c</i> = 20.5695(17) Å β = 103.29(3)°
Volume	2676.7(4) Å ³
Z	4
Density (calculated)	1.475 Mg/m ³
Absorption coefficient	0.591 mm ⁻¹
F(000)	1208
Crystal size (mm ³)	0.106 x 0.089 x 0.061
Theta range for data collection	2.488 to 25.446°
Index ranges	-12 ≤ <i>h</i> ≤ 12, -15 ≤ <i>k</i> ≤ 15, -24 ≤ <i>l</i> ≤ 24
Reflections collected	69374
Independent reflections	4930 [R(int) = 0.0932]
Data / restraints / parameters	4930 / 0 / 334
Final R indices [<i>I</i> > 2σ(<i>I</i>)]	R1 = 0.0331, wR2 = 0.0721
Largest diff. peak and hole	0.781 and -0.336 e.Å ⁻³

Appendix C

Table 3. Crystal data and structure refinement for Complex 5.

Identification code	Complex 5
Empirical formula	C ₂₉ H ₂₃ Cr O ₅ P S
Formula weight	566.50
Temperature	150(2) K
Wavelength	0.71073 Å
Crystal system	Monoclinic
Space group	<i>P</i> 2 ₁ / <i>n</i>
Unit cell dimensions	<i>a</i> = 9.920 (3) Å <i>b</i> = 27.789 (3) Å <i>c</i> = 10.458 (3) Å β = 112.662(5)°
Volume	2660.1(13) Å ³
Z	4
Density (calculated)	1.415 Mg/m ³
Absorption coefficient	0.606 mm ⁻¹
F(000)	1168
Crystal size (mm ³)	0.211 x 0.161 x 0.151
Theta range for data collection	2.343 to 26.372°
Index ranges	-12 ≤ <i>h</i> ≤ 11, -34 ≤ <i>k</i> ≤ 34, -12 ≤ <i>l</i> ≤ 13
Reflections collected	40447
Independent reflections	5367 [R(int) = 0.0656]
Data / restraints / parameters	5367 / 0 / 334
Final R indices [<i>I</i> > 2σ(<i>I</i>)]	R1 = 0.0902, wR2 = 0.1991
Largest diff. peak and hole	1.194 and -0.708 e.Å ⁻³

Appendix D

Table 4. Crystal data and structure refinement for Complex 8.

Identification code	Complex 8	
Empirical formula	$C_{36} H_{32} Mo O_5 P_2$	
Formula weight	702.49	
Temperature	150(2) K	
Wavelength	0.71073 Å	
Crystal system	Monoclinic	
Space group	$P2_1/n$	
Unit cell dimensions	$a = 15.3756(6)$ Å	$\alpha = 90^\circ$.
	$b = 11.7025(5)$ Å	$\beta = 98.1050(10)^\circ$.
	$c = 17.4471(7)$ Å	$\gamma = 90^\circ$.
Volume	3108.0(2) Å ³	
Z	4	
Density (calculated)	1.501 Mg/m ³	
Absorption coefficient	0.568 mm ⁻¹	
F(000)	1440	
Crystal size	0.408 x 0.246 x 0.224 mm ³	
Theta range for data collection	2.358 to 26.369°.	
Index ranges	-19 ≤ h ≤ 19, -14 ≤ k ≤ 14, -20 ≤ l ≤ 21	
Reflections collected	25580	
Independent reflections	6203 [R(int) = 0.0759]	
Completeness to theta = 25.242°	98.2 %	
Absorption correction	Semi-empirical from equivalents	
Max. and min. transmission	0.7465 and 0.7063	
Refinement method	Full-matrix least-squares on F ²	
Data / restraints / parameters	6203 / 0 / 367	
Goodness-of-fit on F ²	1.100	
Final R indices [I > 2σ(I)]	R1 = 0.0389, wR2 = 0.1024	
R indices (all data)	R1 = 0.0441, wR2 = 0.1121	
Extinction coefficient	n/a	
Largest diff. peak and hole	1.338 and -0.847 e.Å ⁻³	

Appendix E

Table 5. Crystal data and structure refinement for Complex 9.

Identification code	Complex 9	
Empirical formula	C ₁₀ H ₅ Mo N O ₆	
Formula weight	331.09	
Temperature	100(2) K	
Wavelength	0.71073 Å	
Crystal system	Monoclinic	
Space group	P2 ₁ /c	
Unit cell dimensions	a = 19.9335(14) Å	α = 90°.
	b = 6.7854(5) Å	β = 114.3890(10)°.
	c = 19.1017(14) Å	γ = 90°.
Volume	2353.1(3) Å ³	
Z	8	
Density (calculated)	1.869 Mg/m ³	
Absorption coefficient	1.133 mm ⁻¹	
F(000)	1296	
Crystal size	0.280 x 0.260 x 0.200 mm ³	
Theta range for data collection	2.138 to 28.924°.	
Index ranges	-11 ≤ h ≤ 27, -9 ≤ k ≤ 9, -25 ≤ l ≤ 10	
Reflections collected	7718	
Independent reflections	4532 [R(int) = 0.0185]	
Completeness to theta = 25.242°	83.9 %	
Absorption correction	Semi-empirical from equivalents	
Max. and min. transmission	0.899 and 0.8032	
Refinement method	Full-matrix least-squares on F ²	
Data / restraints / parameters	4532 / 0 / 339	
Goodness-of-fit on F ²	1.041	
Final R indices [I > 2σ(I)]	R1 = 0.0231, wR2 = 0.0515	
R indices (all data)	R1 = 0.0273, wR2 = 0.0534	
Extinction coefficient	n/a	
Largest diff. peak and hole	0.441 and -0.517 e.Å ⁻³	

Appendix F

Table 6. Crystal data and structure refinement for Complex 10.

Identification code	Complex 10	
Empirical formula	C ₁₆ H ₁₅ Mo N O ₆	
Formula weight	413.23	
Temperature	150(2) K	
Wavelength	0.71073 Å	
Crystal system	Monoclinic	
Space group	P2 ₁ /m	
Unit cell dimensions	a = 9.4381(5) Å	α = 90°.
	b = 9.6189(5) Å	β = 113.1880(10)°.
	c = 10.1394(6) Å	γ = 90°.
Volume	846.14(8) Å ³	
Z	2	
Density (calculated)	1.622 Mg/m ³	
Absorption coefficient	0.806 mm ⁻¹	
F(000)	416	
Crystal size	0.101 x 0.099 x 0.083 mm ³	
Theta range for data collection	2.348 to 26.365°.	
Index ranges	-11 ≤ h ≤ 11, -12 ≤ k ≤ 12, -12 ≤ l ≤ 12	
Reflections collected	38848	
Independent reflections	1834 [R(int) = 0.0401]	
Completeness to theta = 25.242°	99.9 %	
Absorption correction	Semi-empirical from equivalents	
Max. and min. transmission	0.7476 and 0.6647	
Refinement method	Full-matrix least-squares on F ²	
Data / restraints / parameters	1834 / 0 / 127	
Goodness-of-fit on F ²	1.108	
Final R indices [I > 2σ(I)]	R1 = 0.0291, wR2 = 0.0708	
R indices (all data)	R1 = 0.0325, wR2 = 0.0732	
Extinction coefficient	n/a	
Largest diff. peak and hole	1.162 and -0.471 e.Å ⁻³	

Appendix G

Table 7. Crystal data and structure refinement for Complex 11.

Identification code	Complex 11	
Empirical formula	C ₂₇ H ₂₀ Mo N O ₅ P	
Formula weight	565.35	
Temperature	150(2) K	
Wavelength	0.71073 Å	
Crystal system	Triclinic	
Space group	P -1	
Unit cell dimensions	a = 8.9197(3) Å	α = 101.829(2)°.
	b = 15.4383(5) Å	β = 97.949(2)°.
	c = 19.5008(7) Å	γ = 102.128(2)°.
Volume	2523.09(15) Å ³	
Z	4	
Density (calculated)	1.488 Mg/m ³	
Absorption coefficient	0.621 mm ⁻¹	
F(000)	1144	
Crystal size	0.315 x 0.070 x 0.025 mm ³	
Theta range for data collection	2.280 to 27.122°.	
Index ranges	-11 ≤ h ≤ 11, -19 ≤ k ≤ 19, -24 ≤ l ≤ 24	
Reflections collected	79349	
Independent reflections	11136 [R(int) = 0.0532]	
Completeness to theta = 25.242°	99.9 %	
Absorption correction	Semi-empirical from equivalents	
Max. and min. transmission	0.7455 and 0.7204	
Refinement method	Full-matrix least-squares on F ²	
Data / restraints / parameters	11136 / 0 / 631	
Goodness-of-fit on F ²	1.027	
Final R indices [I > 2σ(I)]	R1 = 0.0308, wR2 = 0.0567	
R indices (all data)	R1 = 0.0514, wR2 = 0.0633	
Extinction coefficient	n/a	
Largest diff. peak and hole	0.531 and -0.387 e.Å ⁻³	

Appendix H

Table 8. Crystal data and structure refinement for Complex 12.

Identification code	Complex 12	
Empirical formula	C ₃₆ H ₃₃ Mo N O ₅ P	
Formula weight	686.54	
Temperature	150(2) K	
Wavelength	0.71073 Å	
Crystal system	Triclinic	
Space group	P -1	
Unit cell dimensions	a = 9.5263(5) Å	α = 101.759(2)°.
	b = 10.4311(5) Å	β = 91.060(2)°.
	c = 16.7960(8) Å	γ = 100.185(2)°.
Volume	1605.66(14) Å ³	
Z	2	
Density (calculated)	1.420 Mg/m ³	
Absorption coefficient	0.502 mm ⁻¹	
F(000)	706	
Crystal size	0.113 x 0.087 x 0.074 mm ³	
Theta range for data collection	2.443 to 26.371°.	
Index ranges	-11 ≤ h ≤ 11, -12 ≤ k ≤ 13, -20 ≤ l ≤ 20	
Reflections collected	25743	
Independent reflections	6508 [R(int) = 0.0670]	
Completeness to theta = 25.242°	99.5 %	
Absorption correction	Semi-empirical from equivalents	
Max. and min. transmission	0.7457 and 0.6733	
Refinement method	Full-matrix least-squares on F ²	
Data / restraints / parameters	6508 / 0 / 397	
Goodness-of-fit on F ²	1.029	
Final R indices [I > 2σ(I)]	R1 = 0.0574, wR2 = 0.1206	
R indices (all data)	R1 = 0.0940, wR2 = 0.1352	
Extinction coefficient	n/a	
Largest diff. peak and hole	1.364 and -0.981 e.Å ⁻³	

Appendix I

Table 9. Crystal data and structure refinement for Complex 13.

Identification code	Complex 13	
Empirical formula	$C_{105.19} H_{94.99} Mo_3 N_3 O_{12.80} P_6$	
Formula weight	2079.61	
Temperature	150(2) K	
Wavelength	0.71073 Å	
Crystal system	Monoclinic	
Space group	$P2_1$	
Unit cell dimensions	$a = 19.8402(8)$ Å	$\alpha = 90^\circ$.
	$b = 11.5538(4)$ Å	$\beta = 109.159(2)^\circ$.
	$c = 23.3387(9)$ Å	$\gamma = 90^\circ$.
Volume	$5053.6(3)$ Å ³	
Z	2	
Density (calculated)	1.367 Mg/m ³	
Absorption coefficient	0.523 mm ⁻¹	
F(000)	2131	
Crystal size	0.200 x 0.040 x 0.040 mm ³	
Theta range for data collection	2.173 to 26.372°.	
Index ranges	-24 ≤ h ≤ 24, -14 ≤ k ≤ 14, -29 ≤ l ≤ 29	
Reflections collected	172263	
Independent reflections	20688 [R(int) = 0.0796]	
Completeness to theta = 25.242°	99.9 %	
Refinement method	Full-matrix least-squares on F ²	
Data / restraints / parameters	20688 / 1 / 1043	
Goodness-of-fit on F ²	1.022	
Final R indices [I > 2σ(I)]	R1 = 0.0472, wR2 = 0.1070	
R indices (all data)	R1 = 0.0680, wR2 = 0.1181	
Absolute structure parameter	-0.031(8)	
Extinction coefficient	n/a	
Largest diff. peak and hole	1.357 and -1.249 e.Å ⁻³	